IN-88
61189

NASA CONTRACTOR REPORT 177394

Study of New Systems Concepts for a Titan Atmospheric Probe

Doug Bernard
Todd Citron
Bob Drean
Scott Lewis
Martin Lo
John McCarthy
Robert Soderblom
Dave Steffy
Tina Vargas
Marty Wolff

CONTRACT NAS2– 12049
April 1986

NASA

NASA CONTRACTOR REPORT 177394

Study of New Systems Concepts for A Titan Atmospheric Probe

Doug Bernard
Todd Citron
Bob Drean
Scott Lewis
Martin Lo
John McCathy
Robert Soderblom
Dave Steffy
Tina Vargas
Marty Wolff

Hughes Aircraft Company
Space and Communications Group
El Segundo, California

Prepared for
Ames Research Center
Under Contract NAS2-12049
April 1986

National Aeronautics and
Space Administration

Ames Research Center
Moffett Field, California 94035

Table of Contents

1. SUMMARY AND INTRODUCTION

This final report documents results of a study of new systems concepts for a Titan Probe performed for NASA Ames Research Center under contract NAS 2-12049. This effort extends the work previously performed (Hughes, 1978) where a Titan Probe was conceived based on minimum deviation from Galileo Probe hardware. Though not bounded by existing hardware, this conceptual study was constrained to readily available and low risk hardware projected for the late 1980's time frame. The Titan atmospheric probe concept described in Swenson, 1984 was used as a point of departure for the present study.

This study also reflects the latest thoughts of planetary scientists relative to investigation goals which are somewhat different from the previous studies. Foremost of these is the desire to sample the organic haze layer which surrounds Titan at high altitude, up to 200 km above the surface. Subsonic gas sampling at this altitude requires a low ballistic coefficient. The blunt, large base diameter, light weight Probe design developed in this study provides the desired atmospheric sampling.

A second new requirement is lengthened descent time of 2 to 4 hours, to provide adequate gas sampling. This defines principally, the parachute design, the descent thermal control design, and the power source capacity.

A third new requirement is the ability to image the surface before impact. This leads to a data rate one or two orders of magnitude beyond previous atmospheric probes. However, the relatively close Carrier flyby altitude during the communications relay enables the necessary data transmission.

A fourth new requirement is surface operation. Because of the major effect on probe cost of a hard requirement for surface impact survival and operation under a wide range of surface conditions, the current study only describes the necessary changes; no attempt was made to alter the baseline design to enhance chances of surface survival.

Table 1.-1 lists the key tradeoffs performed during this study and described in detail in this final report.

Figure 1.-1 shows the baseline Probe configuration derived from the study tradeoffs. The Probe basically consists of two major parts, plus separation and radio relay hardware left with the Mariner Mk II Carrier spacecraft after Probe release. The central probe element, the 1 m diameter Descent Module containing all instrumentation and support subsystems, attaches directly to a solid beryllium heat-sink nosecap which provides thermal protection during atmospheric entry. The Probe attaches to the Carrier through three attachment points within the beryllium nosecap. The outer decelerator skirt surrounds the nosecap to provide the necessary low entry ballistic coefficient (high drag area). The skirt uses an ablator entry thermal protection system.

Figure 1.-2 illustrates the mounting of the baseline Probe on the Carrier. Minimum mass and cost result from the nose inward mounting. The fixed decelerator skirt has less risk than a deployable design and fits within the Shuttle envelope.

Figure 1.-3 shows the sequence of events during Probe entry and descent. The Probe first encounters the sensible atmosphere at an altitude of about 700 km. The Probe undergoes supersonic aerodynamic deceleration to an altitude of about 190 km where the velocity drops below sonic speed. At this point, the Descent Module separates from the decelerator skirt by differential drag. As soon as the skirt is clear, a lanyard from the skirt deploys a parachute from the rear of the Descent Module. After this, the optical heads of certain instruments deploy, the communications link is established with the Carrier spacecraft, and the Probe begins the nominal 3 hour descent to the surface.

The individual sections of this report give mass breakdowns of each Probe subsystem or major element. Table 1.-2 summarizes the Probe mass. As shown, the total of 154.8 KG separated mass is over one third decelerator. Carrier mounted hardware comprise 34.7 Kg with a total mass including contingency of 208.5 Kg. Table 1.-3 further breaks down the descent module mass according to its various subsystems.

The next section of this final report describes the mission analysis performed to determine compliance with the high altitude sampling and descent time requirements. It also describes the selection of Probe/Carrier relay geometry to enable high rate surface imaging and defines some of the considerations of surface survival.

Section 3 describes the derivation of a baseline decelerator design. Entry thermodynamics analysis determines the decelerator materials and thickness and aerodynamic stability constrains the shape. For purposes of this study, the parachute is included in the decelerator section.

Section 4 derives the baseline Descent Module design. Tradeoffs result in an integrated descent module/decelerator nose with aft separation of the skirt by differential drag. Some subsystems retain Galileo technology. The most significant advancement from previous probe technology is the Command/Data subsystem reflecting the much higher data rate and increased emphasis on redundancy.

Section 5 describes the elements of the Probe System left on the Carrier after separation. These include the separaration hardware, a simple three spring simultaneous spin/eject mechanism, and the radio relay hardware, a BPSK receiver and antenna.

Finally, section 6 summarizes the study results.

The following individuals are responsible for the preparation of this final report. We also acknowledge the study contributions of our subsystem specialists, of our subcontractor, general Electric Re-entry Systems Organization, under the management of Dwight Florence, and of the NASA contract monitor for this study, Byron L. Swenson of NASA Ames Research Center, Moffett Field, CA. Finally, we acknowledge the support of our secretary, Donna Williams, who typed and assembled this report.

Doug Bernard	John McCarthy
Todd Citron	Robert Soderblom
Bob Drean	Dave Steffy
Scott Lewis	Tina Vargas
Martin Lo	Marty Wolff

TABLE 1.-1 KEY STUDY TRADES

MISSION:	• ENTRY PATH ANGLE
	• CARRIER PERIAPSIS ALTITUDE
	• CARRIER PHASING
	• STAGING SEQUENCE
	• SURFACE SURVIVAL
CONFIGURATION:	• DECELERATOR DIAMETER AND MATERIAL
	• FIXED VS. DEPLOYABLE DECELERATOR
	• DESCENT MODULE SHELF DIAMETER
	• PROBE SEPARATION/CARRIER ATTACHMENT
COMMUNICATIONS:	• MODULATION
	• TRANSMIT ANTENNA SIZE
	• RECEIVE ANTENNA SIZE
	• RECEIVE ANTENNA POINTING
	• RADIO SCIENCE
COMMAND/DATA:	• REDUNDANCY
POWER:	• BATTERY TYPE

TABLE 1.-2 TITAN PROBE SUMMARY MASS STATEMENT

DESCENT MODULE	102.8
DECELERATOR NOSE	10.0
SKIRT	42.0
SEPARATED MASS TOTAL	154.8
RECEIVERS	17.0
ANTENNA	1.7
COAX	0.2
PPIU	3.5
ADAPTER STRUCTURE	8.3
SEPARATION	3.0
WIRE HARNESS	1.0
CARRIER-MOUNTED HARDWARE	34.7
SUBTOTAL	189.5
CONTINGENCY (10%)	19.0
TOTAL MASS	208.5

TABLE 1.-3 TITAN PROBE DESCENT MODULE MASS BREAKDOWN BY SUBSYSTEM

DESCENT MODULE SUBSYSTEMS	(kg)
COMMUNICATIONS	5.8
DATA HANDLING/COMMAND	11.0
POWER	14.8
STRUCTURE	19.3
WIRE HARNESS	8.2
THERMAL CONTROL	11.0
SCIENCE	27.3
SEPARATION	0.9
PARACHUTE	4.5
TOTAL MASS	102.8

FIGURE 1.-1

PROBE CONFIGURATION OVERVIEW

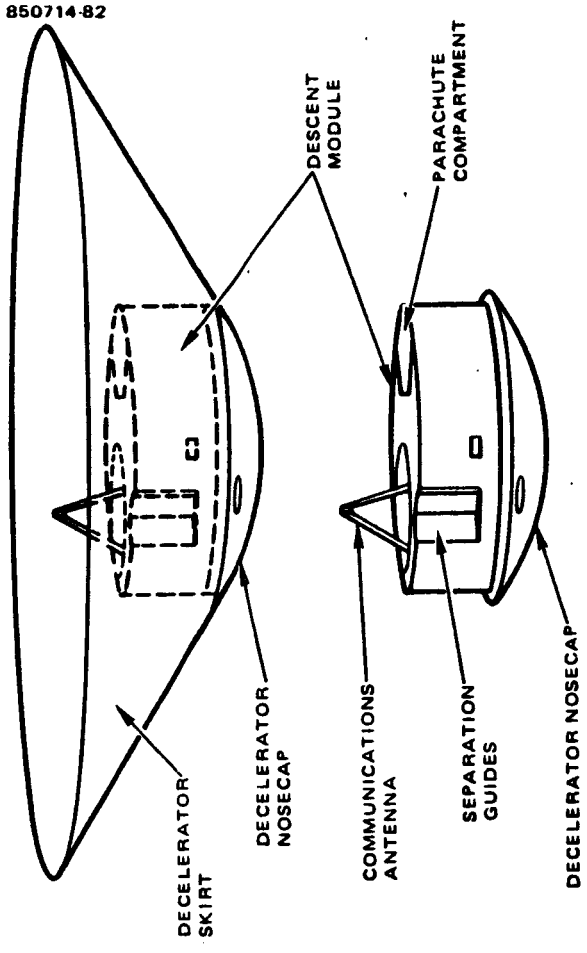

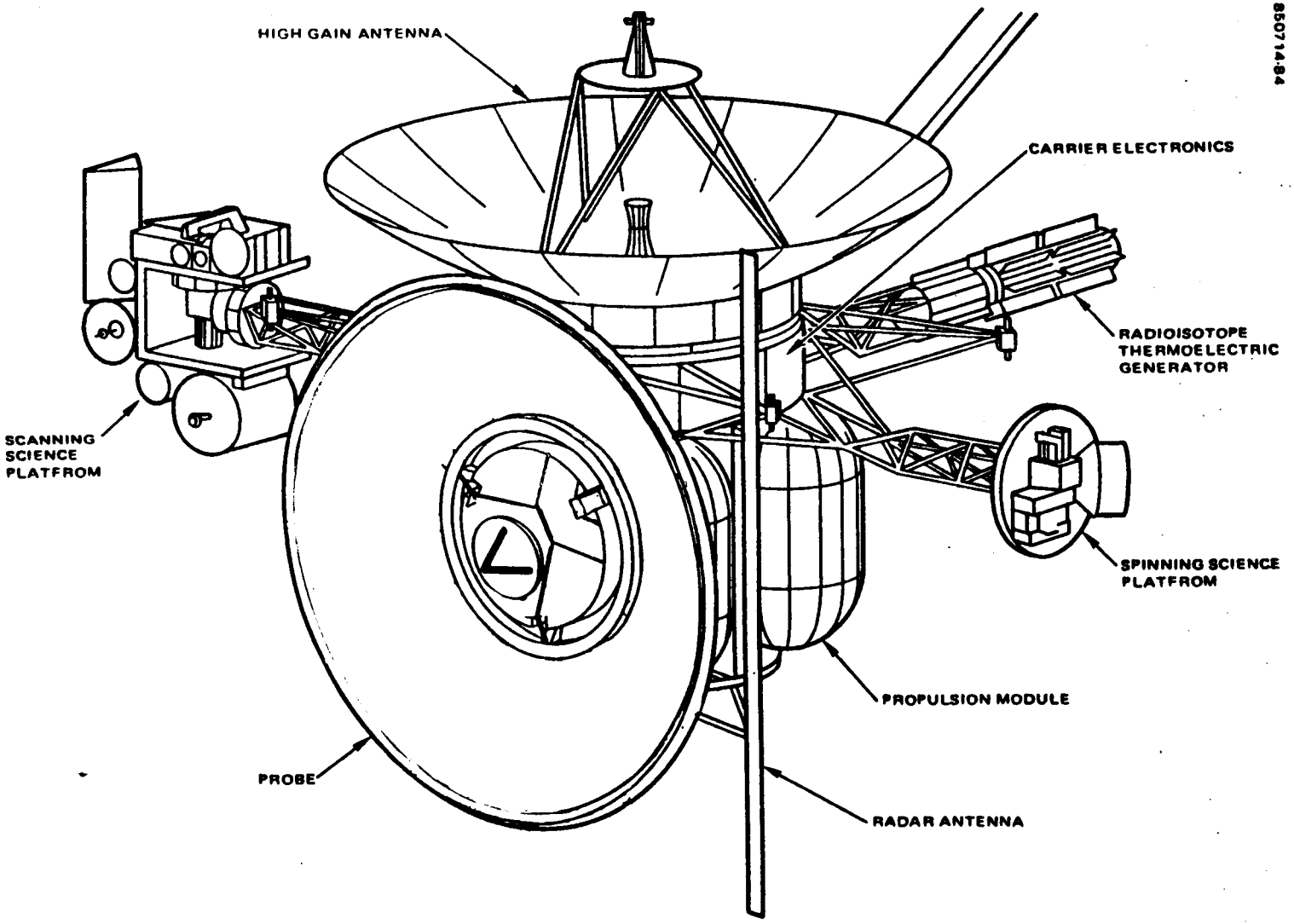

FIGURE 1.-2 PROBE INTEGRATION WITH MARINER MK II CARRIER

FIGURE 1-3 TITAN PROBE ENTRY SEQUENCE

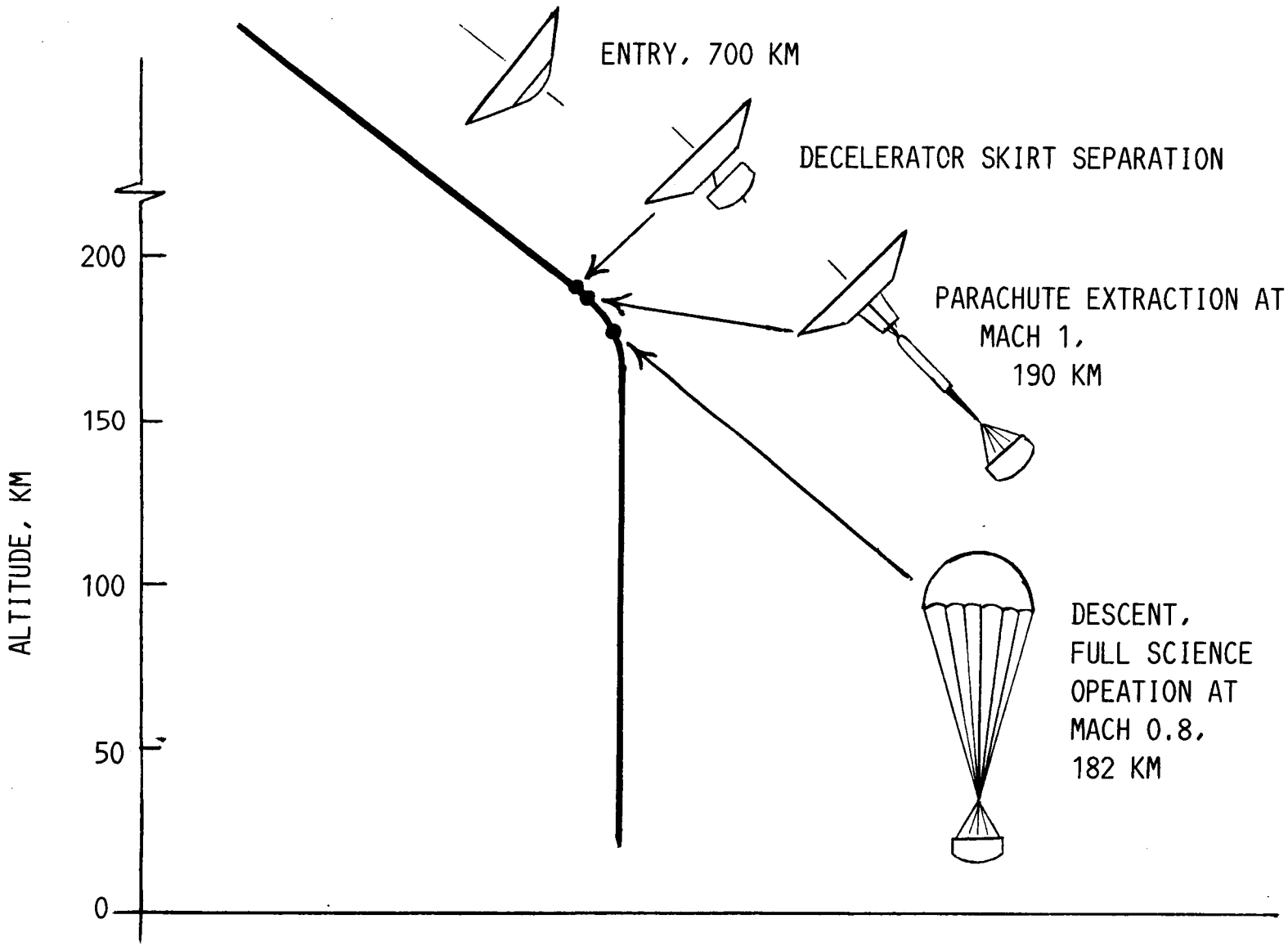

2. MISSION ANALYSIS

Table 2.-1 lists the major assumptions made in performing the mission tradeoffs described in the following sections. The approach velocity of 6.5 km/sec assumes the Carrier is in orbit about Saturn prior to probe release. There is considerable flexibility in Probe targeting and Carrier flyby geometry. Figures 2.-1 and -2 show the overall Probe/Carrier geometry for a set of representative conditions. Tradeoffs have demonstrated small sensitivity to these characteristics. Two model atmospheres were used for this analysis, a model by Hunten, 1982 and a model by Lindal, 1983. The Hunten model atmosphere was imposed as an upper density bound. Figure 2.-3 shows the slight offset for the Lindal model.

It should be noted that for this preliminary analysis, the effects of the small rotation of Titan (approximately 1 deg/hr) were neglected for simplicity. This assumption was made because the precise azimuth of the entry trajectory relative to the pole of Titan is a function of the mission opportunity, the orbit inclination about Saturn, and other Saturn orbit mission characteristics which have not been chosen as yet. The final entry trajectory will have to be appropriately biased to account for this rotation, but for the purposes of this preliminary analysis of Titan probe characteristics, this assumption is sufficiently accurate. Finally, note that no atmospheric winds were considered in the bulk of the present analysis. This assumption was made because at the start of the study, a wind profile for the circulation of the Titan atmosphere had not been defined. Subsequently, a rather strong zonal wind pattern was defined based upon the modelling of Flasar, 1981. The rather substantial effects of that wind profile on the communications link are discussed in Section 2.4.

TABLE 2.-1 MISSION ANALYSIS ASSUMPTIONS

- APPROACH VELOCITY 6.5 KM/SEC (V_∞)
- ENTRY ALTITUDE 700 KM
- TITAN PHYSICAL PARAMETERS

RADIUS	2570 KM
μ	8978.1 KM^3/SEC
ROTATION	IGNORED FOR BASELINE DESIGN

- PROBE CHARACTERISTICS

DESCENT MODULE MASS	105.4 KG
DECELERATOR MASS	35.0 KG
DECELERATOR DIAMETER	2.97 M
ENTRY CONFIGURATION	60.0 DEG BLUNT CONE
ENTRY BALLISTIC COEF.	12.91 KG/M^2 (MACH 5)

- HUNTEN TITAN ATMOSPHERE MODEL, NO WIND
- MASS LOSS DUE TO ABLATION IS NEGLIGIBLE

FIGURE 2.- 1 CARRIER POSITIONING FOR
COMMUNICATIONS RELAY

- 3 HOUR COMMUNICATIONS TIME
- 1000 KM PERIAPSIS ALTITUDE
- 30 MINUTE PHASING

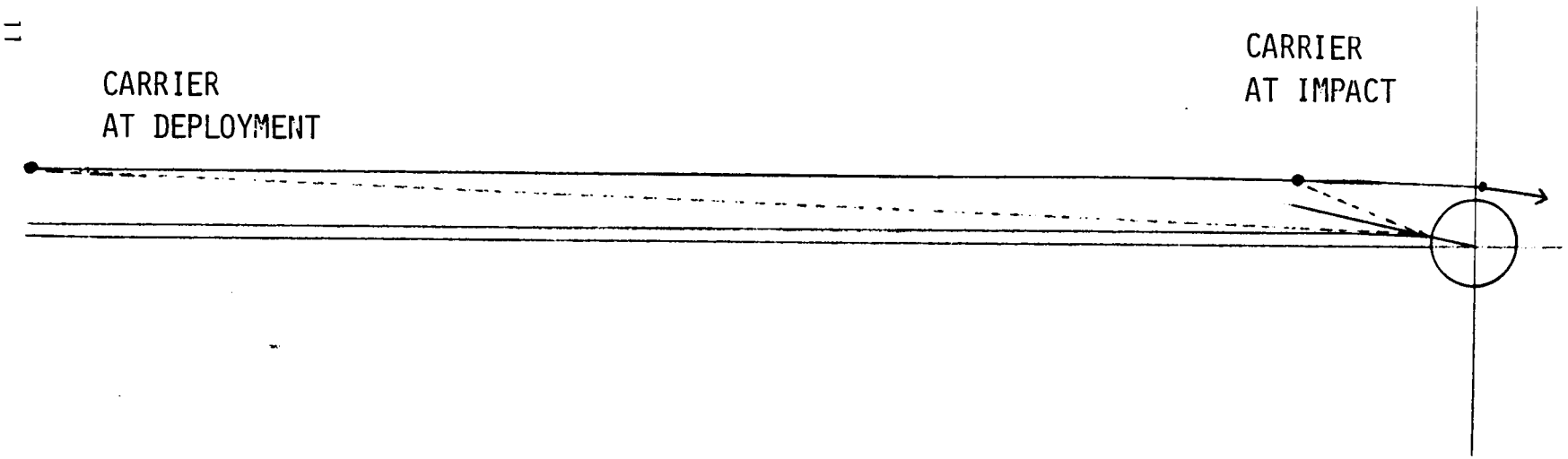

FIGURE 2.-2 REPRESENTATIVE MISSION DESIGN

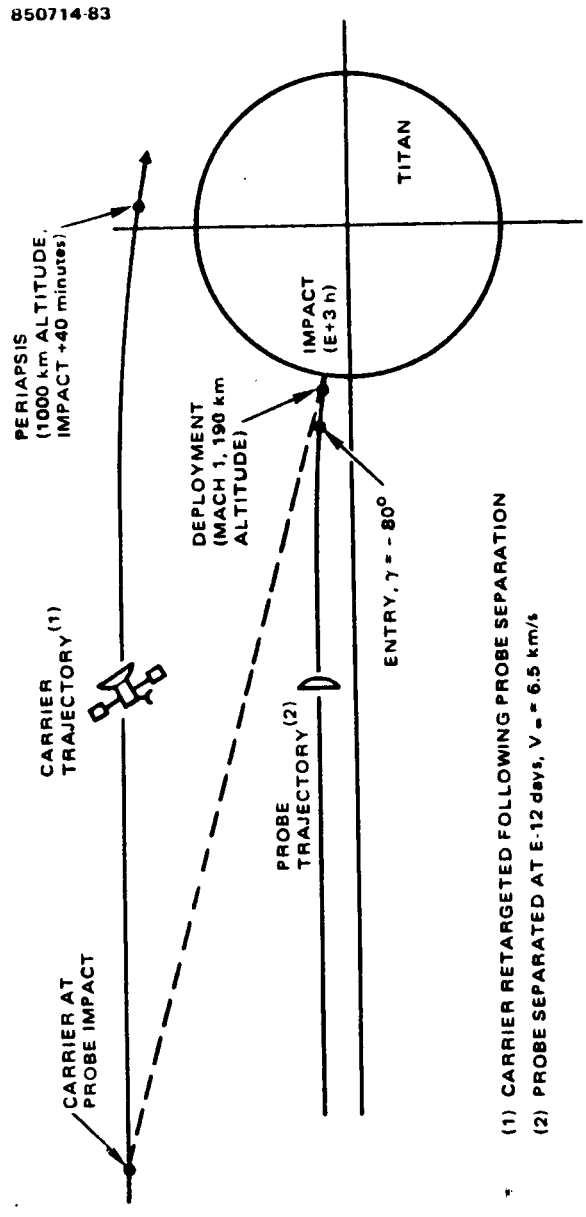

FIGURE 2.-3 COMPARISON OF TITAN MODEL ATMOSPHERES

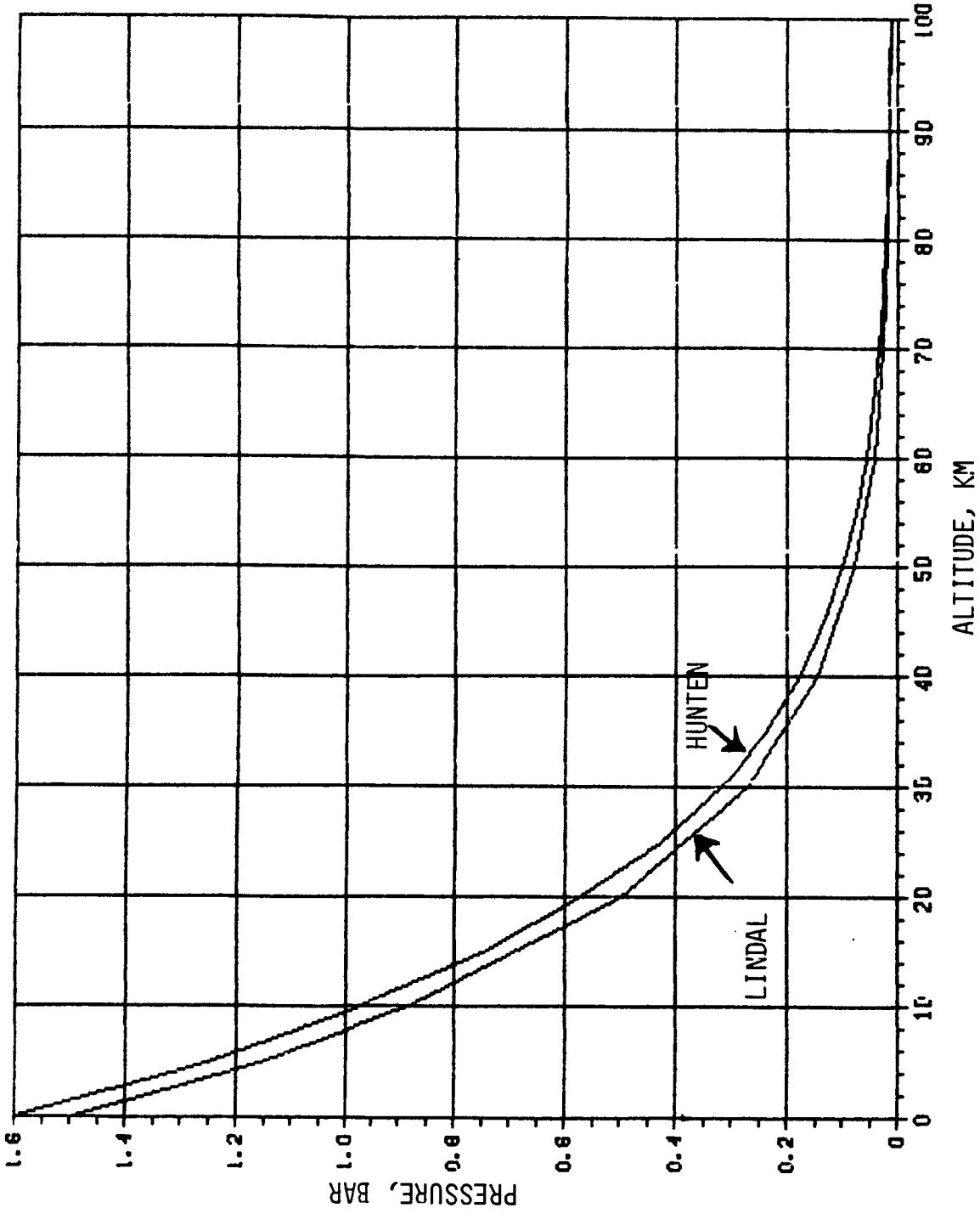

2.1 Carrier Deflection/Coast

The Probe design is relatively insensitive to the time of separation compared to entry. The coast timer imposes a very small battery drain and its stability is not a critical factor since the Probe sequence resets based on direct measurement of entry by acceleration switches. The separation time does have an effect on the Carrier since the Carrier retargeting maneuver (to position the Carrier for flyby and communications relay) is larger for later separation, (see figure 2.1-1). Separation can not be too early, however, as there must be time for orbit determination after the final Carrier orbit correction maneuver at about E-20 days. The figure shows a modest penalty for delaying the Carrier an additional 20 to 40 minutes over the nominal 3 hour delay. Carrier phasing is defined in section 2.4

Probe entry angle is not critically sensitive to Carrier orbit determination. Figure 2.1-2 shows a target plane error of 100 KM results in less than 2^{o} path angle error for steep entry.

FIGURE 2.1-1 CARRIER DEFLECTION REQUIREMENT

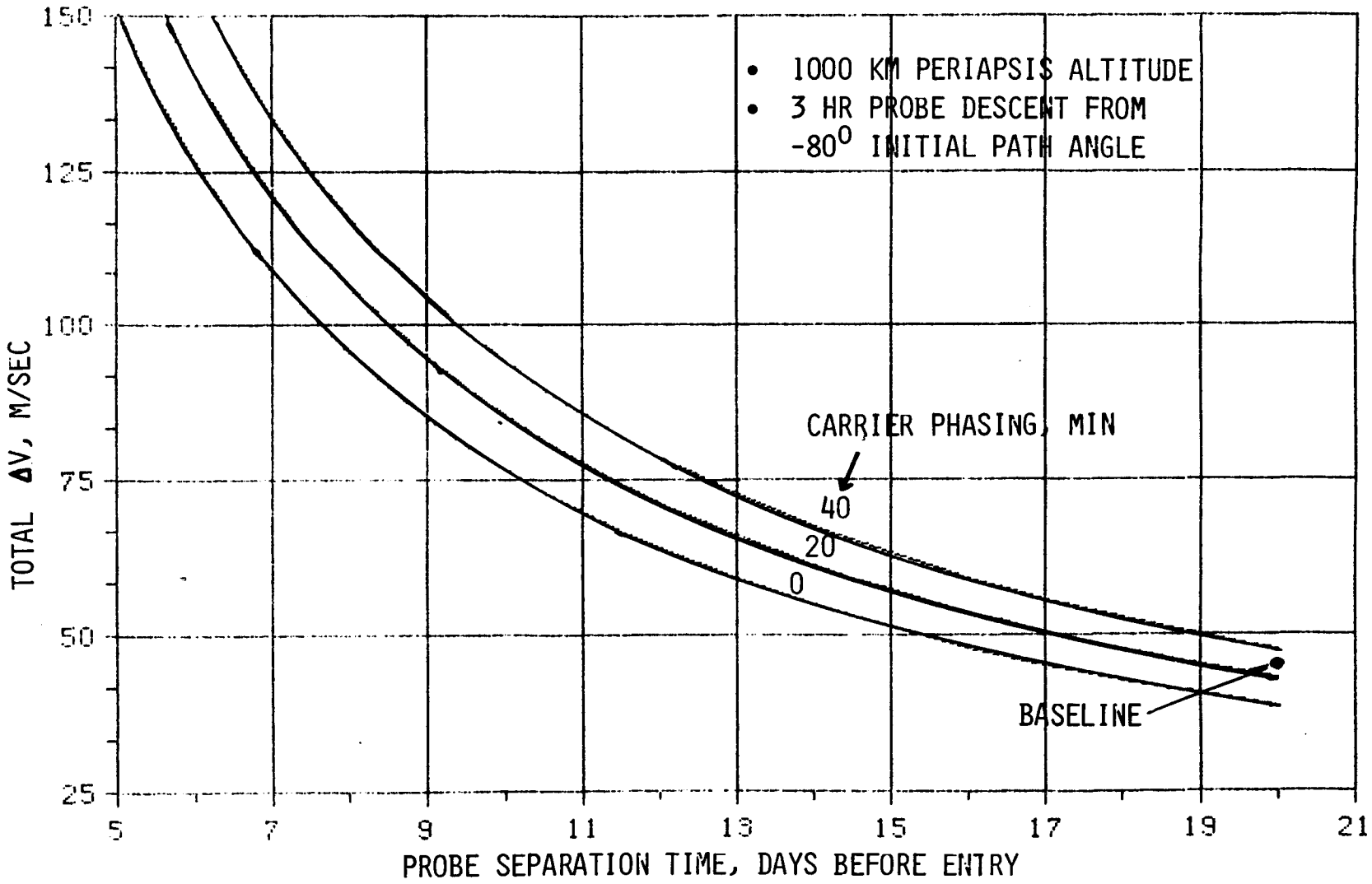

FIGURE 2.1-2 ENTRY PATH ANGLE SENSITIVITY TO TARGETING ERROR

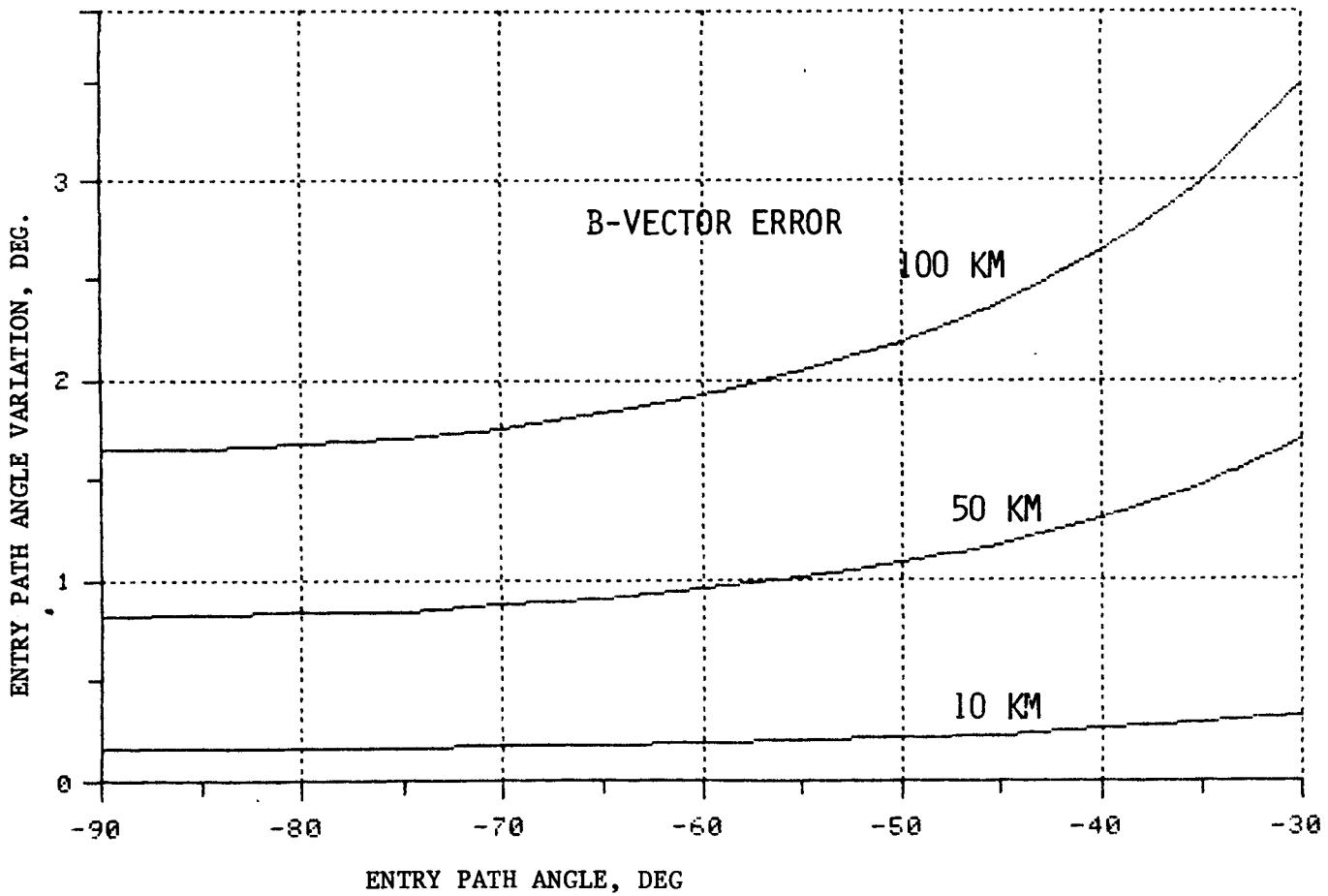

2.2 Entry

Although steep entry path angles impose a greater deceleration load than shallow entry path angles, figure 2.2-1 indicates that the worst case deceleration load at a -90^{o} path angle of 20 g_E is still very benign and comparable to the launch load environment. Figures 2.2-2 and -3 show the time variation of several key trajectory parameters during entry for entry angles of -40^{o} and -90^{o}, respectively.

The entry path angle also has an influence upon the altitude where subsonic speeds are reached. Figure 2.2-4 shows that the baseline probe design with a ballistic coefficient of 14.49 Kg/m^2 a Mach number of unity at 190 KM. It is not easy to increase the altitude. As shown, a 10% larger probe diameter (as could be realized through a complex deployment) only adds an additional 10 KM to the sonic altitude. Shallow path angles offer somewhat greater performance. At a practical communication limit (i.e. 70^{o} probe aspect angle) the resultant -35^{o} entry path angle adds 35 KM to the sonic altitude.

FIG. 2.2-1 ENTRY LOAD VARIATION WITH PATH ANGLE

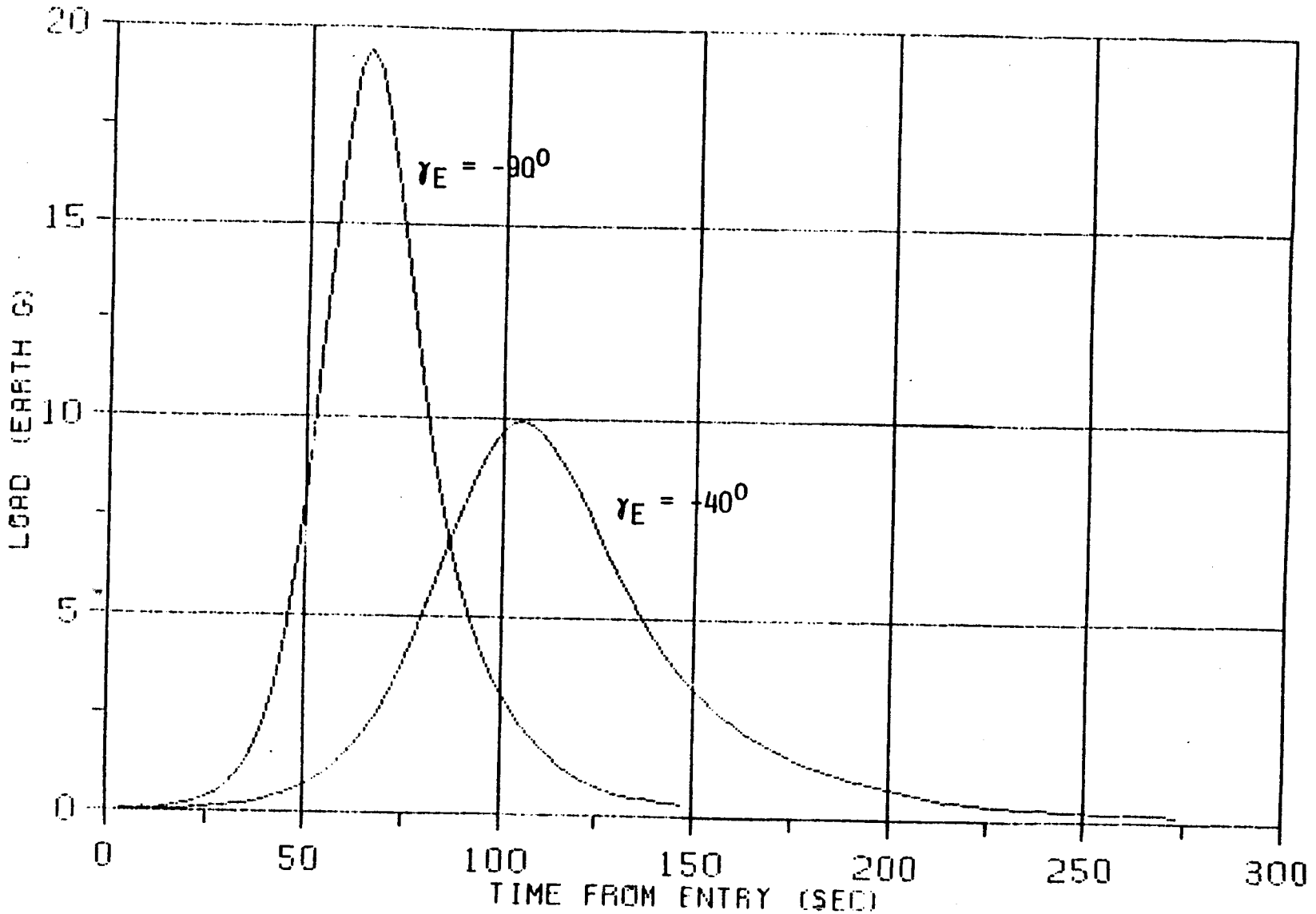

FIGURE 2.2-2
TITAN PROBE ENTRY PARAMETERS
PATH ANGLE -40°, BALLISTIC COEFFICIENT 12.9 KG/M²

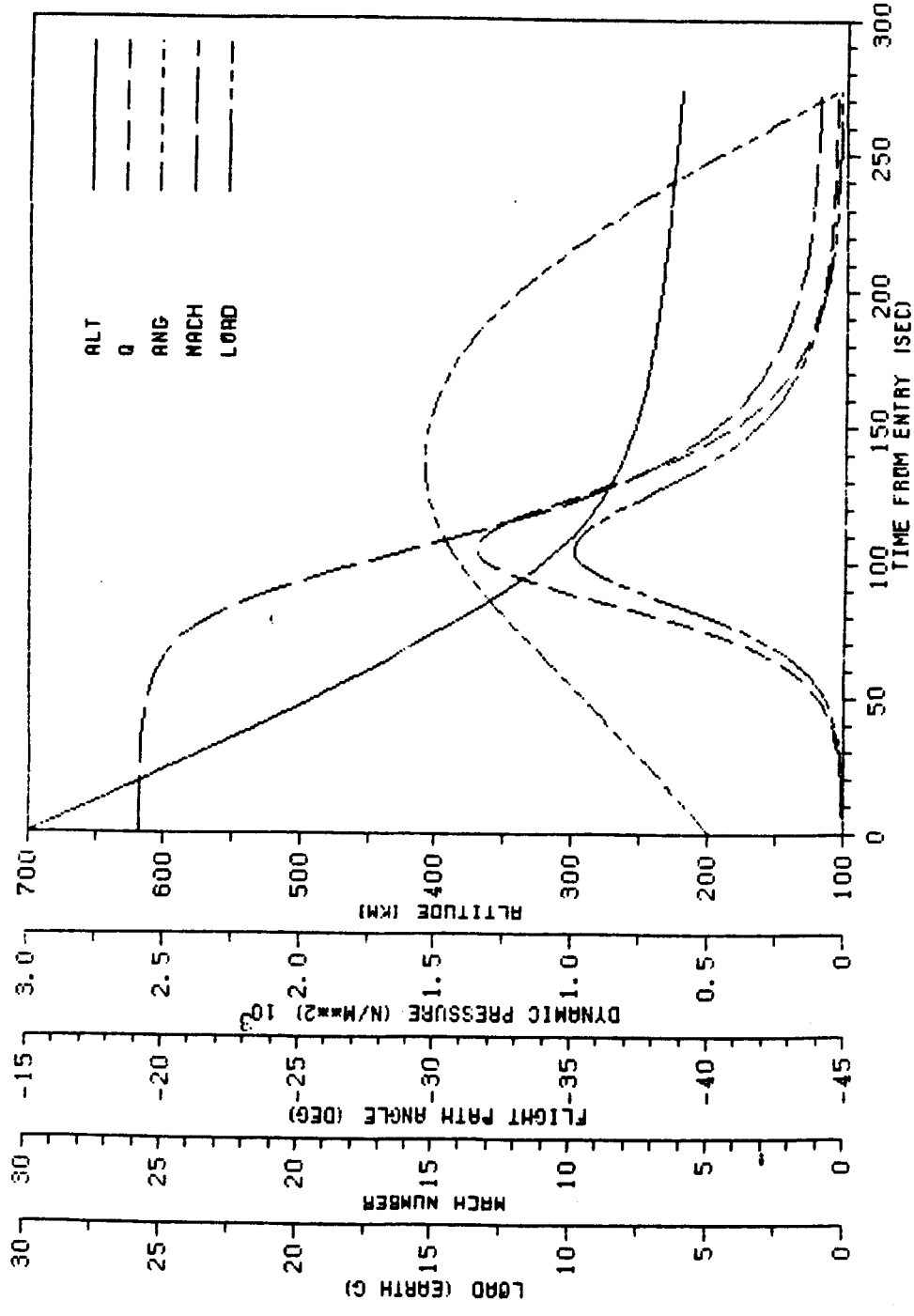

FIGURE 2.2-3
TITAN PROBE ENTRY PARAMETERS
PATH ANGLE -90°, BALLISTIC COEFFICIENT 12.9 KG/M²

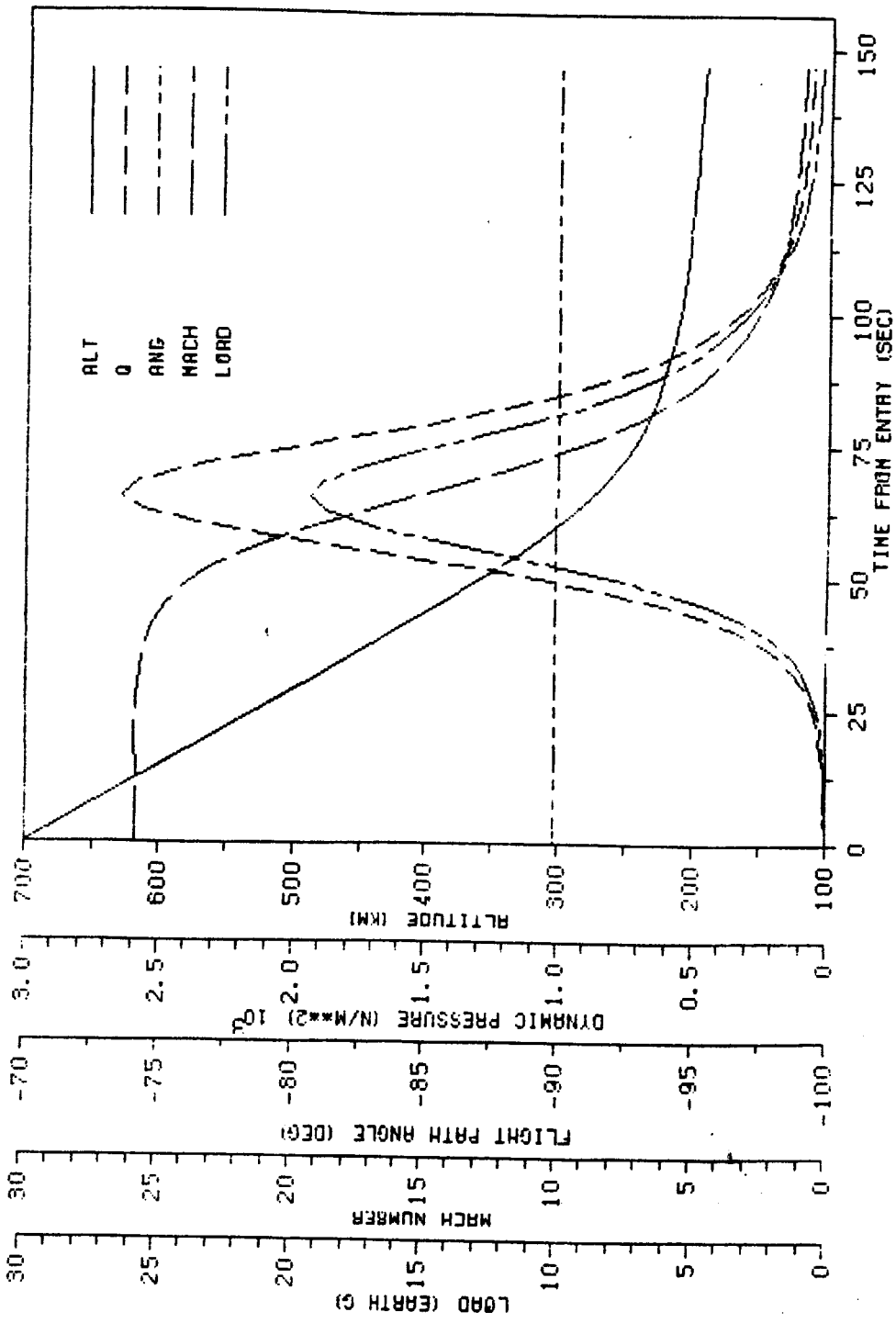

Figure 2.2-4 Altitude at Mach 1 Variation with Entry Path Angle and Ballistic Coefficient

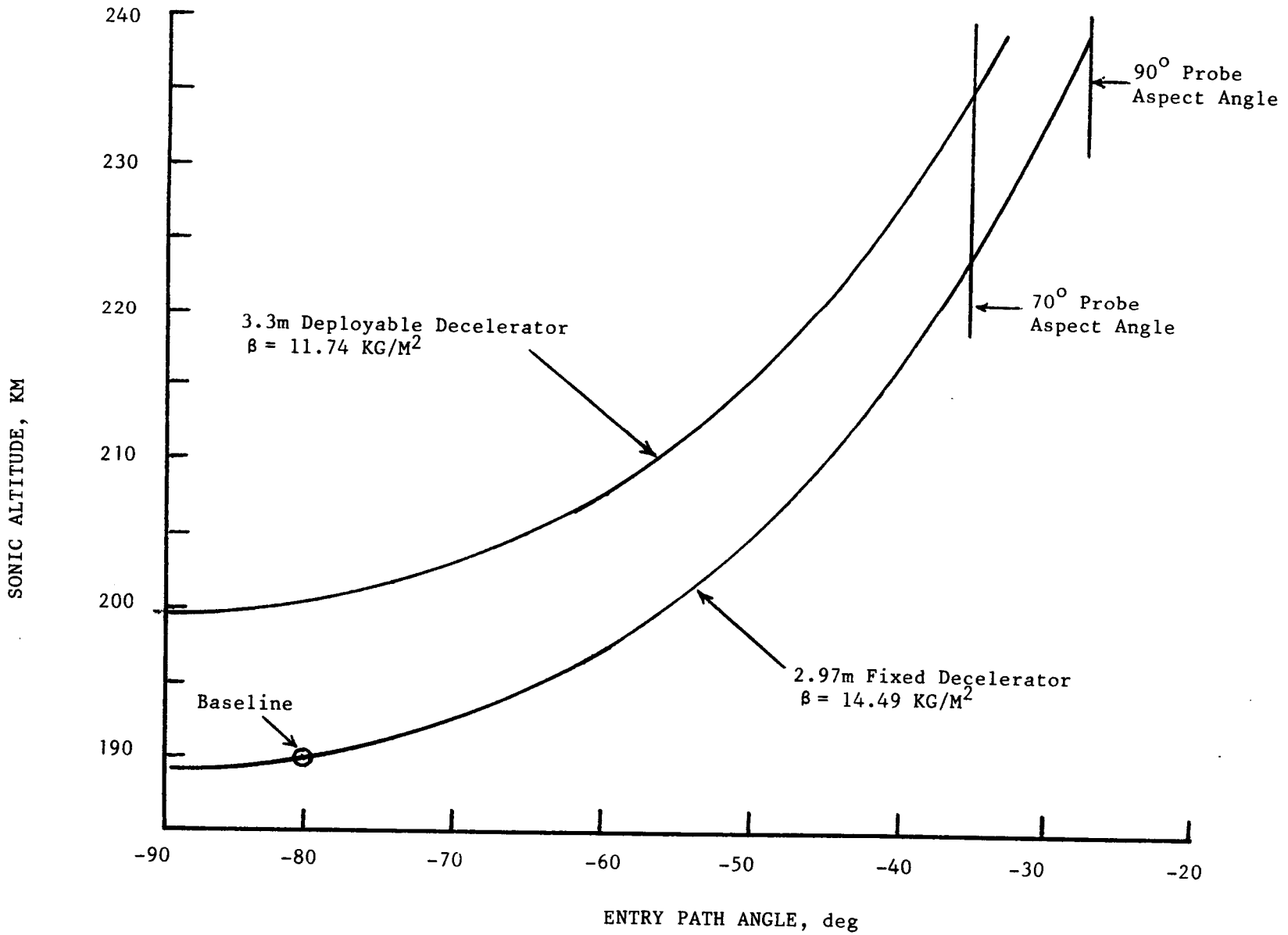

2.3 Descent

The diameter of the parachute is the principal parameter to adjust the descent time from parachute deployment to impact. Figure 2.3-1 shows that a 3.13 M diameter parachute gives the desired nominal 3 hour descent. Figure 2.3-2 shows the corresponding descent velocity profiles. Small parachutes (e.g. 2m diameter), result in an initial speed-up since they have less drag than the decelerator. The descent time can not be exactly controlled due to various uncertainties. The total uncertainty is important to the relay communication analysis as described in the next section. Table 2.3-1 shows how errors combine to a $\pm$8.1% RSS or a sum of $\pm$13.3%.

TABLE 2.3-1 DESCENT TIME UNCERTAINTY

ERROR SOURCE	DESCENT TIME VARIATION	
MODEL ATMOSPHERE (LINDAL VS. HUNTEN)	-5.7%	
PARACHUTE DRAG (±10%)	±5.3%	
SURFACE FEATURES (±1 KM)	±2.3%	
TOTAL RSS	8.1%	(± 15 MIN FOR 3 HOUR DESCENT)
TOTAL SUM	13.3%	(± 24 MIN FOR 3 HOUR DESCENT)

FIGURE 2.3-1 DESCENT PROFILE VARIATION WITH PARACHUTE DIAMETER

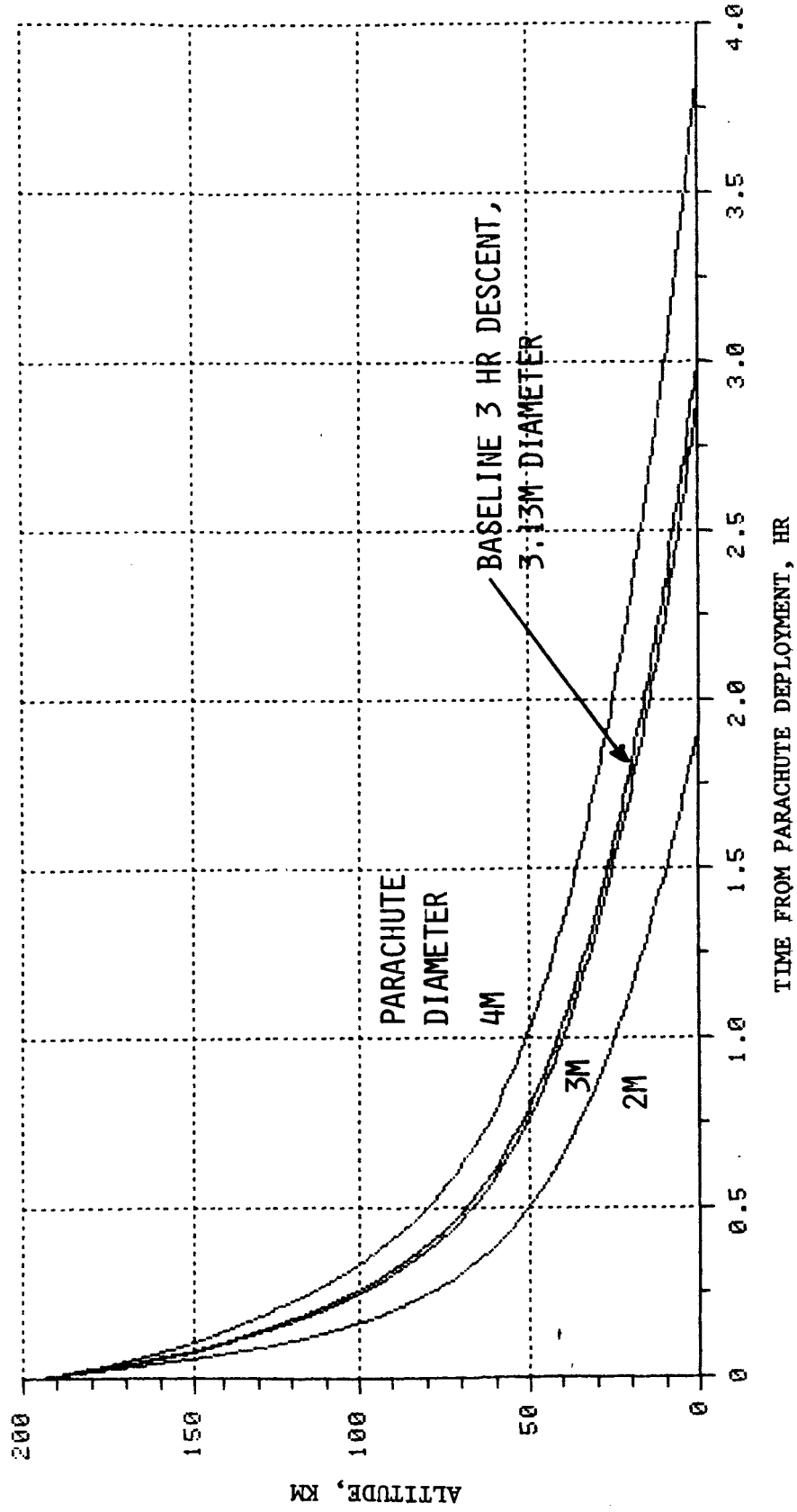

FIGURE 2.3-2 DESCENT VELOCITY DEPENDENCE ON PARACHUTE DIAMETER

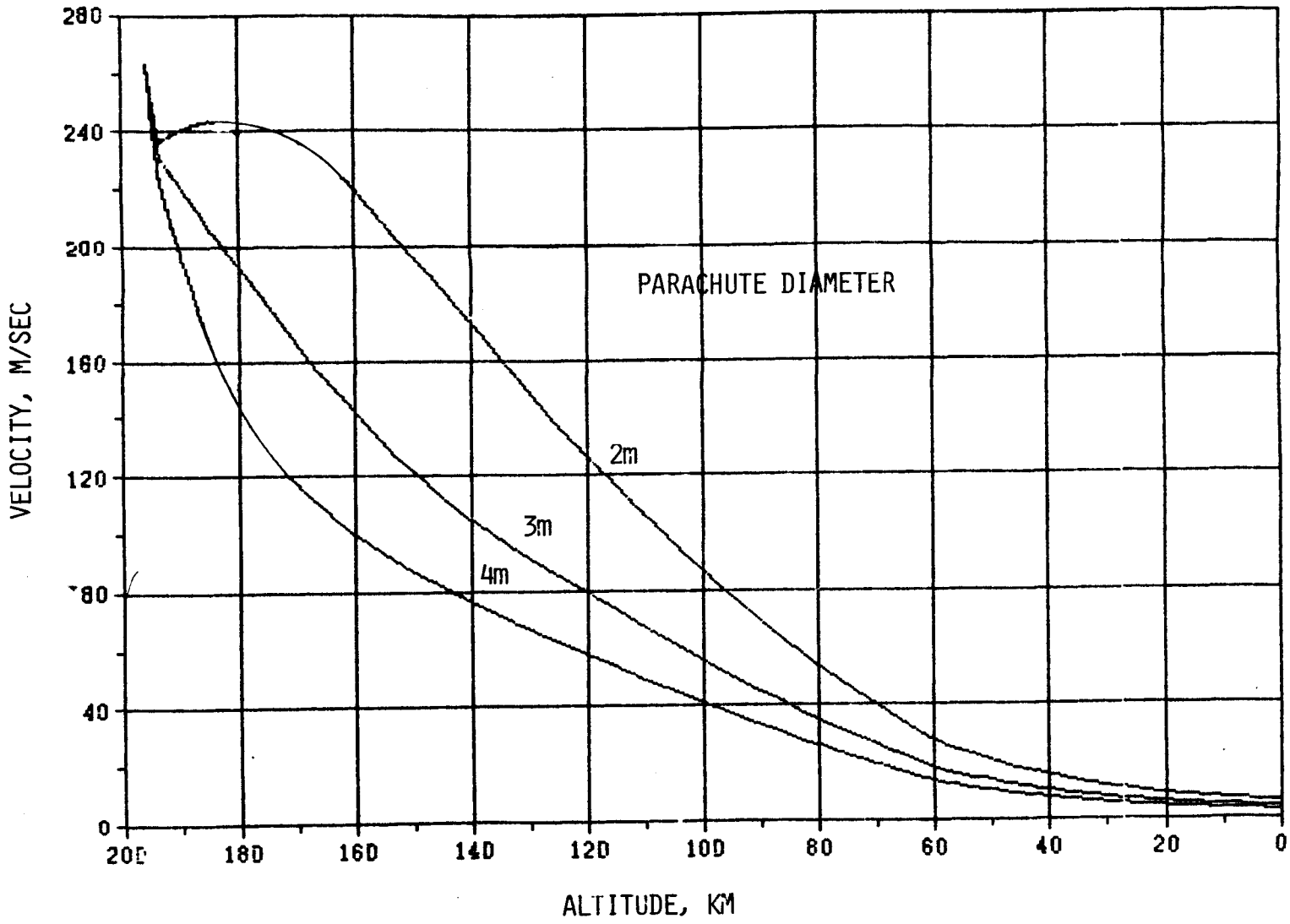

2.4 Relay Communications

Probe communication to the Carrier has two basic phases. The initial phase is characterized by a low rate of 100 bps to support basic atmospheric structure and composition measurements. This phase does not critically size the link. The second phase requires a much higher rate of 10,000 bps to satisfy surface imaging. The mission parameters affecting the link include the Probe entry trajectory and the Carrier flyby trajectory (i.e. periapsis altitude and phasing) which in turn determine Probe aspect angle, Carrier aspect angle, and doppler frequency shift and rate. Hardware variables including transmitter power, probe antenna size, receive antenna size and pointing mechanization, and modulation type combine with the mission parameters to determine link margin, E_b/N_o as shown schematically in figure 2.4-1.

Figure 2.4-3 defines the communications aspect angles. Since the exact mission date is not yet defined, the Carrier attitude (Earth oriented) is not known. Therefore, Carrier aspect angles refer to the direction of approach velocity.

Figure 2.4-4 further defines the Carrier communications angles. The key performance factor depends on the offset of the receive antenna boresight (look angle) and Probe line of sight (Carrier aspect angle). This offset (communications angle) is nominally zero (with a 2^o pointing error) if the receive antenna is mechanized to track the probe.

For purposes of this analysis, the mission parameters given in Table 2.-1 will be assumed together with the following constraints

2.5W transmitter power
S-band frequency (2295 MHz)
10,000 bps

Figure 2.4-5 depicts the time variation of Probe aspect angle during descent for several entry angles. As shown this angle begins at a nominal value which is offset most from local vertical, for shallow path angles. As the Carrier flies overhead, this angle quickly goes through zero and then exceeds a value of 90^o as the Carrier passes over the local horizon. By arranging for Probe impact some 30 minutes or more before Carrier periapsis, the Probe antenna beamwidth depends only on the entry path angle. Since entry path angle may be selected independently of any communications performance considerations, two representative entry conditions and associated Probe antenna beamwidths have been studied as indicated in Table 2.4-1.

The first constraint imposed on the communications relay is that all lines of sight fall within antenna 4 dB cutoff points. Table 2.4-2 summarizes the key characteristics of all considered Probe and Carrier antennas. Figure 2.4-6 shows the effect of the cutoff for the two representative missions and as a function of Carrier periapsis attitude. The lower limit periapsis altitude 1000 km is selected since it allows the latest communications before cutoff.

A second constraint involves doppler shift or rate, the exact limit depending on the modulation technique (see section 5.3). For a BPSK receiver, the

doppler rate must be less than 2 Hz/sec (2nd order tracking loop) and 110 Hz/sec (3rd order loop). As shown in figure 2.4-7, this also requires targeting such that the Probe impact is at least 30 minutes before Carrier periapsis. An FSK receiver is sensitive to doppler shift. Figure 2.4-8 shows that a typical 5 kHz filter also is consistent with about 30 minutes of phasing.

A third constraint comes from the receive antenna geometry if the antenna is not free to track the predicted Probe location. If the receive antenna is positioned for no nominal offset at the start of Probe descent, the 4 dB cutoff requires a minimum phasing limit of 30 to 45 minutes as shown in figure 2.4-9.

Table 2.4-3 summarizes the phasing constraints resulting from the above considerations. As shown, the baseline design (i.e. steep probe entry, BPSK 2nd order loop receiver, and a pointed receive antenna) requires a minimum phasing of 40 minutes.

The final measure of performance is the link margin which varies with range and communications angles. Figure 2.4-10 shows for the shallow entry case (i.e. case 1) a short time where 10,000 bps can be supported. Figure 2.4-11 shows the much longer high rate communications time is available for the steep entry case.

This characteristic time provides a bench mark to compare the various factors in the communications tradeoff. Table 2.4-4 shows the maximum time where 10,000 bps can be supported (considering all the constraints and link margin) as a function of Probe entry angle and antenna diameter (Case 1 and 2), pointed or fixed Carrier antenna, Carrier antenna size, and Probe communications modulation technique. As noted the minimum desired time is 70 minutes to account for timing uncertainty (see section 2.3) and a minimum 10 KM descent at 10,000 bps. The 145 minutes provided by the baseline design has ample margin. This margin is required to account for uncertainties in the wind environment (see next section).

Wind Effects

After completion of the preceding mission analysis a wind model has been suggested which significantly alters the quantitative results, but does not significantly alter any conclusions. To ensure the fundamental validity of the analyses, a brief examination was made of the impact of the wind model. Figure 2.4-12 shows the wind velocities experienced by the Probe as a function of time for the 3 hour descent. For this preliminary study, an analysis has been made of the effect of the Probe horizontal motion due to this wind on the Probe position and the increased Probe communication angle due to the rotation of Titan about its axis. The modeling did not include any attitude offset due to wind shear. Figure 2.4-13 shows the Probe longitude rotation due to the wind. The contribution of Titan rotation is also shown. The wind model results in a 296 KM shift of probe impact site compared to no wind. This motion results in change in the communication angle profile as shown in figures 2.4-14 through -16. The Probe aspect angle exceeds the $\pm 11.40^{o}$ cutoff of the previous baseline thereby requiring a broader Probe antenna beamwidth. As shown a $\pm 13.7^{o}$ cutoff matches the new geometry. Table 2.4-5 lists the appropriate Probe antenna characteristics.

Figure 2.4-17 shows the effect the broader Probe antenna has if there is no wind. The time where the link margin exceeds the 4.8 dB BPSK threshold decreases from 145 minutes to 125 minutes. Figure 2.4-18 shows the performance with wind. Whereas the previous Probe antenna would have a significant data outage where the communications angle exceeds the 4 dB cutoff, the new antenna would support the 100 bps and 10,000 bps phases with the later high rate phase allowed for 87 minutes.

In the first analysis, Titan rotation is ignored. Now, coupled with the wind, the rotation must be considered. Table 2.4-6 lists the various performance factors. With rotation, the high rate time becomes 75 minutes, just meeting the 70 minute target time (fig. 2.4-19).

TABLE 2.4-1 TWO EXAMPLE CASES COMPARE
SHALLOW AND STEEP ENTRY

CASE 1

$\gamma_E = -60^o$

$\pm 28^o$ PROBE ANTENNA BEAMWIDTH

CASE 2

$\gamma_E = -80^o$

$\pm 10^o$ PROBE ANTENNA BEAMWIDTH

TABLE 2.4-2 ANTENNA CONSTRAINTS

	DIAMETER, M	PK. GAIN, dB	3 dB Half Beamwidth, deg	4 dB Cutoff Half Beamwidth, deg
PROBE ANTENNA	0.45	18.08	±10.0	±11.4
	0.2	9.6	±28.0	±32.0
CARRIER ANTENNA	0.5	19.0	± 9.2	±10.4
	0.75	22.52	± 6.1	± 7.0
	1.0	25.0	± 4.6	± 5.2

TABLE 2.4-3 SELECTION OF CARRIER PHASING

CONSTRAINT	REQUIRED PHASING T, MIN		
	CASE 1	CASE 2	
PROBE ASPECT ANGLE WITHIN 4 dB CUTOFF	10	30	
CARRIER ASPECT ANGLE WITHIN 4 dB CUTOFF (FIXED RECEIVE ANTENNA)	30	45	
DOPPLER OR DOPPLER RATE WITHIN RECEIVER OPERATING POINT			
2nd ORDER BPSK (2 Hz/sec)	30	[40]	BASELINE DESIGN
3rd ORDER BPSK (110 Hz/sec)	10	0	
FSK (5 KHz FILTER)	20	25	

*LIMITING CONDITION FOR BASELINE (STEEP PROBE ENTRY, BPSK, POINTED RECEIVE ANTENNA)

TABLE 2.4-4 LINK FIGURE OF MERIT IS TOTAL TIME HIGH RATE IS SUPPORTED

		MAXIMUM TIME 10,000 bps CAN BE SUPPORTED, MIN					
RECEIVE ANTENNA MECH.			POINTED			FIXED	
RECEIVE ANTENNA DIA.		1.0m	0.75m	0.5m	1.0m	0.75m	0.5m
CASE 1	3rd ORDER BPSK	70	55	40	45	30	20
	2nd ORDER BPSK	50	35	20	45	30	20
	FSK	30	25	10	10	-	-
CASE 2	3rd ORDER BPSK	205.	155	105	155	130	100
	2nd ORDER BPSK	195.	145*	95	155	130	95
	FSK	110.	80	50	85	70	45

NOTE ±15 MINUTE TIMING UNCERTAINTY AND 40 MINUTE DESCENT TIME FOR LAST 10 KM REQUIRES 70 MIN MINIMUM

*BASELINE, 40 MIN PHASING

TABLE 2.4-5: CHARACTERISTICS OF REVISED PROBE ANTENNA (WHICH ACCOUNTS FOR WIND)

ANTENNA DIAMETER, M	.384
PEAK GAIN, dB	16.71
3 dB BEAMWIDTH, DEG	± 11.9
4 dB BEAMWIDTH, DEG	± 13.7

TABLE 2.4-6 MAXIMUM TIME 10 Kbps CAN BE SUPPORTED

PROBE ANTENNA DIAMETER	TIME WITHOUT WIND, min	TIME WITH WIND, min	TIME WITH WIND AND ROTATION, min
0.45 M	145	-	-
0.384 M	125	87	-
0.34 M	-	-	75

note: MINIMUM TIME REQUIRED TO ENSURE FULL COVERAGE FOR LAST 10 KM = 70 MIN

FIG. 2.4-1 RELAY COMMUNICATIONS VARIABLES

MISSION VARIABLES WHICH CAN BE ADJUSTED TO IMPROVE LINK PERFORMANCE (AT SOME EXPENSE)

- γ = PROBE ENTRY ANGLE
- hp = PERIAPSIS ALTITUDE
- T = TIME OF CARRIER PERIAPSIS WITH RESPECT TO PROBE IMPACT

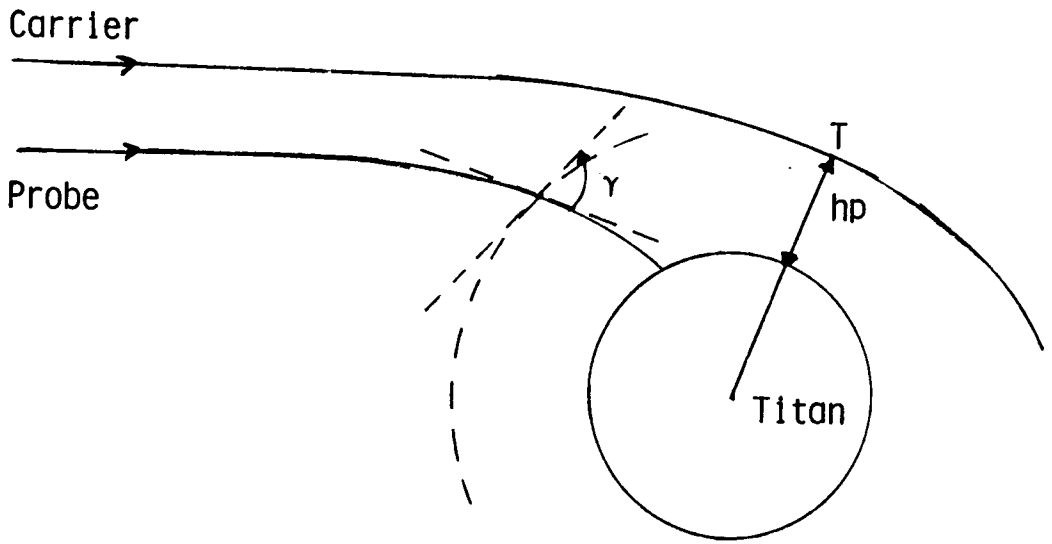

HARDWARE VARIABLES

- TRANSMITTER POWER
- PROBE ANTENNA SIZE
- RECEIVE ANTENNA SIZE AND POINTING MECHANIZATION
- MODULATION TYPE

FIGURE 2.4-2 CARRIER TO PROBE RANGE

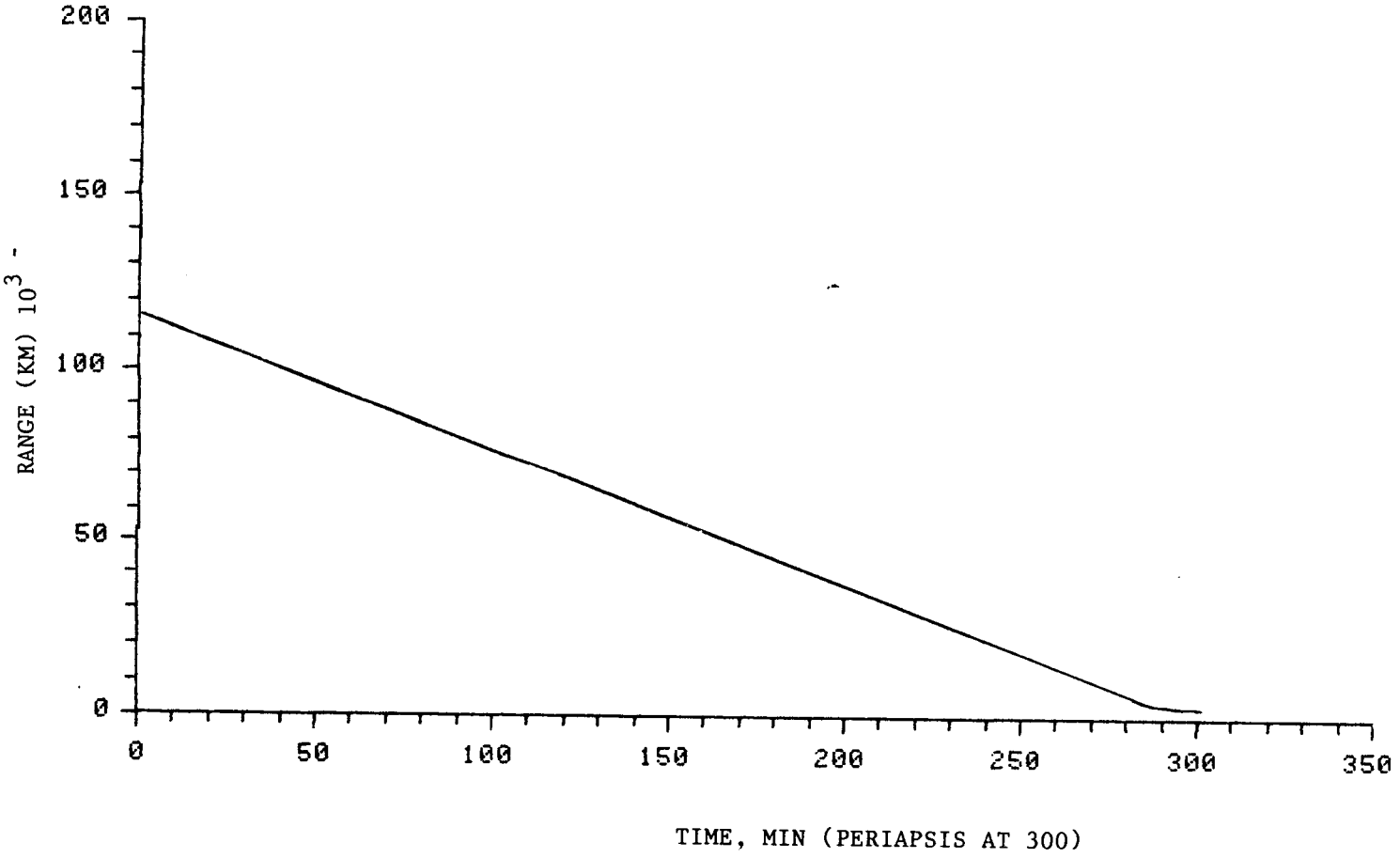

FIG. 2.4-3 COMMUNICATIONS GEOMETRY

- CARRIER ORIENTATION DEPENDS ON EARTH POSITION WHICH DEPENDS ON DATE
- SINCE ENCOUNTER DATE UNKNOWN CARRIER ASPECT ANGLE MEASURED FROM V_{∞}

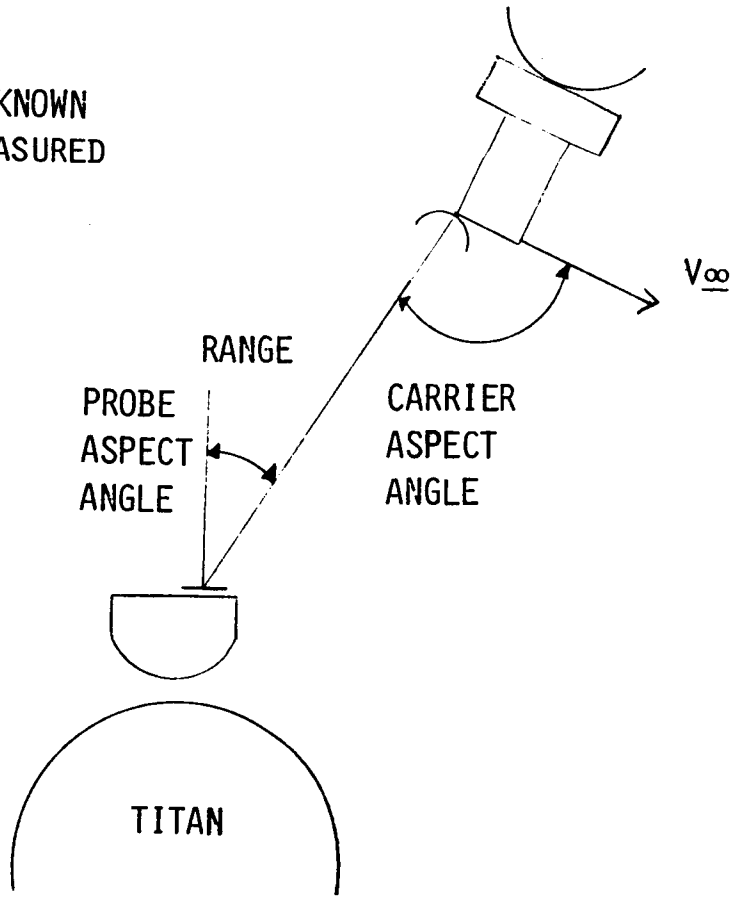

FIG. 2.4-4 RECEIVE ANTENNA COMMUNICATIONS ANGLES

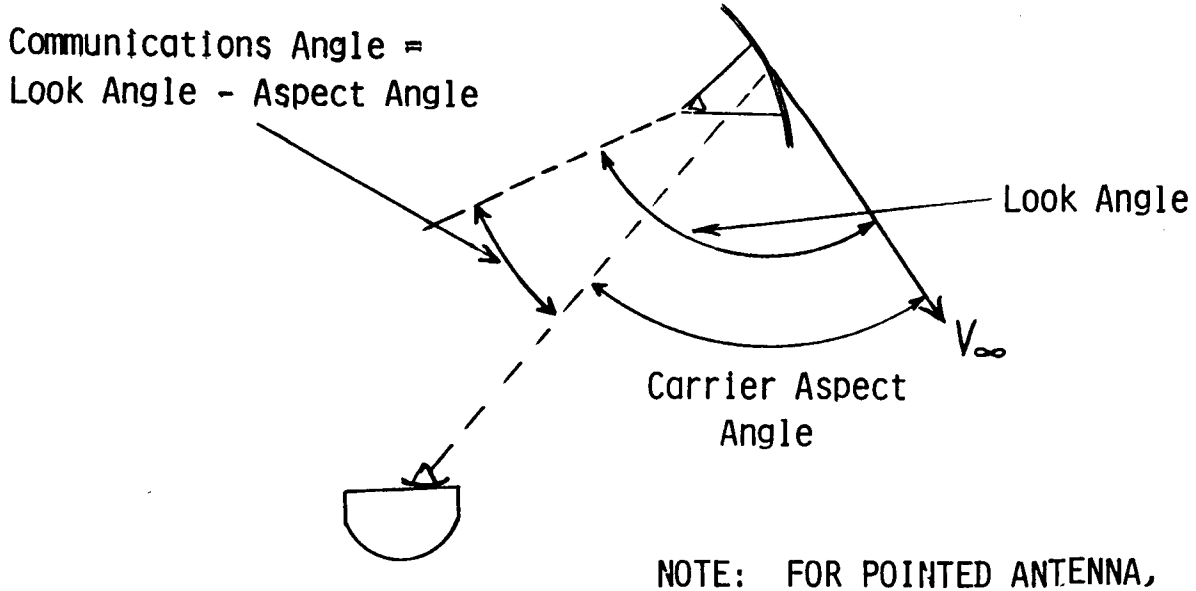

NOTE: FOR POINTED ANTENNA, MECHANISM ASSUMED TO POSITION LOOK ANGLE WITHIN 2^0 OF CARRIER ASPECT ANGLE

FIG. 2.4-5 PROBE ANTENNA BEAMWIDTH
CONSTRAINS ENTRY PATH ANGLE

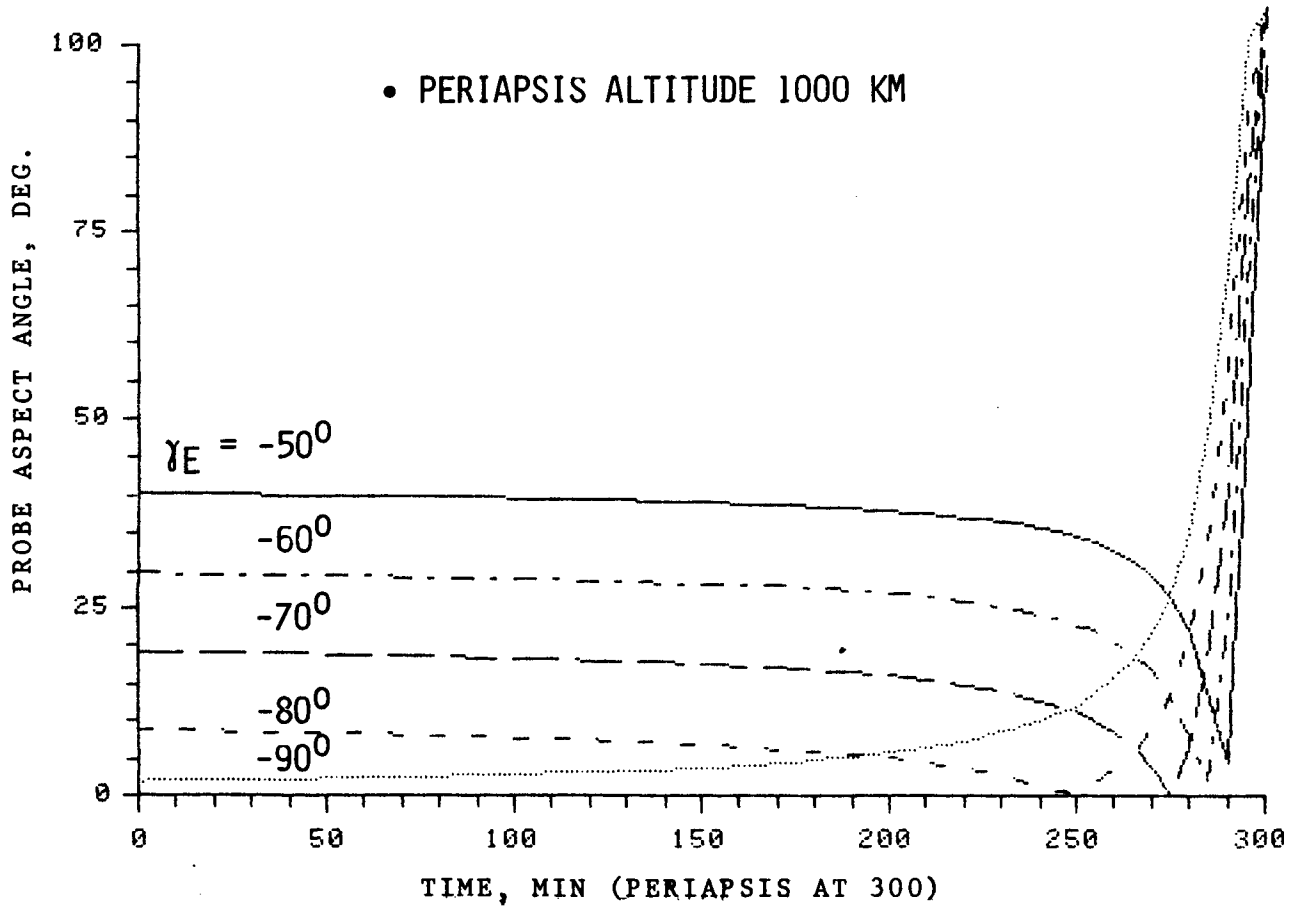

FIG. 2.4-6 LOWER PERIAPSIS ALTITUDE GIVES
LONGER AVAILABLE COMMUNICATIONS TIME

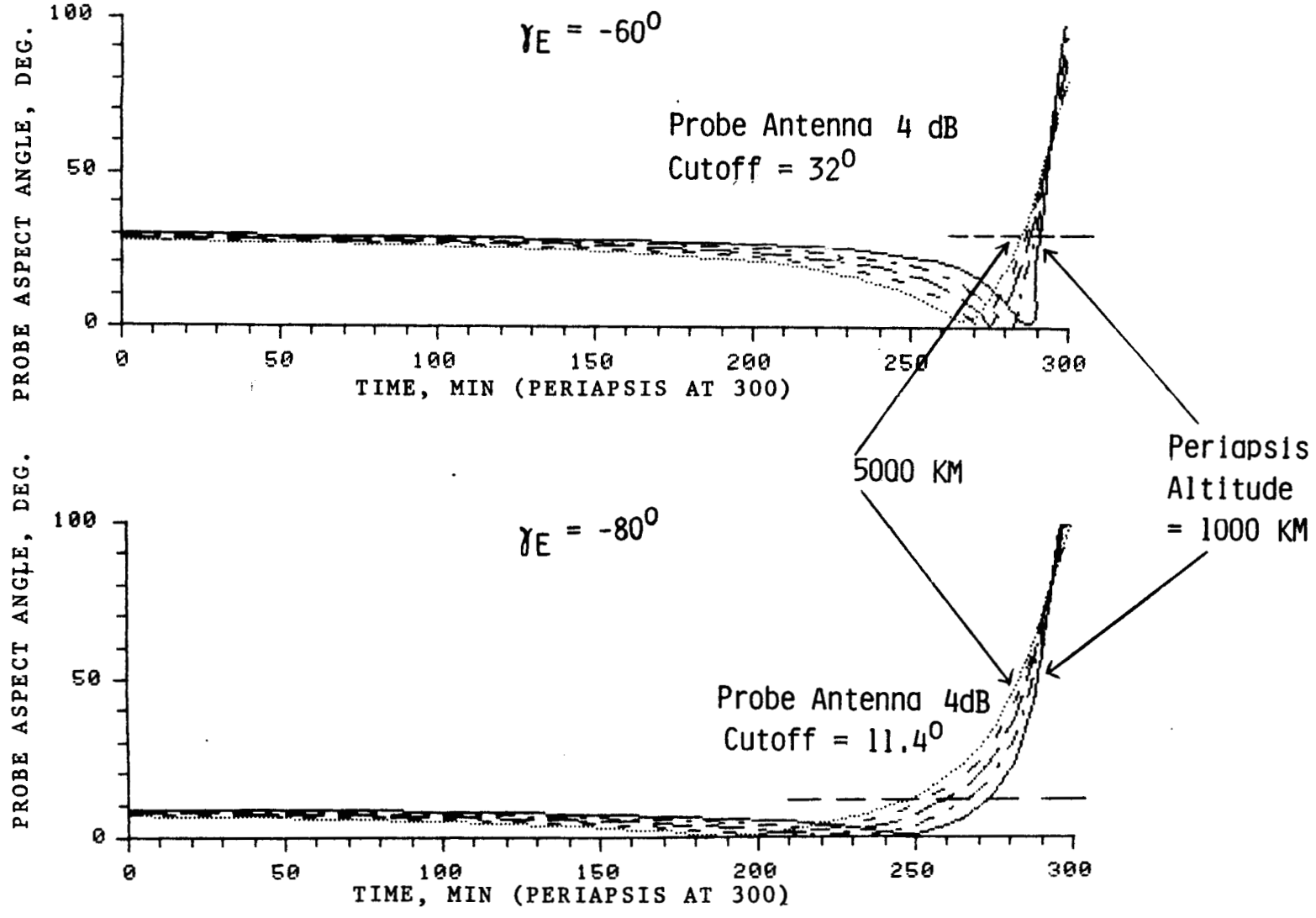

FIG. 2.4-7 BPSK LIMITATION ON DOPPLER RATE

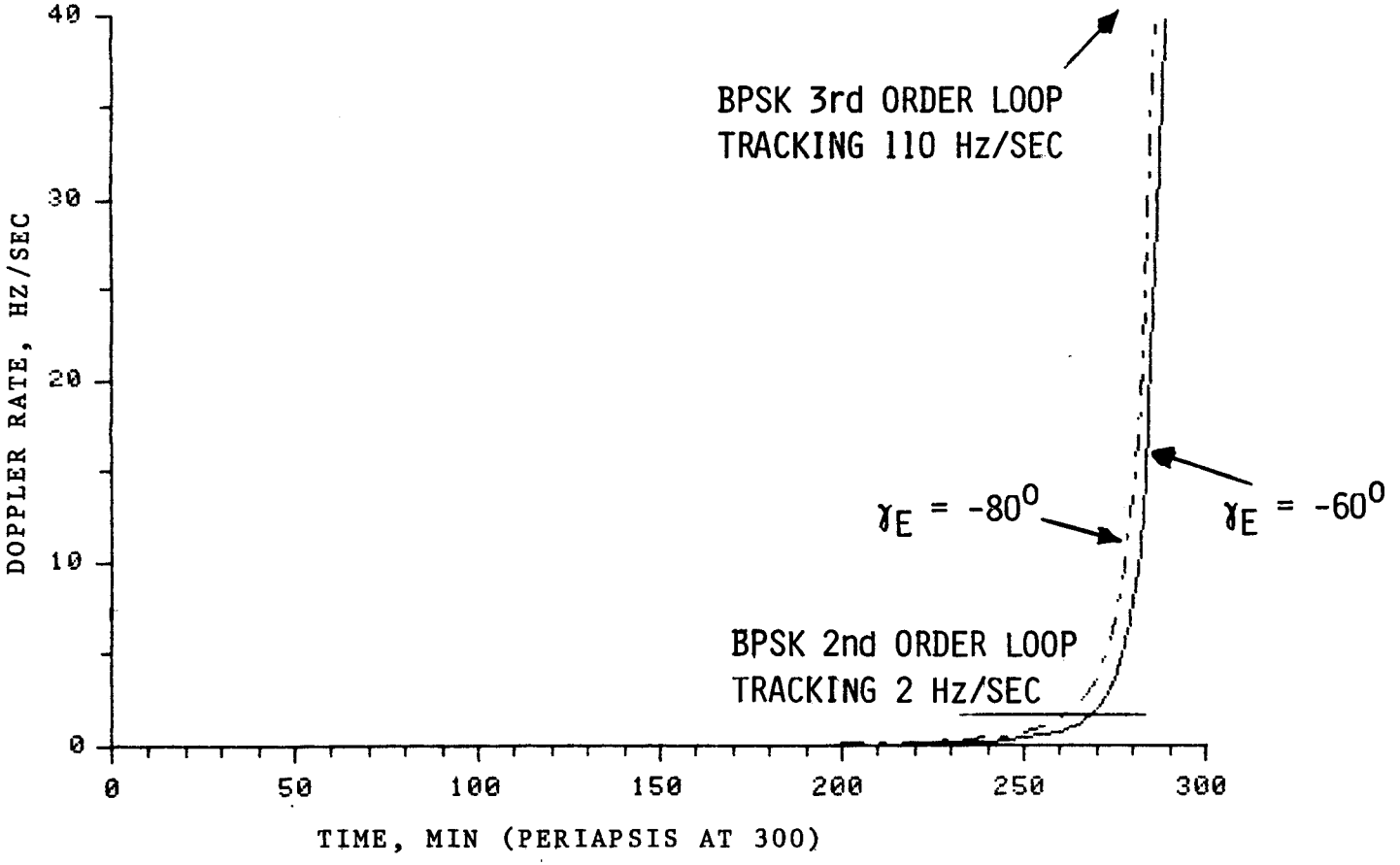

FIG. 2.4-8 FSK LIMITATION ON DOPPLER SHIFT

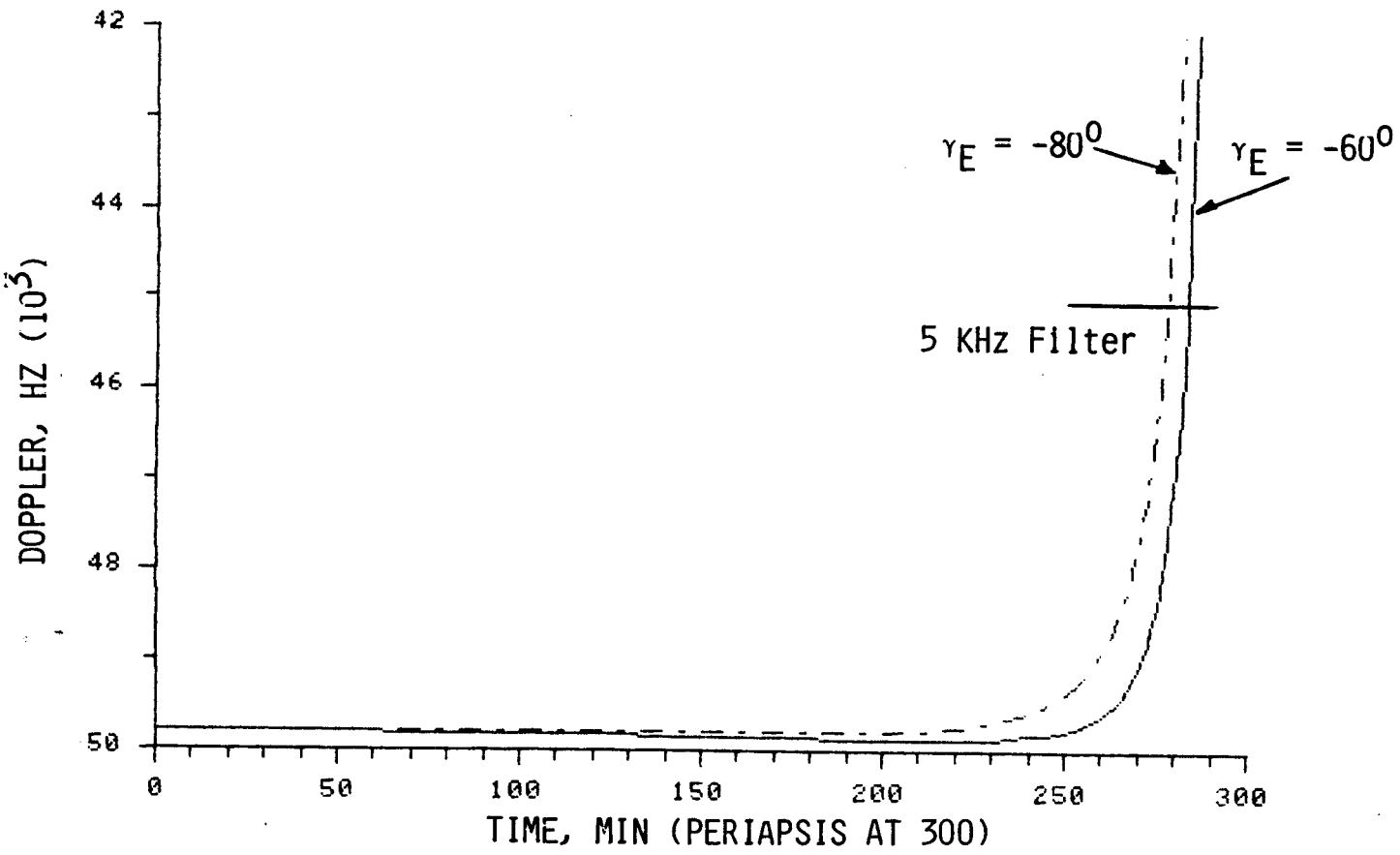

FIG. 2.4-9 CARRIER ASPECT ANGLE FURTHER CONSTRAINS PHASING FOR FIXED POINTED RECEIVE ANTENNA

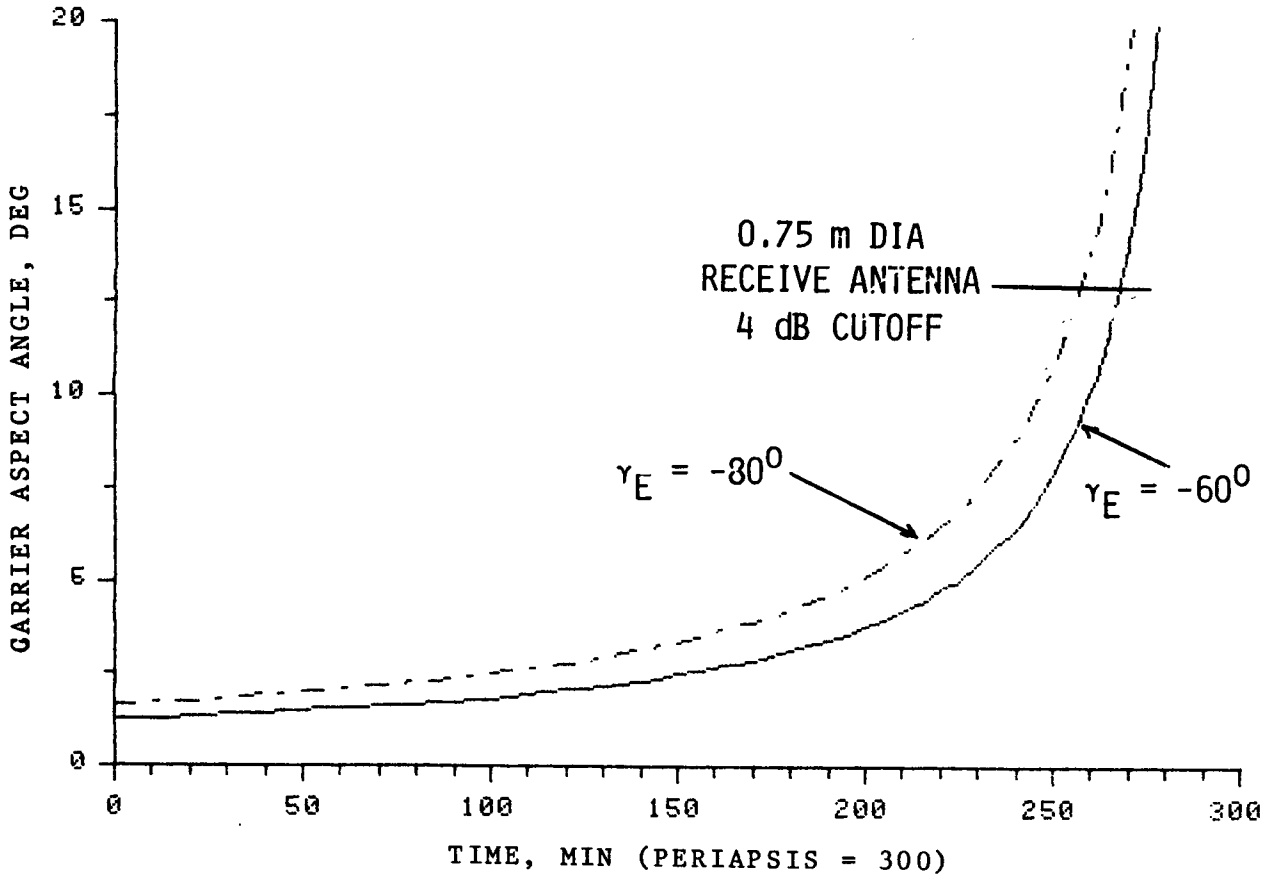

FIG. 2.4-10 SHALLOW ENTRY (CASE 1) PROVIDES
INADEQUATE TIME AT 10,000 BPS RATE

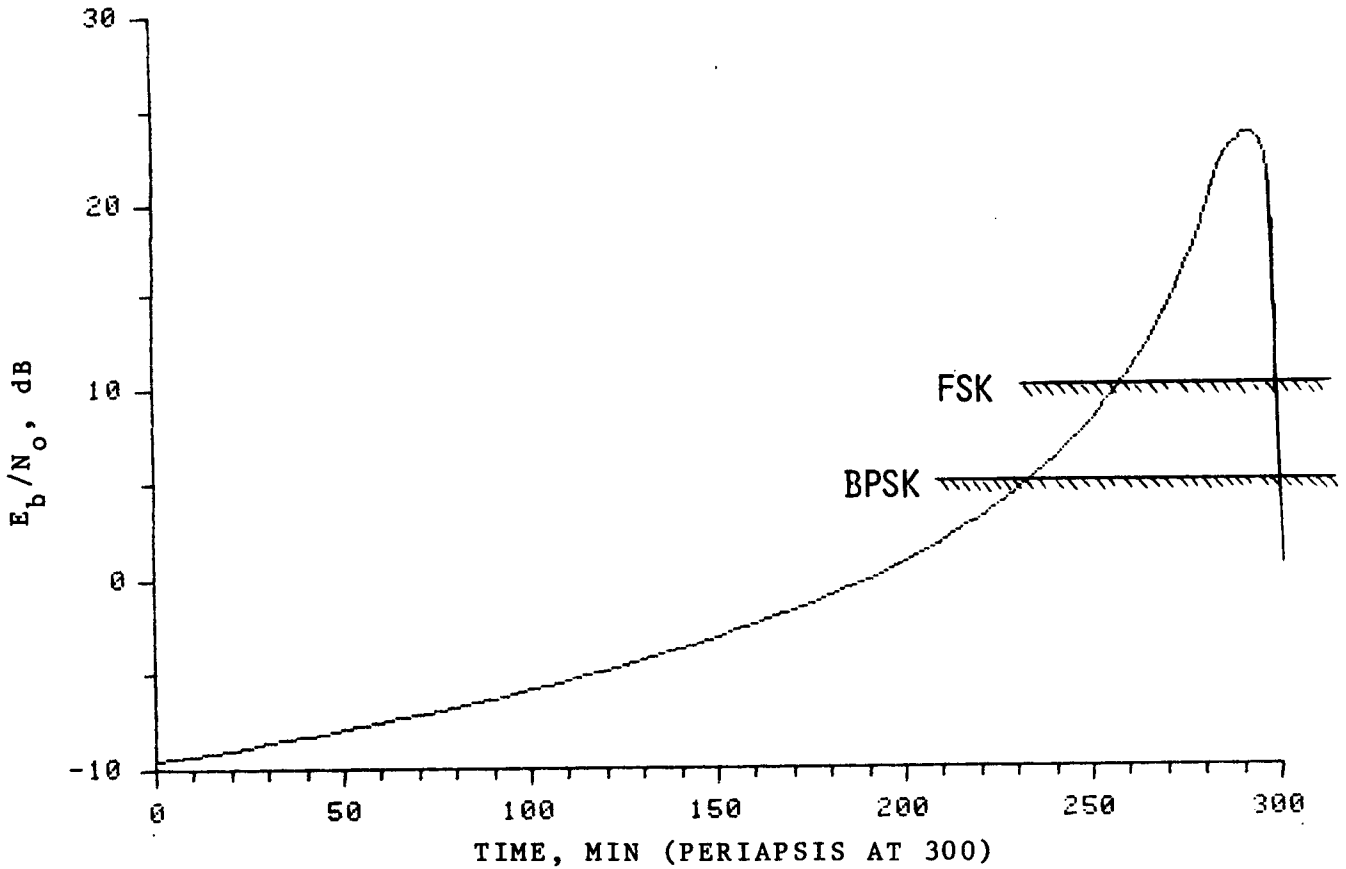

FIG. 2.4-11 STEEP ENTRY (CASE 2) PROVIDES ADEQUATE TIME AT 10,000 BPS

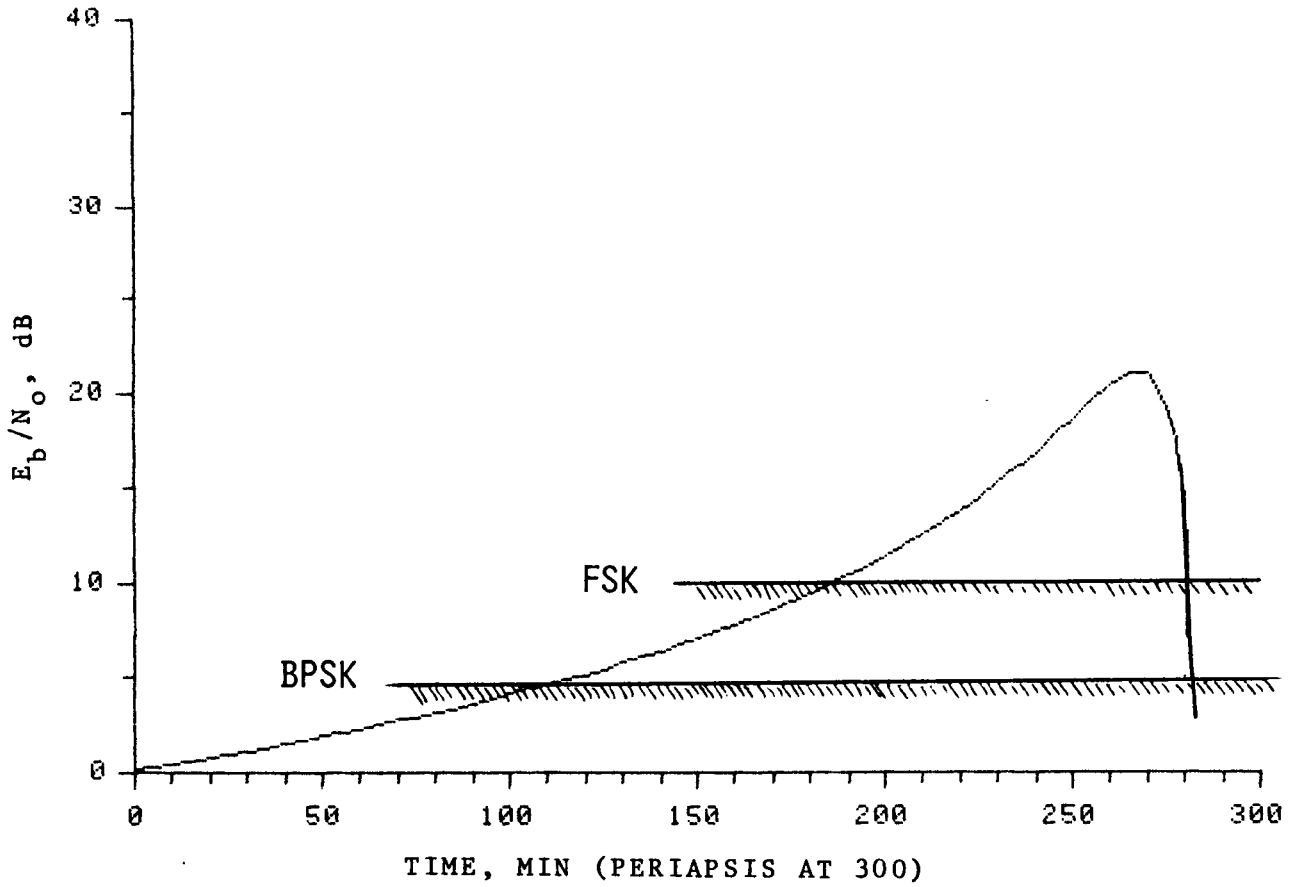

FIG. 2.4-12

TITAN WIND VELOCITY PROFILE FOR 3 HOUR DESCENT

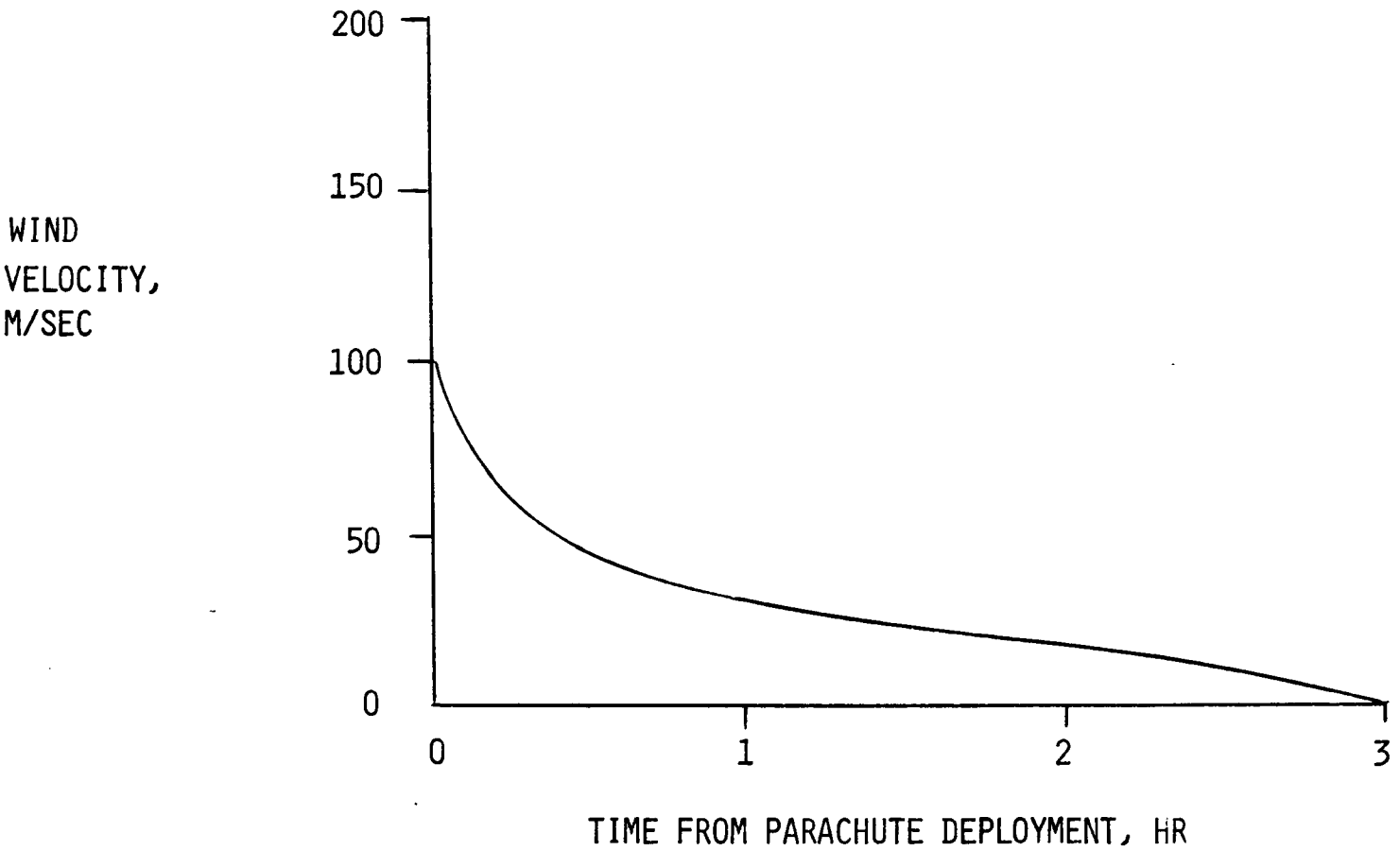

FIG. 2.4-13

EFFECT OF WIND ON PROBE DESCENT

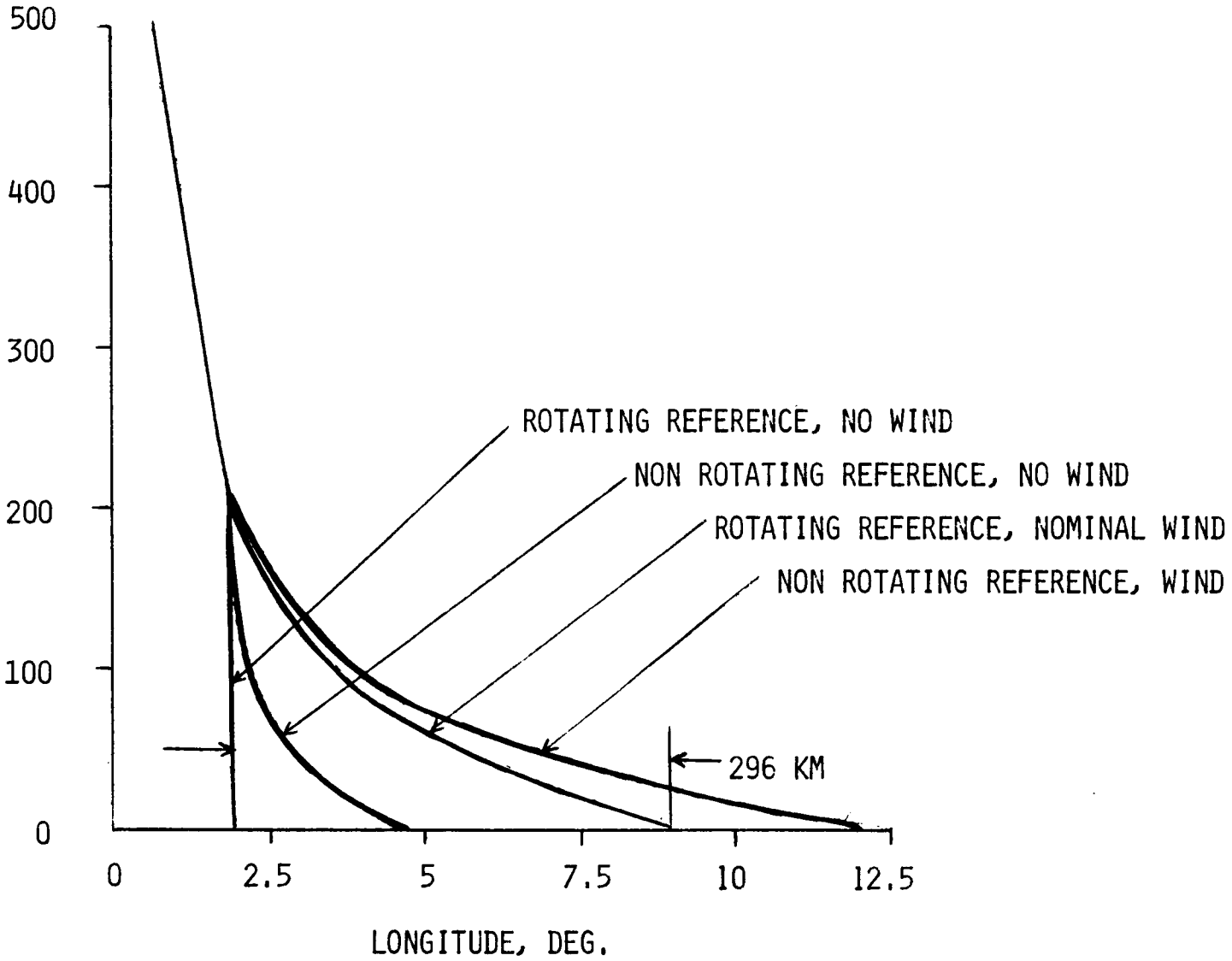

FIG. 2.4-14

COMMUNICATIONS GEOMETRY AT PROBE IMPACT

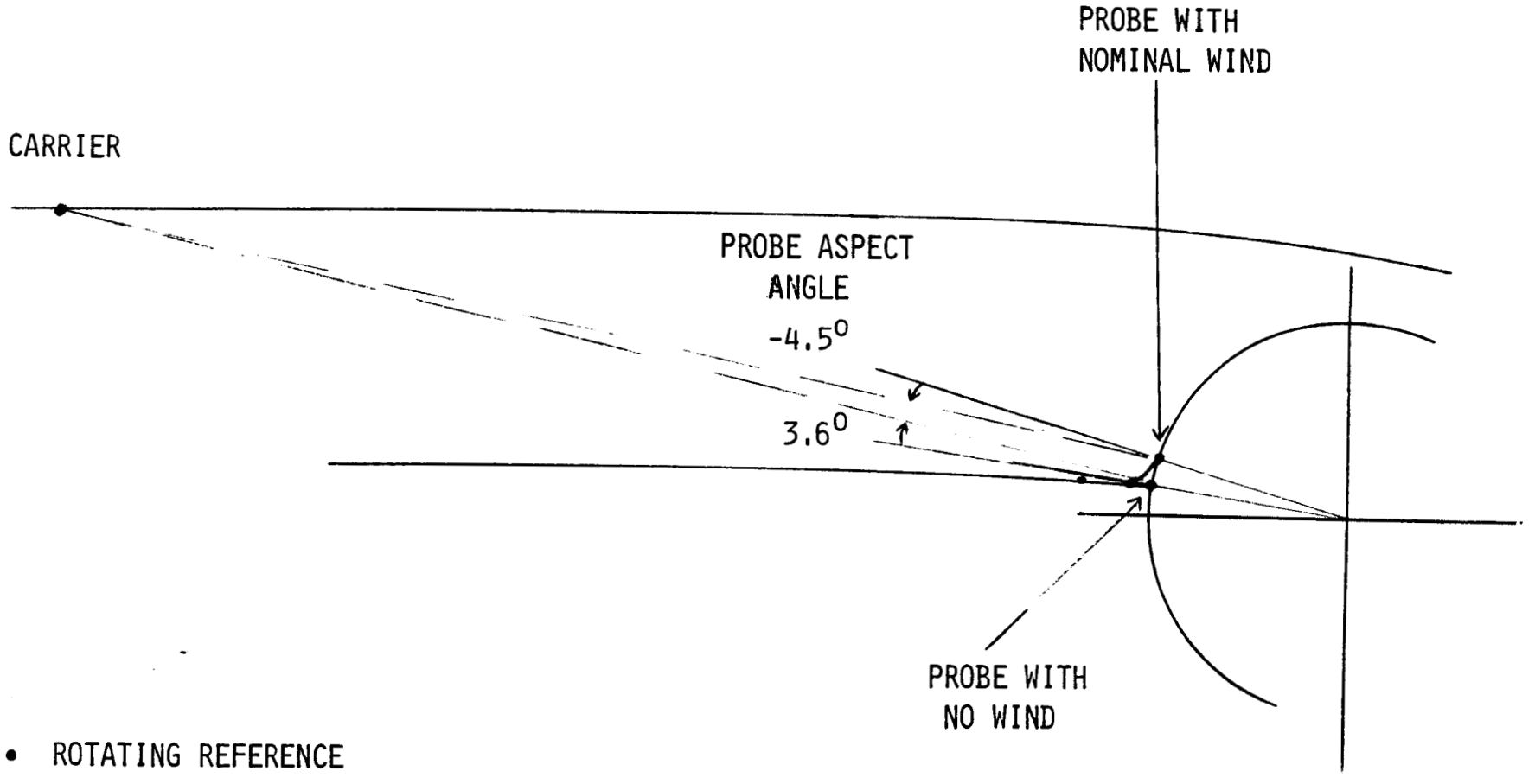

- ROTATING REFERENCE

FIG. 2.4-15
VARIATION OF PROBE ASPECT ANGLE
DURING DESCENT WITH AND WITHOUT WIND

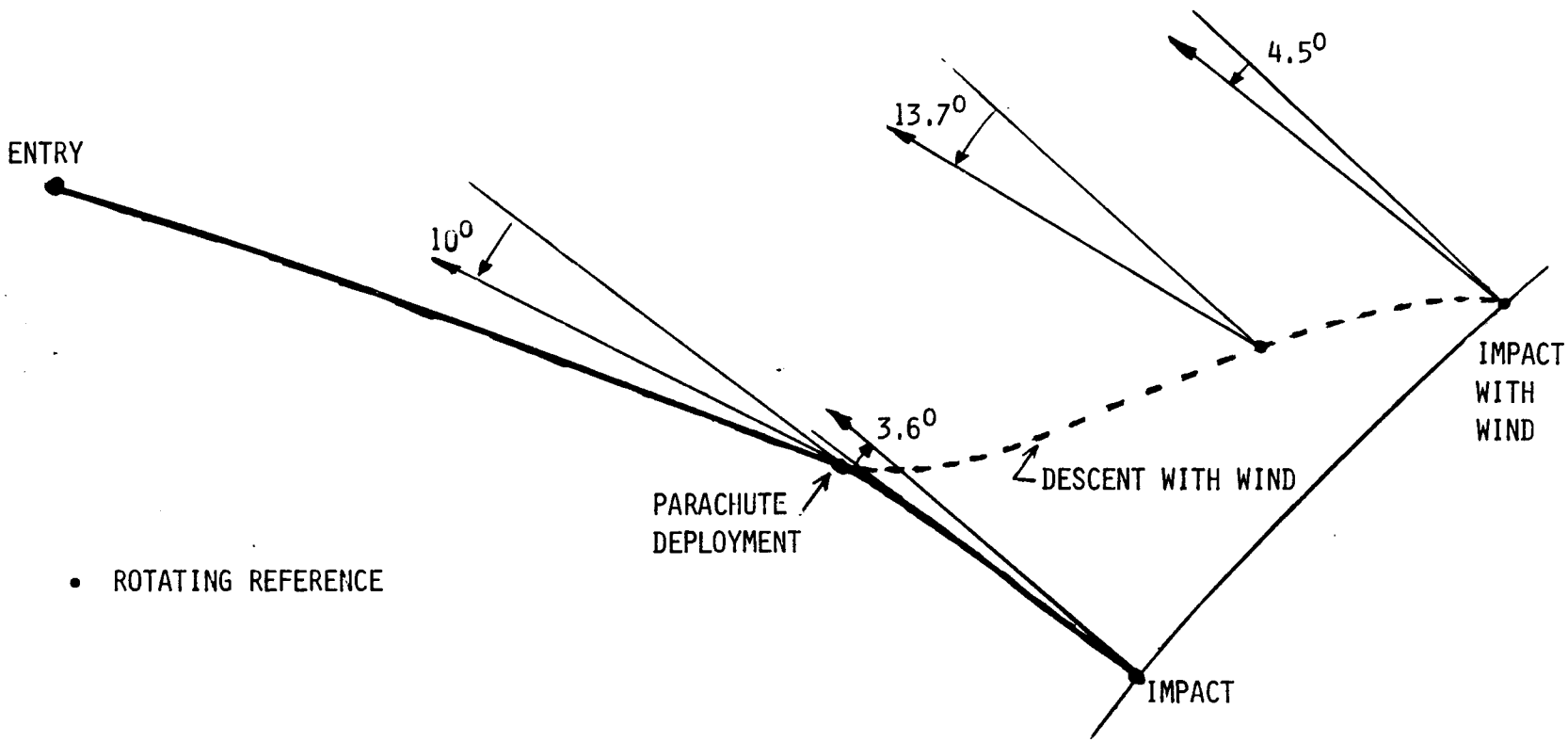

FIG. 2.4-16

WIND REQUIRES BROADER PROBE ANTENNA BEAM

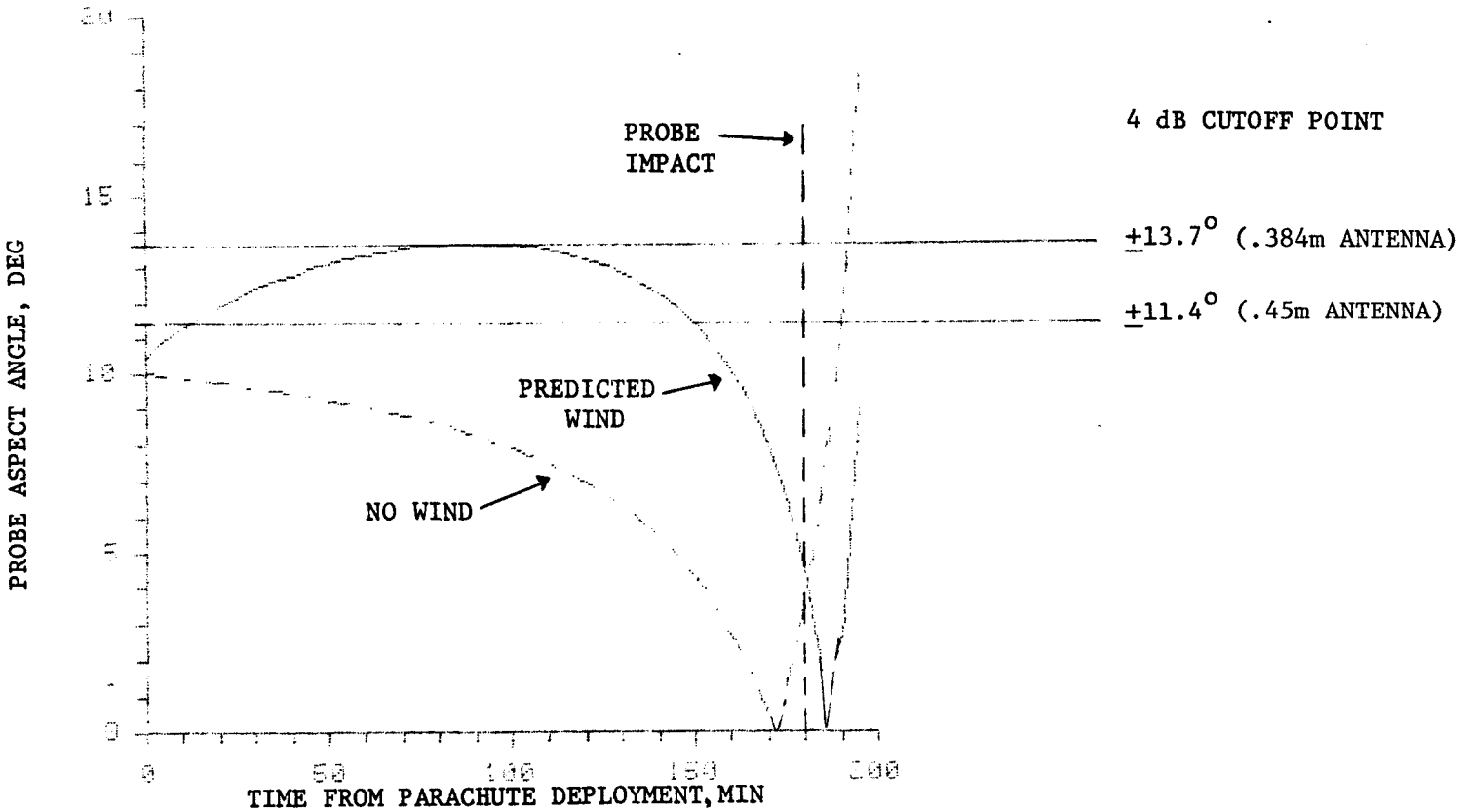

FIG. 2.4-17
LINK PERFORMANCE AS FUNCTION
OF PROBE ANTENNA DIAMETER, NO WIND

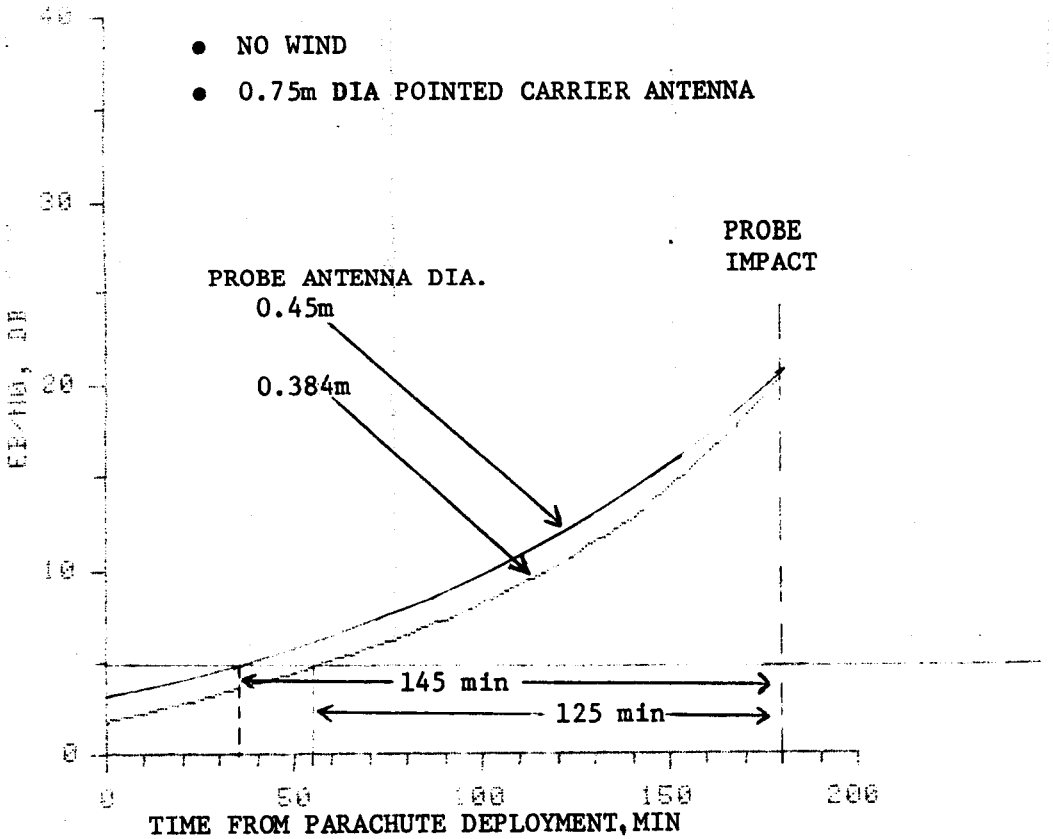

FIG. 2.4-18
BROADENED ANTENNA BEAM
SHORTENS TIME AVAILABLE FOR HIGH DATA RATE

- BASELINE MISSION (145 MIN HIGH RATE DATA IF NO WIND AND 0.45m DIA PROBE ANTENNA)
- PREDICTED WIND
- 0.384m dia PROBE ANTENNA

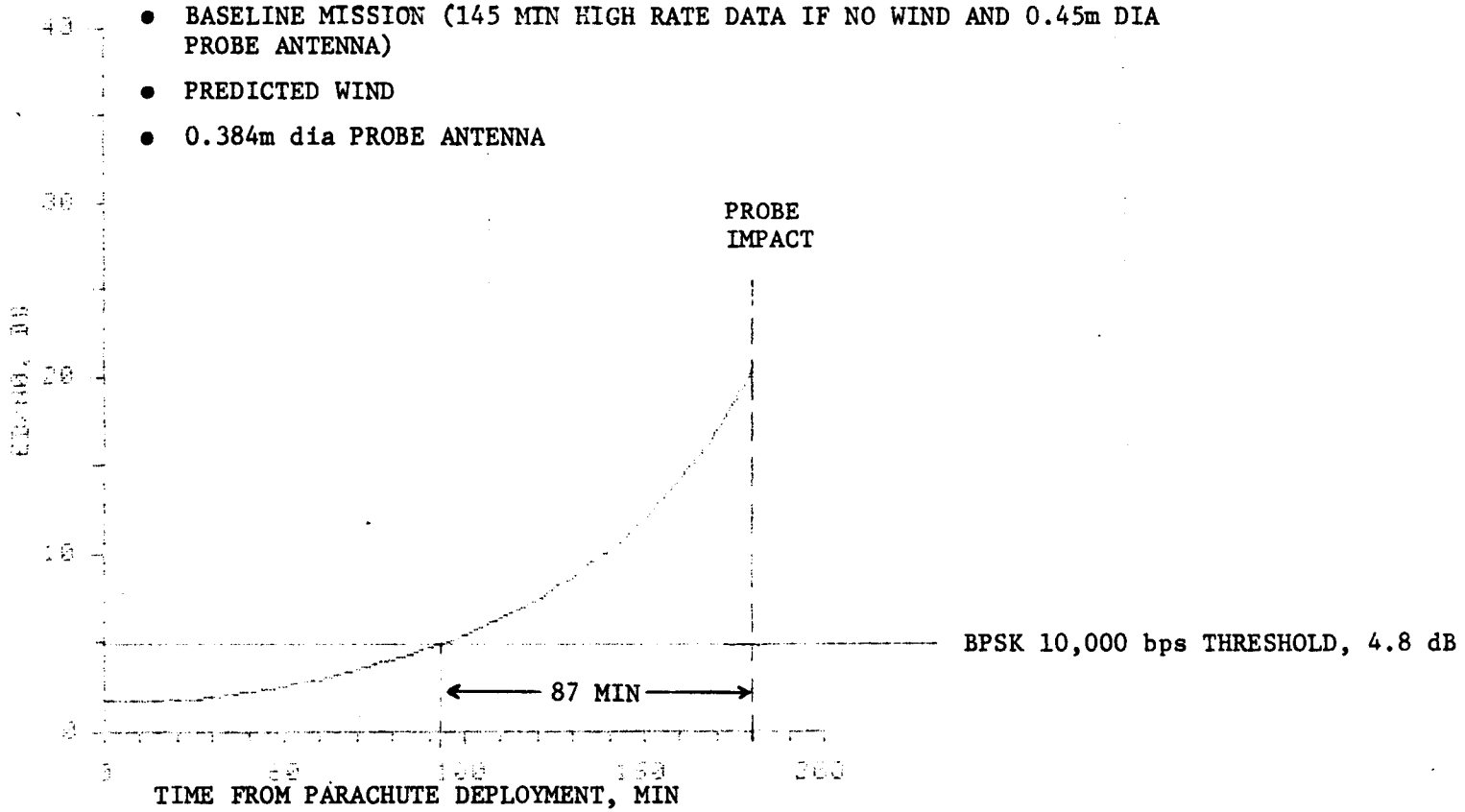

FIG. 2.4-19 INCLUSION OF ROTATION REQUIRES EVEN BROADER PROBE ANTENNA BEAM

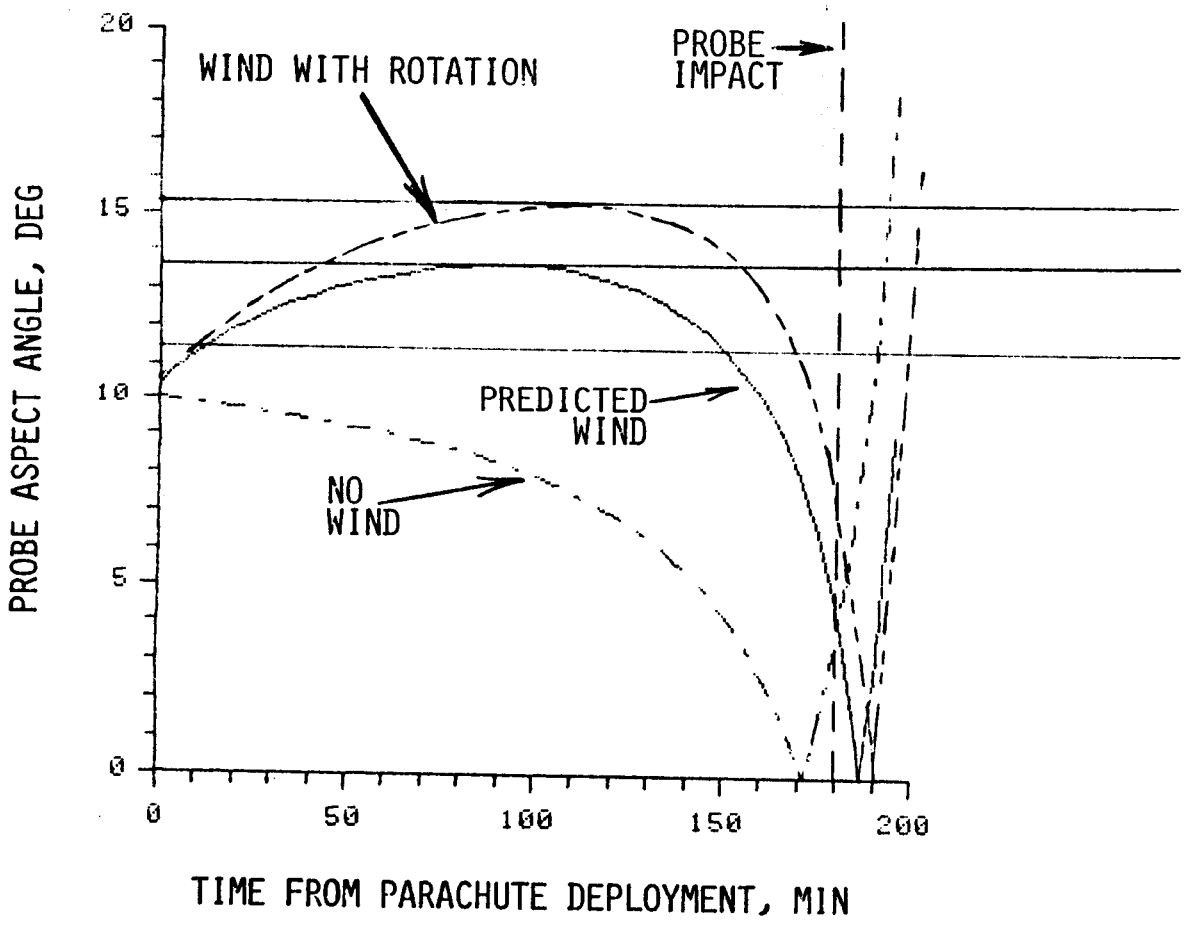

4 dB CUTOFF POINT

± 15.4° (.34 m ANTENNA)

± 13.7° (.384 m ANTENNA)

± 11.4° (.45 m ANTENNA)

TIME TO SUPPORT 10 Kbps WITH WIND AND ROTATION, 75 MINS.

2.5 Surface Survival

Approach

For the purposes of this study, the following approach was adapted to determine requirements for surface survival and operation for a period of 10-20 minutes. First, the baseline design was developed without imposing surface survival requirements. Second, an assessment of the survival potential of the baseline design was made and problem areas were identified. Finally, design modifications were conceived to enhance the survival potential of the Probe. Since the state of the surface is unknown, both liquid and solid surfaces have been considered.

Specific concerns fall into three classes. The first class includes questions about the Probe's ability to survive the shock of impact. The second class addresses the problems of operating on the surface, including thermal control, power availability, and probe buoyancy. The final class includes the various problems associated with maintaining communications with the Carrier.

Surface Conditions

At present, there are conflicting theories of the nature of Titan's surface. If solid, the surface is expected to consist of a mix of ices and clathrates. If liquid, present theories predict a global ocean of liquid ethane mixed with some liquid methane and liquid nitrogen (Lunine 1983). The estimated density of the ethane ocean is 0.61 g cm^{-3}, and the estimated depth is 1 km.

Based on Voyager measurements, a surface temperature of approximately 95K, surface pressure of 1.5 to 1.6 bars, and composition primarily of diatomic nitrogen (N_2) is expected. According to the Conrath model (Conrath 1985), there is no wind at the surface although wind profiles (described in section 2.4) indicate the possibility of non zero surface wind.

Science requirements for surface operation are not specified at present. There is some interest in obtaining samples of the surface for chemical analysis. In addition, it may be worthwhile to deploy a spike forward of the probe to provide an easily interpreted deceleration signal at impact.

For the purposes of this study, no special science requirements have been assumed. However, some of the difficulties of using the existing science complement on the surface have been identified.

Surviving Impact

As shown in Figure 2.5-1, the probe's impact velocity (without winds) varies from 5.7 m sec^{-1} (for a two hour descent) to 2.9 m sec^{-1} (for a four hour descent). To give an intuitive feel, Figure 2.5-2 expresses these impact velocities in terms of the height from which the probe would have to be dropped on Earth to reach the same speed. The worst case equivalent drop height is 1.7m.

The baseline design has a special beryllium nosecap about 1 cm thick. Dropped from a height of 1.7 m, this nose is unlikely to crush. However, the impact load is likely to exceed the Probe structure capabilities since it is sized for relatively low loads (20 g's or less at launch and upon entry).

The details of the impact, either in liquid or on a solid, are difficult to analyze. For example, the low velocities involved are outside the range of validity for empirical equations for solid surface penetrators. Furthermore, the amount of energy dissipated in splashing down in a liquid is comparable to the total impact energy of the probe, so one must develop a method of analyzing the complex behavior of the splash. For these reasons and the resources available for this study, no attempt was made to predict transient landing loads.

A purely kinematic approach to the problem yields interesting results. Figure 2.5-3 shows the relation between impact velocity, stopping distance, and average deceleration. If the deceleration is limited to the 20 g entry load value and the descent time is two hours, then the probe must somehow be stopped over a distance of no less than 8 cm. In principle, the stopping distance can be controlled by the use of crushable materials or perhaps spikes. To accommodate a two hour descent, at least 8 cm of crushable material is needed. For longer descents, the crushable layer can be thinner.

Winds at the surface have two effects upon these results. First, the probe has a transverse velocity at impact. Although the Conrath model of Reference 3 predicts zero wind at the surface, the wind at 5 km is 12 m sec-1, which is twice as large as the worst case vertical impact velocity. The net velocity vector would be substantially rotated from the vertical, implying that the loads might be shifted from the relatively strong nose to the weaker probe side walls. Second, wind shear may induce pendulum-like motions, contributing another component of transverse velocity at impact. Further study of surface survival requires an upper limit on wind velocity at the surface.

Operating on the Surface

The first question to ask about survival on an ocean is whether or not the probe will float. As long as the probe does not leak and the probe's mean density is less than that of the liquid, it will float. The first condition is violated in the baseline design, which is vented to the atmosphere. Assuming that the probe is made leak-tight, then the probe will float, because the probe's mean density of 0.35 g cm^{-3} (probe mass of 105 kg, volume of 302 x 10^3 cm^3) is appreciably less than the density of the ethane ocean and of the other candidate surface liquids listed in Table 2.5-1. In fact, as shown in Figure 2.5-4, the probe will float with roughly half of its volume out of the liquid.

Table 2.5-1
Densities of Candidate Liquids on Titan

Liquid	Density (g cm^{-3})
Ethane	0.61
Methane	0.42
Nitrogen	0.81

Another concern is probe stability on the liquid surface. To prevent the probe from floating upside down, the center of gravity must be kept below the center of buoyancy. Although detailed mass properties are unavailable at present, the baseline configuration appears to satisfy this requirement.

In the baseline design, the outer probe surfaces are within a few degrees of the atmospheric temperature during the descent. The insulation contained within the probe itself controls the environment of the units and maintains a large temperature difference between the units and the outside world. The atmosphere does leak into the vented units, but with limited convection it quickly warms up. The small heat capacity of the vented atmosphere has a negligible cooling effect on the units.

When the probe lands, this situation is basically unchanged. The Probe's exterior temperature does not change significantly, and the insulation continues to maintain the proper environment. One can then extrapolate the temperature predictions for the baseline design. At the end of the mission, the time rate of change of temperature is approximately -2 degrees C per hour, so an extra 20 minutes of surface operation will only lower the bulk Probe temperature by 0.7 degrees C.

The above argument presupposes that the Probe stays "dry", that is, that no significant amount of liquid gets into the interior of the probe. For a vented design, it is likely that this condition will be violated, leading to several undesirable effects. First, the insulation will cool, bringing the cold surface closer to the units. The resulting heat loss rate is much higher than quoted above. Furthermore, the liquid will vaporize, further cooling the units through heat of vaporization effects. In addition, the vaporized liquid will generate pressure with effects difficult to predict. For all these reasons, a leak-tight probe is very desirable for thermal control.

In the baseline design, four lithium battery modules supply power. For a three hour descent, the depth of discharge at impact is 67% (based upon a conservative derating of battery capacity). The limit on depth of discharge is estimated at 98%, leaving a margin of 31%. As shown in Figure 2.5-5, this margin is equivalent to 106 minutes of operation after landing.

The baseline probe design provides inlets for seveal of the science instruments. Some of those inlets are in danger of being plugged or broken during landing. Should surface survival become a hard requirement, instrument accommodation will have to be reviewed carefully to prevent these problems.

Maintaining Communications with Carrier

To maximize communications time at the higher data rate, the optimum Probe landing time is as late as possible in the mission sequence. However, the nominal landing time must be earlier than this optimum to ensure that the probe reaches the surface before the link deteriorates if there are errors from the target plan. A preliminary error analysis indicates that the nominal landing time will be 15 minutes earlier than optimum. Hence, if the descent is nominal, then full communications from the surface will be available for 15 minutes. However, if communications from the surface are required for worst case slow descents, then the nominal probe landing must be pushed back even

earlier in the sequence, reducing the duration of high data rate communications in the atmosphere.

Excessive probe tilting will degrade the communications link. A wide beam-width probe antenna mitigates but does not eliminate the problem. The presence of surface winds will favor jettisoning the parachute and raises concerns about the effects of ocean waves on the Probe's attitude. If the Probe lands on a solid surface, stabilizing legs may be required to maintain suitable antenna geometry.

The survival of the Probe's antenna is another concern. Since the dielectric properties of the surface are unknown, there is a risk of RF absorption or electrical shorting if liquid or snow gets into the antenna. Some sort of RF transparent housing may be required.

Conclusions

Since the probe structure is being sized for entry and launch loads, which are 20 g's or less, there is considerable concern about the probe's ability to survive impact. Crushable materials may offer a way of limiting the landing loads. Approximately 8 cm of crushable material will reduce the load to 20 g's for a worst case impact velocity. Substantial uncertainties exist because of the uncertainties in surface wind speeds.

Thermal control and buoyancy considerations indicate that the Probe design should be modified to prevent liquid leakage if surface survival is required. Providing this is done, the probe will float, and the probe temperature will drop only 0.7 degrees over a 20 minute period. Substantial battery power margin is available. Science instrument accommodation will need further review if surface operation is required.

If the descent is nominal, 15 minutes of communications time will be available from the surface. If communications is required for worst case conditions, then some high data rate communications time in the atmosphere must be given up. Concerns about probe tilting and antenna survival will require further study if surface survival is required.

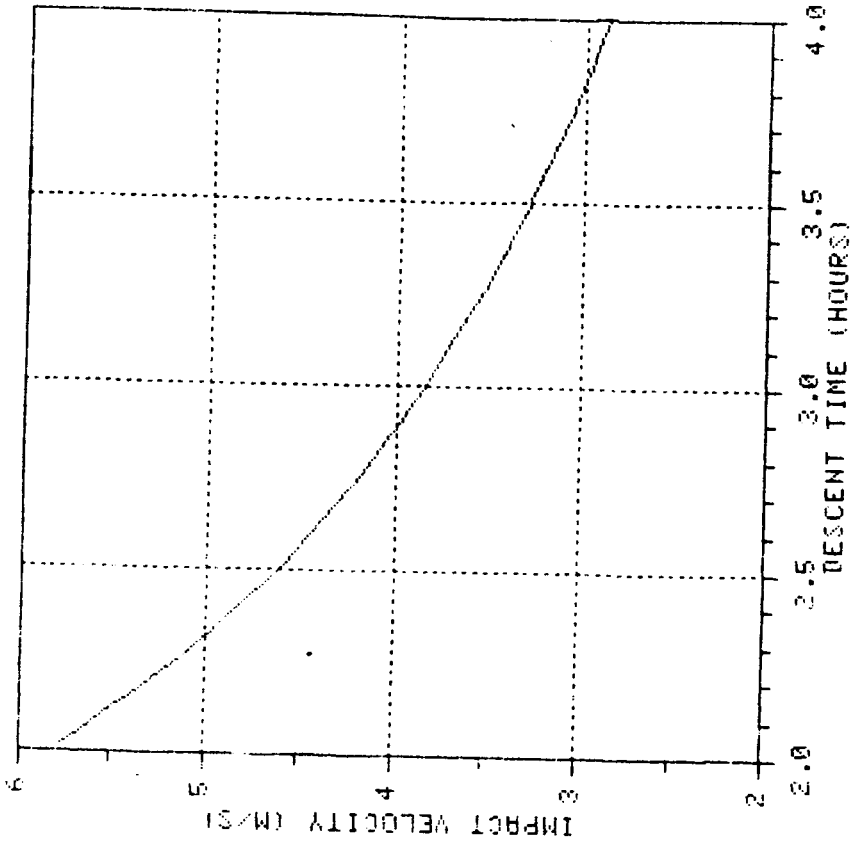

FIGURE 2.5-1:

Probe impact velocity.

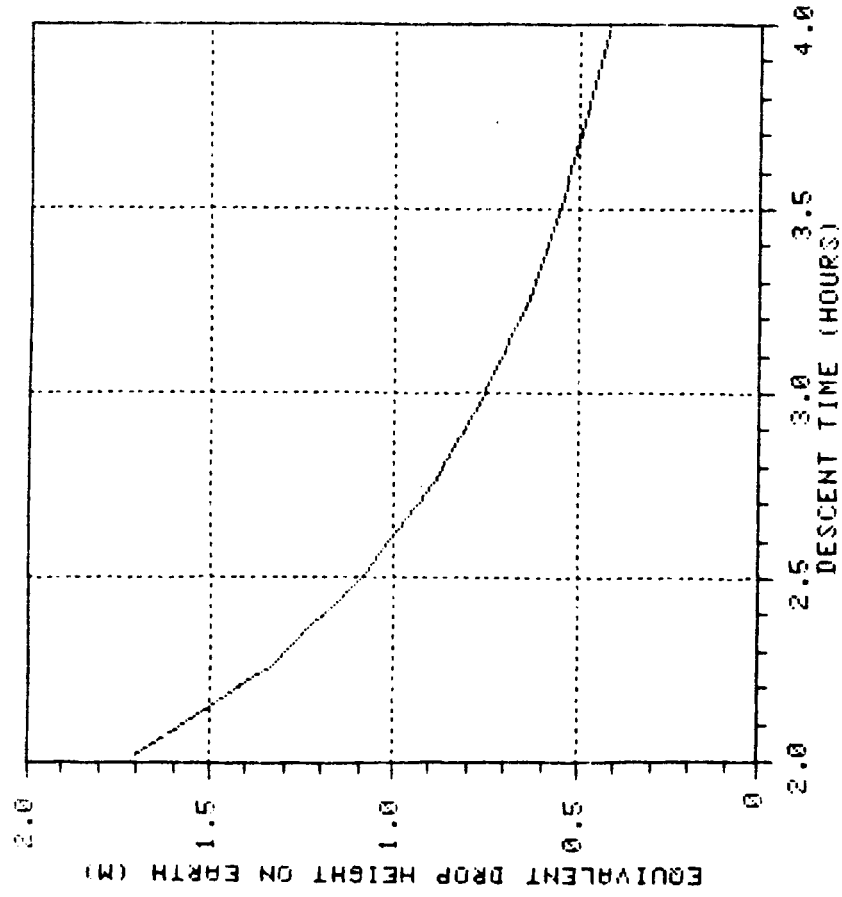

FIGURE 2.5-2:

Probe impact velocity expressed in terms of equivalent drop height on Earth.

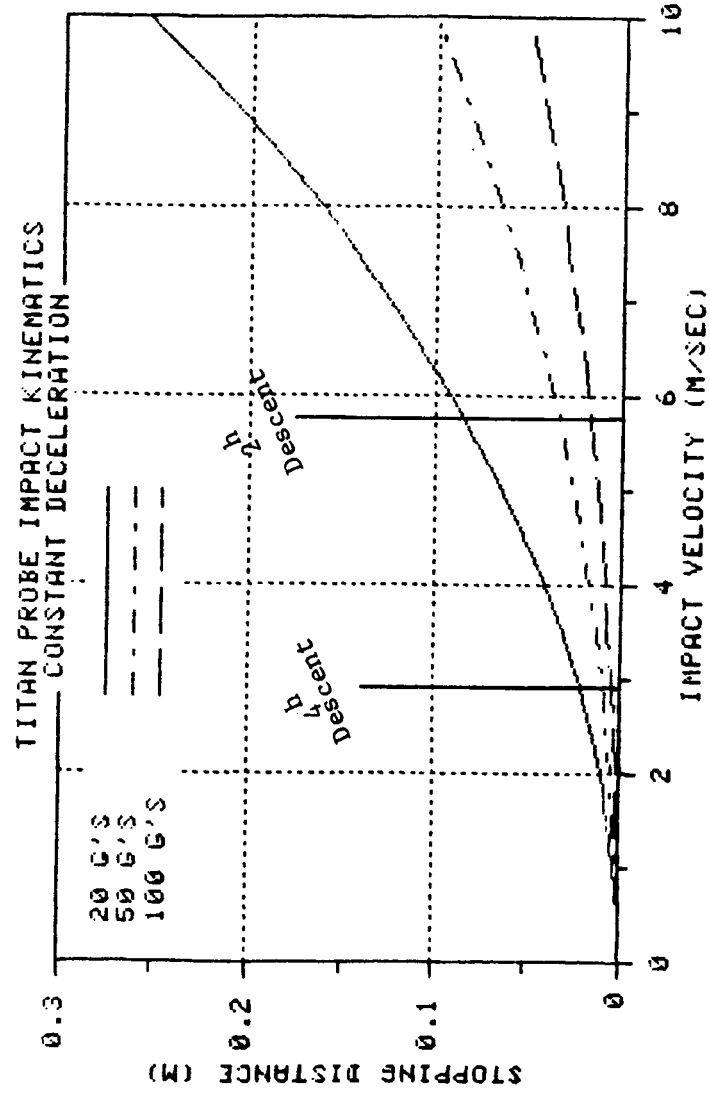

Figure 2.5-3:

Kinematics of probe impact.

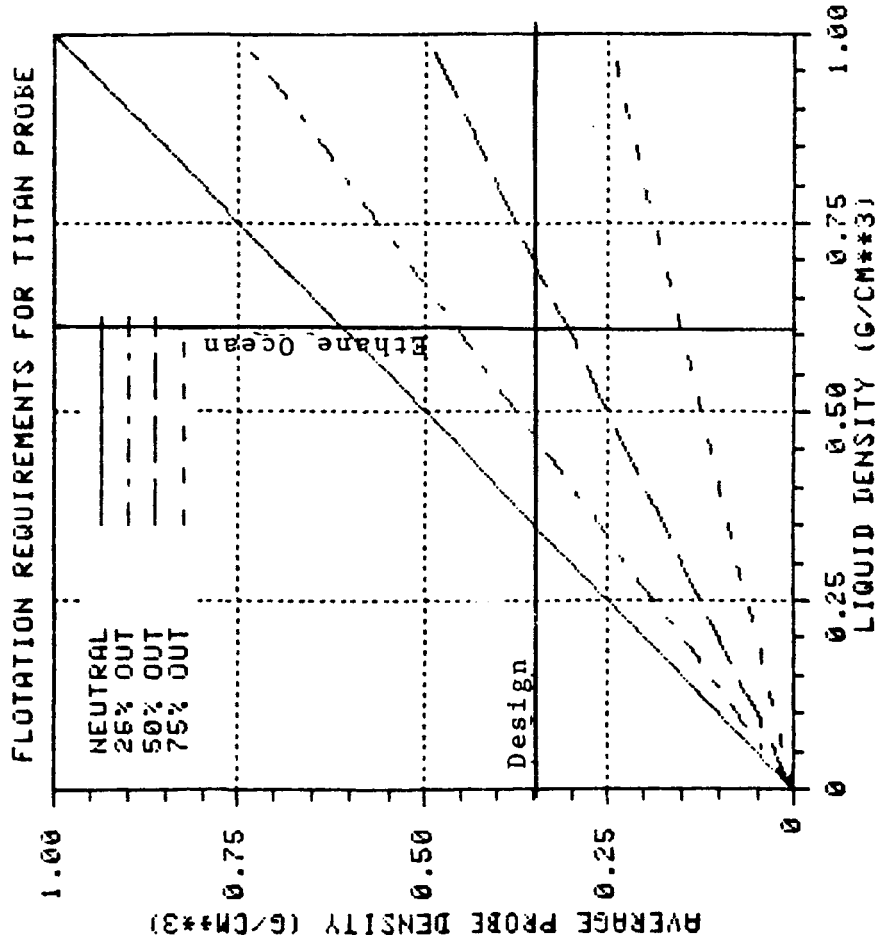

Figure 2.5-4:

Probe buoyancy

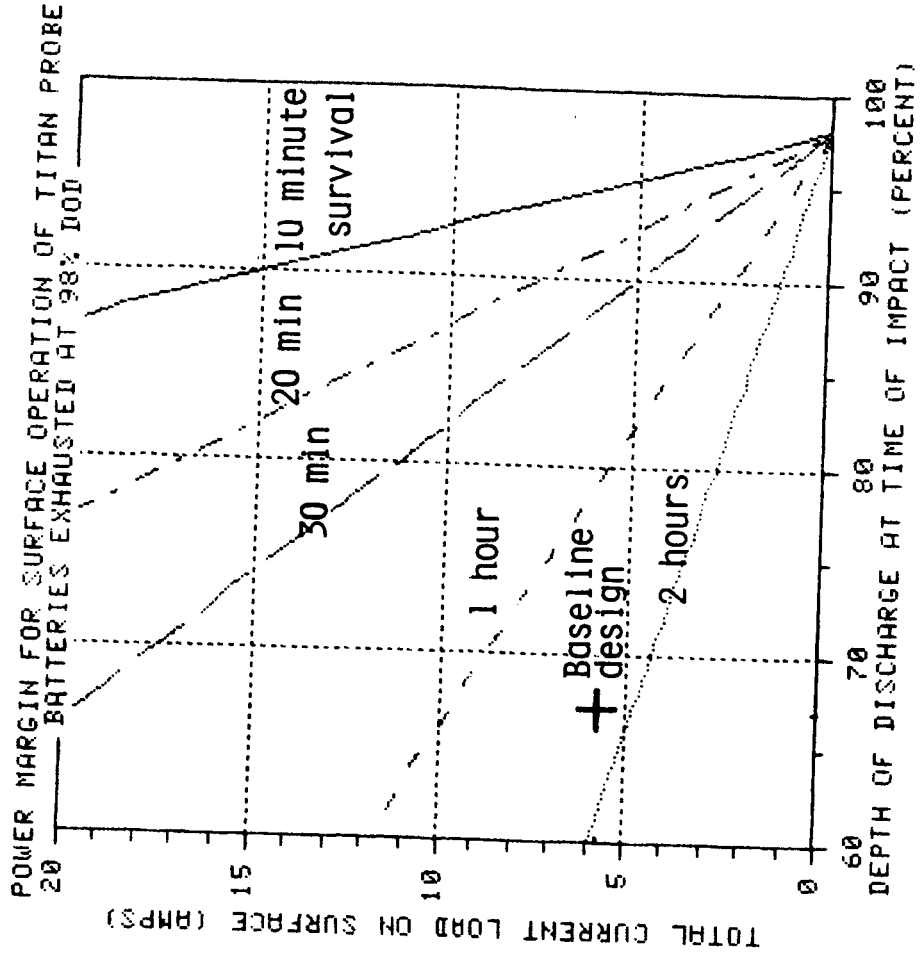

Figure 2.5-5

Probe power margin at impact.

3. DECELERATION MODULE

The deceleration module consists of the decelerator skirt, nosecap, and parachute. The skirt slows the probe during entry; both it and the nosecap protect the descent module from entry heating. When the skirt separates at subsonic speed, it extracts the parachute, which stows on the aft side of the descent module, to provide the correct descent drag.

3.1 Decelerator Configuration

The decelerator configuration strongly affects the entry ballistic coefficient and science deployment altitude. Mild entry loads permit designs with large area and the benign heating allows flatter designs with higher drag coefficients. As shown in Section 2.2, a ballistic coefficient of about 14.5 kg/m^2 results in a sonic altitude of 190 km; halving the coefficent increases the altitude by about 25 km. The design effort has focussed on 60^o spherically-blunted cones with diameters of 3.3 m or less to accommodate the launch envelope of the Shuttle.

Decelerator Concept

Both fixed and deployable decelerator skirts allow fitting reasonable drag areas in the available envelope on the Carrier. Deployable designs allow a larger drag area, desirable because of the corresponding increased sonic altitude. However, deployable designs have higher risk and cost. The study compared the more promising umbrella and hinged panel deployment concepts with a fixed solid material design.

The umbrella design (Figure 3.1-1) consists of cantilevered struts supporting a flexible skirt material. For stowage the struts fold toward the center, meeting at a common point and the material folds along pleats much like a conventional umbrella. Although flexible materials exist that can protect against the heat loads of the Titan entry, all have significant insulation, flow-through, and structural problems. Common failures include internal material abrasion and burn-through caused by porosity. The deployment of the material to a smooth surface following 9 years of in-space storage also poses a design risk. Finally, the performance of the flexible material at low (100 K) temperatures is not known.

The hinged panel concept, proposed for the VOIR aerobrake, avoids the material problems of the umbrella design (Figure 3.1-2). The skirt consists of multiple triangular panels that approximate the desired conical shape when deployed. Hinges along the panel edges allow the decelerator to fold to a star-shaped pyramid configuration for stowage. Because each of the panels remains flat, folding does not affect the material selection. Despite the number of hinges, floating pins and standard mechanical design practices ensure reliable deployment. However, each of the hinge lines must have a seal to prevent flow-through, a major design complication.

The decelerator deployment sequence for either option begins by releasing the stowed members, which allows centrifugal force to deploy the skirt. Dampers slow the deployment as the struts reach their final positions. If the spin-to-transverse inertia ratio of a deployable decelerator design is less than 1.0, the decelerator deployment and the probe itself must meet additional symmetry requirements to assure successful deployment. These requirements affect geometry, probe mass properties, release times, and the deployment dampers.

Although constrained to a slightly smaller diameter, a fixed decelerator (Figures 3.1-3 and 3.1-4) eliminates the cost, risk, and complexity of the deployable designs. A honeycomb structure covered with thermal protection material forms the skirt portion, which separates from the nose when the probe slows to subsonic speed.

While Titan Probe can use either a fixed or deployable decelerator skirt, this study focussed on the fixed design because of its many engineering advantages. The scientific advantages of the slightly higher deployment altitude of a larger diameter deployable design comes with increased design complexity, cost, and mass.

Envelope

Although deployable decelerators of about 3.5 m diameter are possible, the Mariner Mark II Carrier envelope constrains the fixed decelerator to about a 3 m diameter, as shown in Figures 3.1-5 to 3.1-8. The probe mounts nose-in on the opposite side of the Carrier from the RTGs, keeping the c.g. close to the Carrier for the stiffness-driven attachment. The moderate level of entry aerodynamic heating makes penetrations of the nose by the attachments practical.

Allowing 1.5 in. clearance to the JPL-defined fuel tanks, the 175 in. diameter Mariner static envelope constrains the probe diameter to 2.97 m. (Figure 3.1-6). Additional tank clearance reduces the decelerator diameter, at least in local areas. The location of the Carrier thruster outriggers provides more than 45^{o} clearance to the edge of the skirt.

Clearance to the high gain antenna determines the Probe's longitudinal station on the Carrier (Figure 3.1-7). Increasing the clearance forces the Probe aft, complicating the two attachments to the equipment bay corners. The third Probe support attaches to the propulsion module bulkhead. Section 5.1 describes the interface in more detail.

Decelerator Design and Integration

Figures 3.1-9 and 3.1-10 show the fixed decelerator design and attachment to the descent module. A 6 mm thick aluminum honeycomb frustum with 0.18 and 0.15 mm face sheets rigidly supports the thermal protection material. A ring at the outer edge of the skirt stiffens the structure. The forward edge attaches to an inner box-section torsion ring that surrounds the outboard edge of the descent module shelf and lies slightly aft of it. Three brackets attach this inner ring to the shelf. Locating these attach points at the same angular positions as the Carrier attachments transfers the decelerator launch loads directly to the Carrier.

To jettison the decelerator skirt, fully-redundant cutters sever the bolts holding the three brackets to the shelf. Differential drag pulls the skirt aftwards. The mild entry loads allow the use of existing, qualified, dual bolt cutters. Separation guides prevent skirt rotation and ensure that the ring and brackets clear the descent module.

Table 3.1-1 details the decelerator mass. This mass represents a conservative design, using aluminum structure and maintaining comfortable thermal margins at the bond that attaches the thermal material to the decelerator skirt. Further analysis can assess the feasibility of more agressive designs that use higher-temperature substrates and use the transient thermal capabilities of the adhesive bond.

Table 3.1-2 lists the decelerator structural design considerations. Table 3.1-3 lists the dimensions of each decelerator element.

TABLE 3.1-1 DECELERATOR MASS (KG)

BERYLLIUM CAP AND CARBON FOAM	10.0
HONEYCOMB SHELL	15.3
OUTER RING	5.0
INNER RING	1.8
ESM HEAT SHIELD	24.7
LITAFLEX INSULATION	3.4
TOTAL	60.2

TABLE 3.1-2 TITAN PROBE DECELERATOR STRUCTURAL DESIGN CONSIDERATIONS

- NOSECAP SIZED TO KEEP THE MAXIMUM TEMPERATURE BELOW 1500 F FOR WORST CASE ENTRY t = 0.37 cm (0.145 inches)
- OUTER SKIRT SIZED TO MAINTAIN ITS SHAPE UNDER ULTIMATE LOAD, ULTIMATE = 1.25 x LIMIT (NO BUCKLING ALLOWED)
- HONEYCOMB SHELL WITH RINGS AT THE INNER AND OUTER RADIUS ADOPTED OVER SEMI MONOCOQUE SHELL SINCE PRELIMINARY ANALYSIS SHOWS SIGNIFICANT MASS SAVINGS
- HONEYCOMB FRONT FACE TEMPERATURE 350 F UNDER WORST CASE ENTRY

TABLE 3.1-3 - DECELERATOR ELEMENT DIMENSIONS

HONEYCOMB	FRONT FACE	t_f = 0.018 cm	(0.007 inches)
	BACK FACE	t_b = 0.015 cm	(0.006 inches)
	CORE DEPTH	H = 0.61 cm	(0.240 inches)
	CORE DENSITY	= 83.3 Kg/m^2	(5.2 lbs/ft^3)
BERYLLIUM CAP		t = 0.37 cm	(0.145 inches)
ESM HEAT SHIELD		t = 1.74 cm	(0.687 inches)

FIGURE 3.1-1 UMBRELLA CONCEPT FOR DEPLOYABLE DECELERATOR

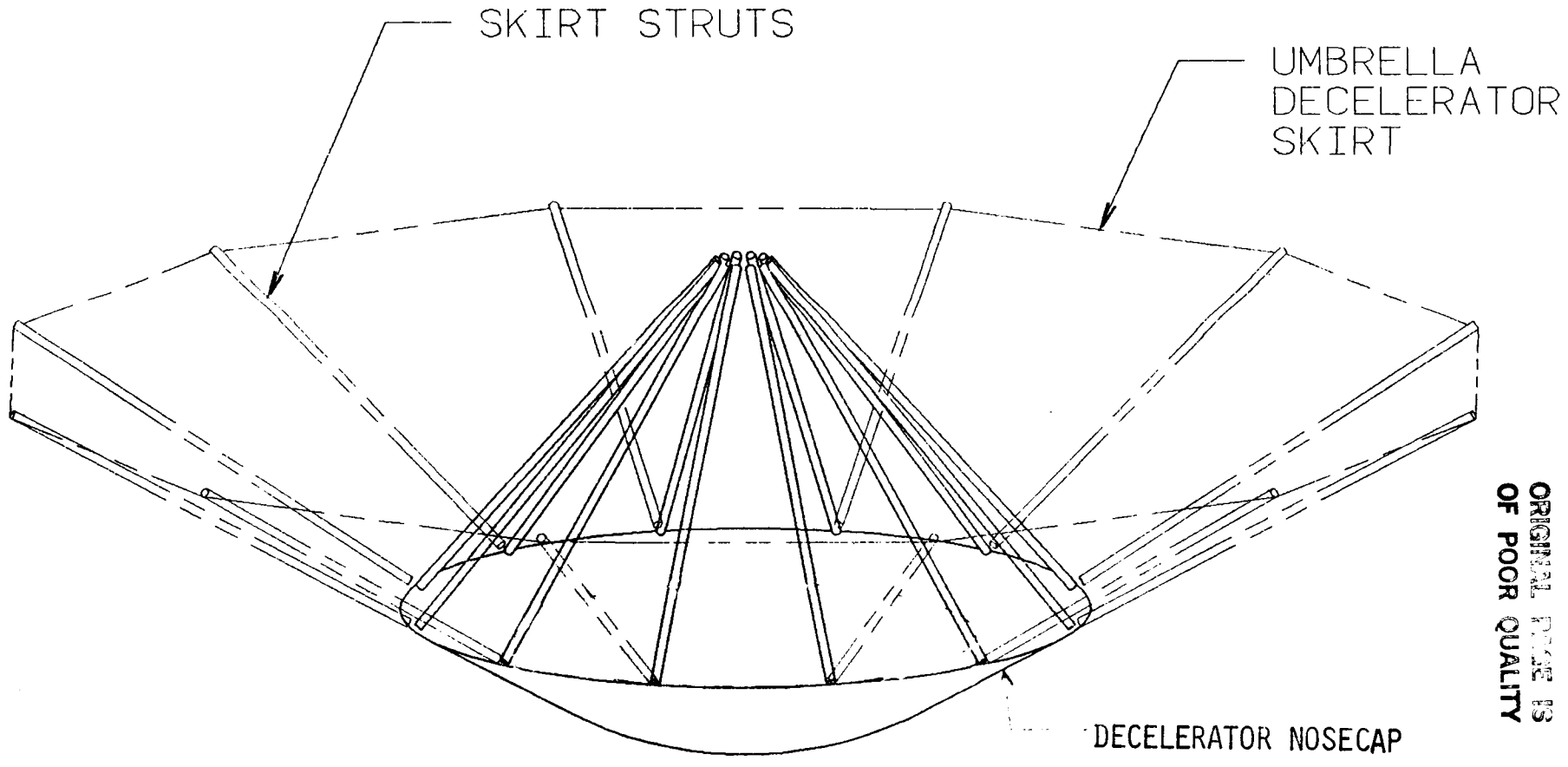

SOLID LINES ARE DECELERATOR STOWED

PHANTOM LINES ARE DECELERATOR DEPLOYED

FIGURE 3.1-2

HINGED PANEL CONCEPT FOR DEPLOYABLE DECELERATOR

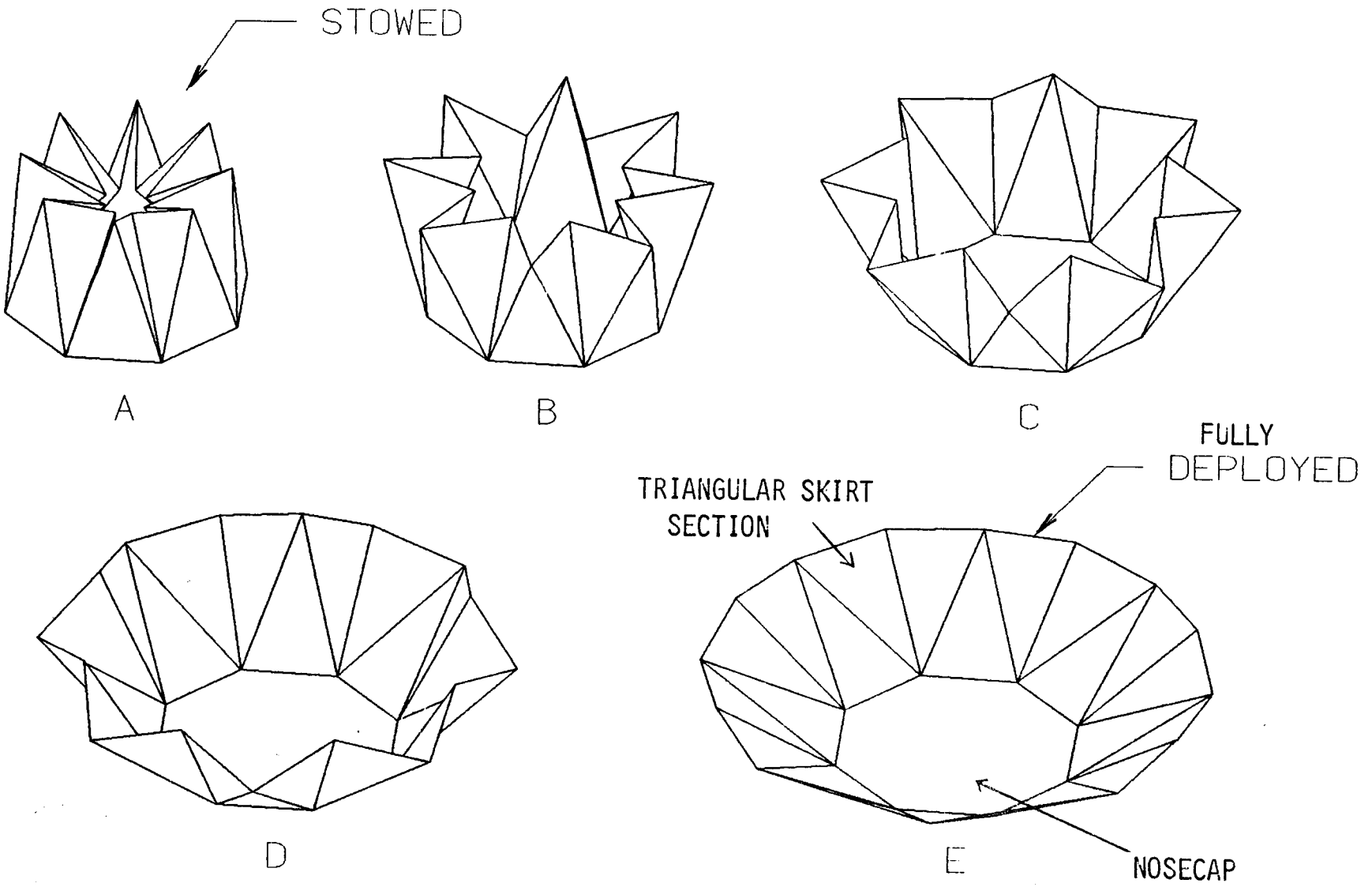

FIGURE 3.1-3

FIXED DECELERATOR (SEPARABLE NOSECAP)

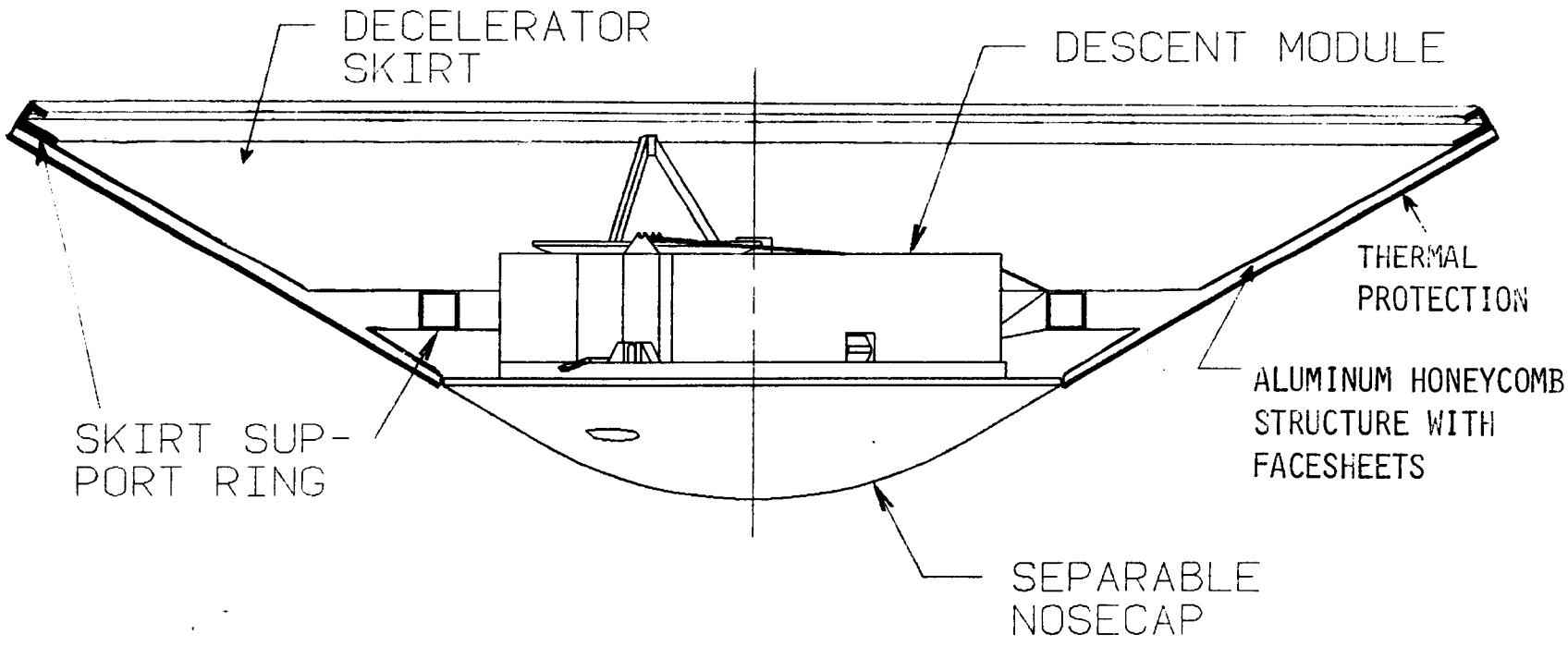

FIGURE 3.1-4:

FIXED DECELERATOR (INTEGRAL NOSECAP)

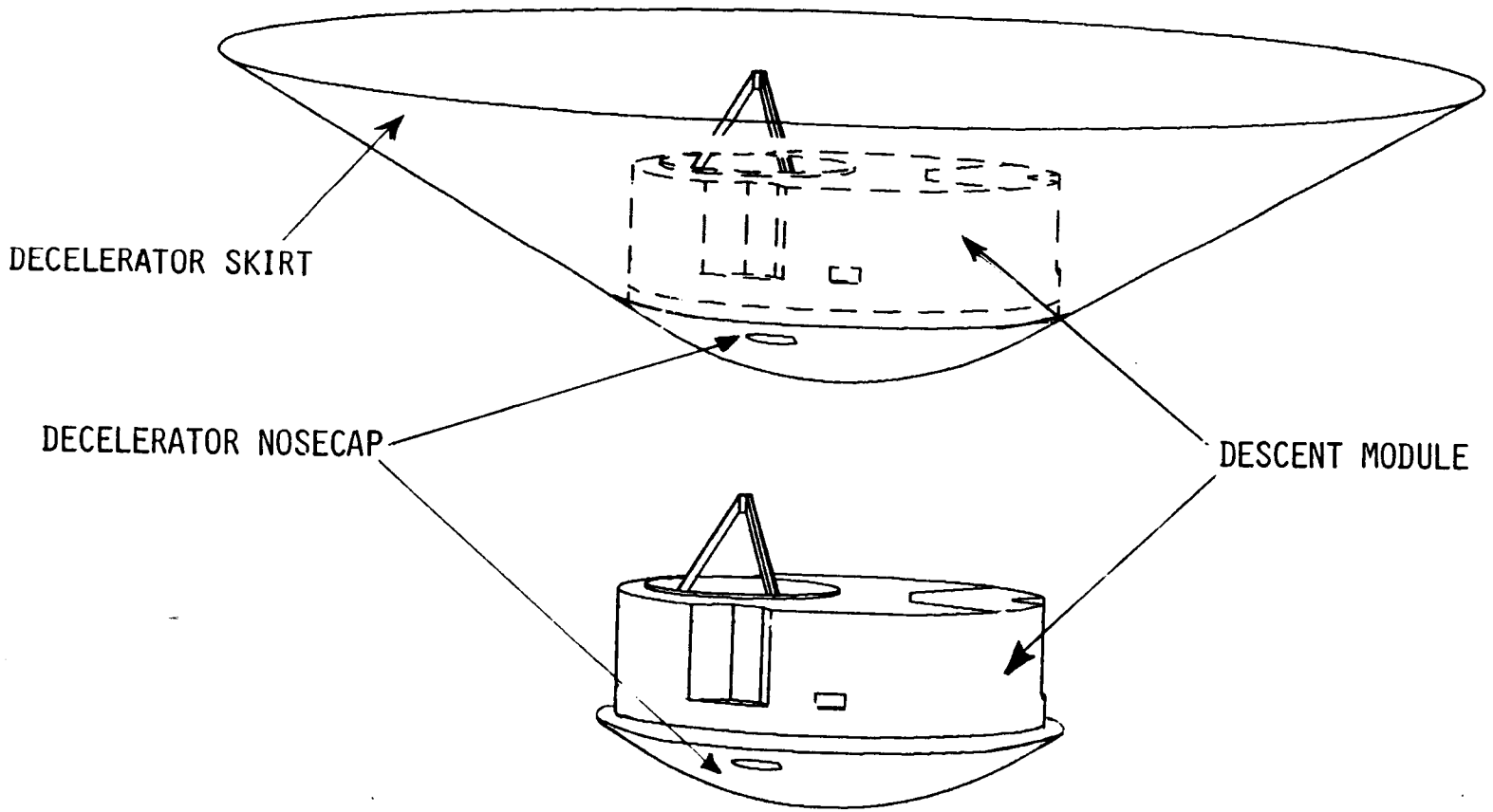

FIGURE 3.1-5

TITAN PROBE ON MM II CARRIER (NOSE ATTACHMENT)

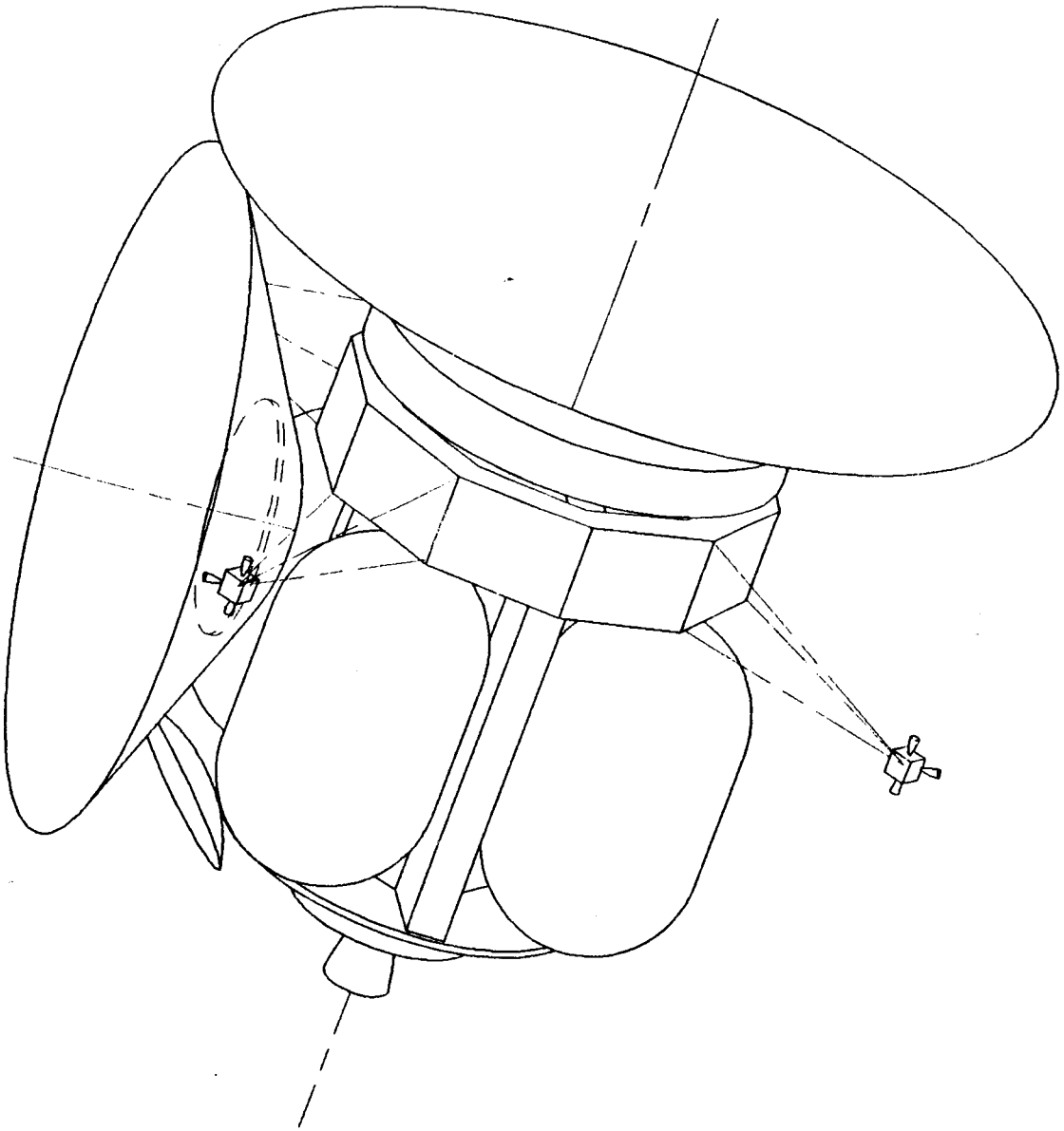

FIGURE 3.1-6
PROBE/CARRIER INTEGRATION - TOP VIEW

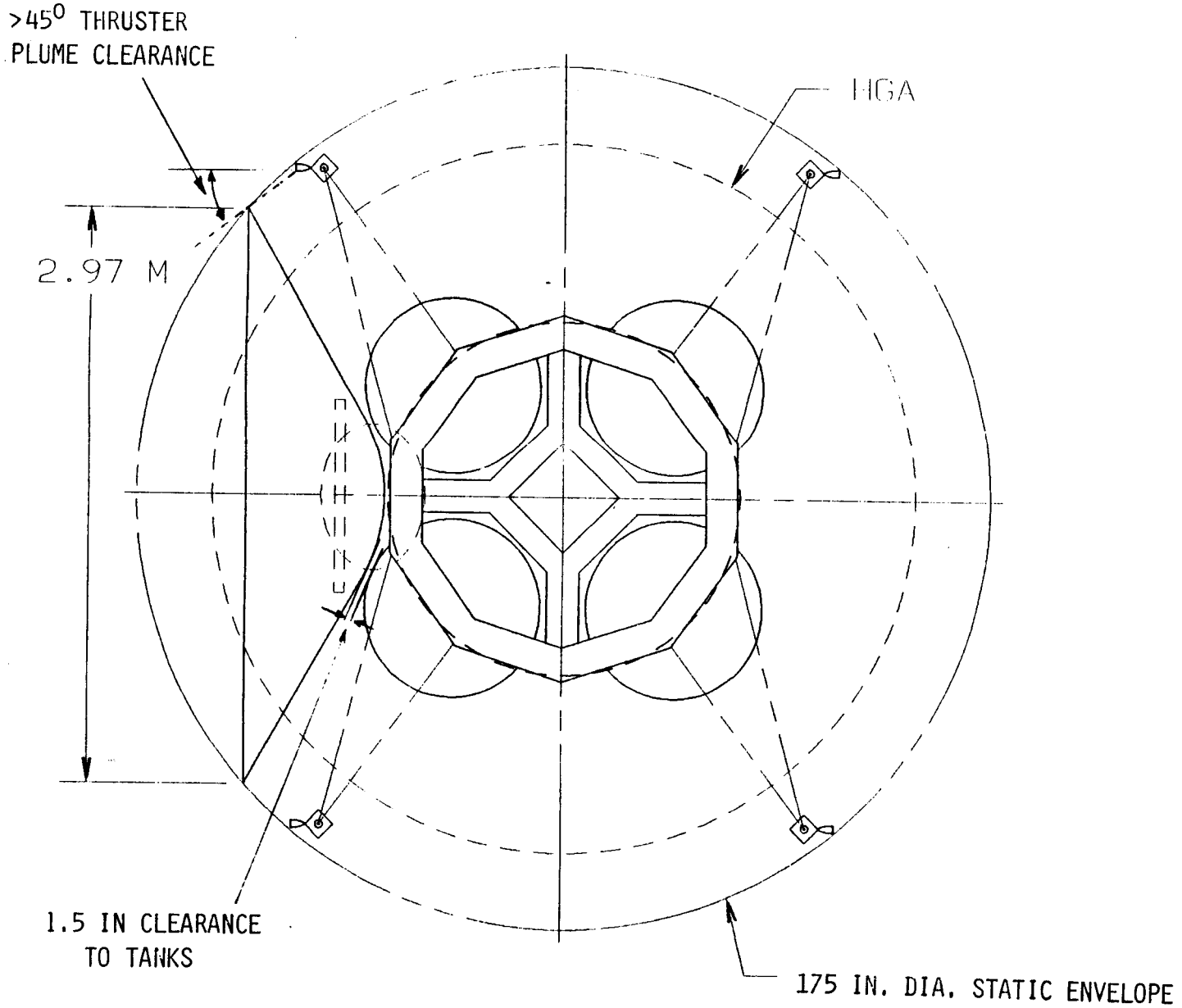

FIGURE 3.1-7
PROBE/CARRIER INTEGRATION - SIDE VIEW

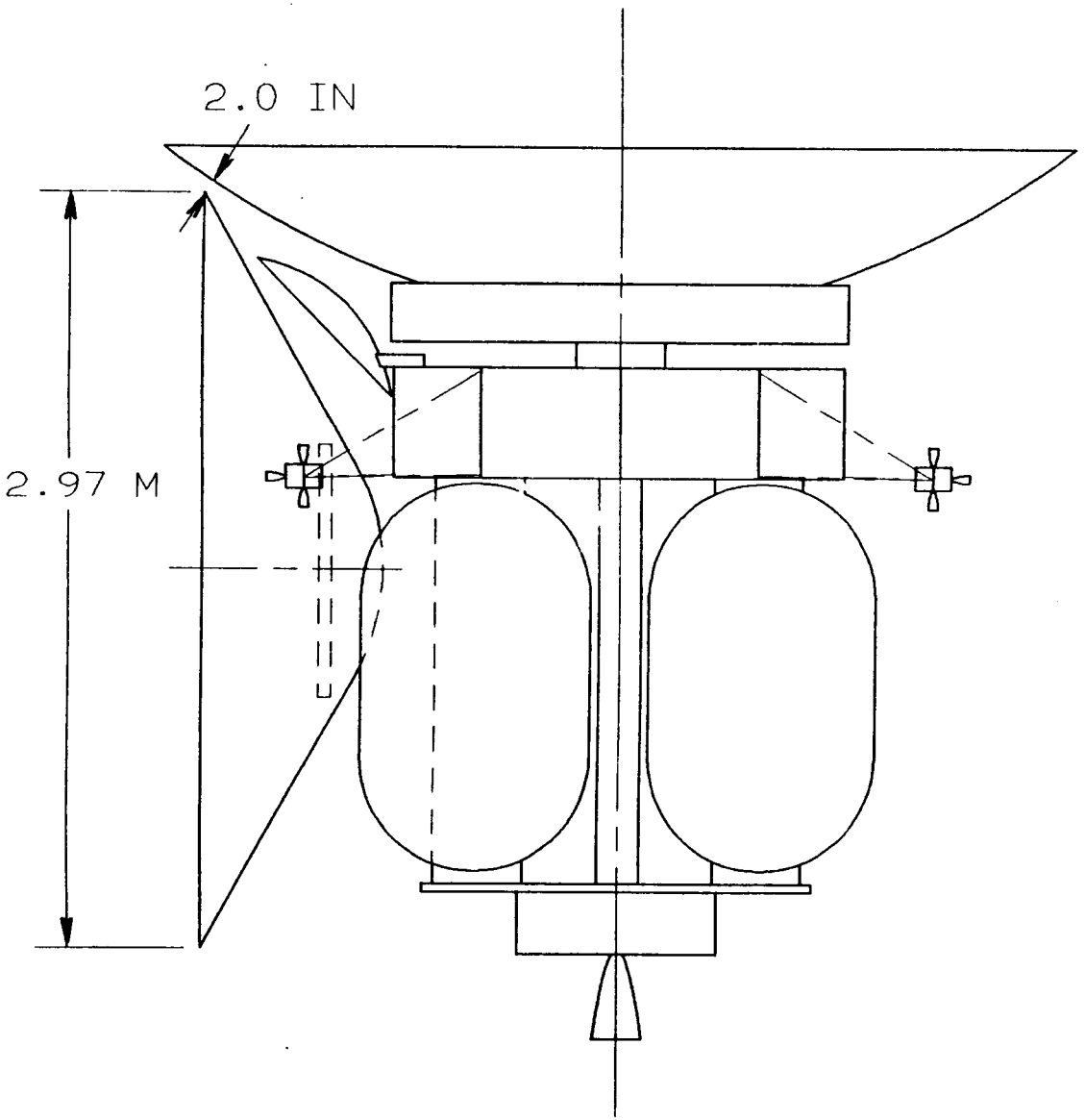

FIGURE 3.1-8
PROBE/CARRIER INTEGRATION - VIEW LOOKING INTO PROBE

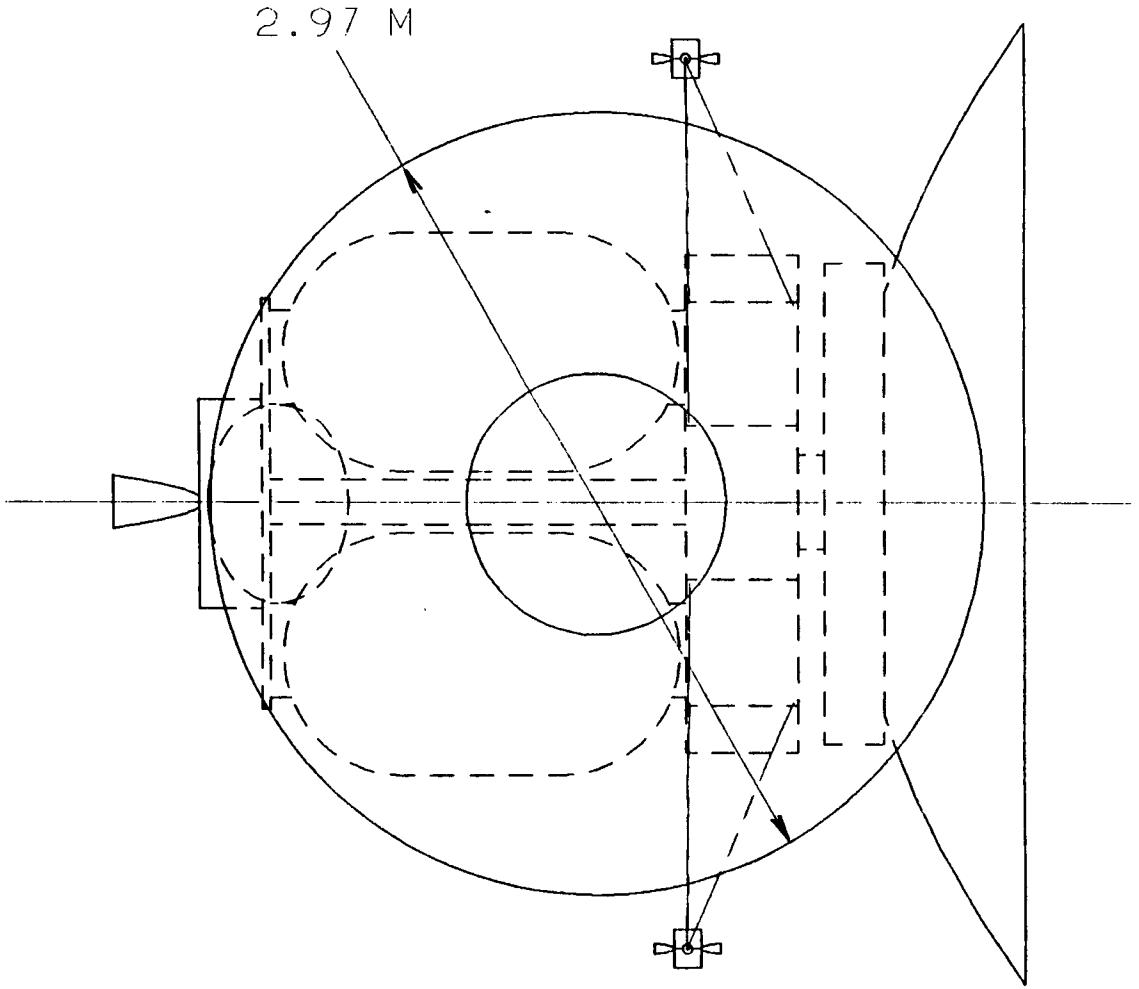

FIGURE 3.1-9

DECELERATOR TO DESCENT MODULE INTEGRATION TOP VIEW

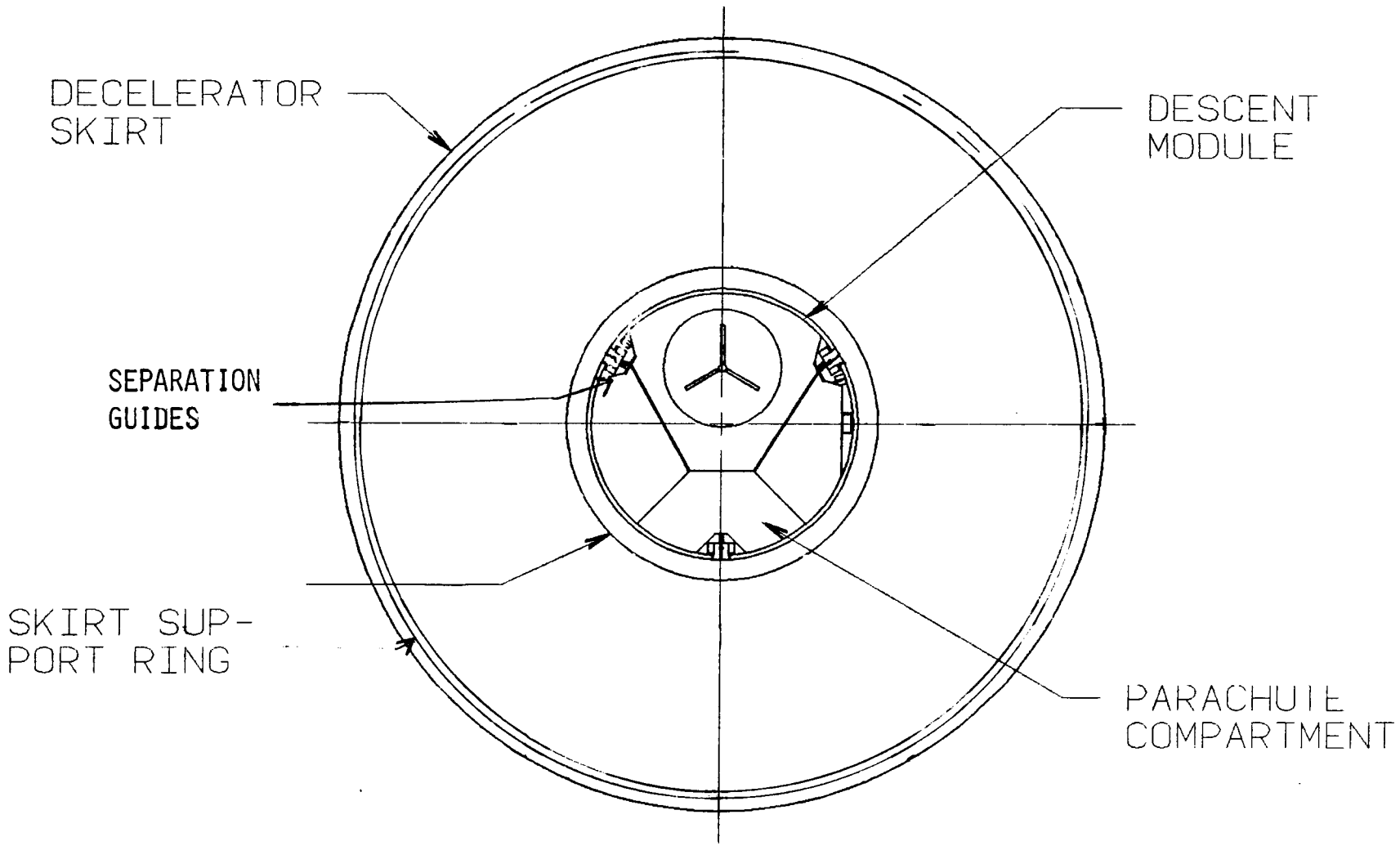

FIGURE 3.1-10:

DECELERATOR TO DESCENT MODULE INTEGRATION SIDE VIEW

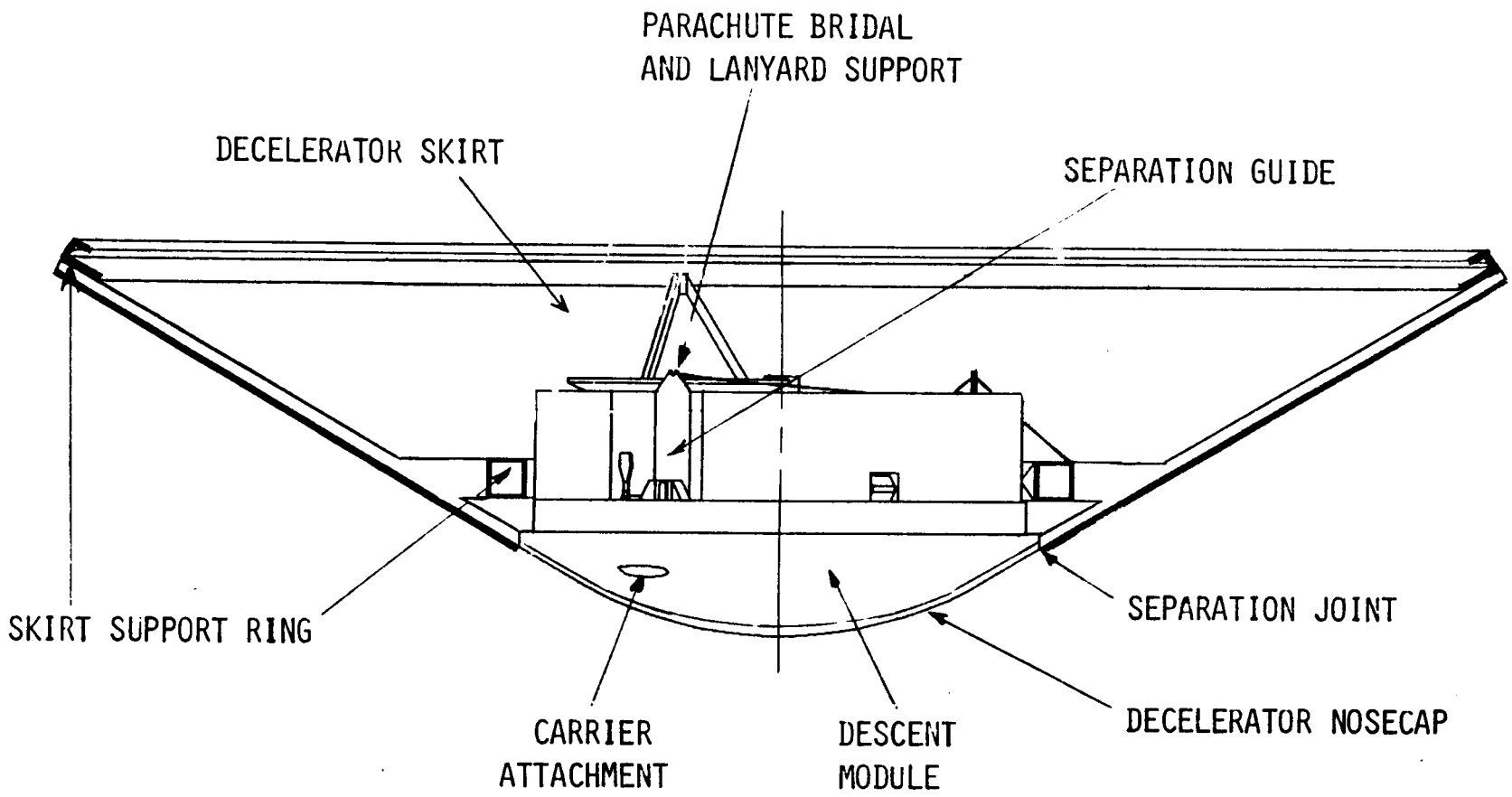

3.2 Thermodynamics

Model Verification

The Titan Probe entry regime falls within the range of previously-developed models for spherically-blunted cone bodies used on Pioneer Venus, Galileo Probe, Viking, and classified missions. However, much of the existing data base applies to entries in air or other atmospheres that differ from Titan's. In addition, the Titan entry extends over a longer than typical duration.

Approximate analytic models exist for simulating the aerothermodynamics of the Titan entry, but they assume the parameters of an air atmosphere. However, NASA/Langley developed more exact entry models for outer planet probe studies which assumed 90% nitrogen/10% methane atmospheres, Tiwari, 81.

Comparison of the air model with the Langley results verifies its applicability for the Titan analysis. As shown in Figure 3.2-1, the models predict similar heating rates, with the air model being conservative toward the end of the 6 km/sec entry. Entries using lower ballistic coefficients should differ by less. Therefore, the Titan Probe aerothermodynamics analysis can safely use existing approximate solutions developed for entries in air atmosphere.

Entry Heating

Figure 3.2-2 shows a heating rate pulse for a typical Titan entry. While the maximum heating rate is low, about 30 BTU/ft^2-sec, the relatively long (100 second) duration causes a significant integrated heat load.

Figure 3.2-3 shows the dependence of the heat load on ballistic coefficient and entry path angle. Although steeper trajectories increase the peak heating rate, they alleviate the integrated heat load, simplifying the heat shield and internal insulation. Since the Titan entries present only mild heating rates which do not drive the design, the thermodynamics favor a steep entry.

Material Selection

Heating rates on the outer portions of the decelerator decrease with increasing distance from the nose, reaching about 60% of the stagnation point values at the edge of the skirt (Figure 3.2-4). Tests performed for the Viking aeroshield configuration in air and carbon dioxide verified the analytic model used to predict these heating rates.

The mild heating rates allow either an ablative or heat sink nose cap design and do not require ablation of the skirt material although an ablative skirt has been chosen due to its minimum mass. Figure 3.2-5 shows the amount of solid beryllium needed at the stagnation point for 500° and 1000° backface temperatures as a function of the integrated heat load. Typical entries require 1.5 to 2 cm thickness at the stagnation point.

Although the thick beryllium heatsink nosecap can provide adequate stagnation point heating protection, a thin beryllium cap backed by carbon foam weighs less and provides comparable thermal protection in the same volume. Figure 3.2-6

shows the performance of the carbon foam insulation with a 3.7 mm beryllium shell. With a shell this thin, the stagnation point temperature responds rapidly to the heating pulse (Figure 3.2-7), but the 4.9 cm of carbon foam keeps the internal temperature below 450 ^{o}K.

The decelerator skirt experiences much milder heating loads than the nose. Figure 3.2-8 shows the demands on heat protection materials for several different entry missions; the Titan entry places minimal demands on the low density abalator materials. Use of ESM 1004-X RTV-impregnated quartz cloth, a typical low-density ablator, can adequatley protect the skirt. Figures 3.2-9 and 3.2-10 show the ESM thickness required to maintain the aluminum substrate temperature below 450 ^{o}K, accounting for the heat sinking effects of the substrate. Figure 3.2-11 shows the response of the substrate to the entry heat pulse. The ESM material, used for backface protection on many Earth reentry vehicles, avoids the mass and thermal expansion problems of metals. However, the RTV develops glass-like properties at low temperatures that require further study.

In addition to the protection on the forward side of the skirt, the back requires a closeout made of uncompressed Litaflex. This closeout lines the inside of the skirt and covers the back of the descent module. Figure 3.2-12 shows the required thickness.

Conclusions

The existing entry aerothermodynamics models apply to the Titan Probe entries and predict mild heating rates. Steeper entries minimize a relatively long heating pulse. Beryllium proves practical for local heat sinks or the entire nosecap; ESM-1004-X material provides adequate low-mass protection for the skirt.

FIGURE 3.2-1 :
MODEL VERIFICATION -
COMPARISON OF APPROXIMATE AND "EXACT" PREDICTIONS

- APPROXIMATE STAGNATION POINT EQUATION FOR AIR
- "EXACT" SOLUTION FROM NASA LRC (90% N_2, 10% CH_4)
- $\theta_C = 45^o$; $R_N = 0.2$ M
- $\beta = 800$ KG/M^2 ; $\gamma = 45^o$

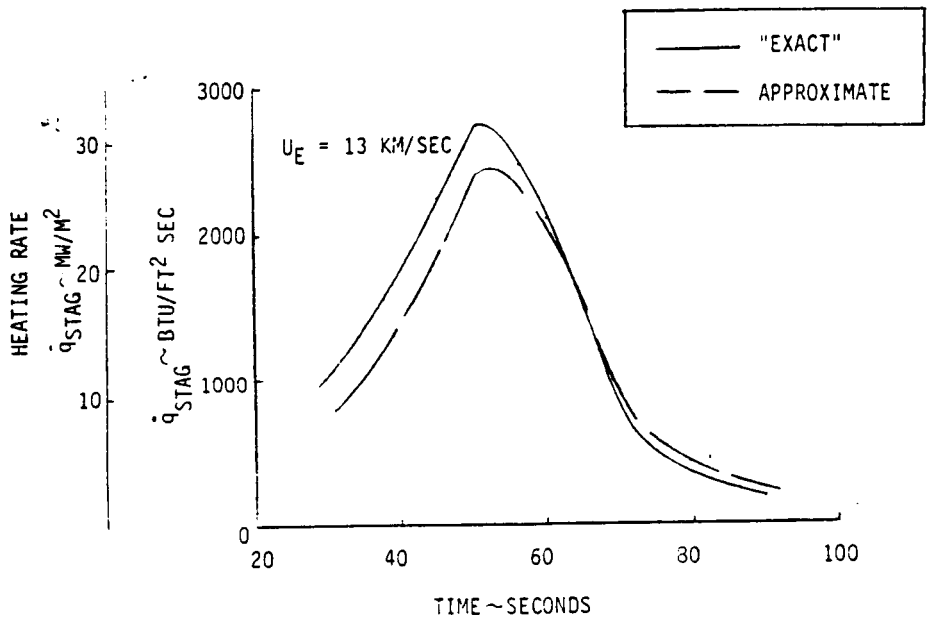

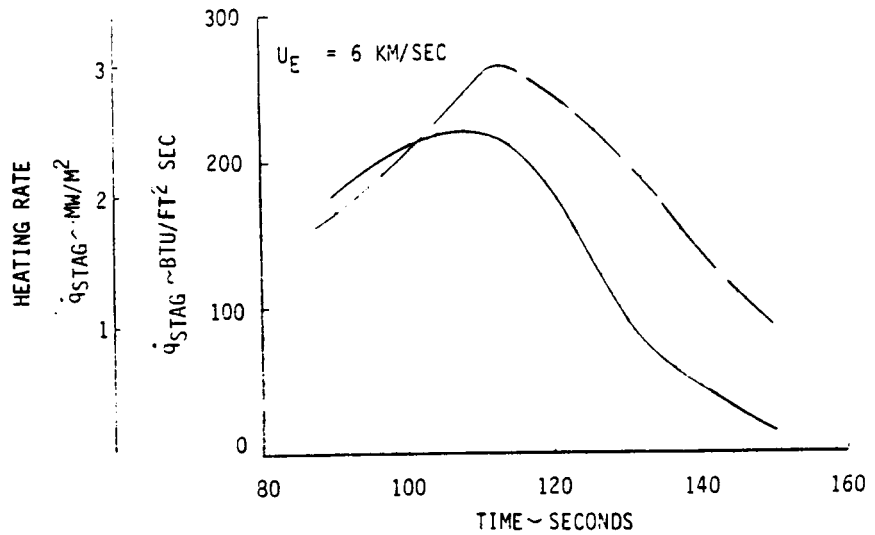

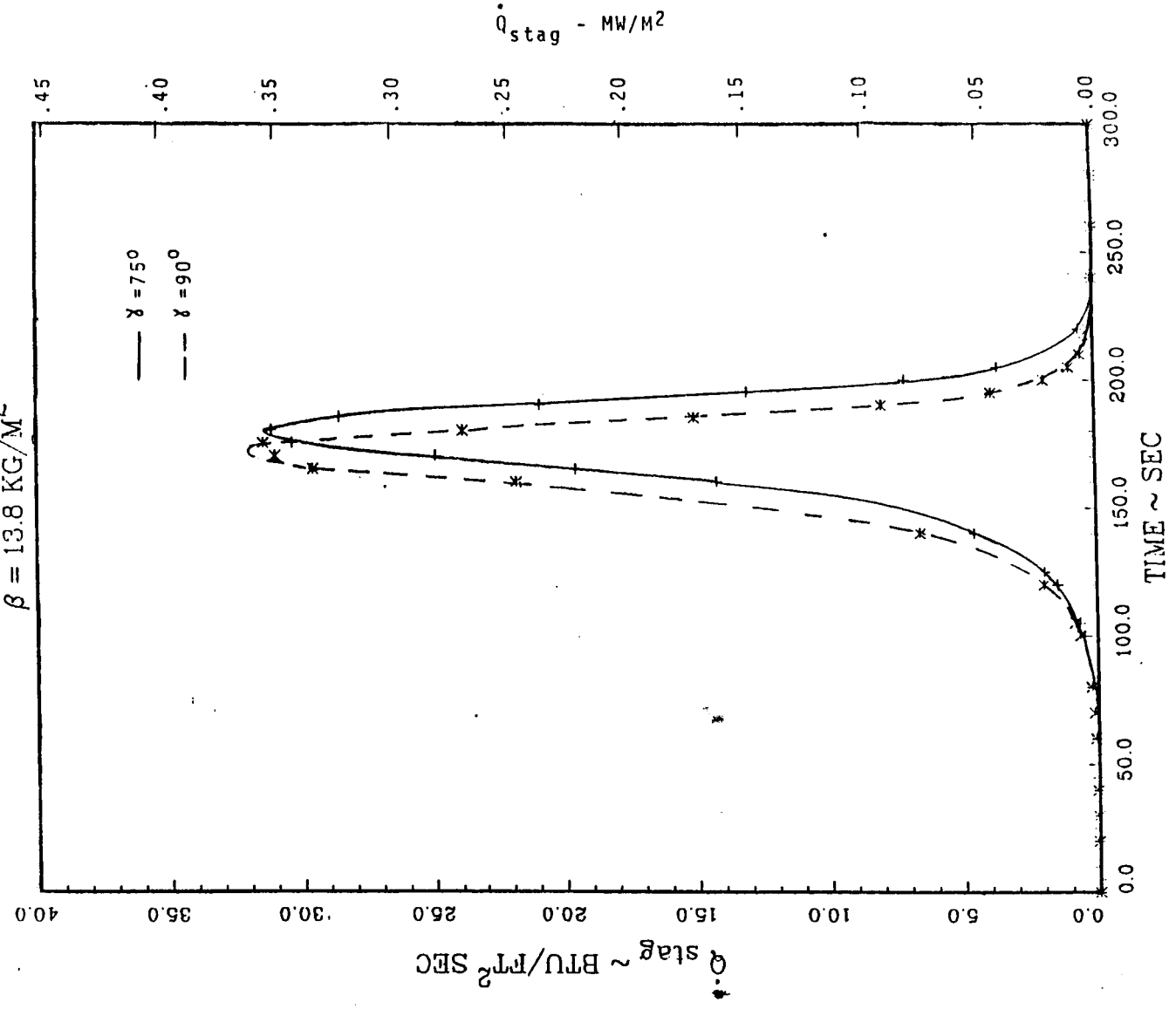

FIGURE 3.2-2:
TITAN PROBE HEATING
STAGNATION

FIGURE 3

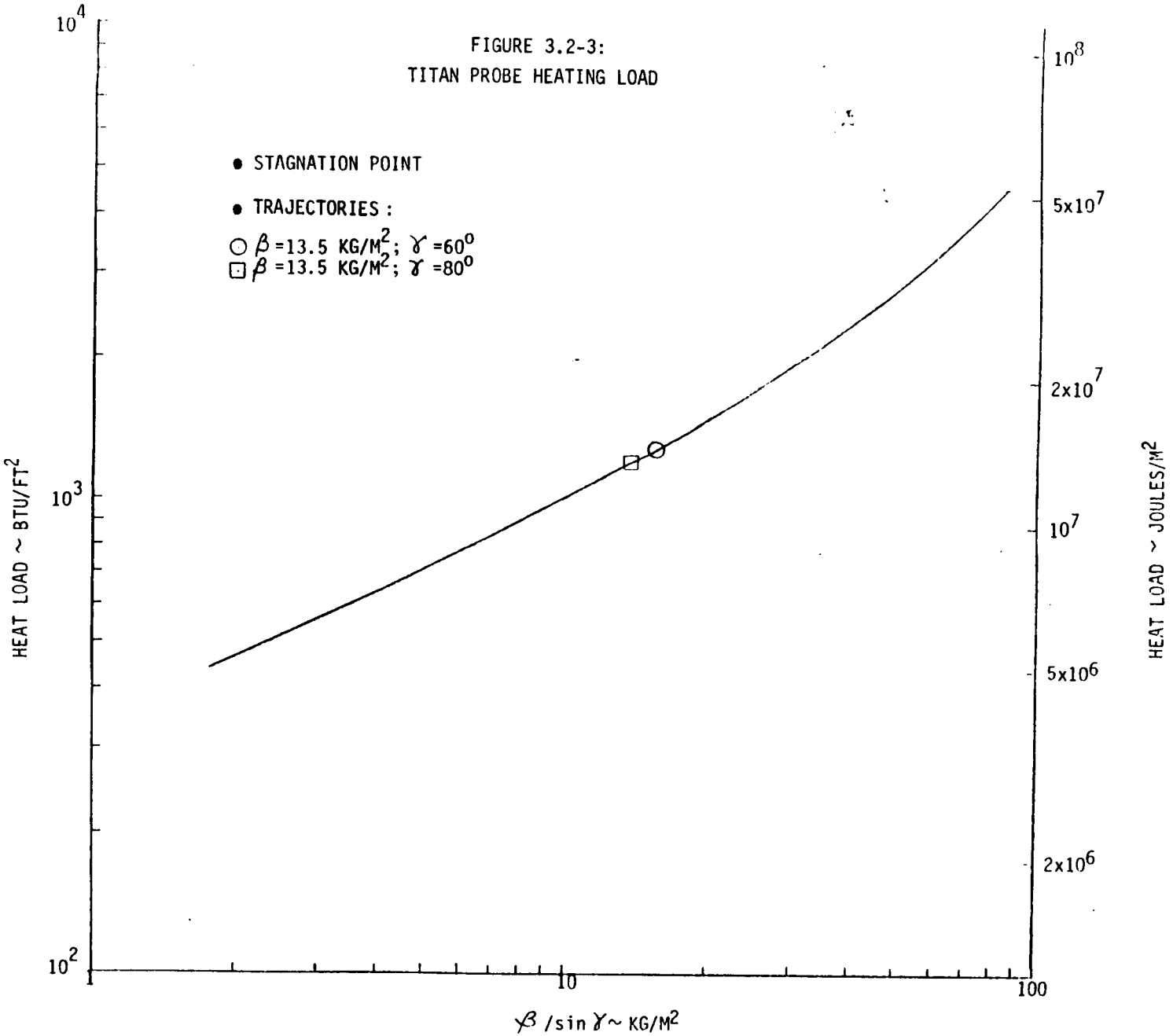
FIGURE 3.2-3:
TITAN PROBE HEATING LOAD
• STAGNATION POINT
• TRAJECTORIES :
○ β =13.5 KG/M2; γ =60°
□ β =13.5 KG/M2; γ =80°
HEAT LOAD ~ BTU/FT2
HEAT LOAD ~ JOULES/M2
10^4
10^3
10^2
10^8
5x10^7
2x10^7
10^7
5x10^6
2x10^6
10
100
β /sin γ ~ KG/M2

FIGURE 3.2-4:

CALCULATED VS. MEASURED VIKING CONFIGURATION

HEAT TRANSFER DISTRIBUTIONS

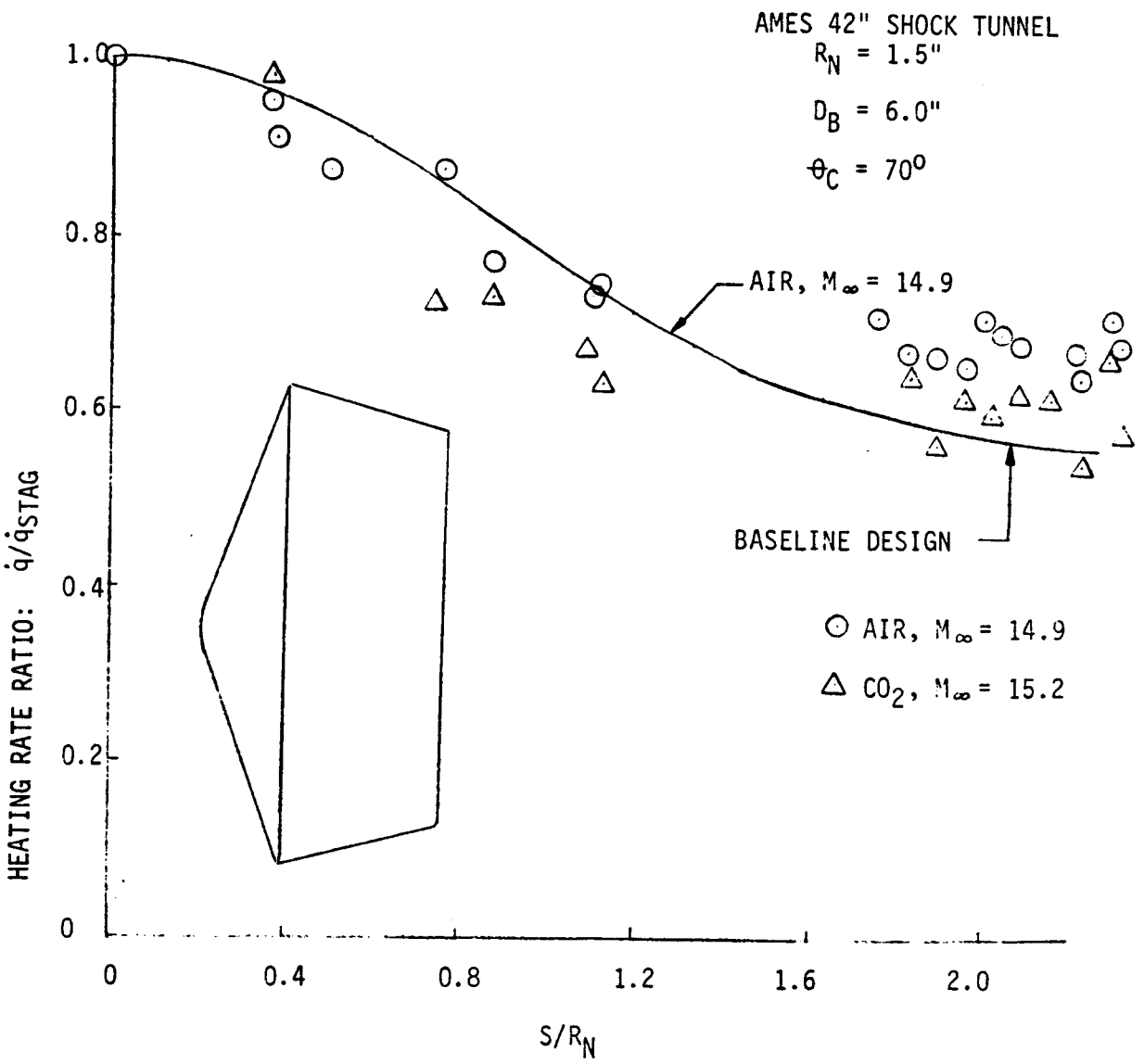

FIGURE 3.2-5:

TITAN PROBE BERYLLIUM REQUIREMENTS

AT STAGNATION POINT

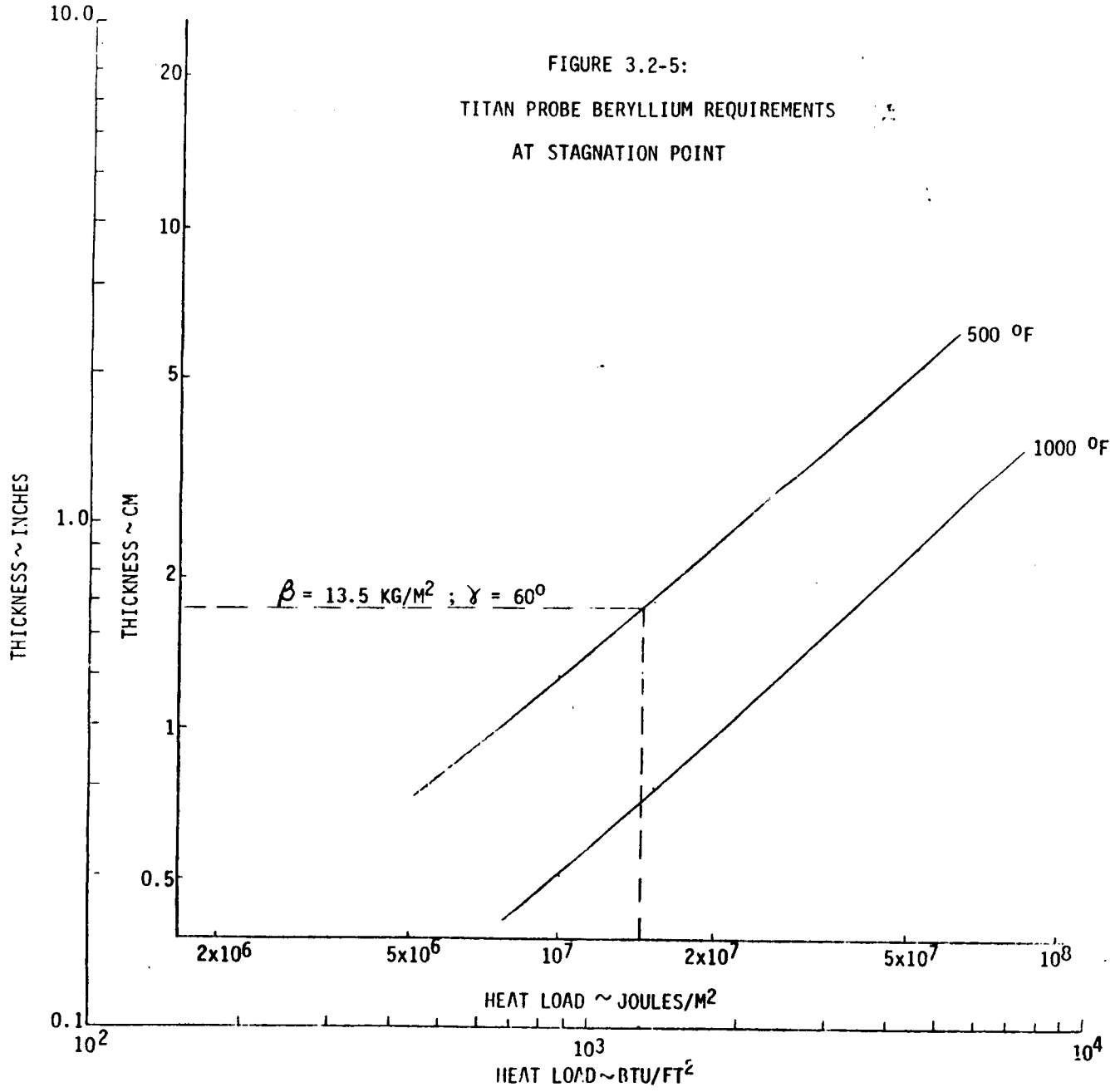

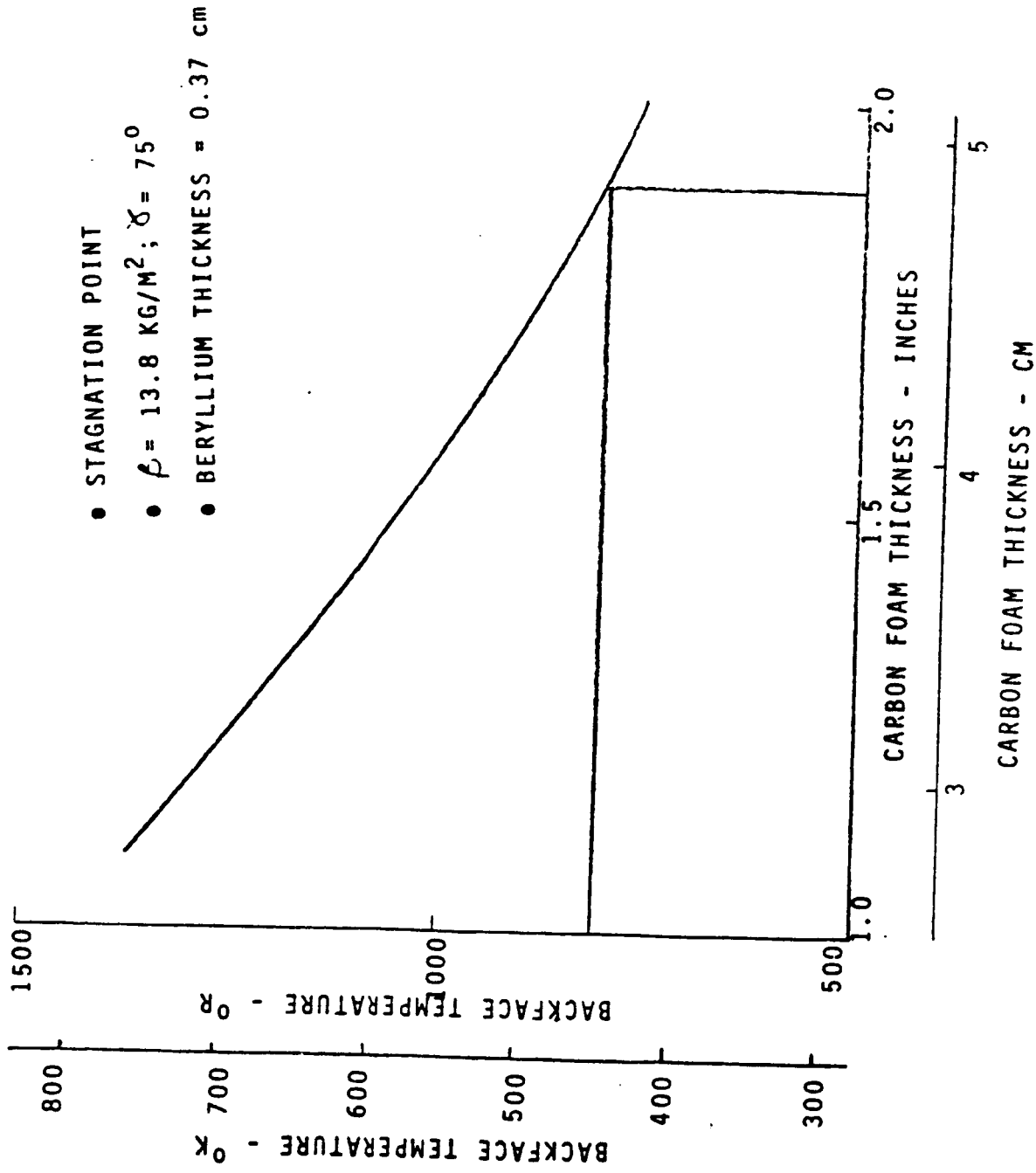

FIGURE 3.2-6: PREDICTED CARBON FOAM BACKFACE TEMPERATURE VS. THICKNESS

FIGURE 3.2-7 : BERYLLIUM SURFACE TEMPERATURE HISTORY

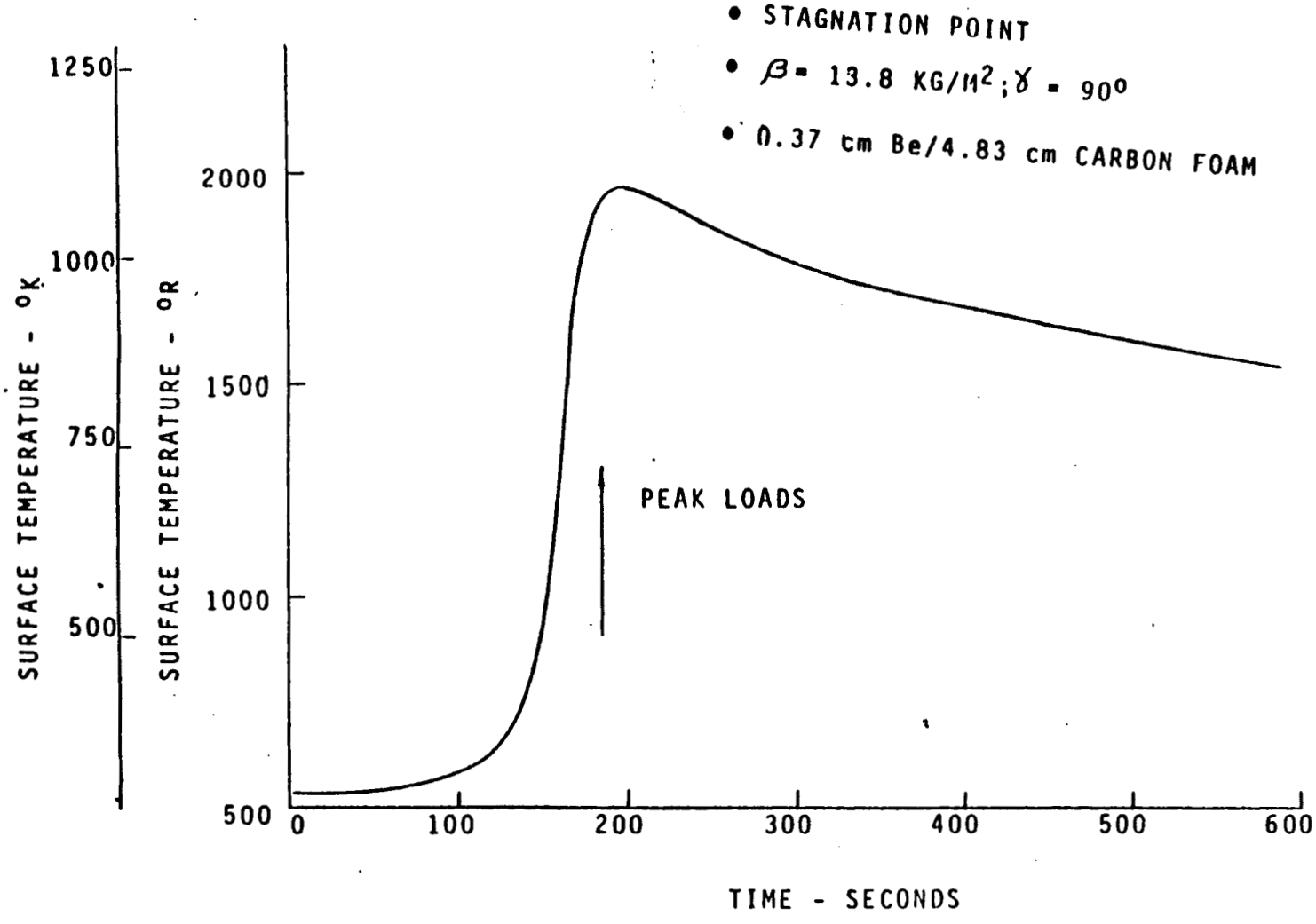

FIGURE 3.2-8: Thermal Protection Material Selection

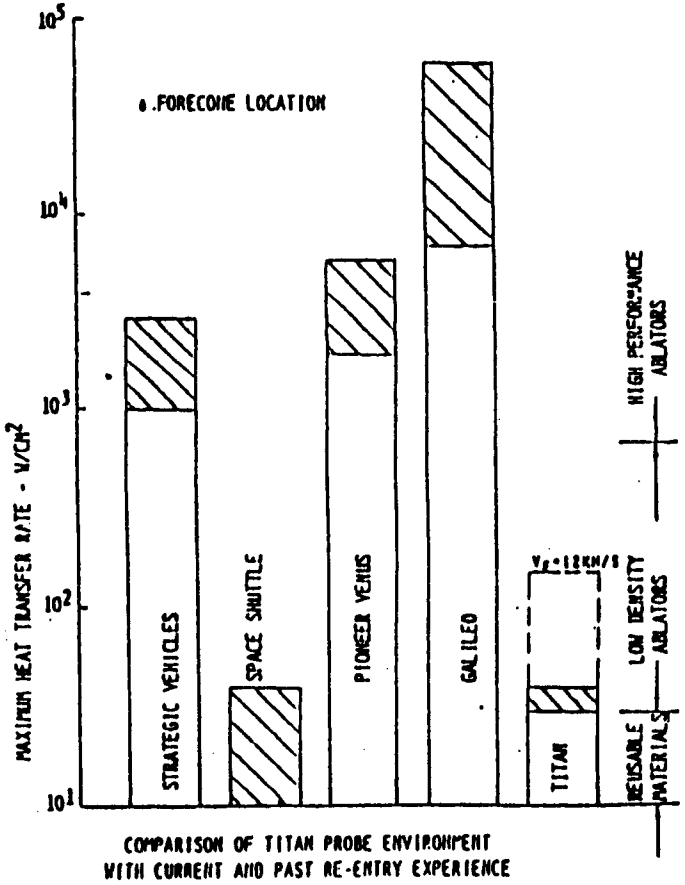

COMPARISON OF TITAN PROBE ENVIRONMENT WITH CURRENT AND PAST RE-ENTRY EXPERIENCE

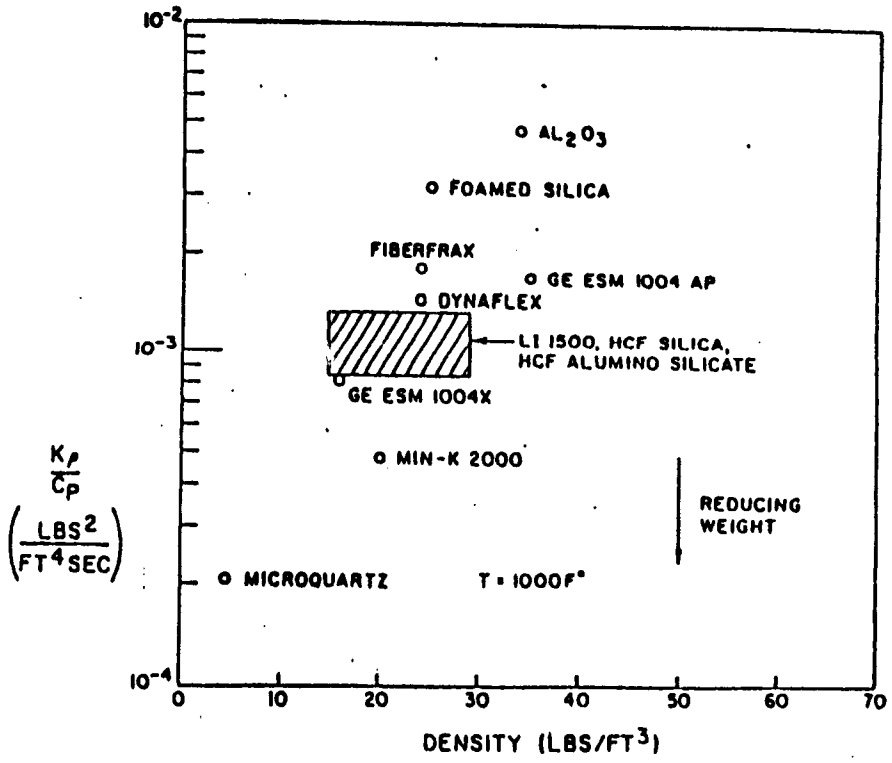

Weight Minimization for Insulation Materials

FIGURE 3.2-9 ESM BACKFACE TEMPERATURE VS. THICKNESS FOR VARYING ALUMINUM STRUCTURE THICKNESS

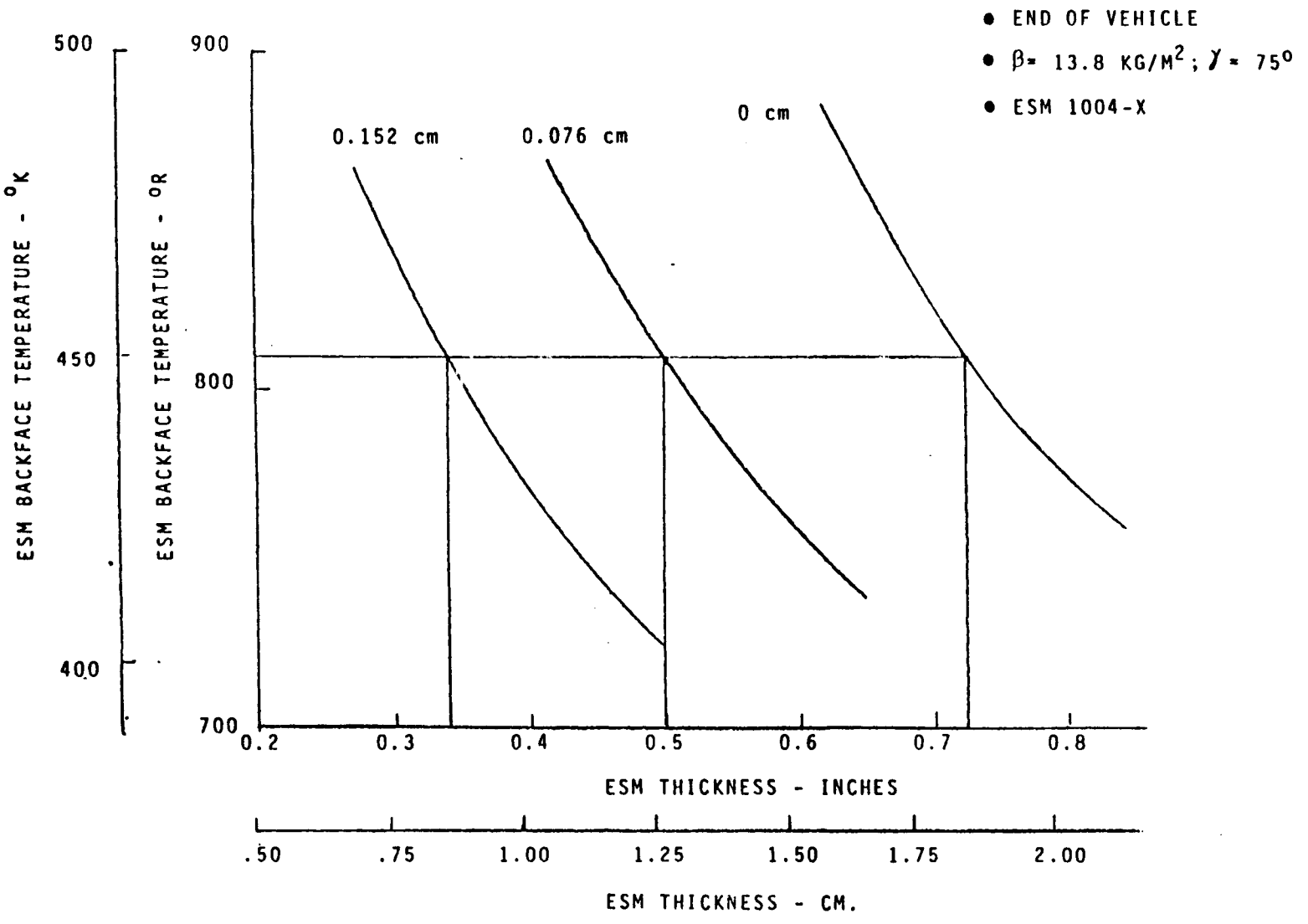

FIGURE 3.2-10: ESM REQUIREMENT VS. ALUMINUM STRUCTURE THICKNESS

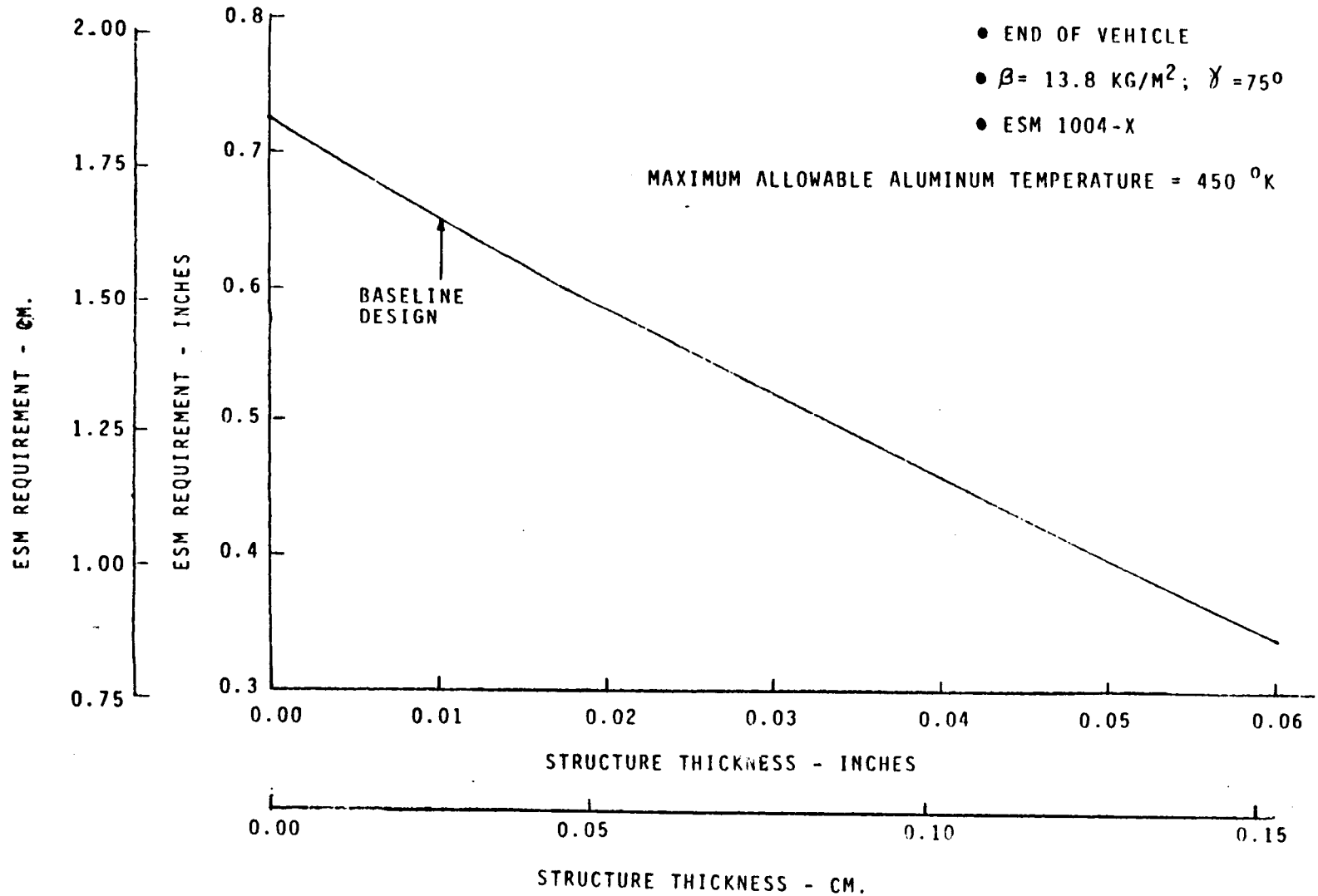

FIGURE 3.2-11 ALUMINUM STRUCTURE TEMPERATURE HISTORY

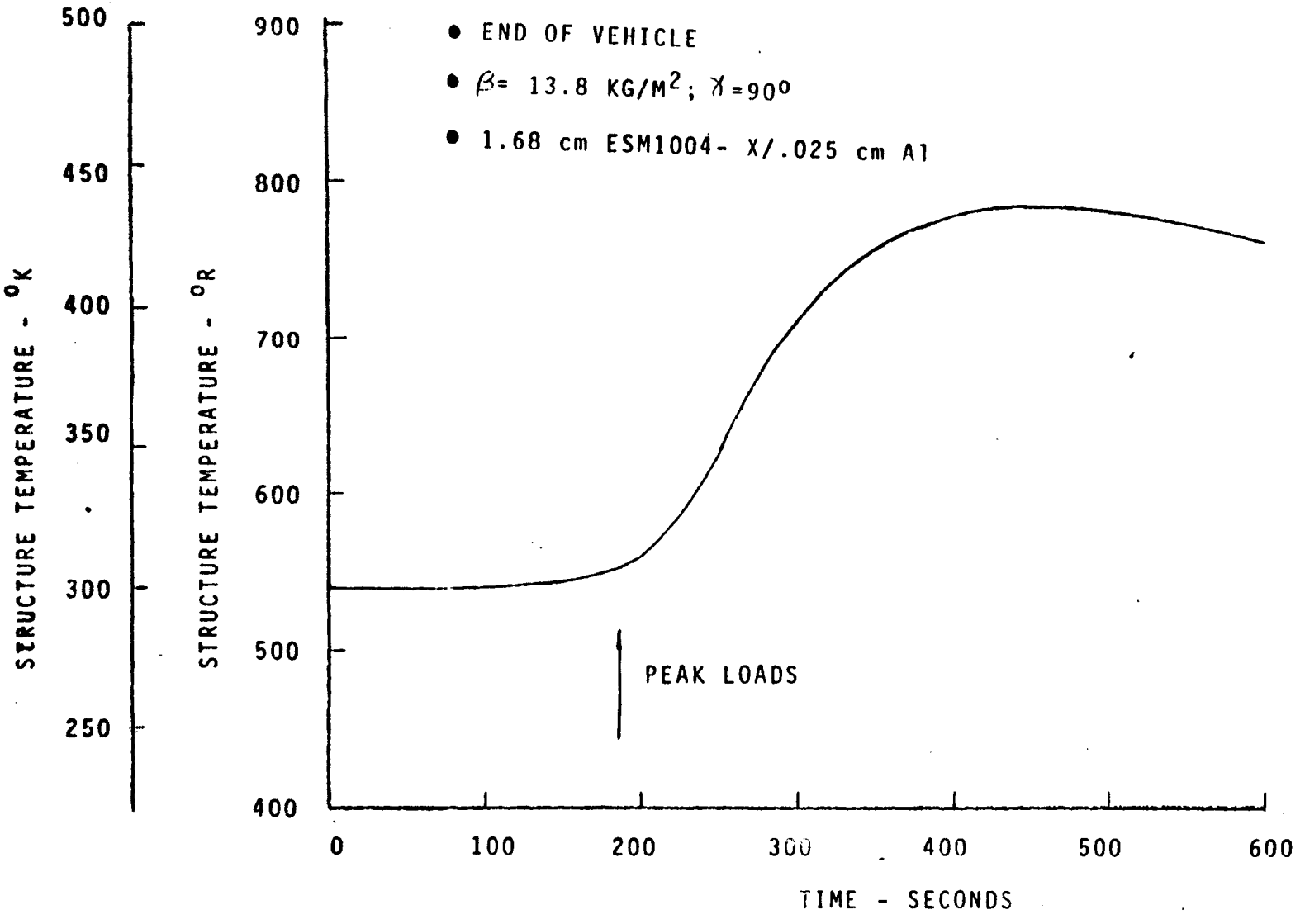

FIG. 3.2-12 THERMAL PROTECTION REQUIREMENT FOR VEHICLE BASE

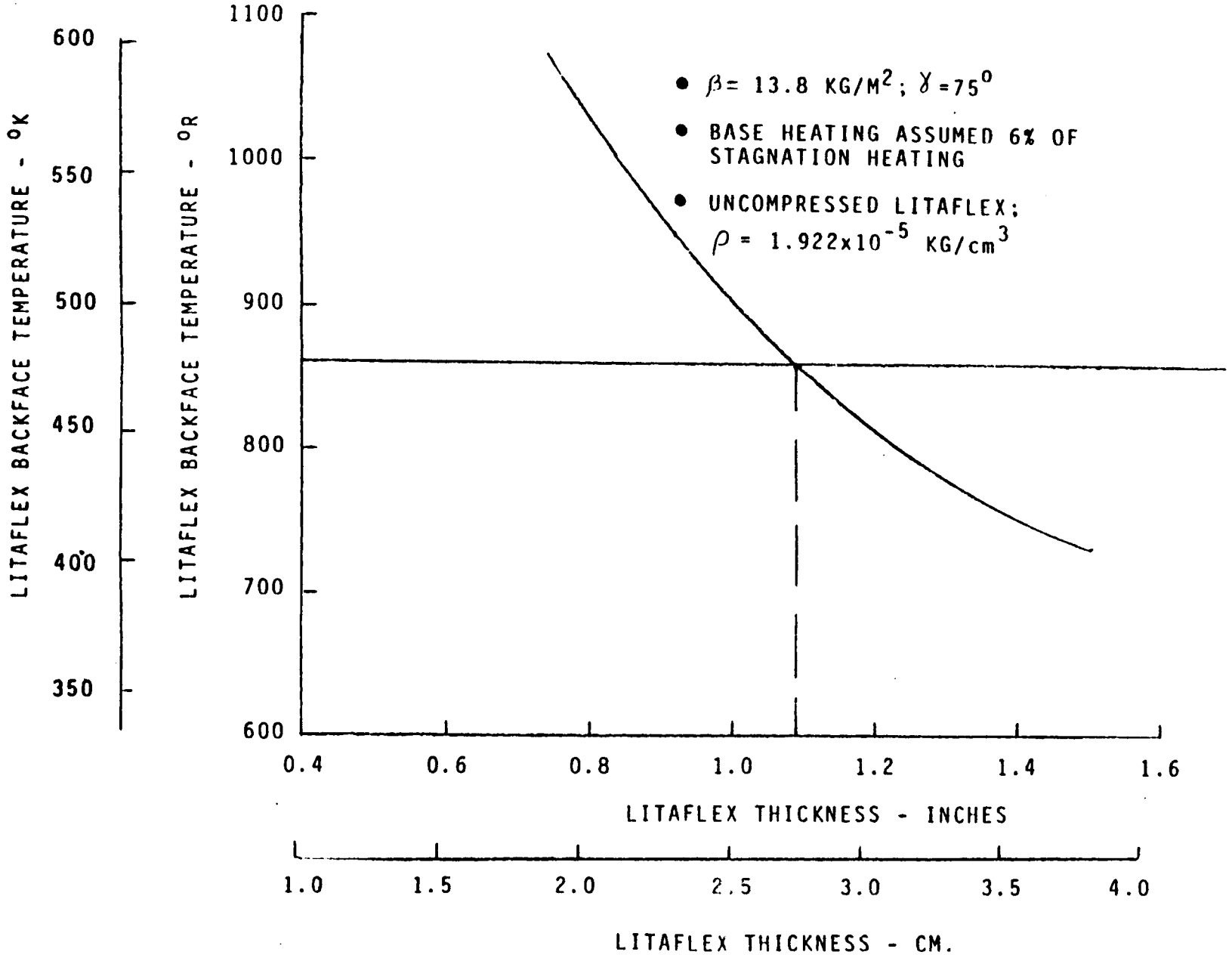

3.3 Aerodynamics

Entry Analysis

Using three-degree-of-freedom entry simulation, the dynamic pressure, heating rate, deceleration loads, and Mach 1 altitude for path angles from -40 to -90 degrees and ballistic coefficients from 8 to 60 kg/m^2 have been determined. Figure 3.3-1 shows the effect of path angle and ballistic coefficient on the deployment altitude and deployment dynamic pressure. Reducing the entry angle from straight-in to -60^o has a minor effect on sonic altitude. Although more shallow entries further raise the Mach 1 altitude, they present communications, targeting, and heating concerns that mitigate this advantage.

Figure 3.3-2 shows the variation in velocity, altitude, dynamic pressure, and axial load during a typical entry. Table 3.3-1 summarizes the key parameters for entries with flight path angles of -45, -60, and -90 degrees; Section 2 describes the entry analysis in more detail.

Entry Dynamics

Separation analysis (section 5.1) and six degree-of-freedom simulations verify the proper attitude of the Probe throughout coast and entry. Spin stability imparted at separation preserves throughout coast the initial attitude set by the carrier. The spin rate must be large enough to provide low coning due to separation tipoff, but small enough to

1) allow practical generation by a simple spin-up mechanism
2) allow angle of attack convergence by aerodynamic forces before peak heating, and
3) give an acceptably small angle of attack at the onset of transonic instability.

Section 5.1 describes the separation attitude perturbations.

Aerodynamic forces during entry cause the Probe's initial angle of attack to converge toward the velocity vector at the time of peak heating. To facilitate the process, the separation attitude of the Carrier places the Probe in this nominal orientation. However, errors cause some misalignment at entry. Figure 3.3-3 shows the attitude convergence for arbitrary initial misalignment of 6 and 12 degrees, several times larger than predicted values. Although a slower spin rate aids the convergence, in all cases the angle of attack drops to less than 4^o before peak heating occurs. Angles this small do not affect decelerator performance during the heating; little or no ablation occurs during the Titan entry.

Aerodynamic forces also cause potential roll and transonic instabilities (Figure 3.3-4). The slow spin rate minimizes the destabilizing roll effects; a 10 rpm entry shows mild divergence in angle of attack at a slightly higher altitude than the entry with a 5 rpm rate. However, the higher spin rate minimizes the effect of transonic instability. The simulations show little angle of attack divergence in all the cases studied, so spin rates of 5 to 10 rpm are acceptable for these entries. The final choice of spin rate depends on the separation mechanism design and induced errors.

TABLE 3.3-1

BASELINE 60 DEGREE SPHERE-CONE ENTRY PARAMETERS

Path Angle	Peak q_∞ (N/m^2)	Peak $\dot{q}s$ (BTU/ft^2s)	Peak Ax (Earth g's)	@ MACH=1 Time (sec)	@ MACH=1 Altitude (Km)
45	714	21.2	5.34	685	245
60	1858	29.7	13.94	335	207
90	2536	42.0	19.05	260	194

FIGURE 3.3-1:
HYPERSONIC BALLISTIC COEFFICIENT REQUIREMENTS FOR M=1

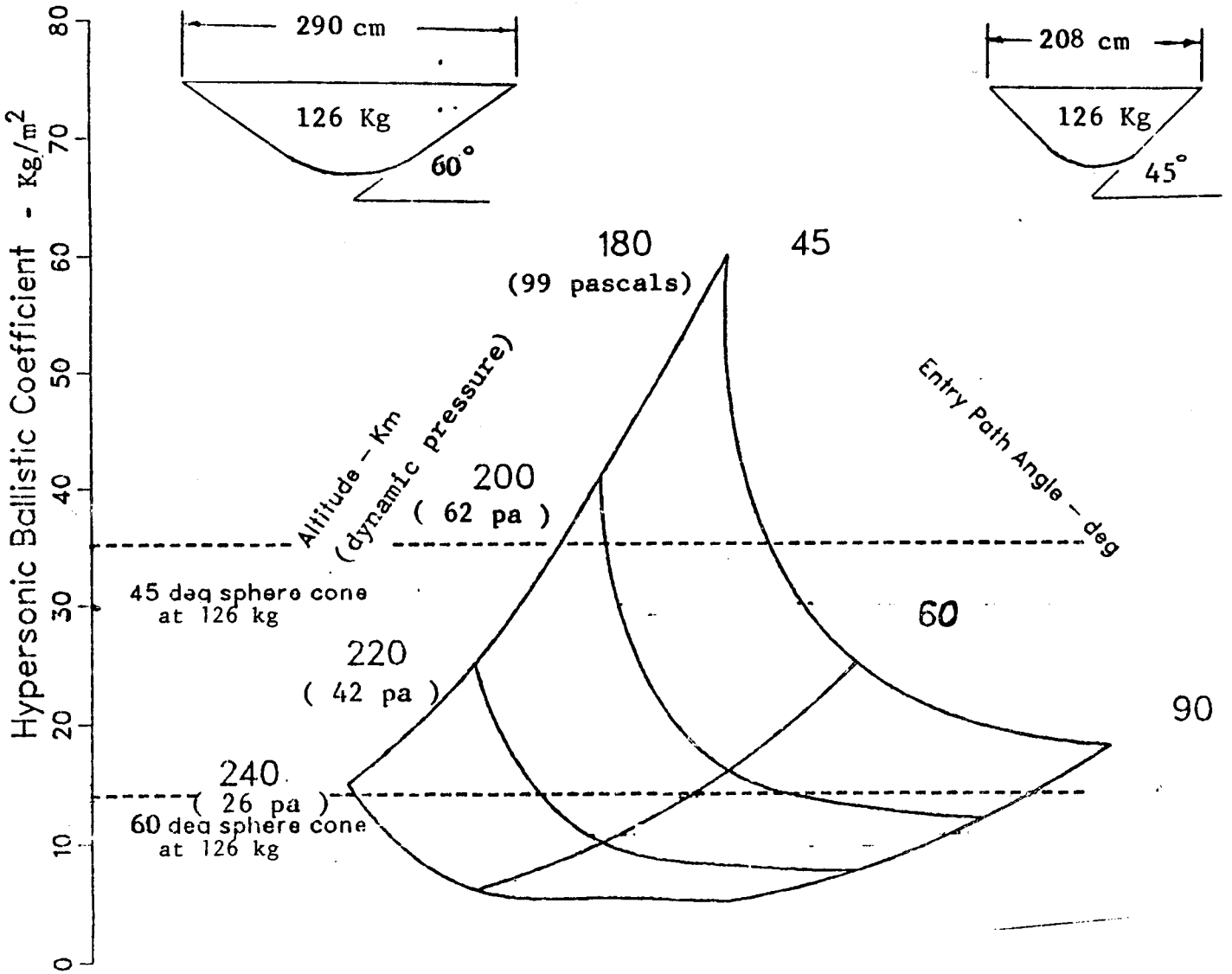

FIGURE 3.3-2

ENTRY TRAJECTORY PERFORMANCE (60^{o} PATH ANGLE)
60 DEGREE SPHERE-CONE, 290 CM BASE DIAMETER

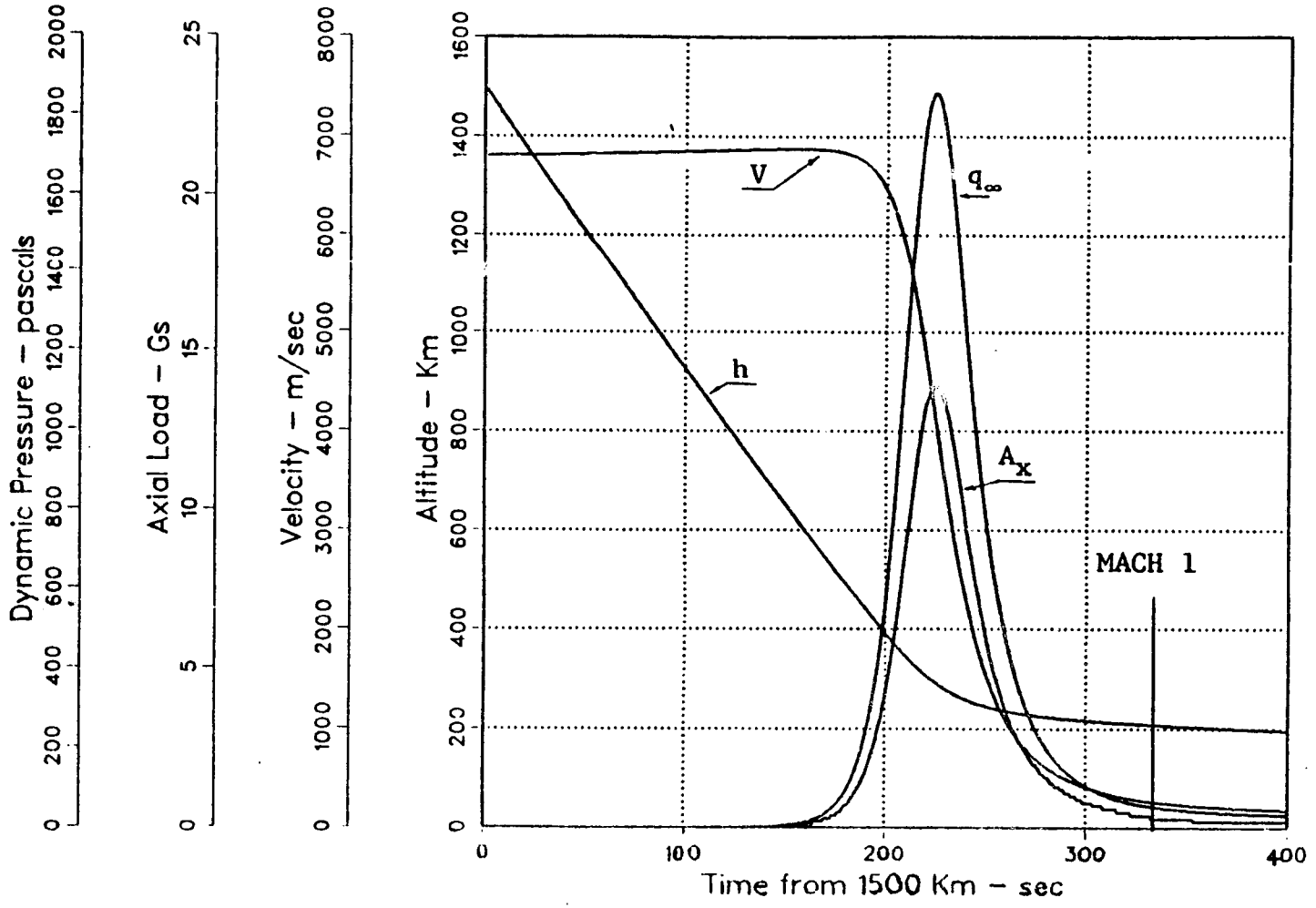

FIGURE 3.3-3

ENTRY ANGLE OF ATTACK CONVERGENCE

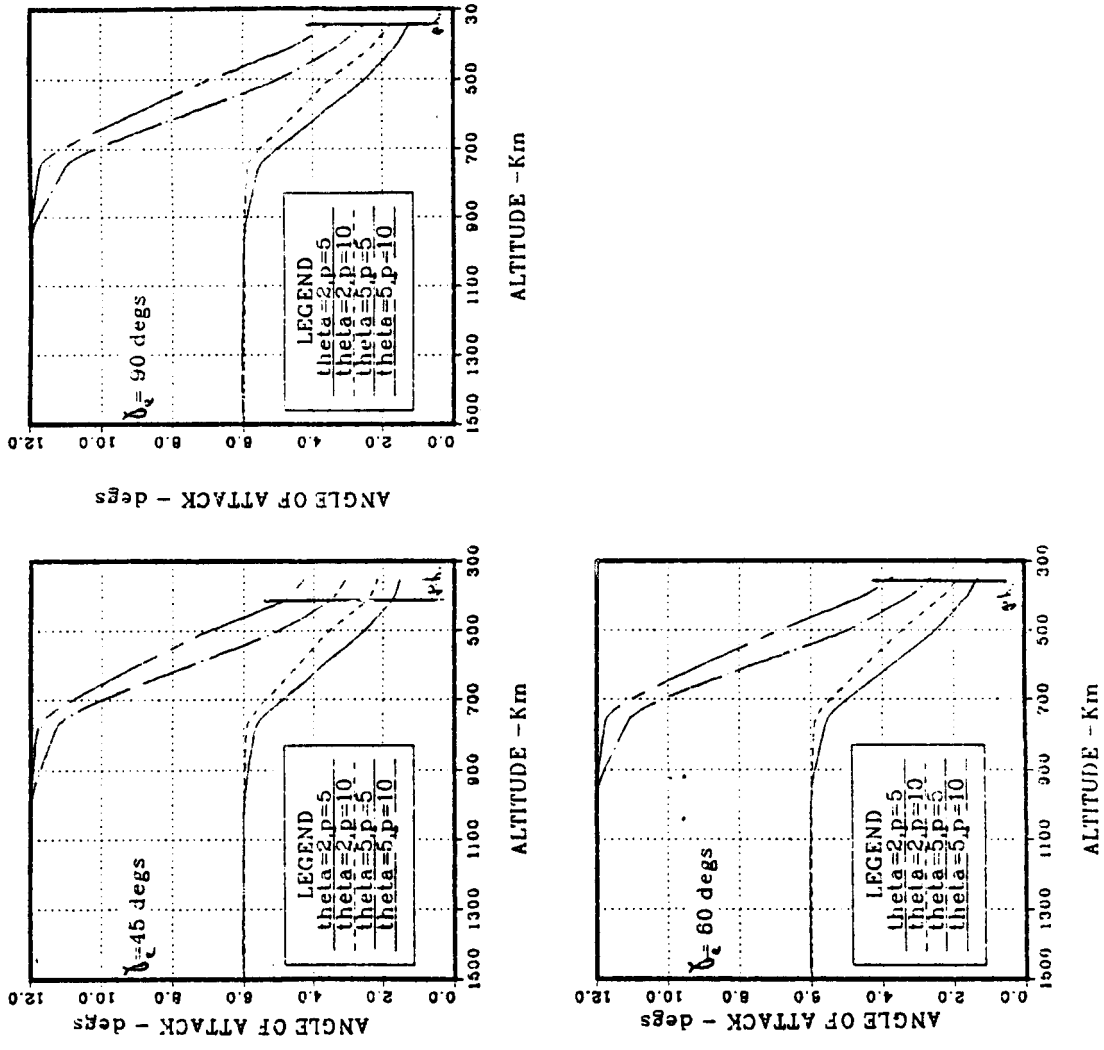

FIGURE 3.3-4:

45 DEGREE SPHERE-CONE CONFIGURATION DYNAMIC STABILITY

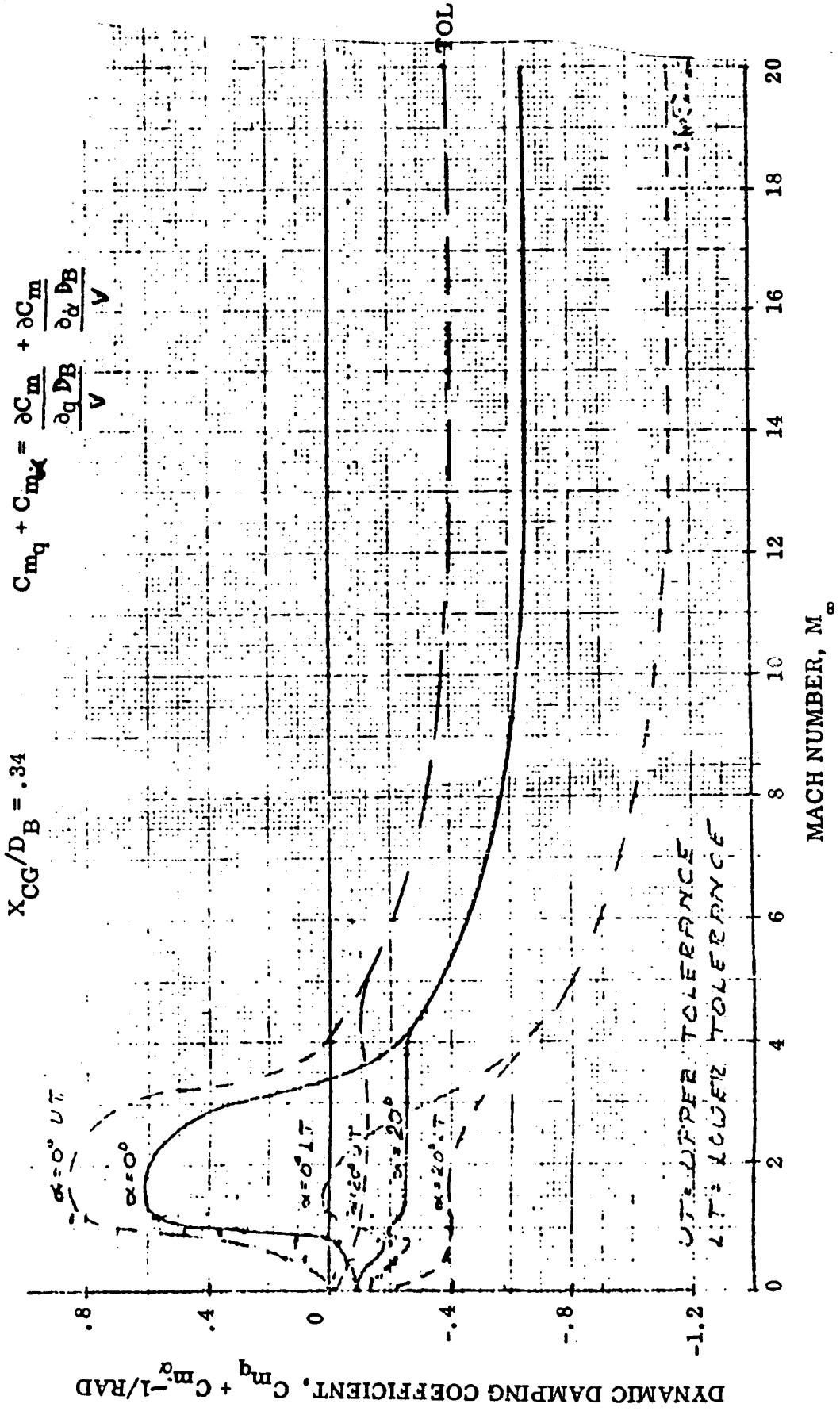

3.4 Staging and Parachute

Staging Sequence

The Probe's angular momentum during coast retains the entry attitude set by the Carrier at separation, aligning the spin axis with the velocity vector at the expected time of peak heating. Small attitude deviations do not affect the heat shield performance; low gyroscopic stiffness (5 to 10 rpm) ensures that aerodynamic torques cause the attitude to converge before peak heating.

For the baseline design, an initial jettison of the gas chromatograph inlet plug enables sampling in the transonic region, (at about 191 km altitude) immediately following peak heating. A sequence of staging events then exposes the remaining science instruments to Titan's atmosphere (Figure 3.4-1 and 3.4-2). These events occur after the Probe slows to subsonic speed (at about 182 km) to avoid the complications of supersonic deployments. For the optional design, a ballasted nosecap drops away from the rest of the Probe to expose the gas chromatograph inlet.

For either design, cutters sever the bolts attaching the decelerator skirt to the descent module equipment shelf. The lower ballistic coefficient causes the skirt to fall behind the descent module. Guides ensure separation clearance.

As the skirt falls behind, it pulls a tether which extracts the bagged parachute from its housing on the descent module, deploying the parachute bridal and risers and stripping the bag from the canopy. Because of the low dynamic pressure, canopy inflation takes longer than on the Galileo Probe or Pioneer Venus Large Probe, and analysis and simulation studies are required to assure limited descent module attitude excursions before full inflation. Once the skirt clears the descent module, instrument sensors deploy for forward view. The optional design allows a larger skirt ring diameter so most instruments can look forward without deployment. However, the larger ring and attachment brackets required to clear the fixed instrument inlets on the side of the Probe increase the skirt structure mass.

Separation Tradeoff

Although the forward release of the descent module results in the simplest hardware, a rearward extraction offers advantages of heritage and heat shield continuity.

As described above, the forward deployment of the descent module uses the inherent difference in ballistic coefficients, avoiding the need for an extraction parachute. The separating skirt pulls out the single descent parachute, although a mortar can deploy it. Forward release requires a seam in the heat shield where the skirt joins the nosecap.

A rearward extraction by parachute takes advantage of the Pioneer Venus and Galileo separation experience. It allows a one-piece decelerator, and the high parachute drag required for extraction slows the initial descent. However, rearward extraction requires a mortar and pilot parachute, and the much larger separation parachute (approximately 10 m diameter) which adds significant mass.

and deployment of a separate smaller descent chute. The large parachute volume requirements presents formidable stowage problems.

A maneuvering extraction parachute moderately reduces the area required by creating horizontal as well as vertical clearance (Figure 3.4-3). Figure 3.4-4 shows two options for such a parachute. However, these designs require large area to separate from the high-drag decelerator (Figure 3.4-5).

Descent Parachute

Descent times of 2 to 4 hours need a much smaller parachute, with a base area about ten times smaller than necessary for rear extraction (Figure 3.4-6). The required descent parachute area is similar to Galileo Probe's with the specific size tailored to the desired descent time.

Ribbon, ring-sail, and disk-gap-band designs have been used in similar applications. However, the ribbon design offers better stability and development heritage from Galileo and Pioneer Venus.

The various entry designs studied have dynamic pressures at Mach 1 from 0.7 to 2.5 psf. This is consistent with the 1 psf minimum desired to ensure deployment; parachutes have deployed at pressures as low as 0.5 psf. Evolving mission and Probe designs must avoid a low parachute deployment pressure.

No parachutes have operated in an atmosphere as cold as Titan's. The Probe warms the parachute until deployment, but strength, bending, and flutter tests must measure the material performance at descent temperatures.

In addition, all parachute designs have a drag uncertainty that may require tests for a sufficiently accurate estimate of the descent time.

Spin Rate Control

Below 10 km altitude, the Probe descent imager desires a constant spin rate of about 10°/sec to scan the surface. Although either a spin parachute or vanes can provide this rotation, both lack predictability and suffer from "helix angle" effects at higher altitude.

The inherent spin of all parachutes and the friction of the connecting swivel dominate the spin effects. Large vanes can overcome the swivel's friction but require actuators and a control system to compensate for the indeterminate parachute spin effects.

Spin parachutes deliberately induce an aerodynamic torque, usually with vents in the canopy. NASA has studied high-altitude spin parachutes of the disk-gap-band design. Although these designs can produce spin rates below 20 rpm during terminal descent, the spin rate, proportional to velocity, exceeds 100 rpm at higher altitudes.

For both the standard and spin-inducing parachute designs, spin rates vary widely, and testing is required to bound the performance. Further definition of imager and parachute design can help to define an acceptable scanning approach.

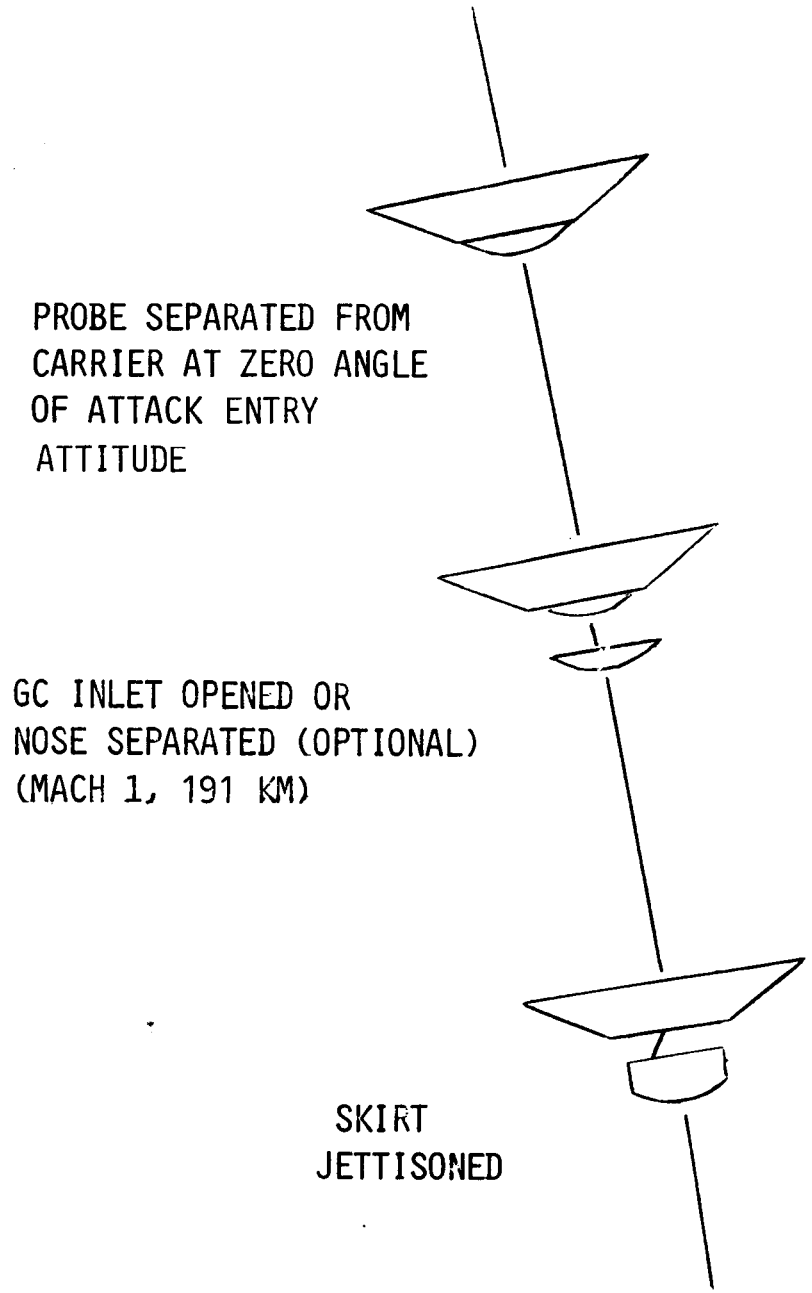

FIGURE 3.4-1:

DECELERATOR STAGING
SEQUENCE -

FORWARD EXTRACTION

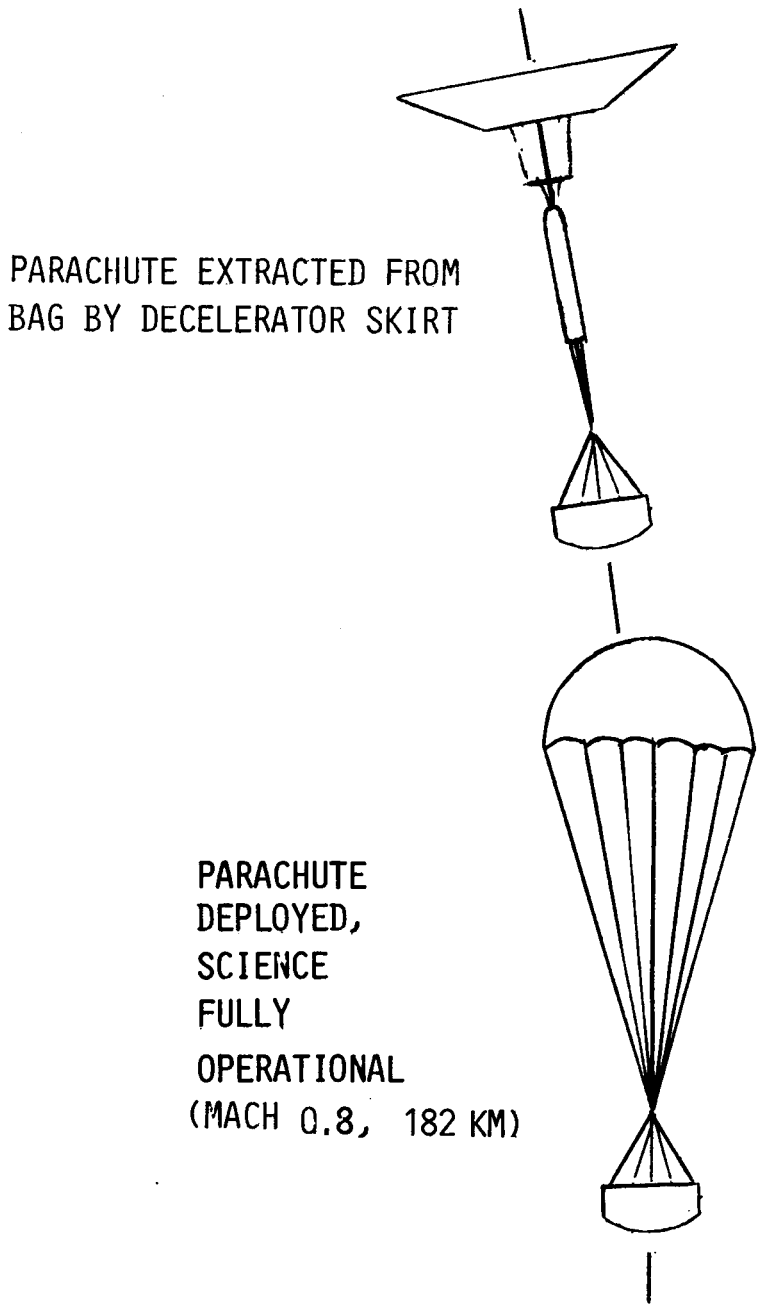

FIGURE 3.4-2:
PARACHUTE DEPLOYMENT SEQUENCE -
FORWARD EXTRACTION

FIGURE 3.4-3:

STAGING SEQUENCE ---
REARWARD EXTRACTION, MANEUVERING PARACHUTE
(LOW TO MEDIUM L/D)

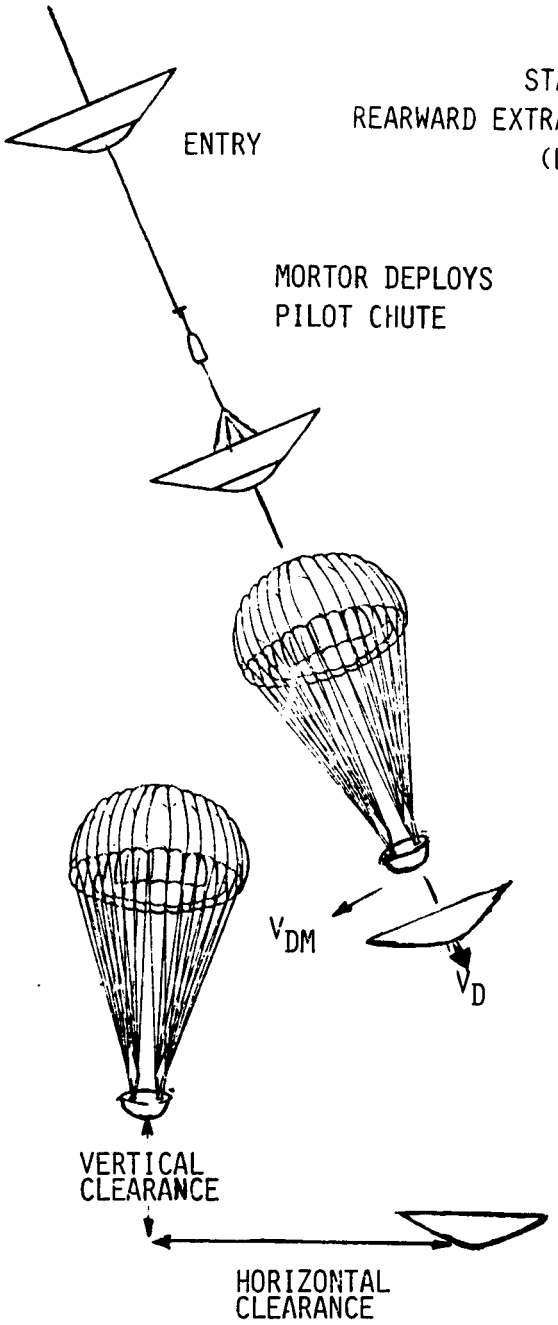

EXTRACTION CHUTE SEPARATED---
DEPLOYS DESCENT PARACHUTE

FIGURE 3.4-4:

MANEUVERING PARACHUTE OPTIONS

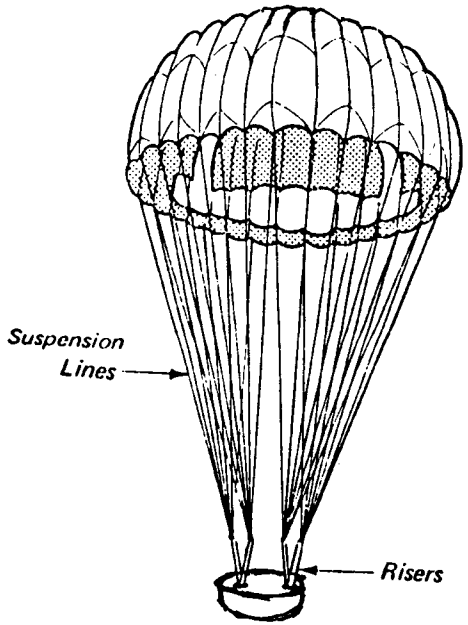

T & U SLOT

(L/D)max = 0.5 to 0.7

Simple circular flat and extended skirt.

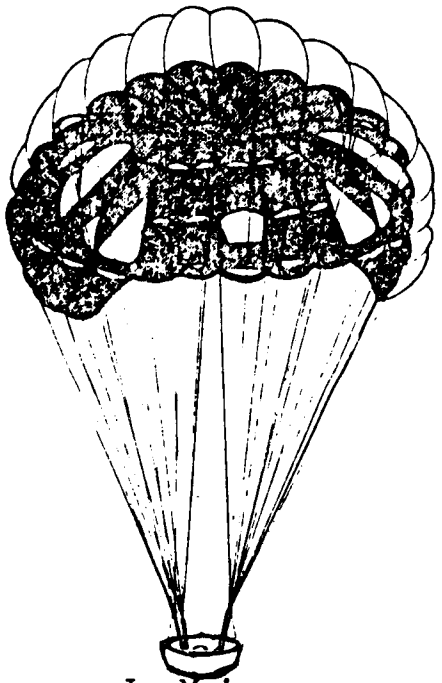

Le Moigne

(L/D)max = 1.2

Similar version developed during Gemini Program

FIGURE 3.4-5
MANEUVERING SEPARATION CHUTE AREA

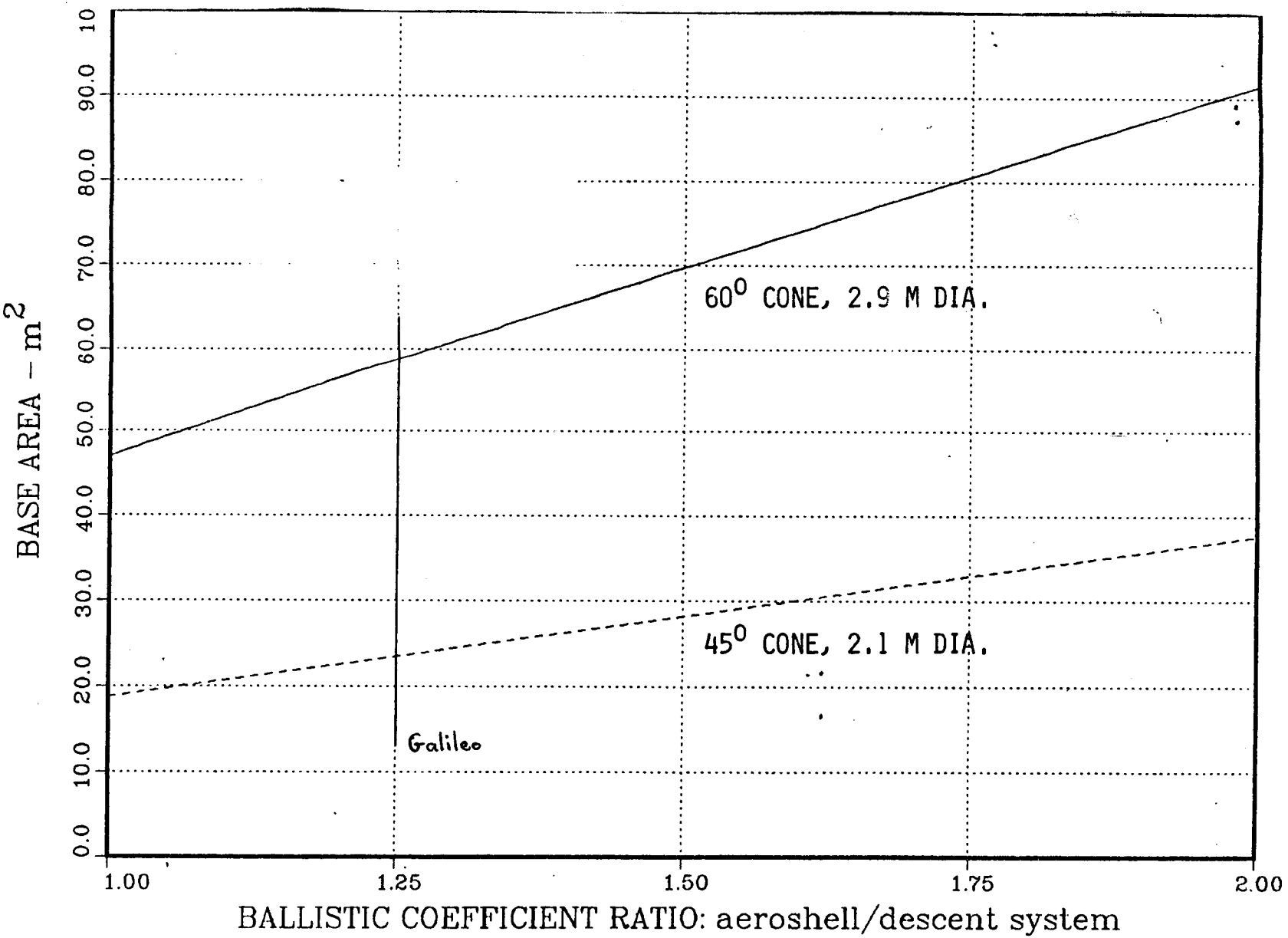

FIGURE 3.4-6
SUBSONIC DESCENT PARACHUTE SIZING REQUIREMENTS

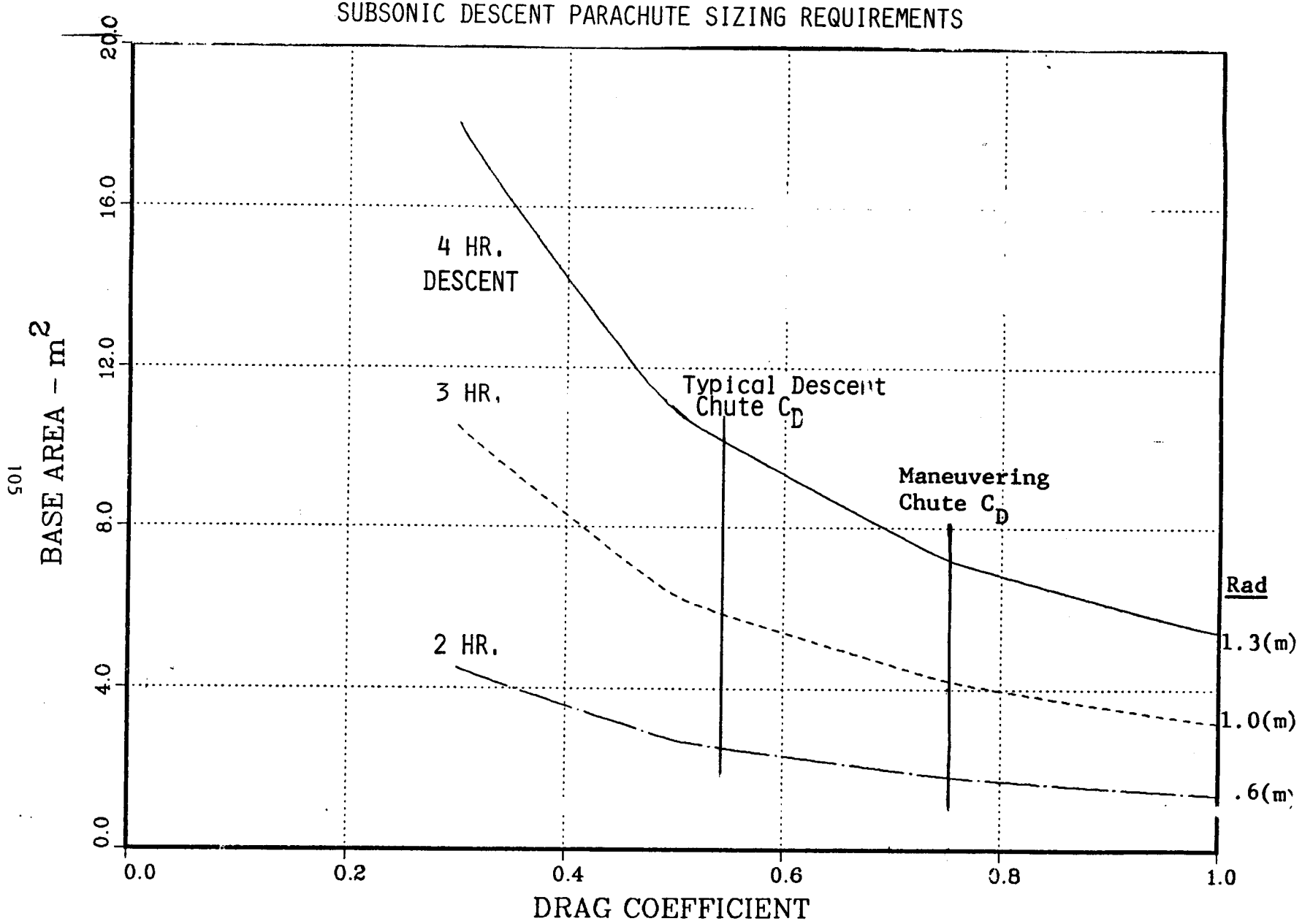

4. DESCENT MODULE

4.1 Configuration

Envelope, mass, and access considerations determine the descent module configuration. A narrow cylindrical envelope requires a small descent module diameter and requires a folding decelerator (see section 3.1). Equipment must be packaged on two or more shelves resulting in an elongated configuration. A sharply curved decelerator nose, steep cone angle, or large equipment shelf forces the descent module aft and increases attachment structure mass; flatter nose configurations permit greater shelf area.

Figure 4.1-1 shows descent module layouts for 50 and 80 cm diameter cylindrical envelopes. These preliminary configurations show somewhat less equipment than the baseline single shelf design, e.g. three battery modules instead of four, and assume tighter unit packing. The 50 cm design shows two shelves, but would probably require a third shelf to properly accommodate harness and blankets. Support of the aft shelves consumes much of the available space, and the second shelf and associated aftward mass introduces cg location and inertia ratio problems. In addition, all instruments must deploy to view along the sides, routing of the gas inlets is difficult, and access to units requires extensive disassembly.

The 80 cm design resembles the Galileo Probe configuration, with the instruments and most of the subsystem units on the main shelf and an aft shelf supporting the communications equipment and a few selected units. Although still cramped, adjustments in the shelf sizes and unit layout permit a two-shelf design of this diameter. Access, though better than the smaller-diameter design, remains difficult, and some instruments still require deployment.

Using the full envelope available on the Mariner Mark II permits a flat 60° decelerator cone with a large spherical nose (Section 3.1). With this geometry, a larger diameter shelf fits near the nose, where it provides favorable mass properties and simplifies the structural design. Figures 4.1-2 show a descent module design based on a 100 cm diameter shelf; the configuration allows adjusting this diameter if required. All the units fit on a single shelf, minimizing the structure mass, avoiding shelf supports, and providing complete access during integration.

Given a strong preference for a single shelf design, two additional options were considered relating to the integration of the decelerator nosecap. The next two sections describe an integral and separable nosecap respectively.

Descent Module Arrangement with Integral Nosecap

Figure 4.1-3 shows the design of the descent module with an integral nosecap. The descent module layout places the heavier batteries and command and data processor units on the forward side of the shelf, keeping the cg forward and close to the Carrier attachments as shown in Figures 4.1-4, 4.1-5 and 4.1-6. The other subsystem units and the science instruments mount on the aft side of the shelf and the NMS rests in a cutout similar to the mounting of the Galileo Probe unit. Slightly elevating the antenna gives it a clear field of view and provides room beneath it for the communications equipment, minimizing the cable runs.

Three brackets on the forward side of the shelf support the fixed beryllium nosecap and the three attachments to the Carrier which penetrate it. The attachment bolt catchers run almost tangential to the inside of the nosecap well away from the batteries and CDP. The three decelerator skirt brackets fasten to the aft side of the shelf above the nosecap supports. The skirt jettison bolt cutter assemblies hold the brackets outside the thermal blankets that envelop the rest of the module.

Because the decelerator skirt requires radial clearance around the shelf for its aftward separation, the nosecap extends slightly outboard of the shelf to meet it. Therefore, this forces deployment of the ASI inlets, nephelometer reflector, and NFR/imager optics. Deploying the sensors places them outboard of the nosecap edge to provide a clear field of view and exposure to clean airflow. Both the GC and NMS inlets pass through the nosecap near the stagnation point. The inlet design prevents interaction with the flow effects. Although two inlets are shown, they might be integrated into one inlet in the final configuration.

Blankets, held by aluminum supports, cover the entire descent module and line the inside of the nosecap. The parachute stows in a separate blanketed compartment to avoid disturbing the rest of the insulation when it deploys.

Descent Module Configuration with Jettisoned Nosecap

Figure 4.1-7 shows integration of the descent module with a jettisonable nosecap. Jettisoning the nosecap allows it to use lower mass organic ablation materials for entry thermal protection that would otherwise contaminate the gas samples. Jettisoning the nosecap eliminates or at least simplifies the instrument deployments. The shelf arrangement is unchanged, but bolt cutters hold the nosecap at the end of the supports. About 24 kg of ballast must be added to the nosecap to separate it from the descent module and skirt when the cutters fire. Removal of the nosecap exposes the instrument gas inlets.

Since the jettisonable nosecap extends further beyond the shelf, a larger hole in the decelerator skirt is required in order to clear fixed instrument sensors. This simplifies instrument design at the expense of an extra separation and the nosecap ballast mass. To avoid an even bigger nosecap, the long nephelometer sensor deploys in a similar manner to that on the Galileo Probe.

Mass

Table 4.1-1 gives the descent module mass for the integral nosecap, single shelf baseline configuration.

Conclusions

A simple configuration using a single 100 cm diameter shelf supports all science and subsystem units while maintaining favorable mass properties and complete accessability. Shelf diameter can grow to provide additional area as required. An integral nosecap reduces overall Probe mass and risk at the expense of additional instrument sensor deployments.

ONE 50 AND
ONE 80 CM
SHELF

TWO 50 CM
SHELVES

FIGURE 4.1-1:
NARROW DESCENT MODULE CONFIGURATIONS REQUIRE TWO SHELVES

FIGURE 4.1.-2:

LARGER CARRIER ENVELOPE ALLOWS SINGLE SHELF CONFIGURATION

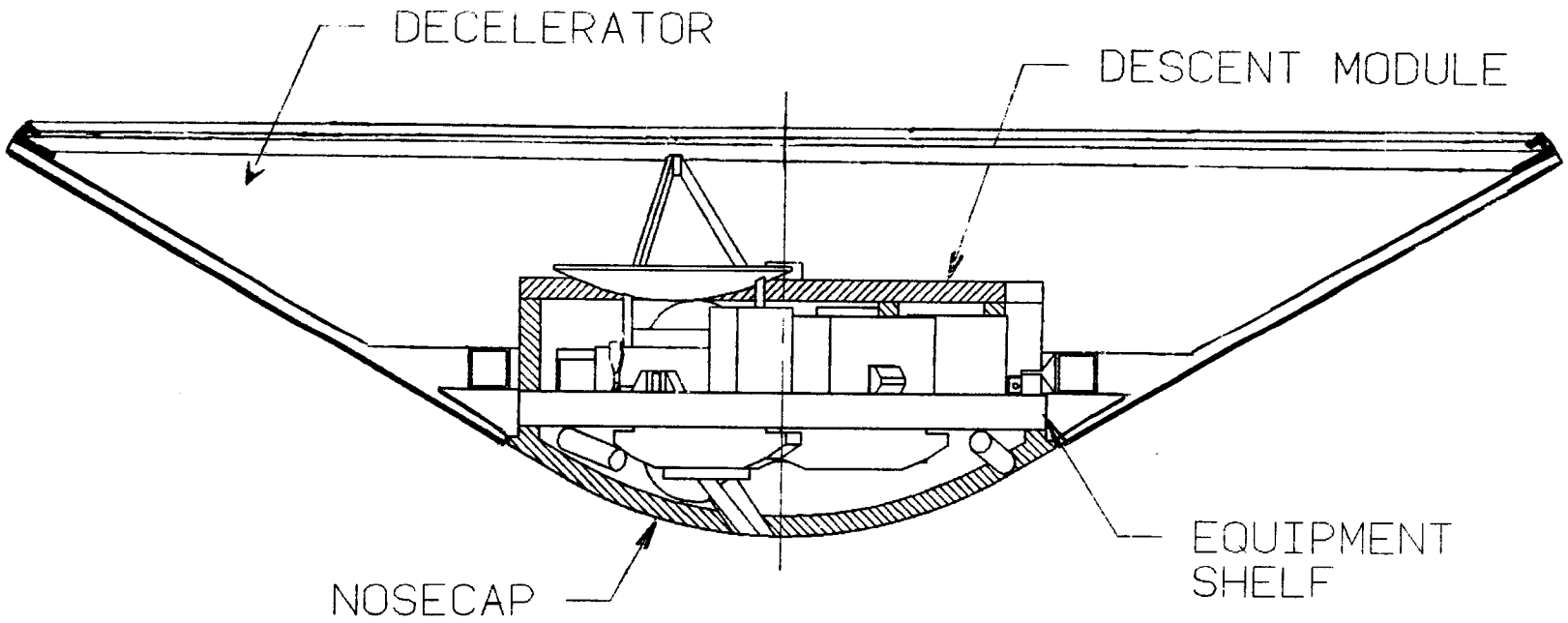

ONE 100 CM SHELF

FIGURE 4.1-3:

INTEGRAL NOSE CAP DESIGN - SIDE VIEW

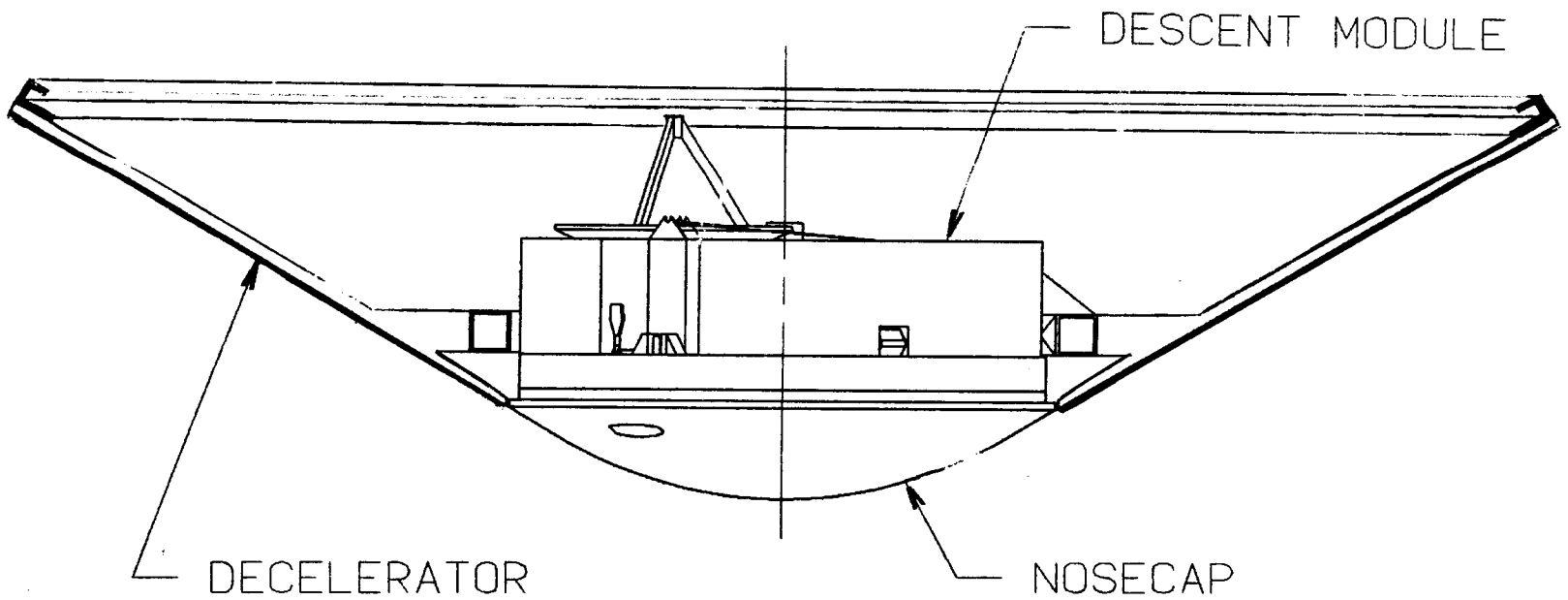

FIGURE 4.1-4:

EQUIPMENT SHELF LAYOUT - FORWARD SIDE

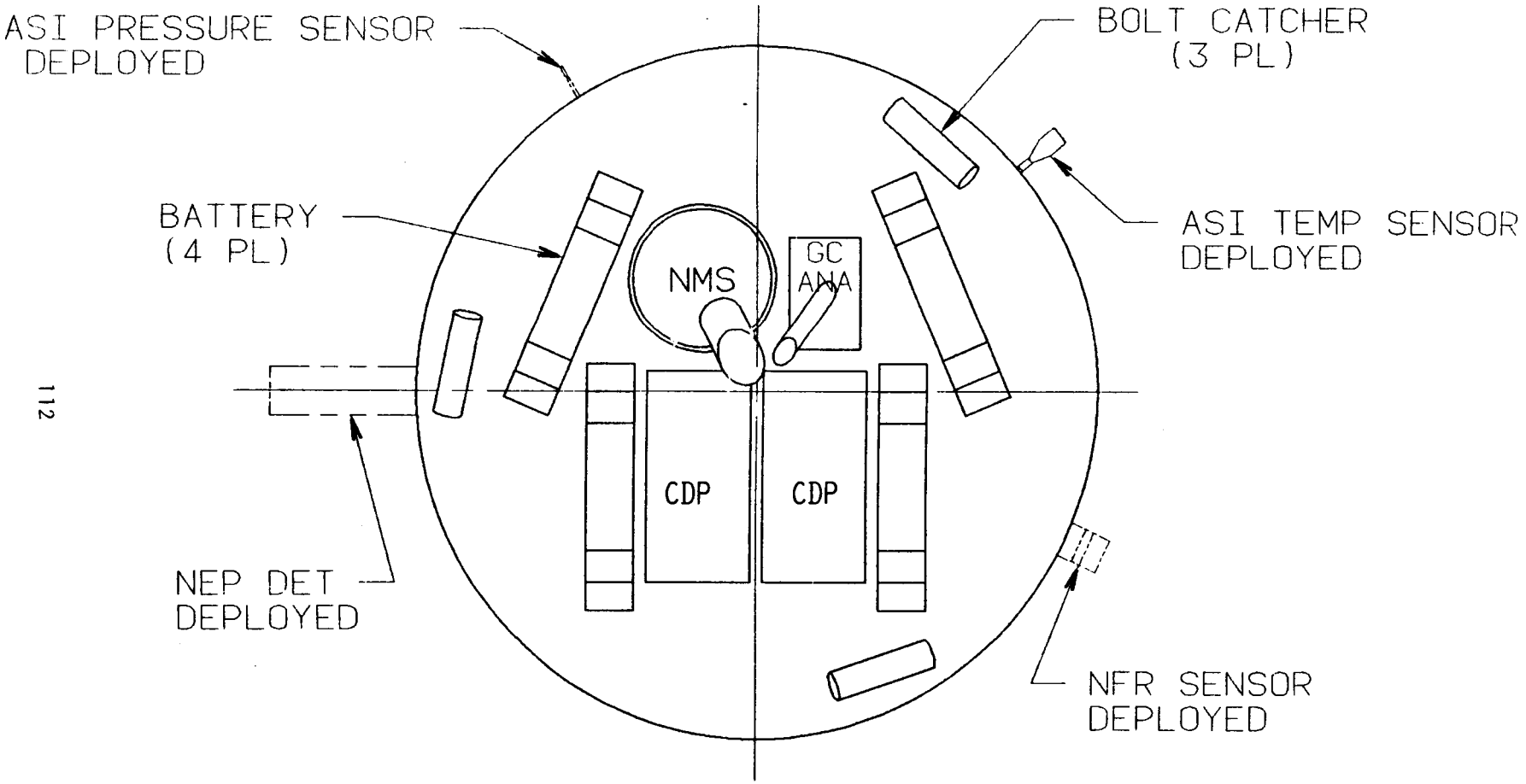

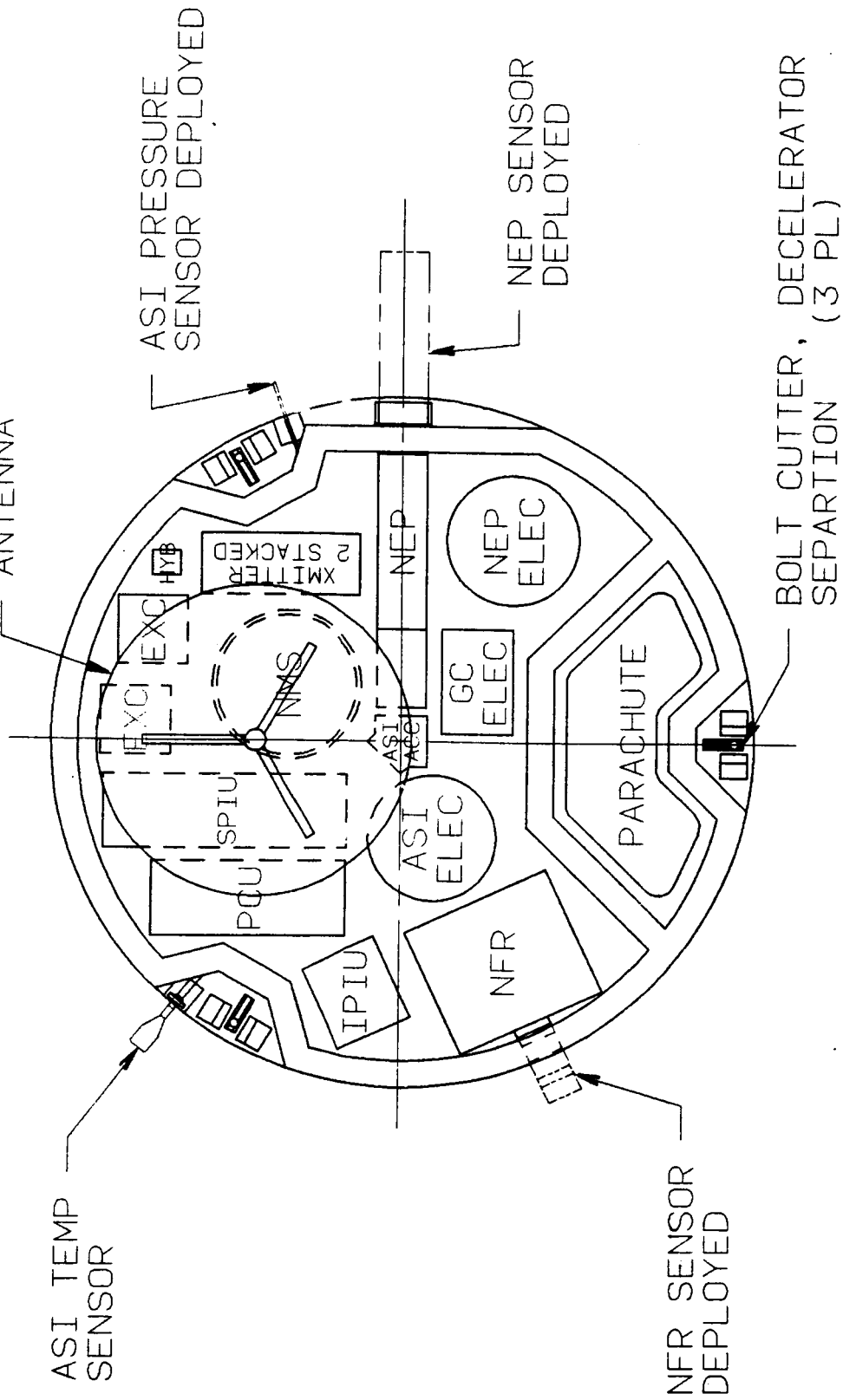

FIGURE 4.1-5:

EQUIPMENT SHELF LAYOUT - AFT SIDE

FIGURE 4.1-6:

DESCENT MODULE DESIGN - SIDE VIEW

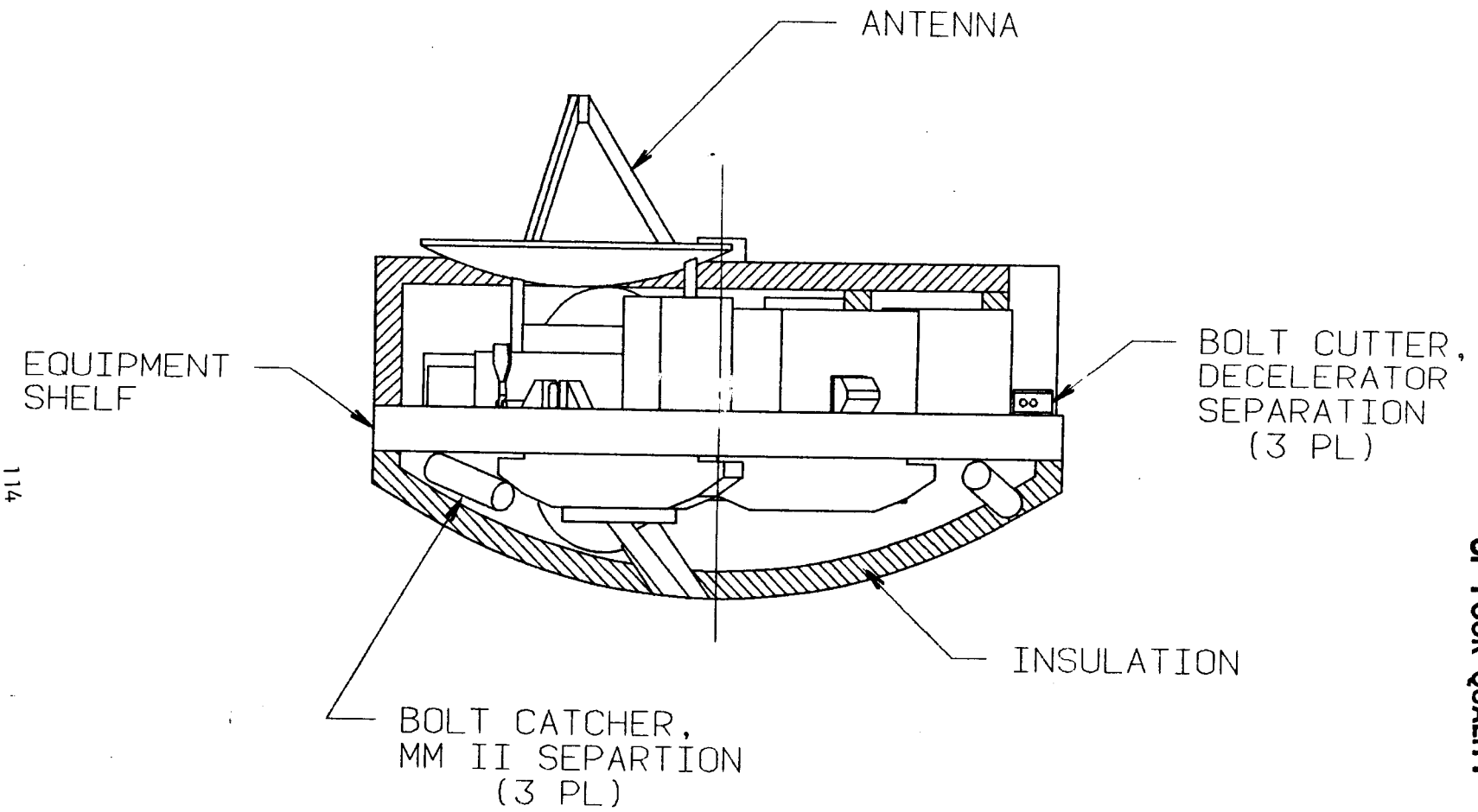

FIGURE 4.1-7:

JETTISONABLE NOSECAP DESIGN - SIDE VIEW

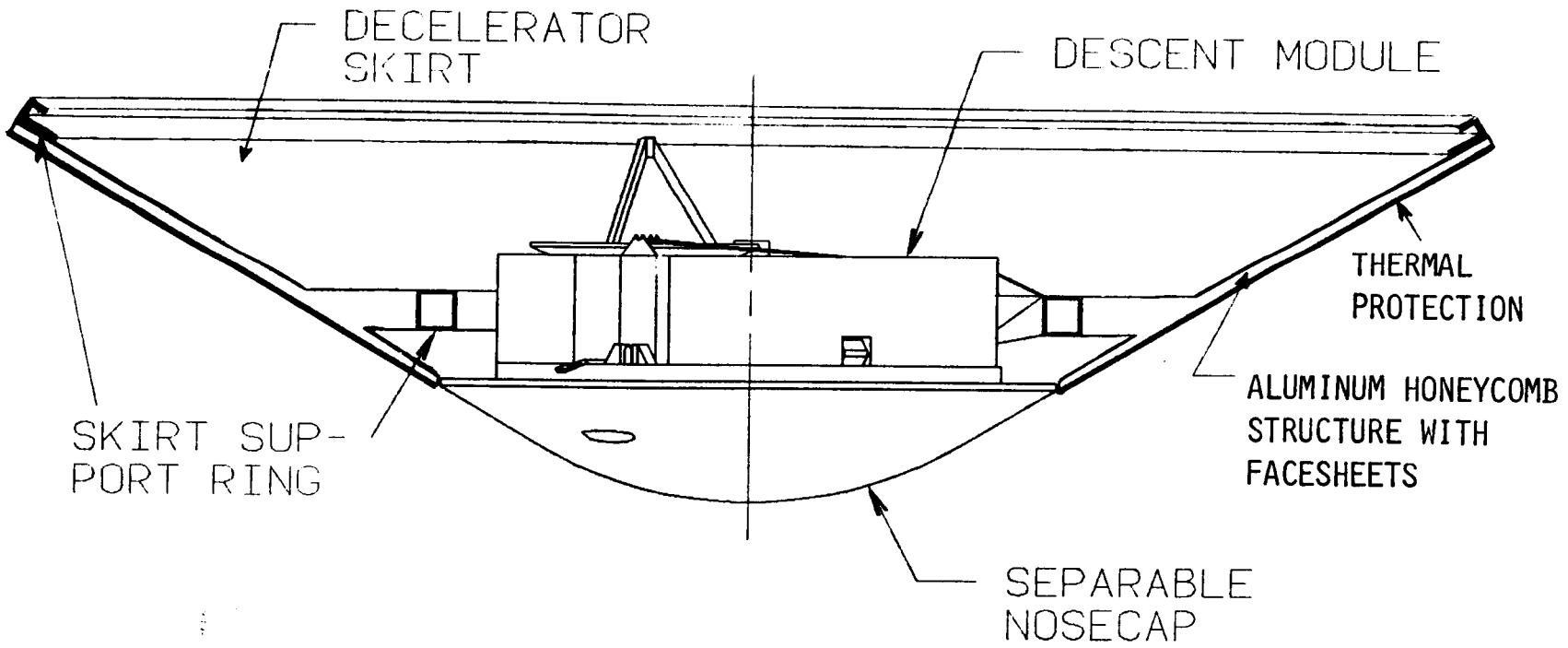

4.2 Structure

The single-shelf configuration, mild entry deceleration, and moderate launch loads simplify the Probe structural design. Table 4.2-1 lists the structural requirements. The entry analysis in section 2.2 defines 20 g axial load as the worst case for the trajectories of interest and JPL has provided estimated launch loads for the Probe location on the Carrier.

Stiffness dominates the structural requirements. The overall Probe natural frequency of 30 Hz allows a 10 Hz margin over the JPL-defined minimum. Coupling of the structural modes then requires that the main shelf frequency exceed 50 Hz.

Equipment Shelf

The single equipment shelf supporting all subsystem and science units dominates the structure. Models of the shelf using NASTRAN show high load margins resulting from the stiff design. A 2.0 inch thick core of 5056 aluminum honeycomb with 50 mil 2024-T81 facesheets maintains the 50 Hz frequency.

Locating the three shelf supports at two-thirds of the radius enhances the shelf stiffness (compared to edge support) while placing the Carrier attachments correctly for separation. Loads from the decelerator pass directly to the Carrier attachments and do not affect the shelf. However, the cutout for the NMS instrument (assumed to resemble the Galileo Probe NMS) lowers the shelf stiffness. A surface-mounted NMS or a local shelf stiffner would offer some saving in shelf mass and thickness.

Mass

Table 4.2-2 lists the mass of each structural element. As the prime load-carrying member, the shelf dominates the structure mass.

TABLE 4.2-1: STRUCTURE REQUIREMENTS

- QUASI-STATIC LOAD REQUIREMENTS

LAUNCH	12 g	(PROBE LONGITUDINAL AXIS)
	14 g	(PROBE LATERAL AXES)
ENTRY	20 g	

- MINIMUM FREQUENCY

PROBE	20 Hz REQUIRED, 30 Hz DESIGN GOAL
EQUIPMENT SHELF	50 Hz (TO MEET DESIGN GOAL)

TABLE 4.2-2: STRUCTURE MASS

SHELF	10.2
THERMAL BLANKET SUPPORTS	2.5
NOSECAP/CARRIER BRACKETS	2.0
SKIRT SEPARATION GUIDES	1.0
MISC ATTACH HARDWARE	2.0
TOTAL MASS	17.7 kg

4.3 Thermal Control

Requirements

The probe must maintain proper internal temperatures during the 9-year cruise to Saturn, 6 to 20 day coast from spacecraft separation to Titan entry, and descent into the cold Titan atmosphere. Table 4.3-1 summarizes the operating temperature requirements. In addition to these ranges, the batteries should remain below 20°C for long-term storage.

Cruise and Coast Thermal Control

Figure 4.3-1 shows the thermal control concept. The approach follows that of the Galileo Probe, with 4 cm thick blankets surrounding the descent module that contains the units. However, for the Titan Probe, the radioisotope heater units (RHUs) that keep the probe warm during cruise and coast are placed inside the descent module thermal blankets where they can also help to warm the module during descent. A separate parachute blanket and RHU for the parachute allow it to deploy without affecting descent module thermal control.

Because the Probe is designed for a thermal balance while coasting alone after separation from the Carrier spacecraft at Saturn, it requires shade from the sun near Earth and isolation from the Carrier. This isolation may include shading from the Carrier RTG thermal radiation, if the small view factor does not sufficiently minimize the effect. The Probe-Carrier attachments may also require conductive isolation; exact values of acceptable radiation and conduction require definition and are beyond the scope of this study.

The RHUs must maintain the Probe between -10° and 20°C with effective blanket emissivity from 0.02 to 0.04 (Figure 4.3-2). Since variations in blanket installation and penetration cause the range of emittances, tests are required to determine the exact number of RHUs. A baseline value of 40 watts falls in the expected range.

Descent Thermal Control

Table 4.3-2 compares the three key parameters of the descent thermal environment to previous probe missions. The conductivity of Titan's atmosphere, about one-sixth of Jupiter's, reduces the rate of heat loss. Free convection is approximately the same as on Pioneer Venus. Although the cold Titan atmosphere tends to cool the Probe, it also results in low conductivity of blankets and metal parts compared to the Galileo descent.

Figures 4.3-3 and 4.3-4 show the variation in Probe temperature during descent for initial temperatures of +10° and -10°C. The profiles show the effects of 4cm and 8 cm (1.5 and 3.0 inch) thick insulation, with up to 65 watts of heater power added to the internal dissipation as described by the power budget in the following section. Heaters would primarily warm the batteries because they are most sensitive to low temperatures. Appropriate heater power and insulation thickness can maintain internal temperatures for any of the descent times considered. The baseline 4 cm thick insulation supports a 3-hour descent with +10° initial temperature and no supplemental heater power; modest heater power ensures maximum battery performance for longer missions or cooler initial temperatures.

TABLE 4.3-1

THERMAL CONTROL REQUIREMENTS

MISSION PHASE	DURATION	OPERATING TEMPERATURE RANGE
CRUISE (CHECKOUT)	9 YEARS	$-15^{o}C$ to $50^{o}C$ $-10^{o}C$ to $20^{o}C$ (batteries)
COAST	20 DAYS	$-10^{o}C$ to $50^{o}C$
ENTRY/DESCENT	3 HOURS	$-20^{o}C$ to $50^{o}C$ (equipment) $-10^{o}C$ to $50^{o}C$ (batteries)

TABLE 4.3-2

THERMAL ENVIRONMENT AT TITAN COMPARED TO JUPITER AND VENUS

- ATMOSPHERIC CONDUCTIVITY:
  - APPROXIMATELY 1/6 OF VALUE AT JUPITER (100° K)
  - K = .01 W/METER K° (TITAN)
  - K = .06 W/METER K° (JUPITER)
- FREE CONVECTION IN PROBE
  - ROUGHLY THE SAME AS PIONEER VENUS
  - h = 7.55 W/METER K° (111° K)
- ATMOSPHERIC TEMPERATURE
  - T = 75° K (28 to 60 km altitude)
  - COOLER THAN JUPITER, IMPLYING CONDUCTIVITY OF BLANKETS AND METAL PARTS IS LOWER THAN THOSE ON GALILEO PROBE
  - MUCH COOLER THAN -20°C EQUIPMENT TEMPERATURE LIMIT

FIGURE 4.3-1

THERMAL CONTROL CONCEPT

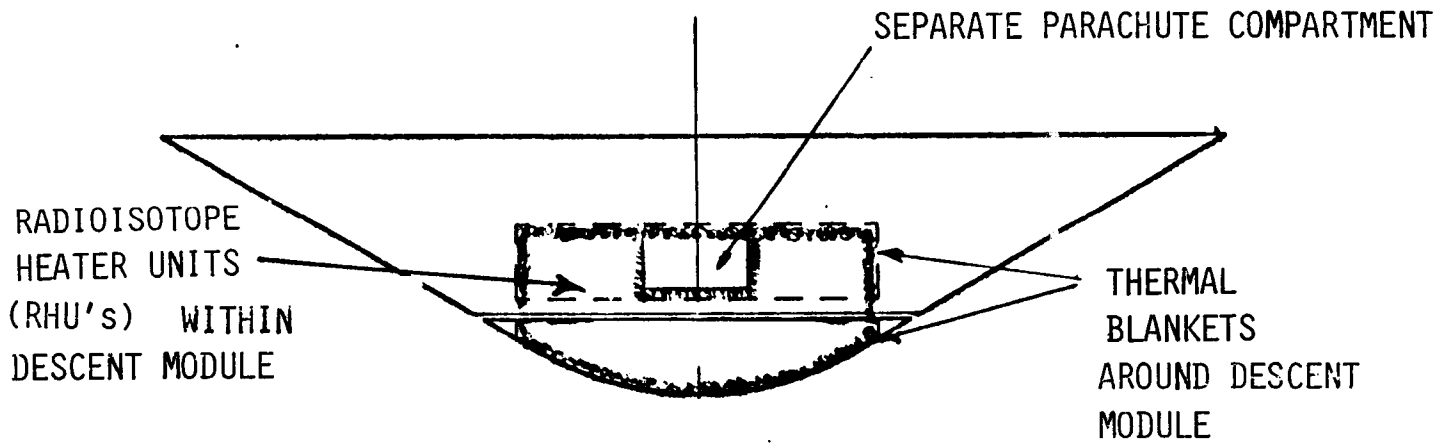

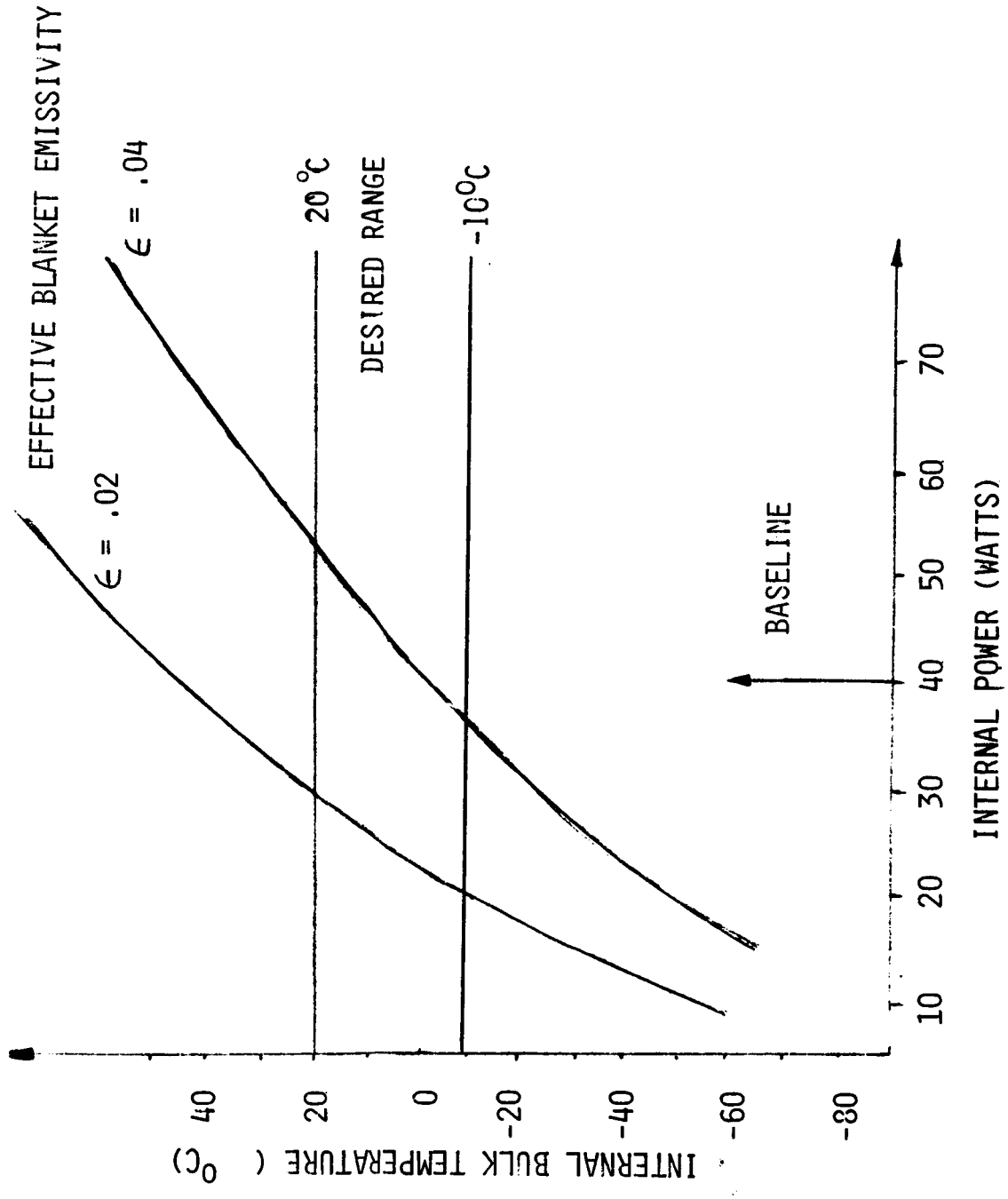

FIGURE 4.3-2:
COAST PHASE THERMAL CONTROL

FIGURE 4.3-3:

DESCENT TEMPERATURE-TIME PROFILES - +10°C COAST TEMPERATURE

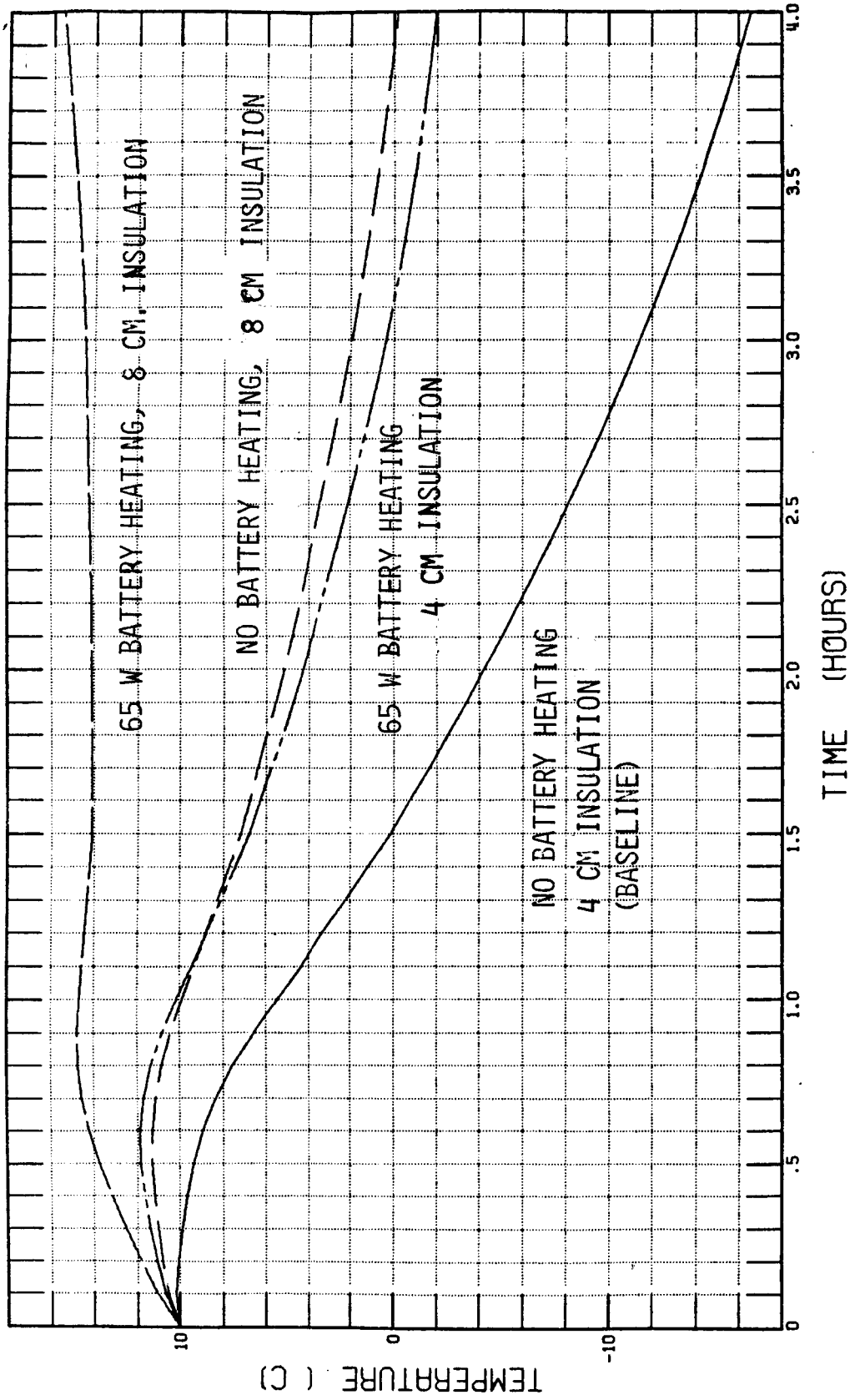

ORIGINAL PAGE IS
OF POOR QUALITY

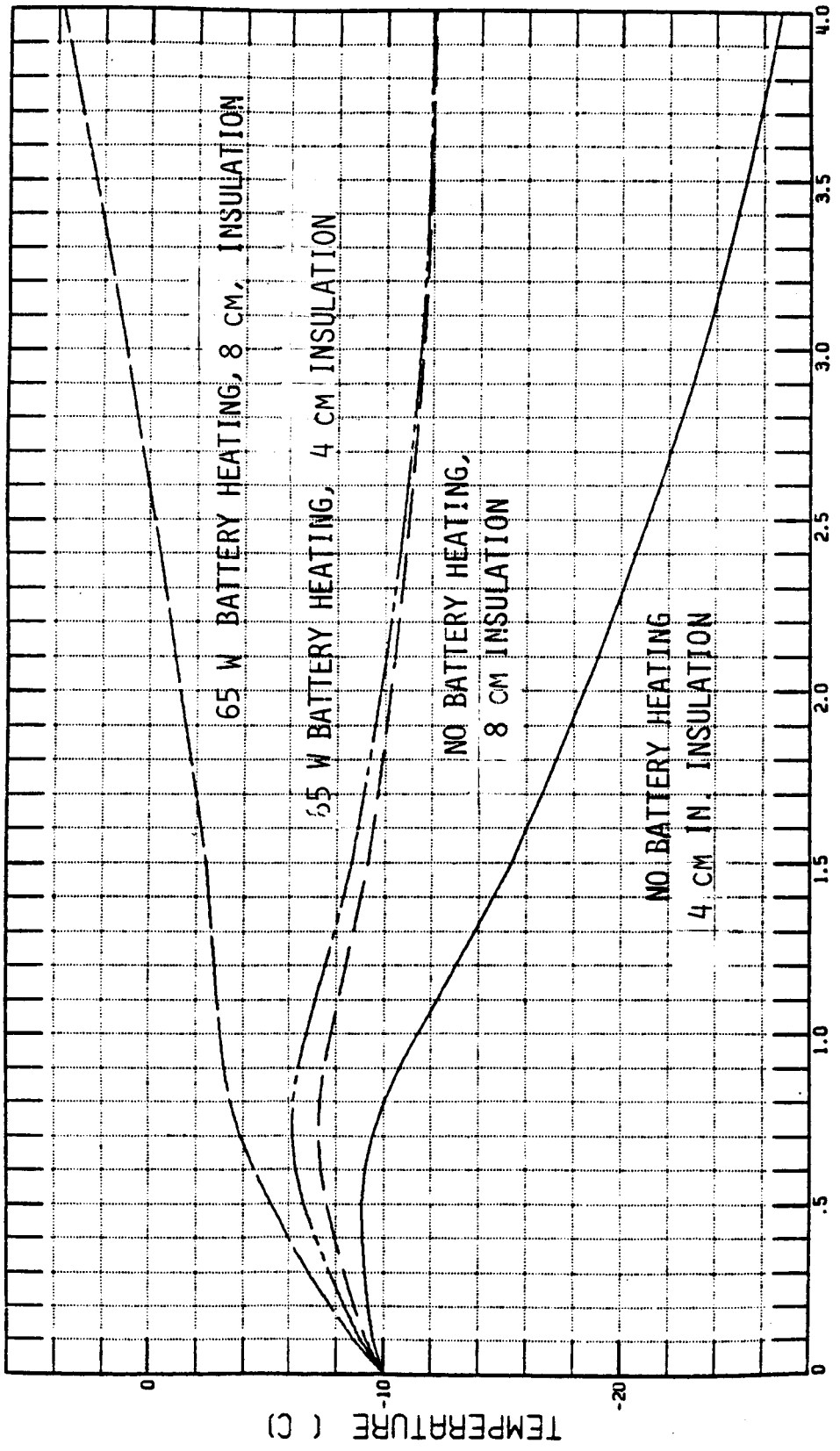

FIGURE 4.3-4:

DESCENT TEMPERATURE-TIME PROFILES - $-10^{o}C$ COAST TEMPERATURE

4.4 Power Subsystem

Operation

The Probe must internally supply 60 mW, 32 W, and 153 W of regulated battery power to the units during coast, pre-entry, and descent, respectively. It also must distribute Carrier power supplied through two Probe power interface units (PPIUs) for checkout during cruise. In addition, the power subsystem must provide firing current for up to six simultaneous separation and deployment pyrotechnic initiators.

Figure 4.4-1 shows the subsystem operation. The subsystem power interface unit (SPIU) diode-ORs and regulates the power lines from four $LiSO_2$ battery modules It also contains reconditioning circuits to depassivate the batteries before entry. Orbiter power supplied by the PPIU passes through the SPIU for switching and distribution.

The SPIU switches power to the command and data processor (CDP), the CDP coast timer, the instrument power interface unit (IPIU), the communications equipment, and the pyro control unit (PCU). The IPIU in turn provides overvoltage regulation, fusing, and switching of science instrument power. The PCU contains the arming and hybrid driver circuits for the pyrotechnic initiators. Based on measured performance of the Galileo Probe $LISO_2$ batteries, battery power can drive the squibs directly; no thermal batteries are required.

Table 4.4-1 lists the subsystem unit masses and required modifications from the Galileo design. The added battery module supports the longer Titan mission and provides the desired margin for this stage of the program. Repackaging the Galileo Probe electronics eliminates the hermetically-sealed, pressure tolerant (20 bar) cases to save mass.

Table 4.4-2 shows the power budget for a 3-hour descent. All loads carry a 10% contingency. In addition, allocated battery shelf losses of 0.1 A-hr/module/year consume 3.6 A-hr, although Galileo Probe has not observed losses this high. The science instruments drive the checkout power requirement; sequencing the checkout would reduce the maximum power if necessary.

Carrier Power Interface

Two Probe power interface units (PPIUs) on the Carrier supply power for Probe operation during the cruise to Saturn (Figure 4.4-2). Each PPIU accepts switched, regulated, current-limited DC lines from the Carrier. Two DC-to-DC converters shift the voltage from the $\pm$15V input to the desired +33 V and +39 V values. Like Galileo Probe, three busses pass from the converters to the probe SPIU. The first powers the command interface functions and contains a Shuttle lockout and bleed resistor circuit for safety. The second bus powers the CDP; the third bus provides current and voltage limited checkout power. The second PPIU redundantly supplies the same interfaces.

Battery Selection

Table 4.4-3 summarizes the characteristics of batteries considered for the Probe. Safety, mass, cost, shelf life, and transition from the coast timing phase of the mission to the higher power required just before entry primarily affect the battery selection. Although other systems offer some advantages, the overall tradeoff favors the Galileo probe $LiSO_2$ batteries because of the low cost and mass, and developed status. Carrying sufficient capacity margin overcomes both the temperature and shelf life disadvantages of this type. The entire power subsystem therefore retains most of its Galileo Probe heritage.

TABLE 4.4-1:
POWER SUBSYSTEM UNITS

UNIT	CHANGES FROM GALILEO	MASS (kg)
BATTERIES Li/SO_2 (4 modules)	ADDED MODULE	10.0
SUBSYSTEM POWER INTERFACE UNIT (SPIU)	REPACKAGING, AND MINOR CHANGES RELATED TO ADDED BATTERY MODULE	3.2
INSTRUMENT POWER INTERFACE UNIT (IPIU)	REPACKAGING, AND TWO RELAYS CHANGED TO ALLOW HIGHER CURRENT LEVEL	1.6
	* PROBE TOTAL *	14.8 kg
PROBE POWER INTERFACE UNIT (PPIU)	DESIGN CHANGED TO ACCEPT CARRIER SUPPLIED DC VOLTAGE AND SWITCHED INPUT	3.5 kg
		18.3 kg

TABLE 4.4-2:

TITAN PROBE POWER BUDGET

	CHECKOUT (5 min)	COAST (20 days)	ENTRY (10 min)	DESCENT (3 hours)
COMMUNICATIONS	10.2	--	32.6	32.6
DATA HANDLING/COMMAND	20.0	0.05	20.0	20.0
POWER	3.5	0.00	2.3	3.5
SCIENCE	76.1	--	6.3	76.1
SUBTOTAL	109.8	0.05	61.2	132.2
CONTINGENCY (10%)	11.0	0.01	6.1	13.2
TOTAL (Watts)	120.8	0.06	67.3	145.4

BATTERY DEPTH OF DISCHARGE:

MISSION	=	16.73 A-HR
STORAGE	=	3.6 A-HR
TEST	=	0.4 A-HR
TOTAL		20.73 A-HR (66% DOD FOR 4 MODULES)

TABLE 4.4-3
BATTERY TECHNOLOGY TRADE-OFF

Coast Battery + Entry/Descent Battery	MASS (kg)	ADVANTAGES	DISADVANTAGES
BASELINE Li SO_2 + Li SO_2	10.0 kg	1. Understood by HAC 2. Low cost 3. Low weight 4. Pre-packaged and environment. qualified 5. Shuttle safety approved	1. Poor low temperature performance (requires heating) 2. Nine year mission poses shelf-life concerns
Li Mang Dioxide + Li $SOCl_2$	11.4 kg	1. Long shelf-life	1. Expensive (more development $) 2. Safety concerns (volatile system) unusable in System Test, raises Shuttle safety issues 3. Reliability is a concern 4. Transition between low-rate coast and entry/descent batteries 5. Low temperature problem
Li SO_2 + Li $SOCl_2$	13.6 kg	1. Avoids transition problem of other systems	1. Heavier than Baseline 2. Has deficits of both Li/SO_2 storage and Li/$SOCl_2$ volatility 3. Very expensive 4. Low temperature problem
Li Manganese Dioxide + Thermal Batteries	18.2 kg	1. Both battery systems have long well-known shelf-lives 2. No temperature problem 3. Will add heat to descent module 4. Low cost	1. Very heavy 2. Transition problem 3. Noisy voltage source

FIGURE 4.4-1:
POWER SUBSYSTEM FUNCTIONAL DIAGRAM

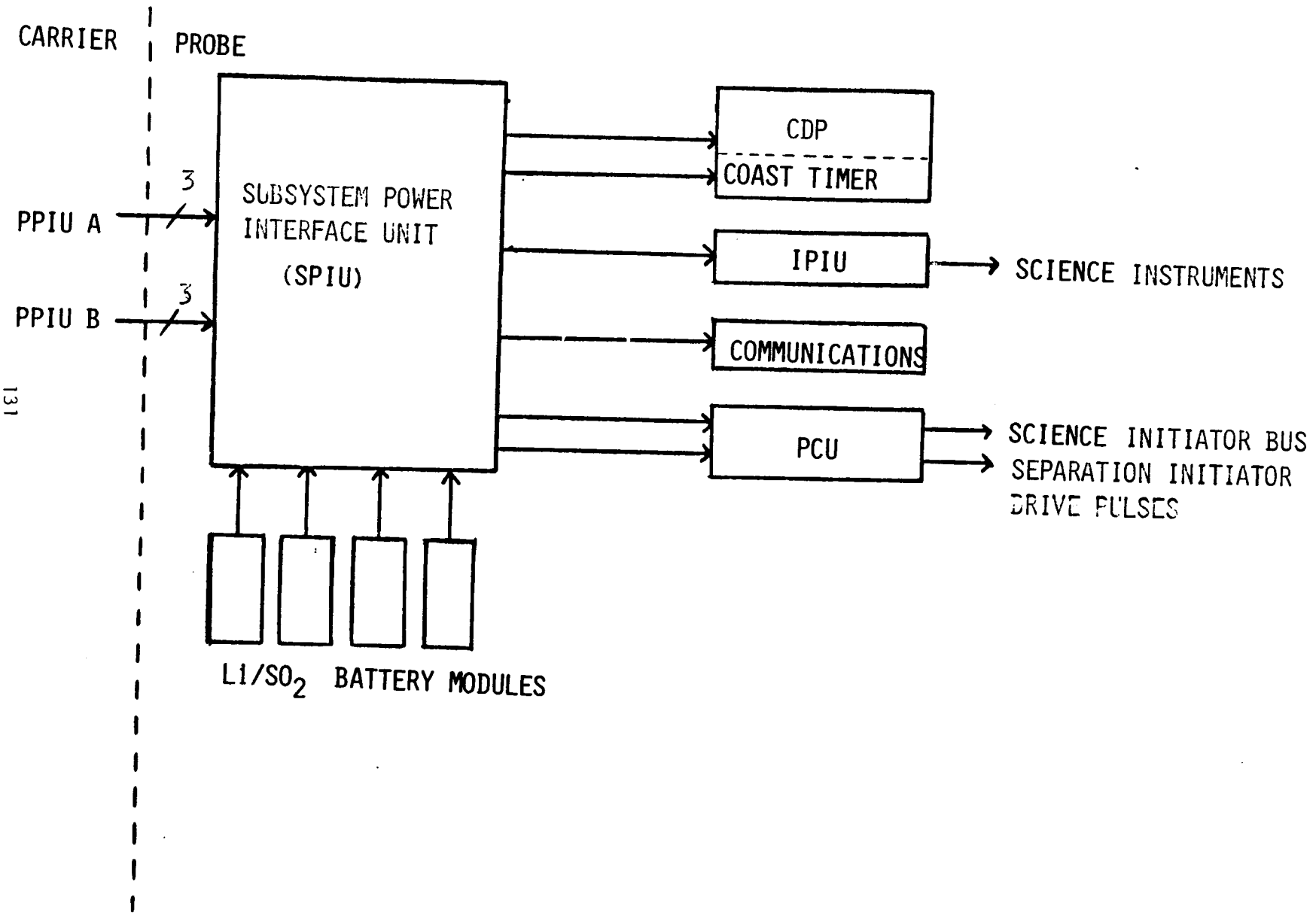

FIGURE 4.4-2:

PROBE POWER INTERFACE UNIT (PPIU) FUNCTIONAL DIAGRAM

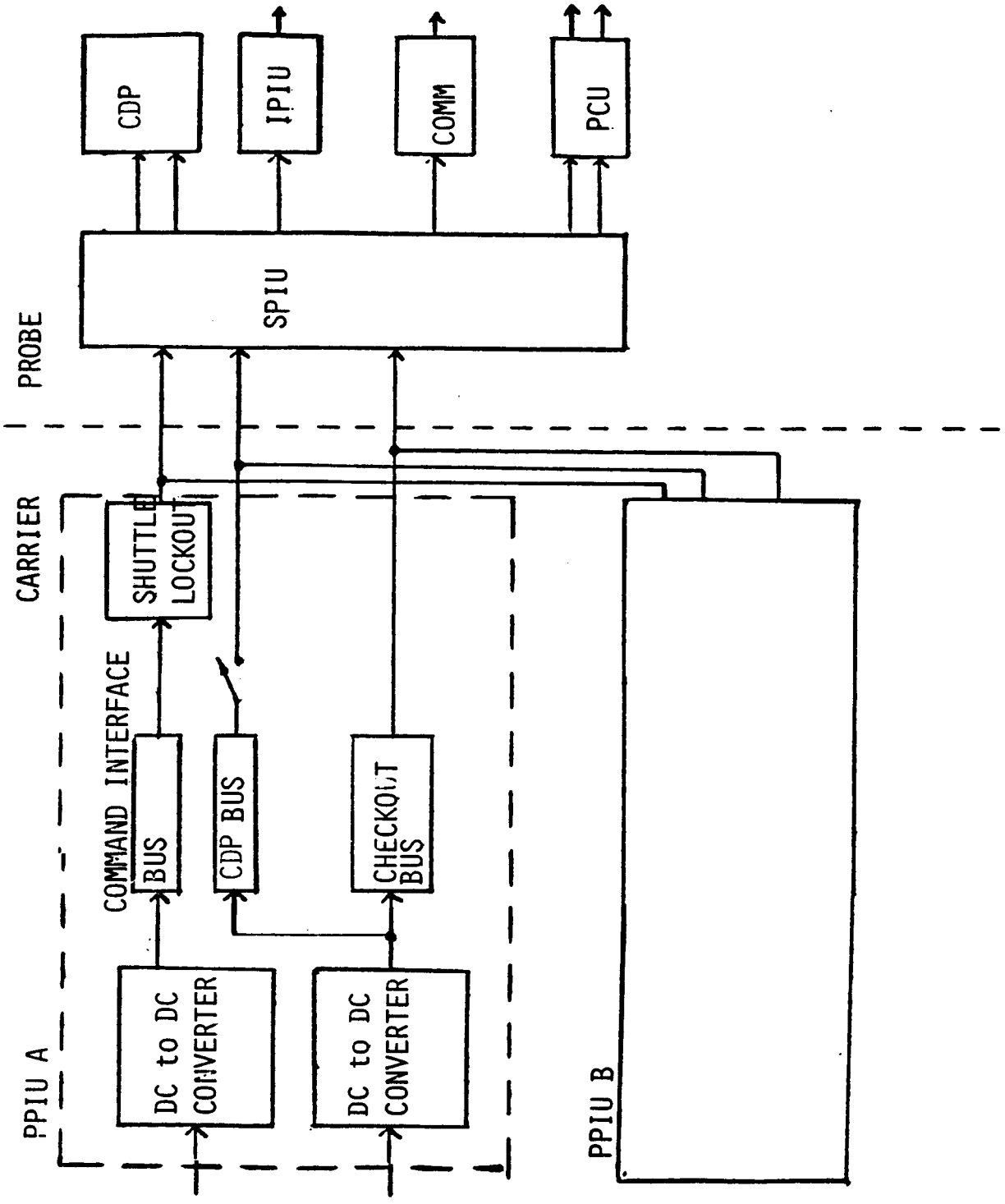

4.5 Communications Subsystem

To simplify the communications analysis the transmitter power was set at 2.5W, S-Band frequency (2295 MHz) was assumed, and atmospheric absorption effects and galactic and synchrotron noise were ignored. . A bit error rate of 10^{-3} was assumed based on the Galileo Probe requirement, and receiver/ demodulation losses, cable loss, and noise temperature (437°K) were set at the values measured for the Galileo Probe. Link budgets assume a worst case disk noise of 90°K.

Section 2.4 describes the tradeoff of other communications parameters and derives a baseline Probe antenna beamwidth, Receive antenna beamwidth, and BPSK receiver design employing a 2nd order tracking loop (see Section 5.3).

The Probe communication subsystem employs a parallel string configuration with no cross-strapping, similar to that used on Galileo Probe (see Figure 4.5-1). The two phase modulated S-band channels are transmitted to the Carrier at orthogonal polarization and offset frequency. The two strings transmit nearly redundant telemetry information from the CDP unit.

Ultra Stable Oscillators (USO) generate the RF carriers with sufficient frequency stability to allow determination of atmospheric wind from doppler measurement. An exciter in each string biphase modulates the carrier with the composite convolutionally encoded data stream from the associated CDP. A power amplifier delivers 2.5 watts to the antenna. All the units have their heritage in existing hardware. Table 4.5-1 shows mass, power, and dimensions for each unit.

Inclusion of radio science impacts both the Probe and Carrier. If radio science is deleted the Ultra Stable Oscillators can be replaced by temperature controlled crystal oscillators decreasing mass, power and dimensions (see table 4.5-2). Eliminating radio science also allows similar simplification of the oscillator in each receiver, a small receiver data rate decrease (250 bps), and some reduction of receiver A/D hardware.

TABLE 4.5-1 COMMUNICATIONS SUBSYSTEM MASS, HERITAGE AND POWER

UNIT	HERITAGE	MASS, kgs	POWER, W @ 28 Vdc	DIMENSIONS, cm. each unit
EXCITER (2)	PV	2.0	7.4	9.9 x 9.9 x 7.87
TRANSMITTER (2)		2.73		
DRIVER AMP (2)	PV	0.38	22.4	12.2 x 6.0 x 3.25
ISOLATORS (2)	PV	0.23	-	6.0 x 6.0 x 1.52
USO (2)	GALILEO	1.18	4.0	15.0 x 6.1 x 4.8
HOUSING (2)	NEW	0.94	-	24.1 x 7.62 x 5.1
HYBRID	PV	0.03	-	4.06 x 3.56 x 1.83
COAX-CARRIER INTERFACE	GALILEO	0.11	-	
PROBE ANTENNA	-	1.13	-	DIAM. 45.0
TOTAL		6.0 KG	33.8 W	

TABLE 4.5-2 COMPARISON OF CRYSTAL OSCILLATOR CHARACTERISTICS

	TCXO	USO
MASS, kg	0.045	0.59
POWER, w	1.4	2.0
DIMENSIONS, cm	5.1x3.3x2.79	15.0x6.1x4.8

FIGURE 4.5-1 COMMUNICATIONS SUBSYSTEM ARCHITECTURE

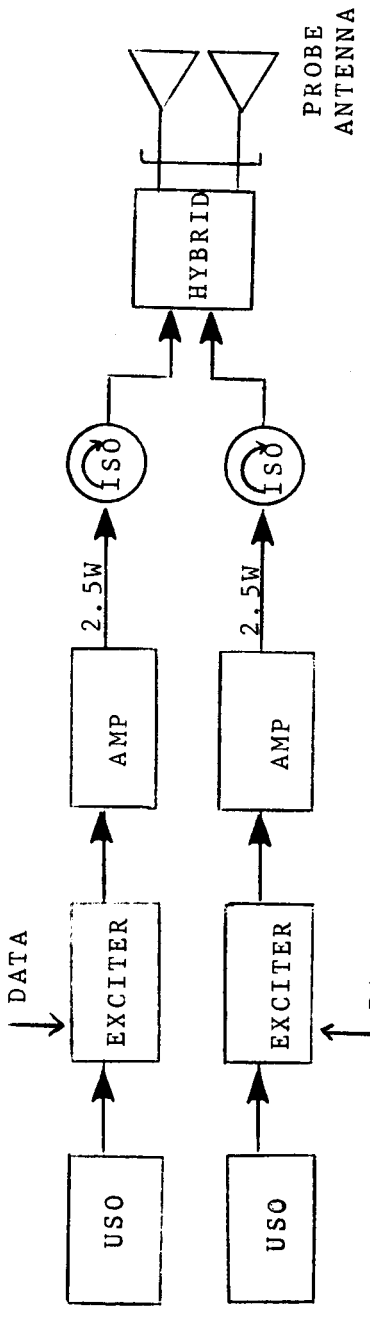

4.6 Command and Data Subsystem

Requirements

The Titan Probe Command and Data Subsystem (CDS) must communicate with the Carrier during cruise to perform Probe checkout. After the Probe separates, the CDS must time the coast period to ensure pre-entry warm-up of the stable oscillator. The g-switches give the CDS an indication of the forces experienced by the Probe as it enters Titan's atmosphere. The CDS must use this information to derive the timing of parachute deployment, decelerator separation, and commands to the science instruments.

As the Probe descends, the CDS must deploy sensors, command instruments to take measurements, format science and engineering data, and send the composite data to the communications subsystem for transmission to the Carrier. The estimated number and type of command and telemetry channels are nearly the same as Galileo Probe.

Hardware Description

The Probe command and data handling subsystem comprises the two halves of the CDP, two PCU's (Pyrotechnic Control Unit), and four g-switches. Table 4.6-1 lists the mass, power, and dimensions of each of these units. The mass and power column has the total for all units on that line, while the dimensions apply to individual units.

Interfaces

Figure 4.6-1 shows the Carrier command interfaces with the Probe, receiver, and separation mechanism. Commands come to the Probe over the Carrier serial bus. Note that the serial bus interface passes through the cable cutter. The Bus Interface Unit (BIU) handles Carrier bus protocol and decodes commands for the Probe. An identical command interface exists between the Carrier and the receiver. The Carrier provides a number of drivers to fire NASA standard initiators in the cable cutter and separation mechanism.

Data interfaces between the Carrier and Probe-related hardware are shown in figure 4.6-2. All Probe data interfaces also pass through the cable cutter. The Probe, separation mechanism, and the receiver have a number of passive analog and bilevel transducers that are sampled by the Carrier CDS. Sampling of these telemetry points does not require the participation of the receiver or Probe electronics.

CDP-formatted checkout data pass through the Probe exciters and travel at RF to the receivers over coaxial cables. The receiver then processes the data as if they were received through the antenna and sends them to the Carrier serial bus via its BIU. This scheme provides an end-to-end checkout of both the Probe and receiver. An option exists whereby the Probe returns data directly to the Carrier through its BIU. This option would allow checkout of the Probe without involving the receiver or Probe RF equipment. The baseline does not employ this option because the increased CDP complexity outweighs the potential checkout power savings.

CDP Redundancy Options

Four redundancy options for the Command and Data Processor (CDP) have been identified. In the following descriptions, the options are ordered by increasing redundancy and complexity. In Option A, shown in figure 4.6-3, the unit simply comprises two identical and independent halves. The Carrier selects the prime half prior to Probe separation, and the other half remains off for the remainder of the mission. This option has the advantage of simplicity, but is vulnerable to single failures after separation.

Option B (figure 4.6-4) offers increased reliability by using a self-test analyzer to test both CDP halves and select the prime one just before entry. The analyzer monitors prime timing signals from then on, and selects the backup half should the timing go out of tolerance. If the backup half is viable, its data function remains synchronized with that of the prime half, and allows redundant data collection and transmission. Finally, the Carrier can disable the self-test analyzer should it fail prior to separation. This option was selected for the Galileo Probe, because volume, mass, and schedule precluded the following options.

As shown in figure 4.6-5, the two CDP halves of Option C operate independently to provide active redundancy. The identical halves are not synchronized, and hence, require asynchronous serial data interfaces with the non-redundant science instruments. The asynchronous data interfaces can be implemented by each instrument or by a separate unit (see following paragraphs). Critical command enabling, coupled with judicious command output circuit assignment, gives protection against single-failure false commands. CDP oscillator fault protection precludes premature command sequencing as a result of a single failure (see following paragraphs). Option C provides increased reliability over Option B, and eliminates the synchronization hardware and self-test analyzer.

Option D, figure 4.6-6, is the most reliable and complex of the four options. The data function is essentially the same as that of Option C. The command function, however, employs three sequencers and majority voting hardware. As with Option C, no self-test analyzer or synchronization hardware is required. Premature sequencing by one of the three command sequencers is not mission critical to this option. Coarse synchrony among the sequencers is necessary, however, and demands a certain stability of the CDP oscillators.

Baseline Subsystem

Option C has been chosen for the baseline subsystem because it offers the necessary reliability with lowest complexity and cost. Figure 4.6-7 shows the independent CDP halves and the remainder of the subsystem. Carrier commands are routed to both halves, either of which responds if powered and properly addressed. G-switch inputs provide timing cues to the CDP for descent sequencing. Each critical command requires an enable to prevent single-failure false commands. In addition, a latching g-switch enable within the PCU prevents execution of critical commands before entry. Non-critical commands do not depend on enables and execute directly if sent by either half. Each CDP half provides asynchronous telemetry timing to the Probe and science instruments, which then return separate, asynchronous data streams. The CDP halves independently format data for parallel transmission by the communication subsystem.

Pyrotechnic Control Unit

The redundant PCU provides isolation diodes, arming relays, and driver hybrids to meet requirements for mission reliability and shuttle safety. Hybridization of the driver circuits has proven to significantly reduce the mass and volume of this unit on the Galileo Probe. These same advantages apply to the Titan Probe. The arming circuit requires a command from the CDP in addition to g-switch activation before the drivers are connected to the power bus. Finally, each fire command from the CDP must be preceded by an enable command.

Oscillator Fault Protection

The baseline subsystem requires that sequencer oscillators be protected from single failures that cause oscillation at some higher frequency, since the resulting premature sequencing is potentially mission catastrophic. This type of failure is characterized by oscillation either at a harmonic frequency or in an undesired mode. In either of these cases, a bandpass filter centered about the fundamental frequency would block the undesired oscillation and halt the faulty sequencer.

Asynchronous Science Data Interfaces

The asynchronous data acquisition of the baseline CDP halves places special requirements on the serial interfaces between the CDP and the science instruments. Implementation of these interfaces requires either a second data output circuit from each instrument or a separate data splitter unit. Figure 4.6-8 shows one option in which the science instrument design remains essentially unchanged. The instrument provides asynchronous data outputs by simply replicating the circuitry from the A/D converter to the output connector. Figure 4.6-9 shows an option in which the science instrument retains the single data interface typical of Galileo Probe instruments. This option requires a separate data splitter circuit, like the one shown, for each instrument. Intermediate options require that the science instruments provide some of the buffering and/or control functions.

In the baseline design, science instruments provide asynchronous data outputs to the CDP. The implementation of these outputs is an instrument design issue whose impact depends on data handling hardware complexity.

Convolutional Encoding

The tradeoff regarding the implementation of convolutional encoding for the Probe-receiver link is essentially hardware vs. software. The hardware option requires an estimated 100 equivalent parts, which is about 2.5% of a Galileo CDP. Software encoding requires about 25 instructions per bit, which occupies 8.3% of the baseline processor's time. The baseline design uses software encoding because it imposes an acceptably low demand on processor time, and requires no additional hardware.

Data Rates

Table 4.6-2 lists the factors that contribute to the rate of data transfer from the receivers to the Carrier for both the high and low Probe data rates. The factors comprise: Probe formatting and convolutional encoding, receiver engineering data, radio science data, receiver packetization, and a factor of 2 to account for receiver redundancy. Packetization follows the CCSDS recommendation, uses 1024-bit packets, and does not employ error control fields. The highest data rate seen by the Carrier is around 45,000 bps - well within the capability of the serial bus.

TABLE 4.6-1 - UNIT MASS, POWER, AND DIMENSIONS

UNIT	QUANTITY	MASS (KG)	POWER (W)	DIMENSIONS PER UNIT (CM)		
				L	W	H
CDP HALF	2	14.4	20	30.5	15.2	8.9
PCU	2	3.45	0	27.9	10.8	8.3
G-SWITCH	4	0.55	0	3.8	3.8	3.8

TABLE 4.6-2 - DATA RATES

DESCRIPTION	HIGH RATE (BPS)	LOW RATE (BPS)
PROBE NET DATA RATE	10,000	100
PROBE FORMATTING	10,492	105
PROBE CONV. ENCODING	20,984	210
RECEIVER ENGINEERING	21.184	410
RECEIVER PACKETIZATION	22,226	430
RADIO SCIENCE	22,476	680
RECEIVER REDUNDANCY	44,952	1,360

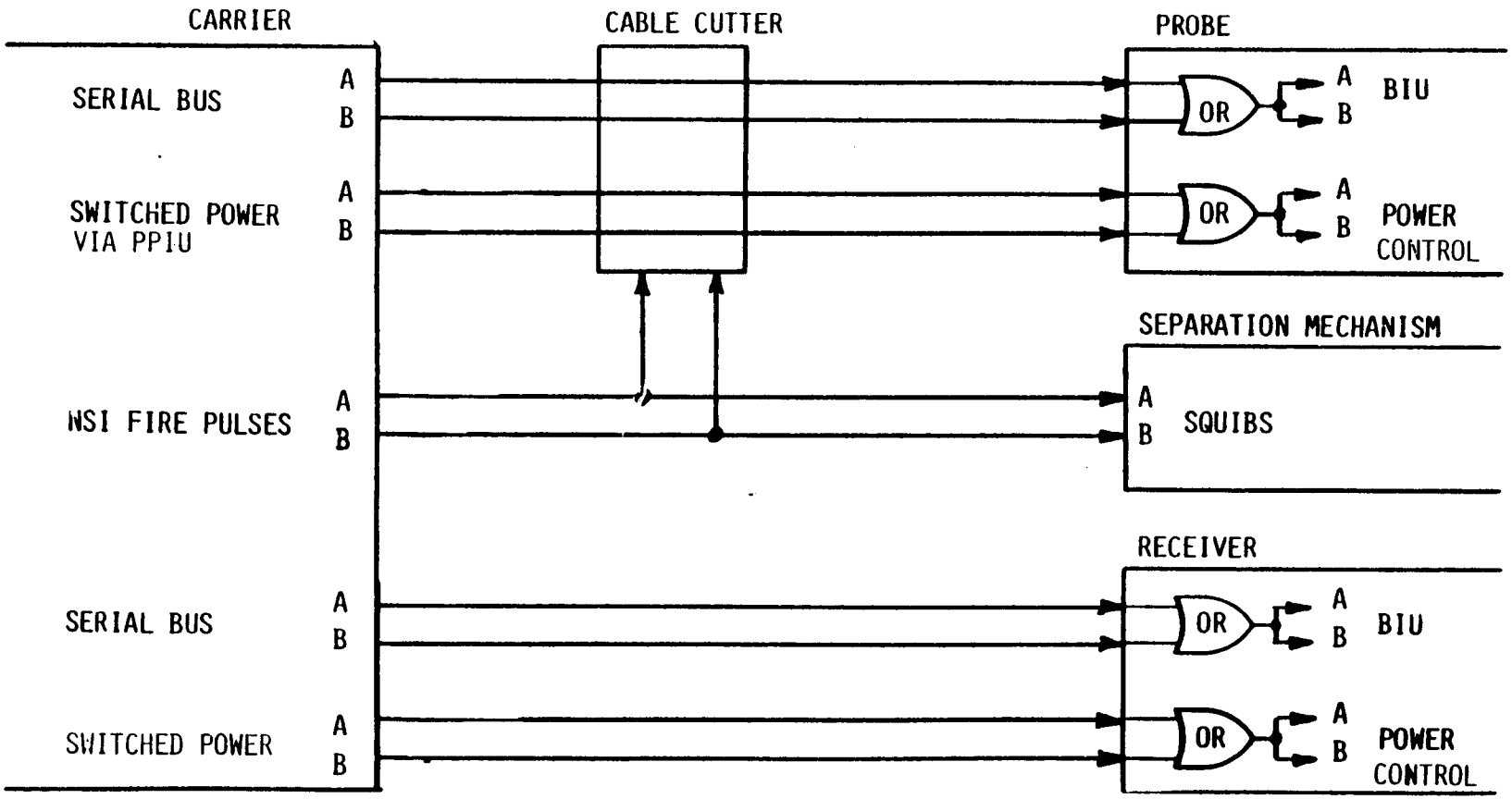

FIGURE 4.6-1 - PROBE COMMAND INTERFACES WITH CARRIER

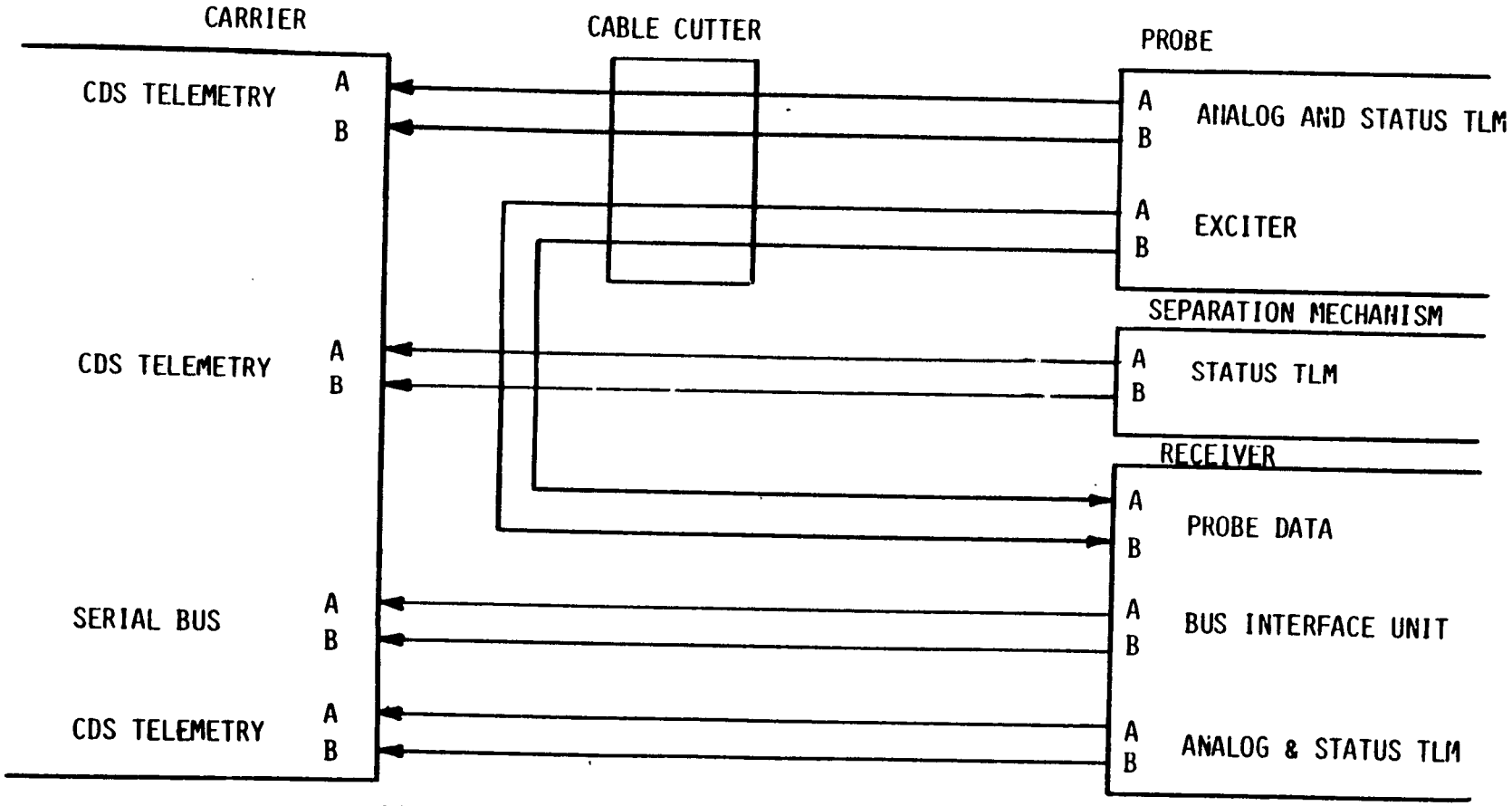

FIGURE 4.6-2 - PROBE DATA INTERFACES WITH CARRIER

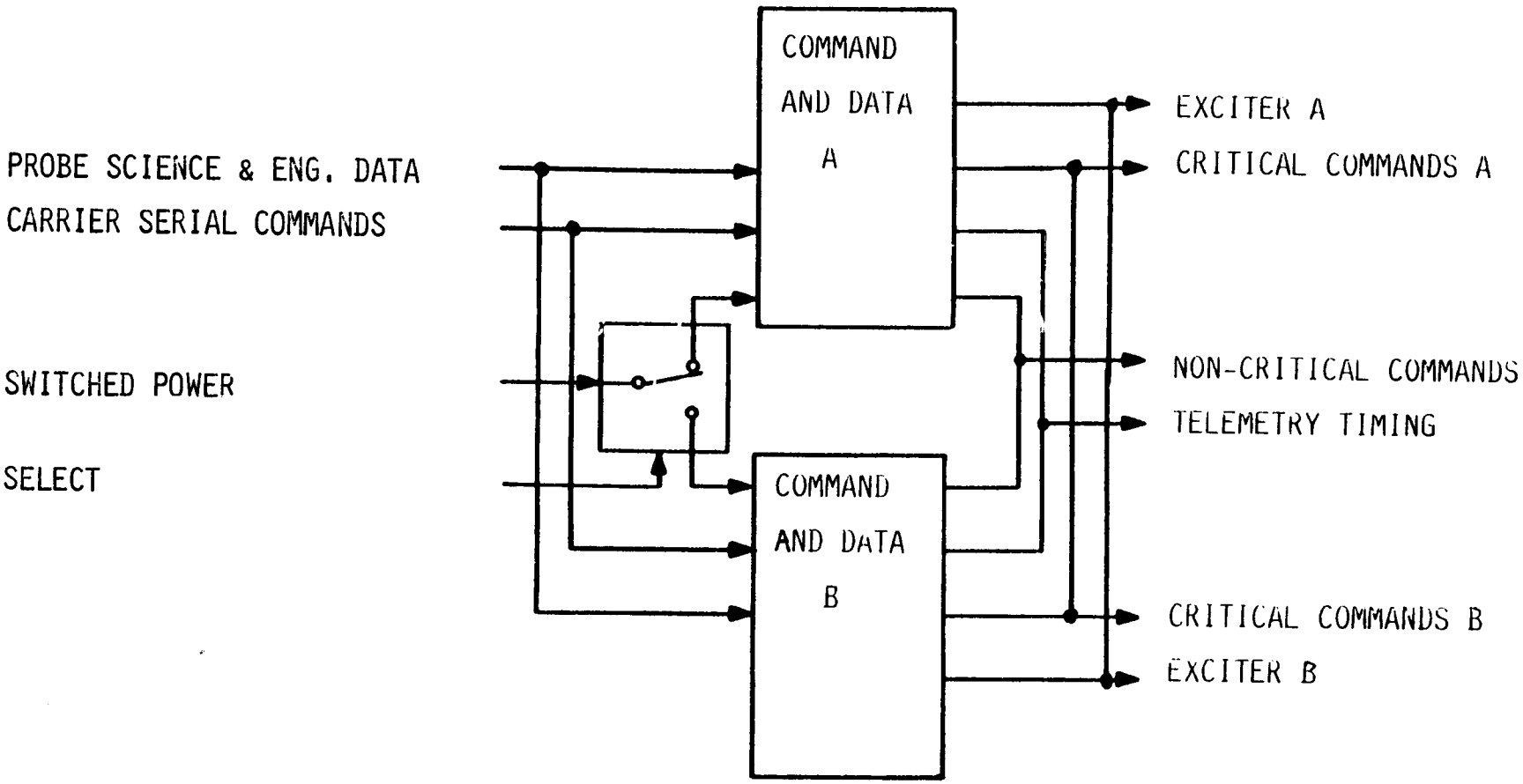

FIGURE 4.6-3 - OPTION A: REDUNDANT UNITS, ONE SELECTED BEFORE PROBE SEPARATION

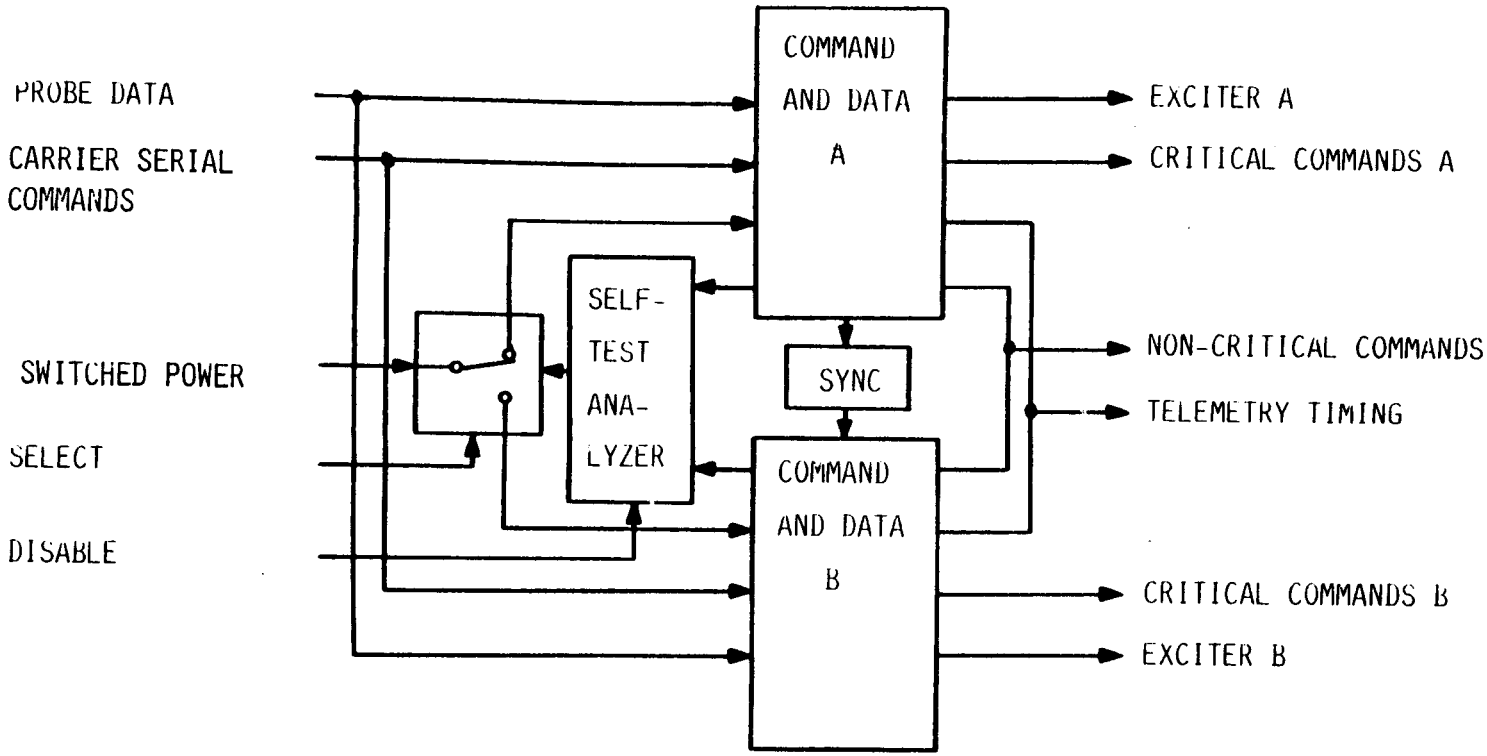

FIGURE 4.6-4 - OPTION B: QUASI-REDUNDANT DATA PROCESSING SELF TEST ANALYZER COMMAND CHECK

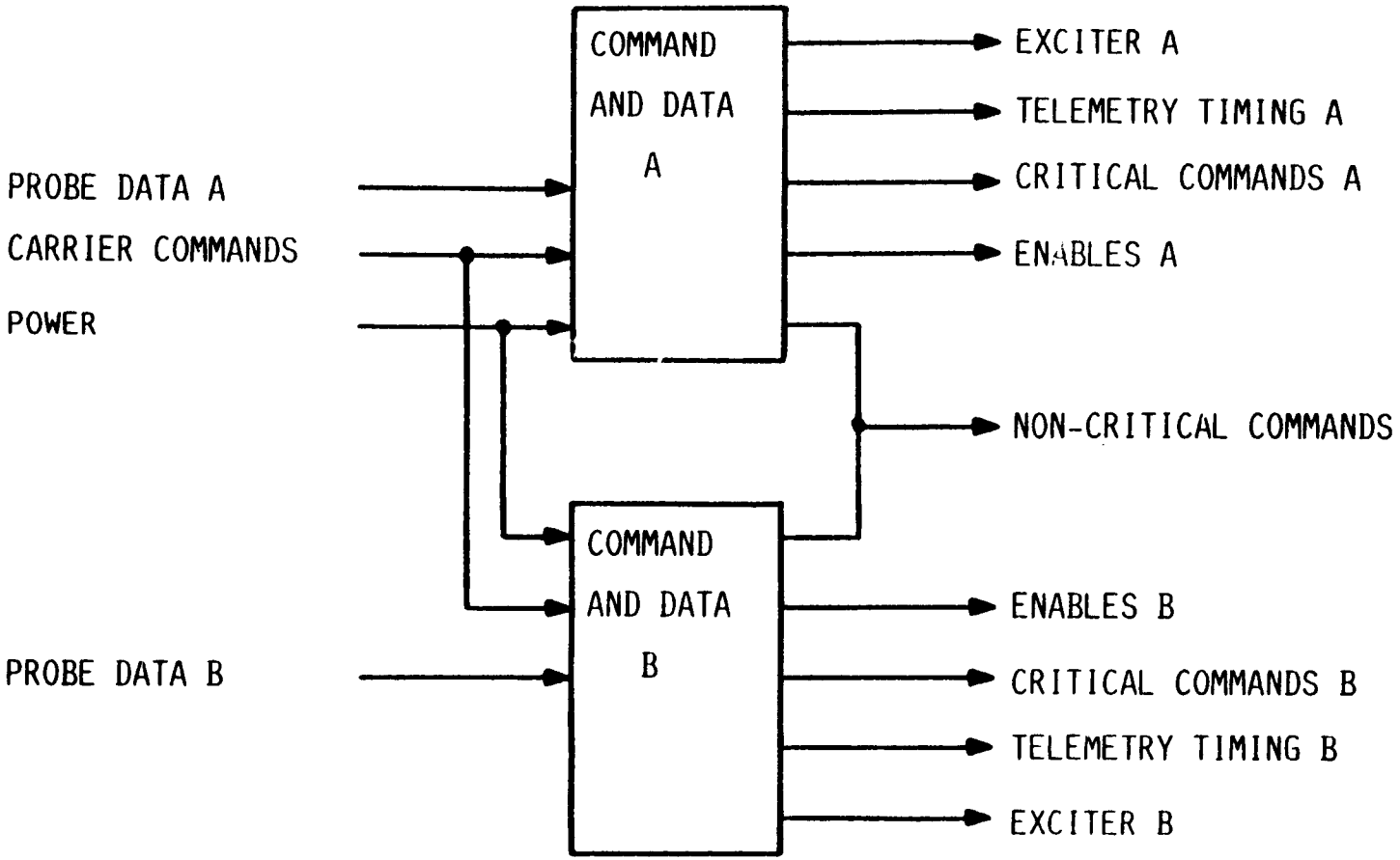

FIGURE 4.6-5 - OPTION C: REDUNDANT DATA PROCESSING WITH CRITICAL COMMAND PROTECTION

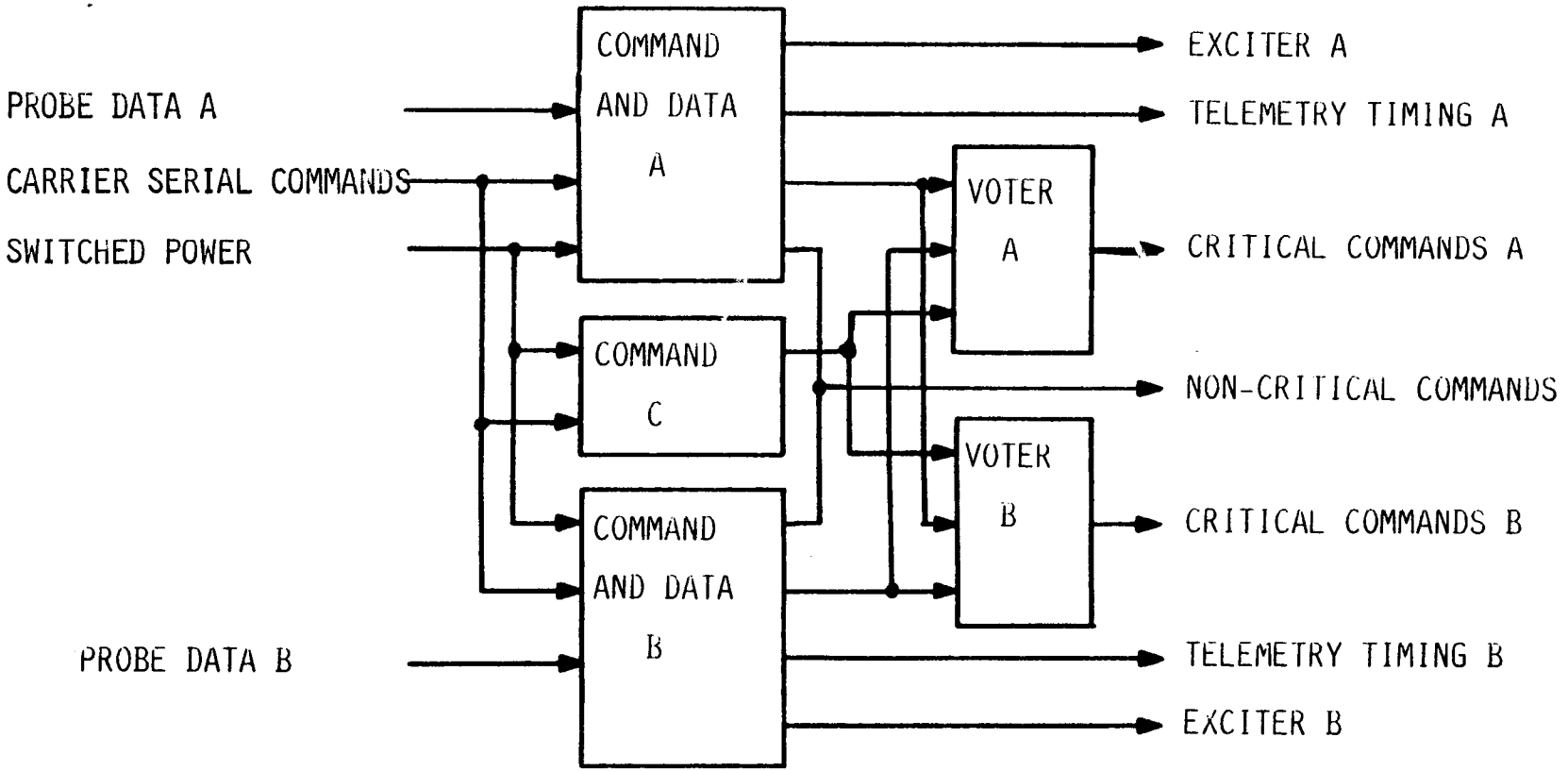

FIGURE 4.6-6 - OPTION D: REDUNDANT DATA PROCESSING AND 2 OF 3 COMMAND VOTING

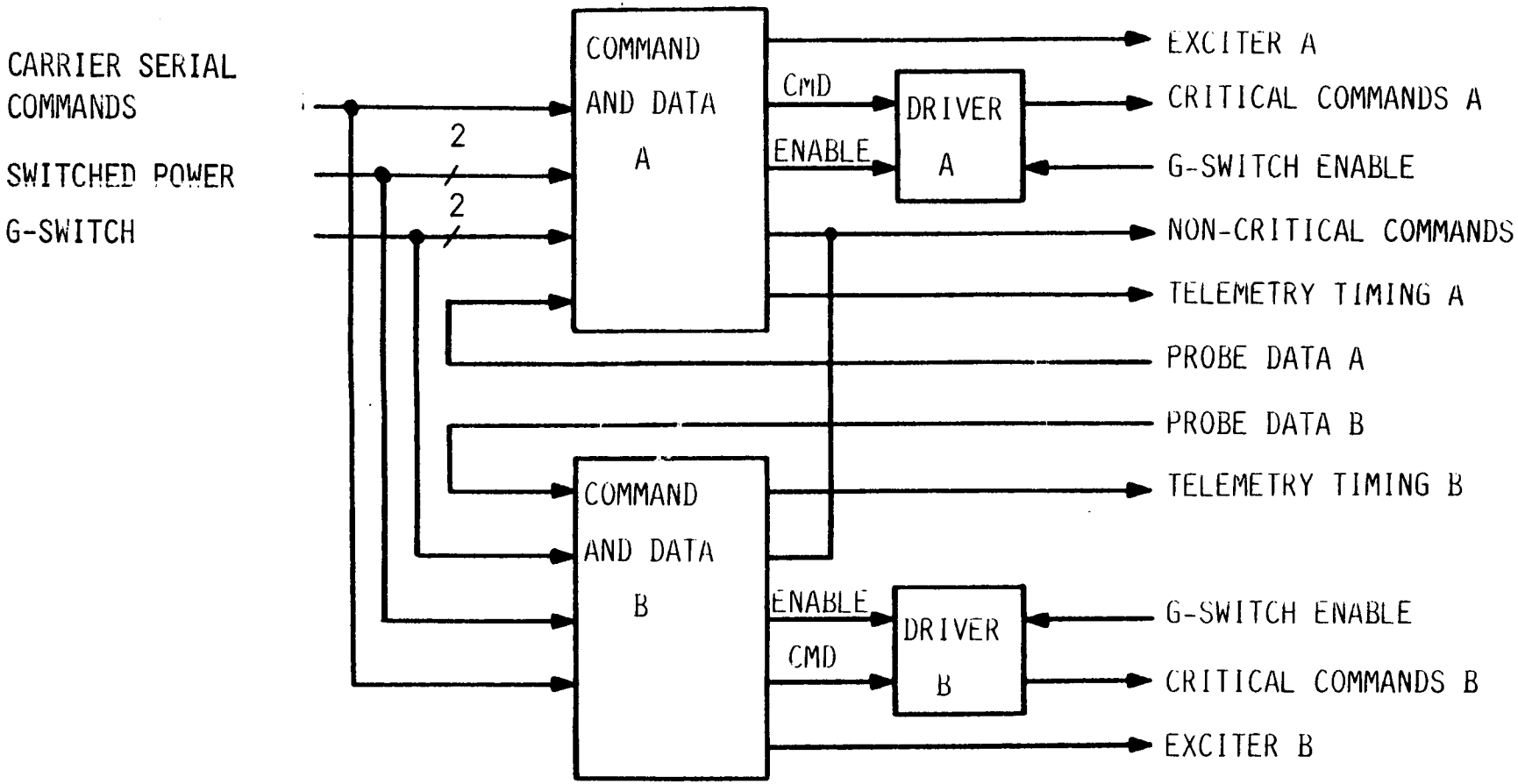

FIGURE 4.6-7 - BASELINE SUBSYSTEM

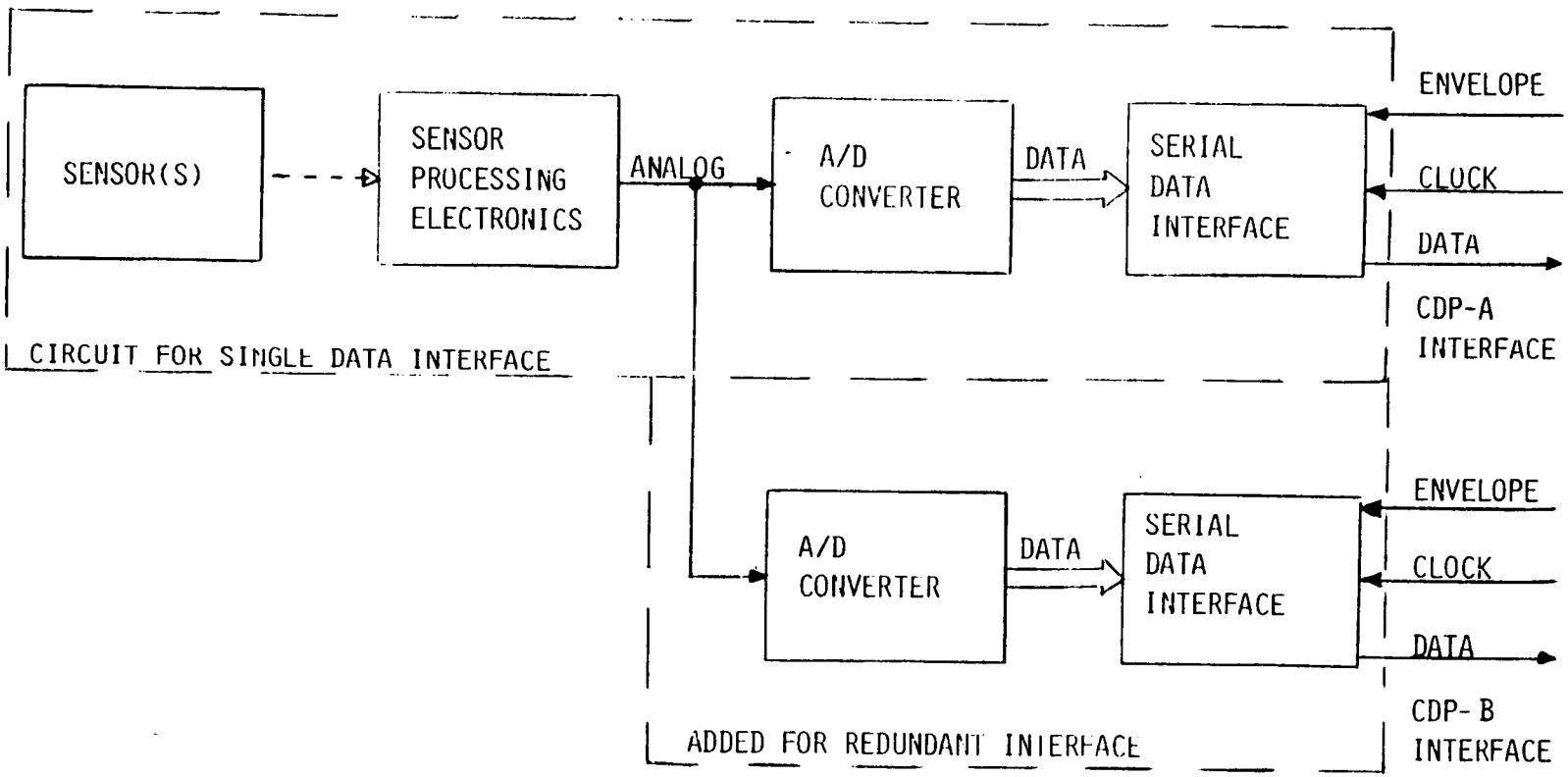

FIGURE 4.6-8 INSTRUMENT DATA INTERFACE FOR REDUNDANT ASYNCHRONOUS SAMPLING

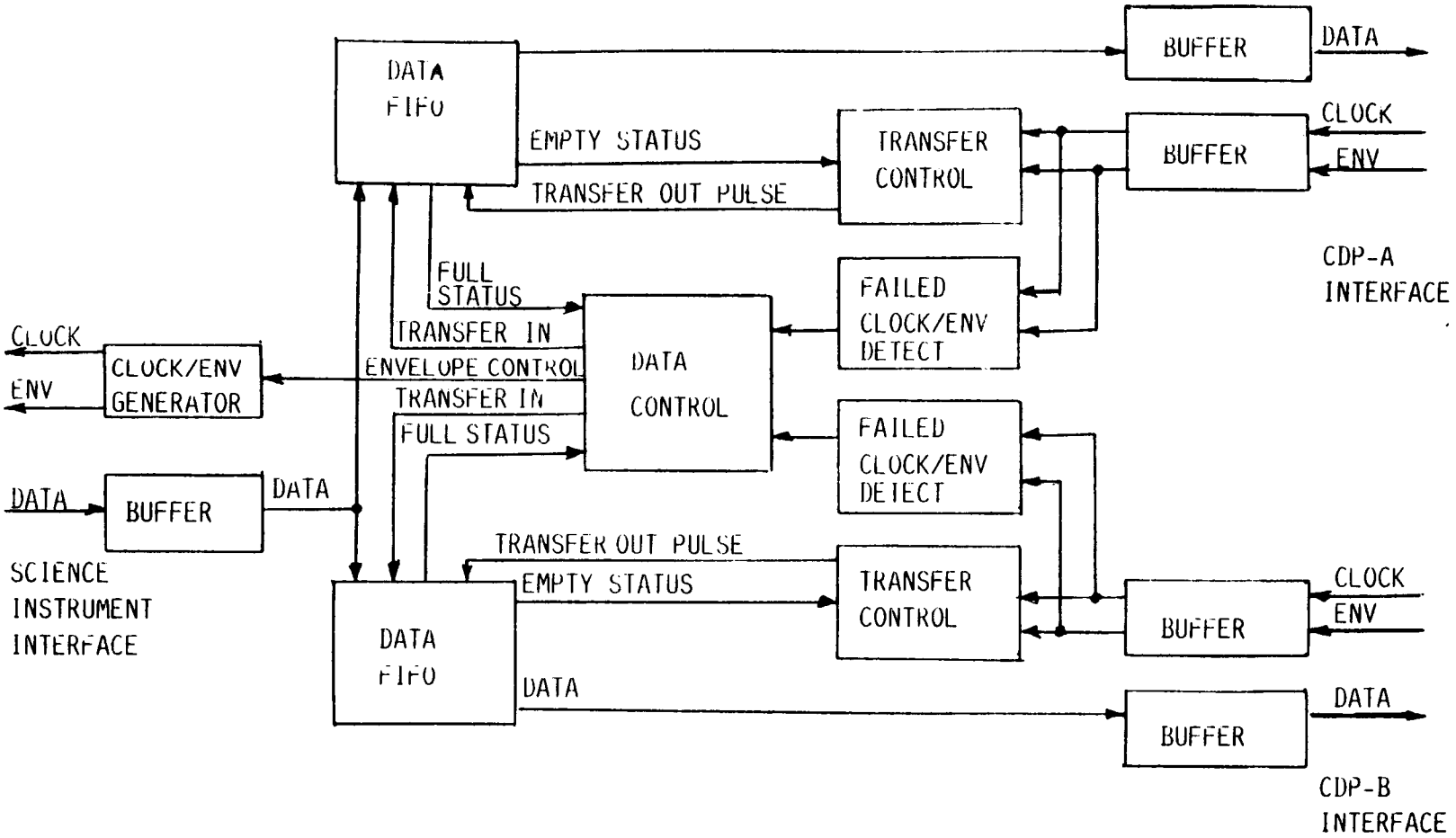

FIGURE 4.6-9 DATA SPLITTER UNIT FUNCTIONAL DIAGRAM

5. CARRIER INTERFACE

5.1 Separation

Requirements

The requirements for Probe separation from the Carrier derive from the basic requirement that the separation velocity be sufficient to assure separation. Furthermore, the Probe angular momentum must be large enough to assure a nose first atmospheric entry and sufficiently small to permit satisfactory Probe precession to zero angle of attack during entry.

Any candidate separation design must be within Carrier requirements for disturbance impulse and must meet mission requirements for separation precision. Imprecision in the separation velocity vector produces targeting errors and imprecision in the angular momentum vector produces errors in the angle of attack at entry.

Design Selection

The requirements can be met with three separation concepts. Each is characterized by the way that the angular energy is applied.

The first is the Galileo approach: ejecting the probe from a spinning carrier. The carrier provides the angular velocity through its spin, allowing the separation hardware to provide only a translational impulse. The gyro control limit (2^{o}/sec) of the 3-axis stabilized Mariner Mark II Carrier eliminates further consideration of this approach.

The second approach is a gradual buildup of angular momentum with a Carrier mounted spin up system. The separation impulse is also only translational.

The third concept is simultaneous translational and rotational impulse. A wide variety of hardware implementations are possible. The difficulty is to meet spin and delta V requirements without sacrificing separation precision.

Table 5.1-1 shows the hardware implementations examined for this study. All three designs can provide the required separation energy but differ greatly in design complexity.

The spin table system applies a gradual spinup through a motor driven platform with springs on the platform separating the Probe when the proper angular velocity is reached. All shuttle launched HS-376 satellites use this approach. Application to the Titan Probe mission necessitates costly scaling down of complex and expensive hardware. Furthermore, the volume of the hardware pushes the Probe into the Shuttle envelope, significantly reducing the allowable size of the fixed decelerator.

The centerline spring system and the three canted spring system are two different methods of applying a simultaneous spin up and ejection. The centerline approach incorporates a single spring mechanism attached at the Probe centerline. The spring is mounted in a helix-slotted cyclindrical housing which

attaches to the Carrier. Guide pins in an outer jacket force the Probe to rotate as the spring extends, constraining the Probe's motion during separation. The angle of the helix determines the ultimate angular velocity of the Probe at release. A single separation bolt initiates separation which occurs in approximately 0.5 seconds.

Some sample design characteristics for this system are given below. The assumed separation parameters are consistent with the requirements listed above.

probe mass - 141 kg
probe inertia - 44 kg-m^2
probe spin rate - 10 rpm
probe velocity - 0.2 m/sec
helix angle - 41.3°
torque radius - 16.9 cm
spring constant - 12.1 kn/m
spring diameter - 5.7 cm
spring compressed length - 3.0 cm
spring length at release - 8.0 cm
release time - 0.44

The primary disadvantage of this system is the complexity of the design for Probe attachment. The centerline application of force significantly complicates nosecap design. It also requires a separate attachment structure to carry launch loads.

By incorporating the springs into the load bearing structure the three canted spring approach minimizes the structural complexity. This system uses three springs mounted near the radius of gyration. Canting the springs at the proper angle provides the proper ratio of angular to translational momentum. Unlike the centerline system, the three spring approach requires the simultaneous release of three mechanisms for proper Probe deployment, introducing additional separation errors due to non simultaneity. Analysis of a similar three spring separation for Galileo Probe indicates a time uncertainty of release of 2 msec.

Concepts for a three canted spring design range from a guided release resembling the centerline spring to an unguided release in which the mass and inertia of the Probe preserve the alignment during ejection. The unguided three canted spring design has the advantage of simplicity and the disadvantage of less precision. The relative structural and mechanical simplicity as well as low cost of the three spring design results in its selection as the baseline separation scheme for this report. Since the predicted targeting error and angle of attack are acceptable, the baseline further assumes unguided separation. A discussion of separation parameters and dynamics for the baseline design follows the hardware description in the next section.

Baseline Separation Hardware - Three Canted Spring Design

Figures 5.1-1, 5.1-2, and 5.1-3 show the Carrier/Probe mechanical interfaces. The three support structure designs (monopod, bipod, and tripod) accommodate the different Carrier mounting locations along the bulkhead and equipment ring (Figure 5.1-1). All three have plates holding the spring cartridges and separation nuts. (Figure 5.1-2). A ring links the three supports together.

Three elliptical penetrations in the Probe decelerator nose allow the spring cartridges to mate to the main Probe structure (Figure 5.1-3). The spring cartridge tube carries loads from the Probe to the support plate. It houses a 10 cm compressed spring which extends to 15 cm for Probe release. A bolt running along the centerline of the spring ties the support to the Probe. The ball-in socket at the cartridge end bears loads in the direction of the Probe's centerline. A bolt catcher within the Probe attaches to the equipment shelf. Insulation around the bolt catcher protects the equipment module from concentrated heating loads during atmospheric entry.

The umbilical cord to the Probe runs along one of the three struts and enters the Probe through another penetration. A cable cutter and retraction springs separate the cable prior to Probe release. Section 4.6 discusses the signals carried by the umbilical cable.

Firing the three explosive nuts forces the bolts entirely into the Probe and frees the springs for Probe release. Tabs in the cartridges impede any further spring extension beyond 15 cm. Crushables at the end of the bolt catcher prevent any damage to the Probe. The Probe separates with a corkscrew motion - simultaneously spinning and translating away from the Carrier. The dynamics of the separation are discussed below.

Separation Dynamics

The following design parameters separate a probe with a mass of 141 kg and inertia of 44 Kg-m 2 at 0.2 m/s and 10 rpm spin rate.

cant angle:	75.2 deg
radius to spring attach points:	0.45 m
spring constant:	7184 N/m (3 places)
spring compressed length:	10 cm
spring stroke:	5 cm
release time:	0.15 s
angular impulse:	46 Nms
linear impulse:	28.2

The resulting impulses applied to the Carrier are within JPL's limiting values for such impulses: . 100 Nms angular, 60 Ns linear. A wide range of separation velocity and spin rate is allowable. Figure 5.1-4 sketches the bounds.

The orientation of each spring provides both a tangential (spin-up) and axial (separation) force to the Probe. There is no radial component. The Probe contact surface is a ball-in socket, as is used for Leasat frisbee ejection. By attaching the spring to the support structure with a pin the cant angle can change slightly during ejection. With the example design, the spring cant angle

rotates from 75.2 deg to about 72 deg during ejection. The springs apply their force at 0.45m, close to the radius of gyration of 0.56m. Mounting the springs further from the Probe radius of gyration would increase the amount of spring rotation. A spring guide prevents excessive spring bending in the Probe radial direction.

The key concern of the three spring spin/ejection scheme is the possibility of undesired torques perpendicular to the intended spin direction causing the Probe to tumble. Tumble will not occur if there is a fast enough spin up -- or large enough inertia.

To help understand the action of this system we can consider the dynamic response of classes of systems to an angular impulse about a transverse axis. For a spinning body this impulse induces nutation about an offset angular momentum vector. For a non-spinning body this impulse induces tumbling (if given enough time). For a body undergoing spin-up this impulse can start the body tumbling but as long as the motion doesn't prevent proper application of the spin-up torque, the motion becomes nutation as the body is spun up. The response approaches the spinning body response as the spinup time approaches zero.

An estimate for the maximum undesired transverse angular impulse comes from previous analysis of the Galileo Probe ejection. In this case, the effect of all misalignments, asymmetries, mistimings, and other separation torques in the transverse direction is calculated to be less than the equivalent of 1 Nms angular impulse applied at the start of separation.

If a 1.0 Nms transverse angular impulse is applied to the Titan Probe at the start of spin/eject and assume separation within 0.2s, the symmetry axis tips less than 0.3 deg, giving displacements less than 5% of the spring stroke. Also, after 0.07s the Probe has acquired half of its final angular momentum. At this time, the symmetry axis has tipped only 0.1 deg and the displacements are less than 1.5% of the spring stroke. Since the displacements are small, they do not prevent the springs from spinning up the Probe, and the Probe achieves a stable spinning condition although the initial condition has no angular momentum. Figures 5.1-5 and 5.1-6 demonstrate successful separation for this case based on dynamic simulation.

A perfect ejection would give the Probe angular momentum and separation velocity vectors with the desired magnitude and direction. The errors in the Probe angular momentum and separation velocity come directly from two sources: 1) Carrier orbit and attitude errors, and 2) asymmetric ejection effects. A two body simulation program has been developed to study asymmetric separation effects. The simulation uses JPL-supplied mass properties for the Mariner Mark II carrier and Hughes estimates for Probe mass properties: 141 Kg mass, 44 KG-m^2 spin inertia, and 24 KG-m^2 transverse inertia. The effects of spring mismatch, Carrier reaction, release mechanism mistiming, and Probe center of mass offset were studied separately.

Simulation #1 assumes an inertially fixed Carrier, matched symmetric springs, simultaneous separation device release, and perfect Probe balance and alignment. Figure 5.1-7 shows that the Probe acquires the desired 0.2 m/s separation velocity and 10 rpm spin rate following an ejection that takes about 0.15 s.

Simulation #2 shows the effect of the Carrier reaction to the separation forces. The separation axis does not pass through the Carrier center of mass and does not lie along a principal axis. As a result, the Carrier rotates about all three axes as the Probe is ejected. Figure 5.1-8 resembles figure 5.1-5. This similarity indicates small errors in magnitude: about 1% in spin angular velocity and 0.5% in axial velocity. Figure 5.1-9 shows the resulting components of separation velocity and angular velocity in the directions perpendicular to the desired direction.

Simulation #3 shows the effect of a large spring mismatch. Spring mismatch is expected to be the largest asymmetric effect associated with separation device asymmetry. This simulation assumes one spring has a spring constant 110% of nominal while the other two have spring constants 90% of nominal. In reality, this mismatch can be reduced by making a special effort to select matched springs. The conservative simulation shows about 2% change in the magnitudes of both the separation velocity and the angular momentum. Figure 5.1-10 shows the lateral velocity and transverse angular velocity profiles.

Simulation #4 shows the effect of a mistiming in one release mechanism. The 0.002 s maximum mistiming estimated for Galileo is used here. The simulation predicts a 1.2% error in separation velocity and a 0.2% error in angular momentum caused by the mistiming. Figure 5.1-11 shows the lateral velocity and transverse angular velocity profiles. Note that the final lateral velocity is much smaller than the lateral velocity in the middle of the ejection.

Simulation #5 shows the effect of Probe center of mass offset. A 1 cm offset from the release system axis of symmetry would cause a 1 cm/s lateral velocity for a 10 rpm release and guided separation. In the unguided system, figure 5.1-12, the final lateral velocity is less than this because of the action of the springs during the ejection. The simulation predicts a 1.2% error in separation velocity and a 0.2% error in angular momentum.

Imprecision in Probe angular momentum vector direction causes angle of attack errors at entry. Imprecision in separation velocity (particularly lateral velocity) causes targeting errors at entry. Table 5.1-2 summarizes the effect of the asymmetries studied in lateral velocity and angle of attack. The exact relationship between separation velocity error and targeting error depends on the Probe trajectory. If there were no gravitational effects, each mm/s of lateral velocity would cause 1.7 Km B-plane targeting error.

TABLE 5.1-1: SPIN/EJECT MECHANISM TRADEOFF

DESIGN	OPERATION	ADVANTAGES	DISADVANTAGES
Spin Table	Motor driven table spins up Probe	*Small springs minimize force imbalance	*Long time for spinup forces Carrier attitude control *Complex hardware includes table, motor, motor driver, rotary interface, 2 step release system (spin + linear) *Reduces fixed decelerator diameter
Centerline spin/eject	Helix-slotted spring housing provides simultaneous angular + linear impulse	*Single release mechanism *Probe motion guided during spinup	*Attachment on or near Probe centerline complicates nosecap design *Requires launch load carrying structure separate from ejection device
3 canted springs	3 canted springs simultaneously release Probe	*Avoids centerline attachment *Common structure for launch loads and mechanism *Low side loads at Probe attach points	*Non-simultaneous release complicates mechanism design *Probe unconstrained during release leads to tipoffs *Varying bends loads through support structure

TABLE 5.1-2 SIMULTION RESULTS

Source of Asymmetry	Contribution to lateral velocity	Contribution to angle of attack
orbiter reaction	0.0014 m/s	0.06 deg
spring mismatch	0.032 m/s	1.0 deg
mistiming	0.0011 m/s	0.05 deg
center of mass offset	0.004 m/s	0.25 deg

FIGURE 5.1-1 PROBE/CARRIER MECHANICAL INTERFACE

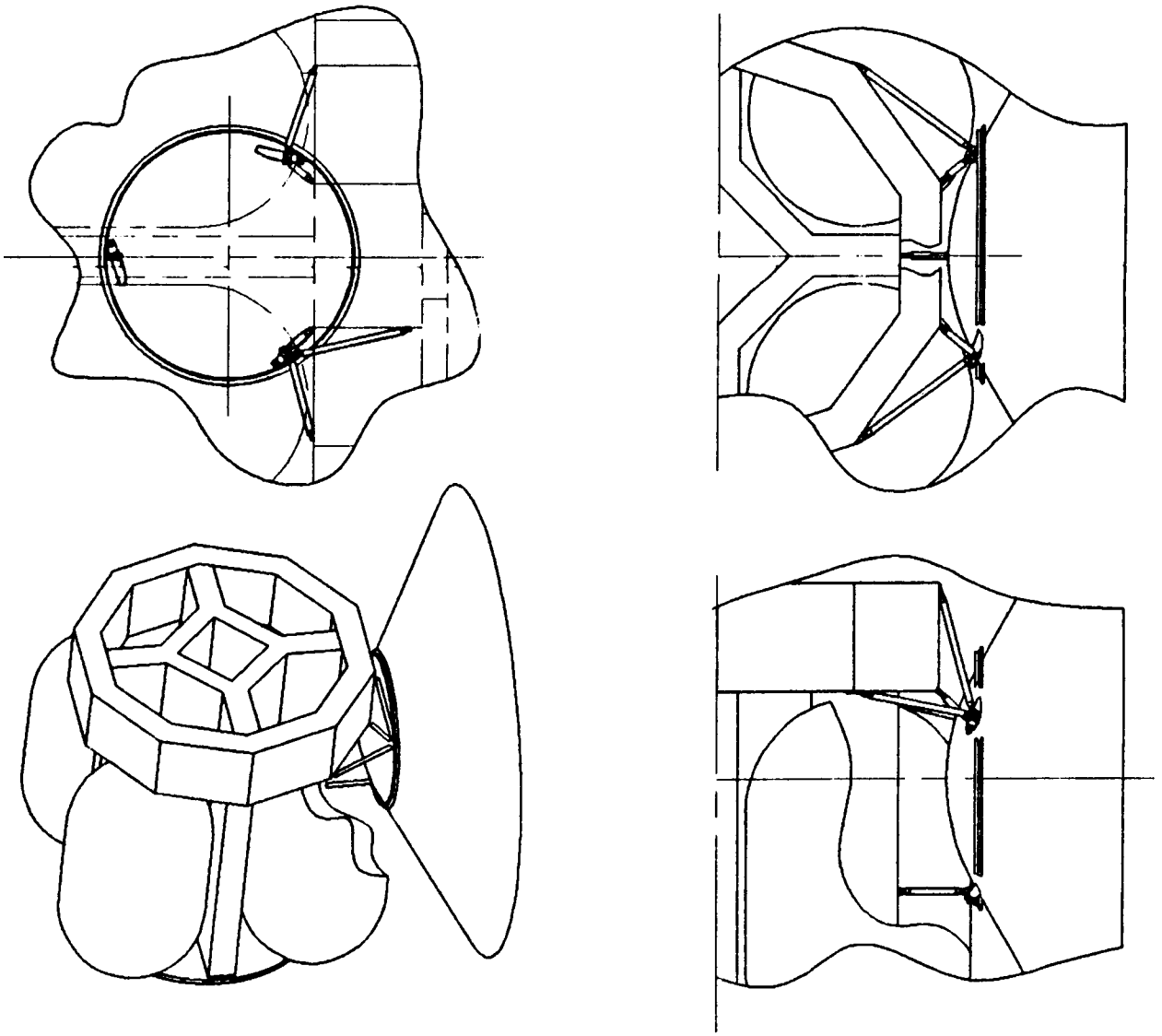

FIGURE 5.1-2 PROBE ATTACHMENT STRUT ASSEMBLIES

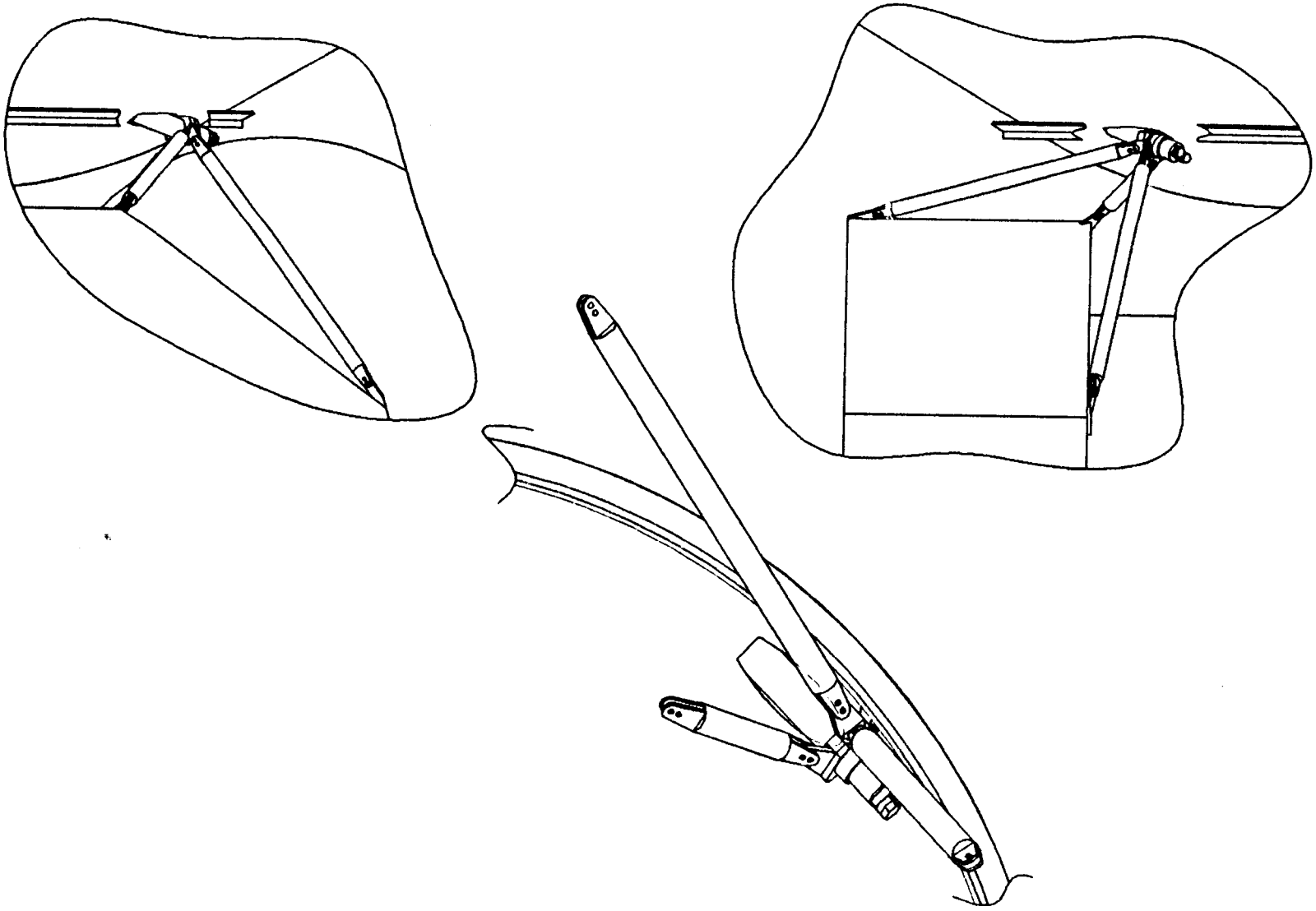

FIGURE 5.1-3 SPIN-EJECT MECHANISM

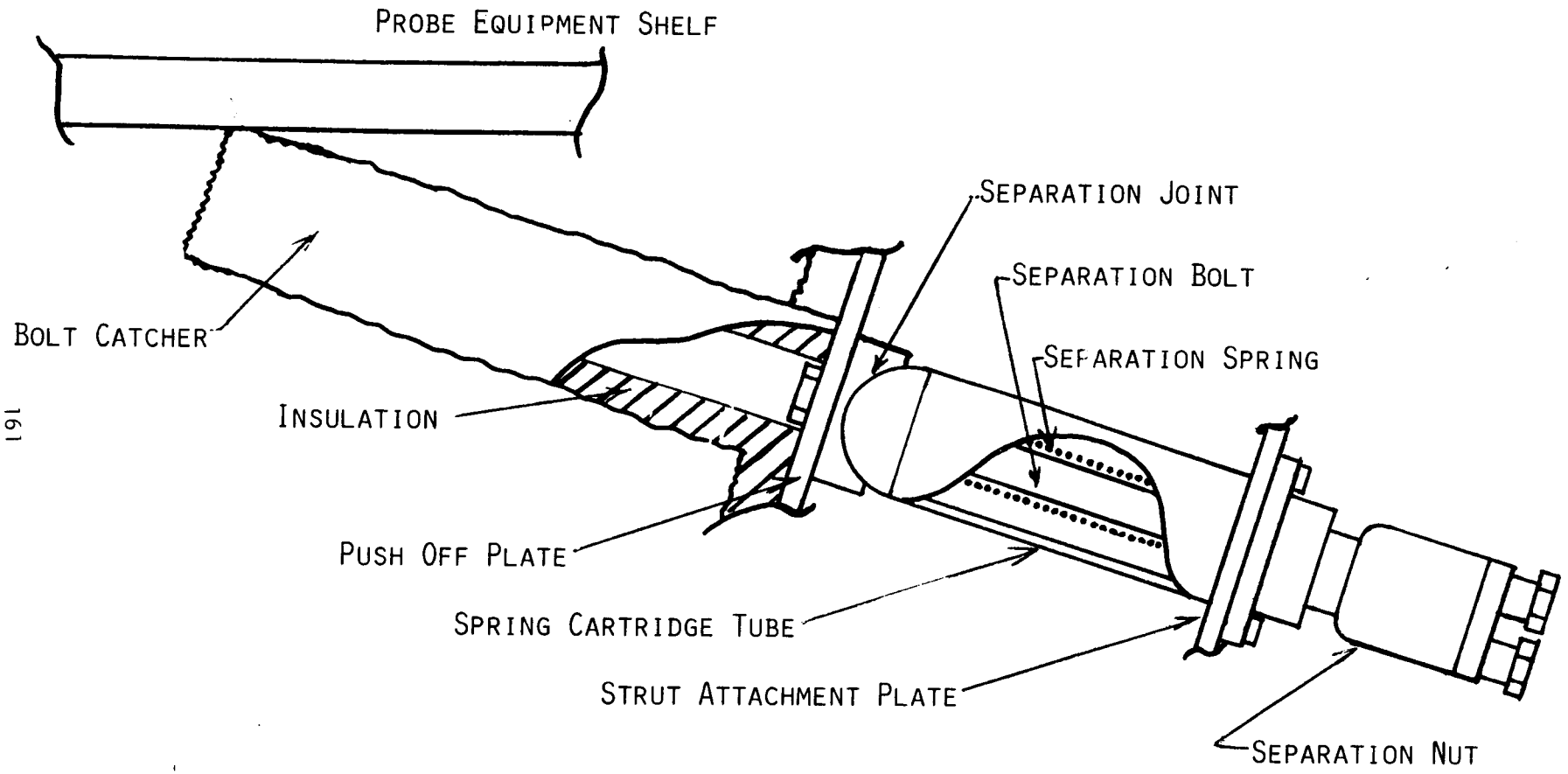

FIGURE 5.1-4 -PROBE SEPARATION PARAMETERS

SEPARATION REQUIREMENTS MAY BE MET WITH A RANGE OF SPIN RATE AND ΔV.
THE FOLLOWING GRAPH SHOWS APPROXIMATE LIMITS.

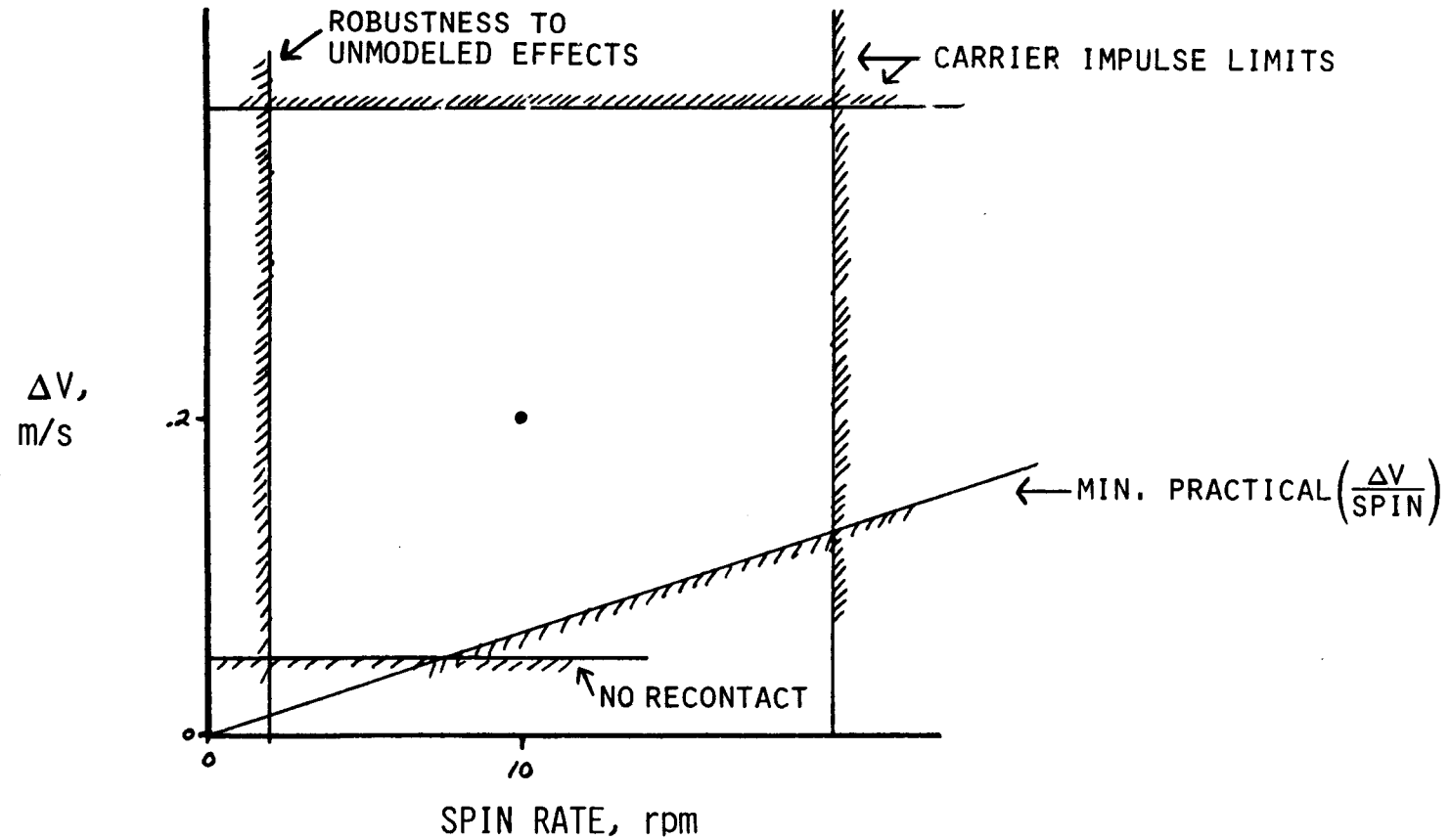

FIGURE 5.1-5-IMPULSE RESPONSE

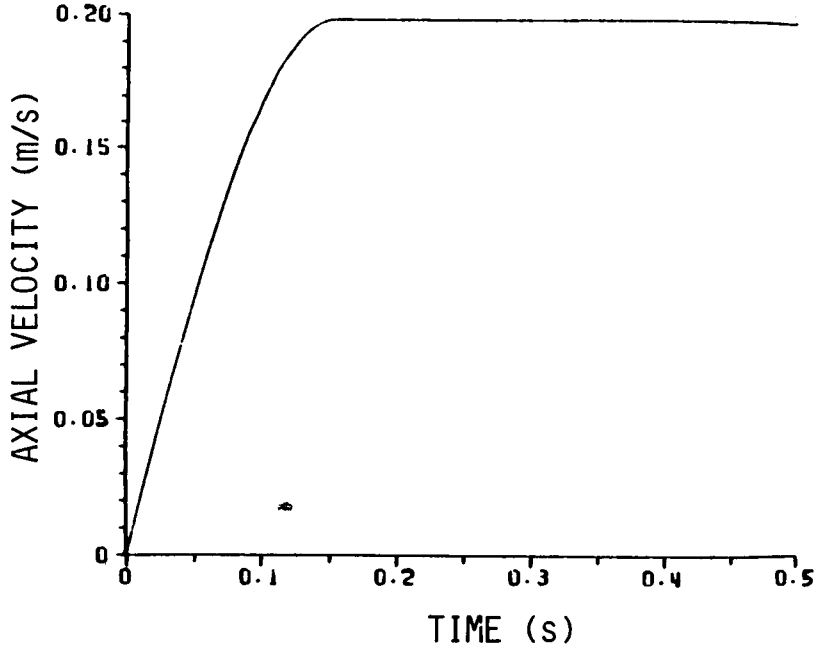

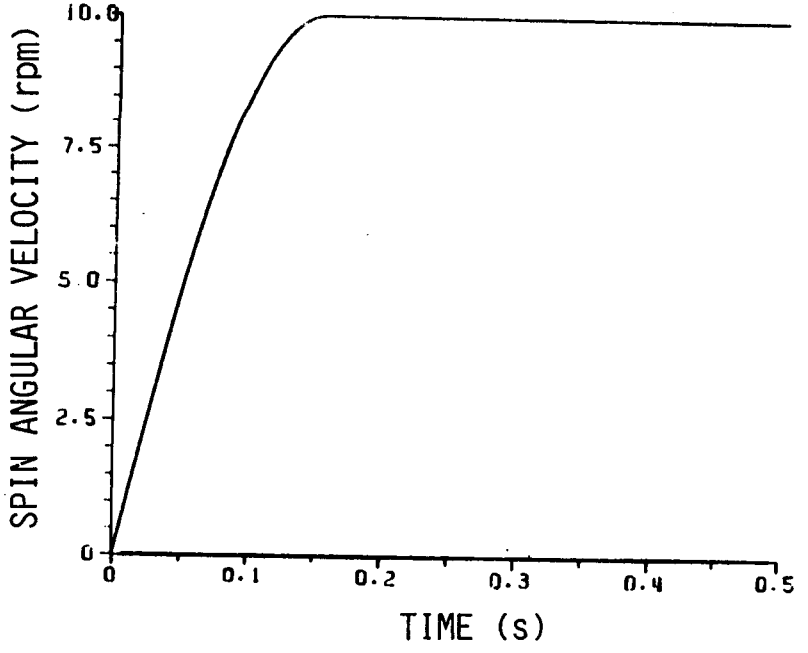

FIGURE 5.1-6 - IMPULSE RESPONSE

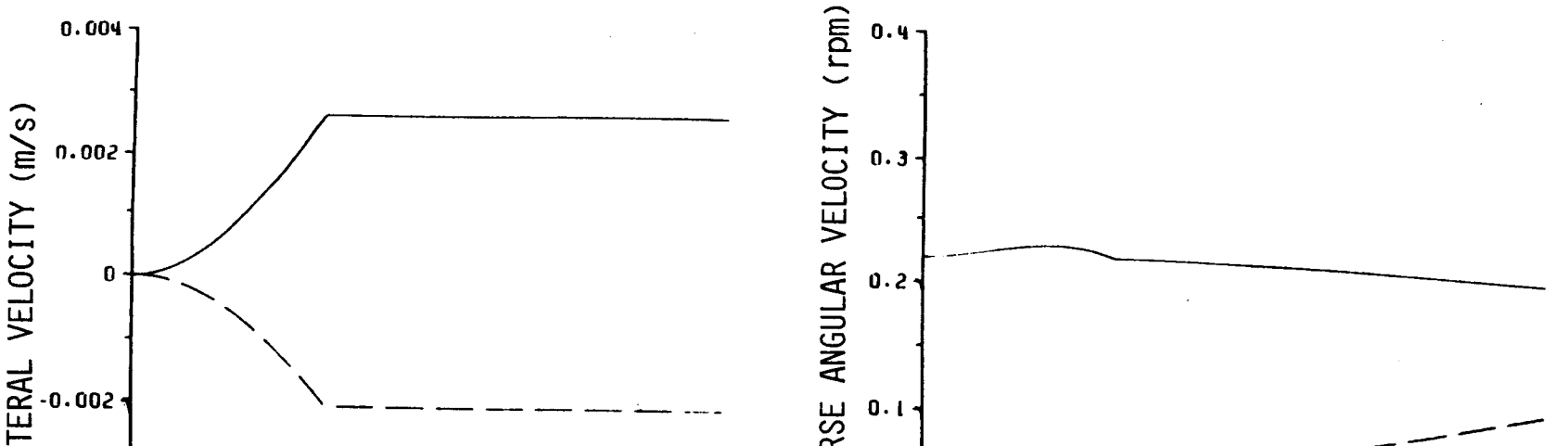

FIGURE 5.1-7 - SIMULATION #1

- CARRIER CONSTRAINED
- NOMINAL SPRINGS

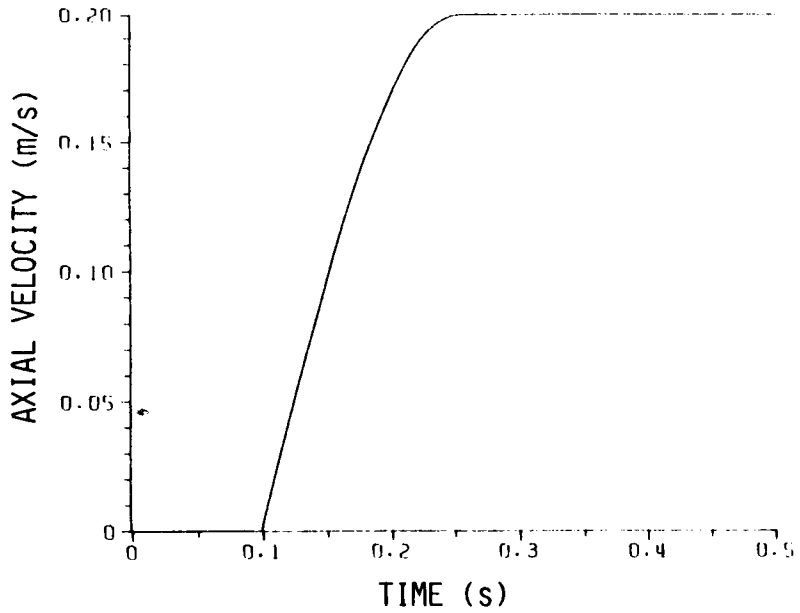

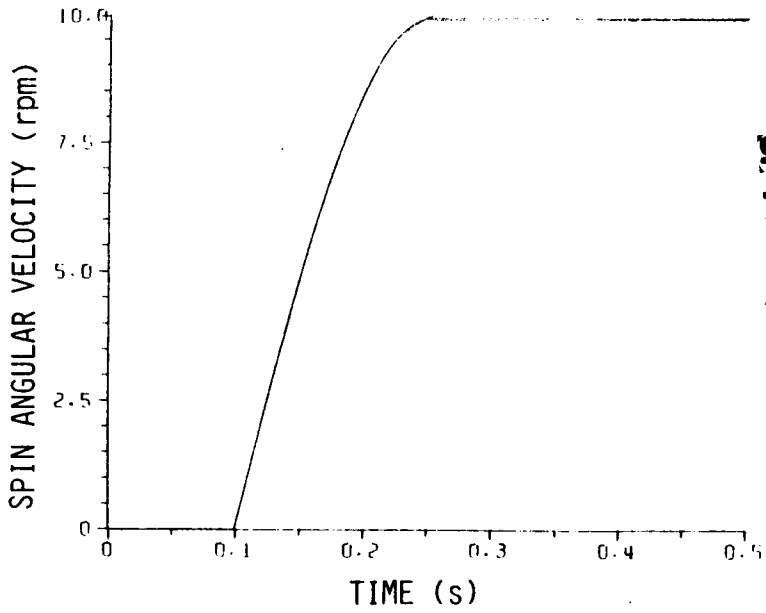

FIGURE 5.1-8-SIMULATION: #2

- CARRIER REACTION INCLUDED
- NOMINAL SPRINGS

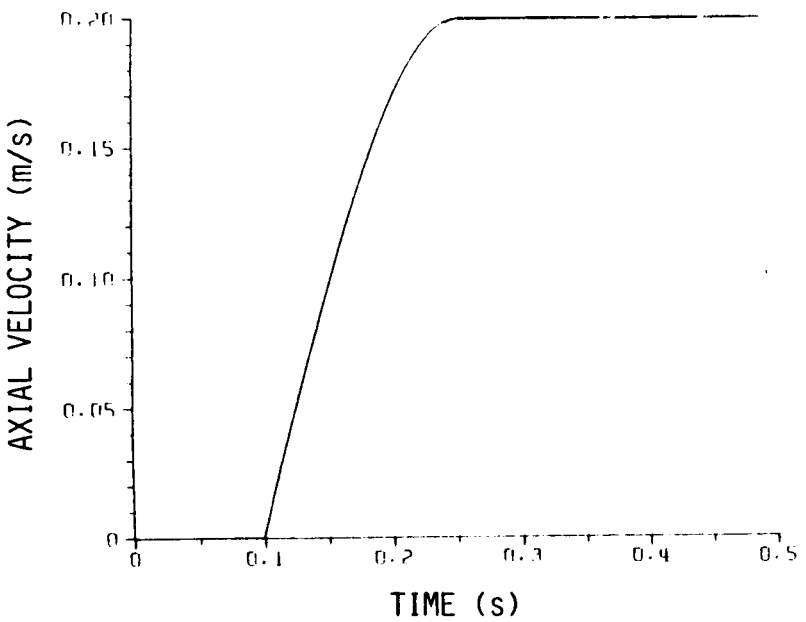

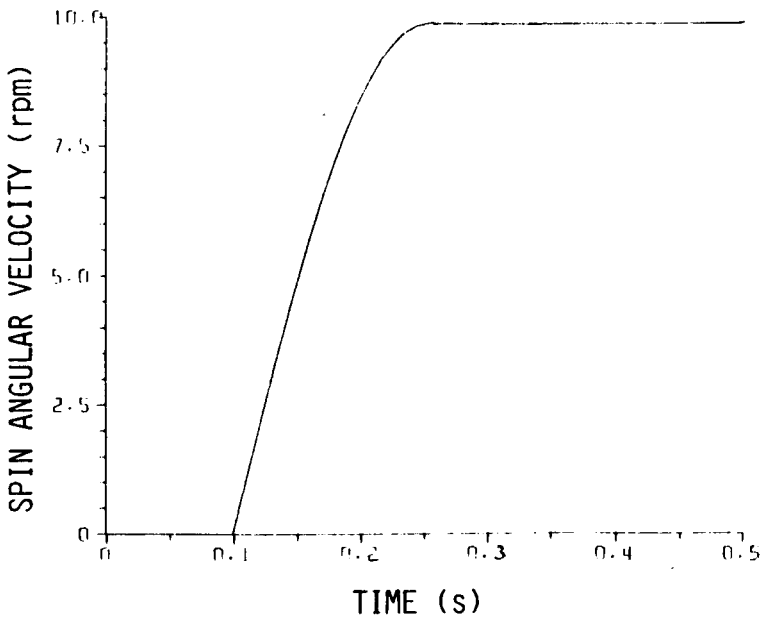

FIGURE 5.1-9 -SIMULATION #2

- CARRIER REACTION INCLUDED
- NOMINAL SPRINGS

FIGURE 5.1-10-SIMULATION #3

- CARRIER CONSTRAINED
- ± 10% SPRING MISMATCH

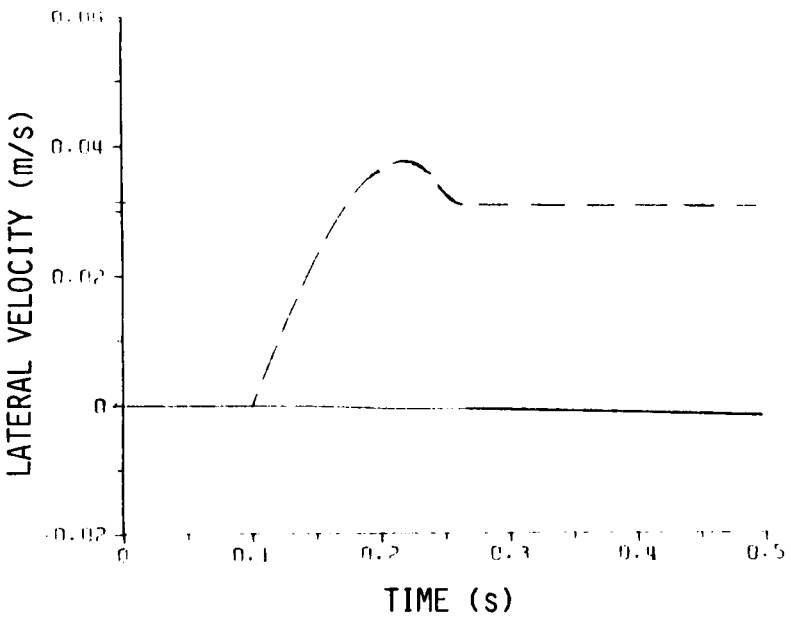

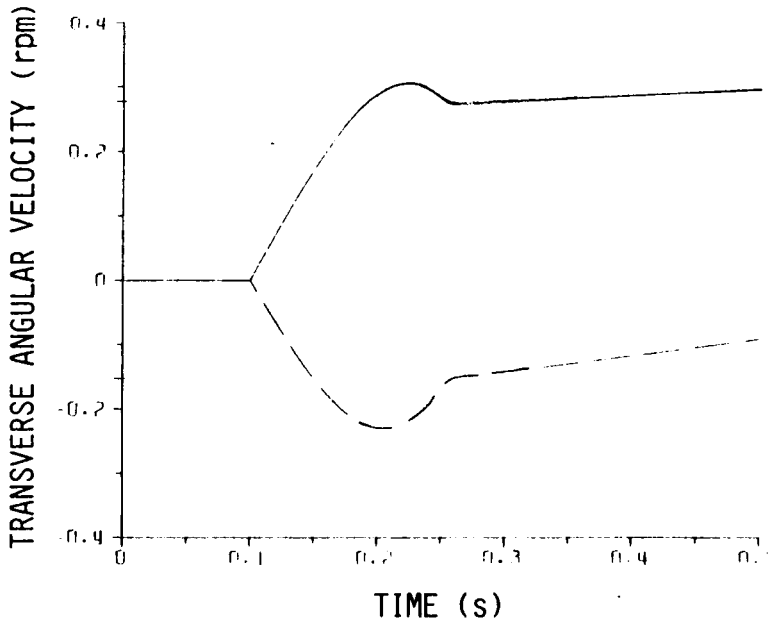

FIGURE 5.1-11- SIMULATION #4

- .002 s MISTIMING

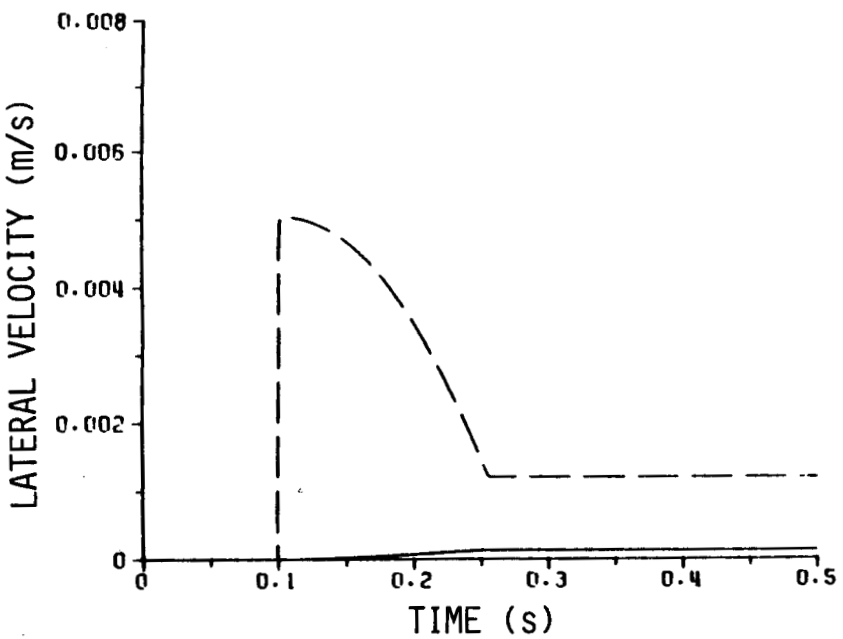

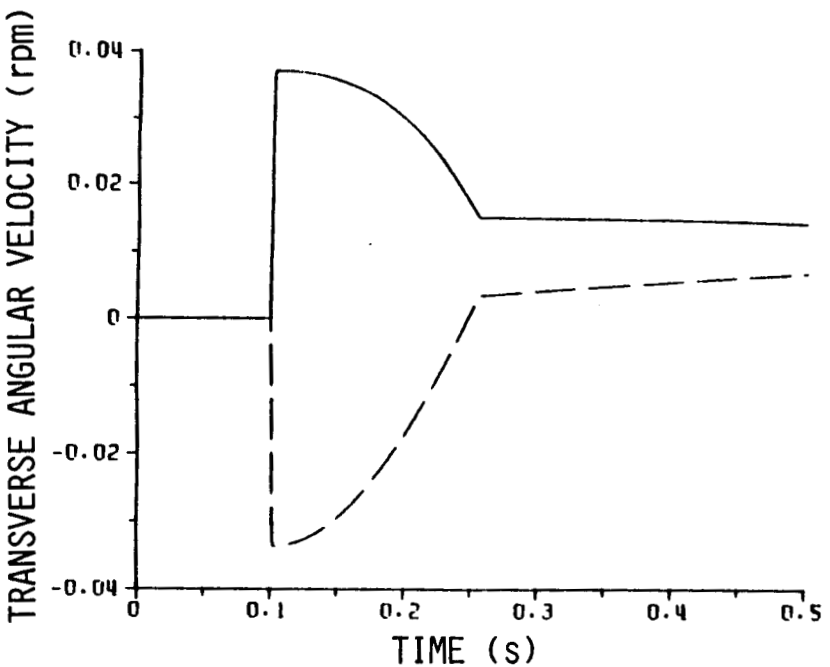

FIGURE 5.1-12 -SIMULATION #5

- 1cm PROBE CENTER-OF-MASS OFFSET

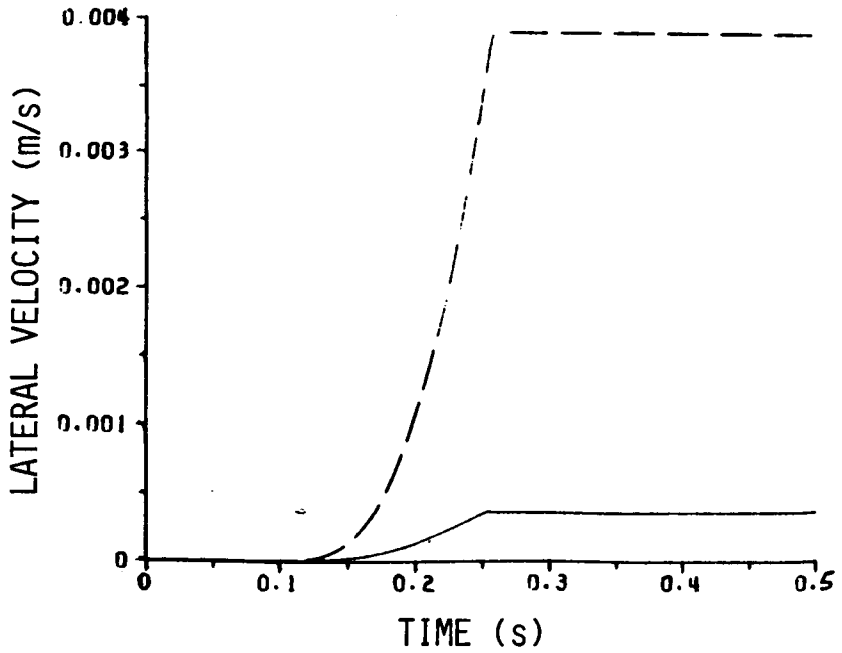

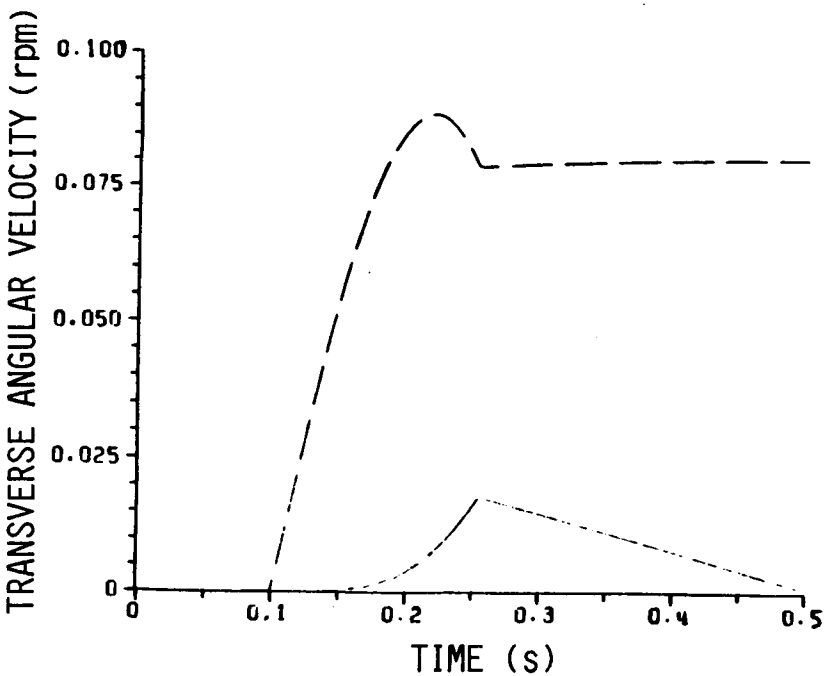

5.2 Receive Antenna

Figure 5.2-1 shows a possible Carrier mechanical integration of the baseline 0.75m diameter receive antenna. The antenna mounts on the top of the spacecraft below the Earth pointing high gain antenna. Preliminary configuration studies indicate that an antenna up to 1 m diameter can mount in this area, but the integration of any antenna requires a detailed examination by the Mariner Mk II configuration engineers at JPL. Depending on the final mission plan the antenna may be required to point anywhere from -5^{o} to -140^{o} from the anti-Earth line. An antenna positioner is necessary to allow this mission flexibility and, as shown in section 2.4, considerably increases communications performance if used to track the Probe position during Carrier over flight. The receive antenna may also mount to the scan platform which eliminates the need for a separate pointing mechanism, but requires a longer cable run to the receiver. A thorough tradeoff of antenna integration options requires refinement of Carrier design constraints and link performance requirements.

FIGURE 5.2-1 RECEIVE ANTENNA INTEGRATION

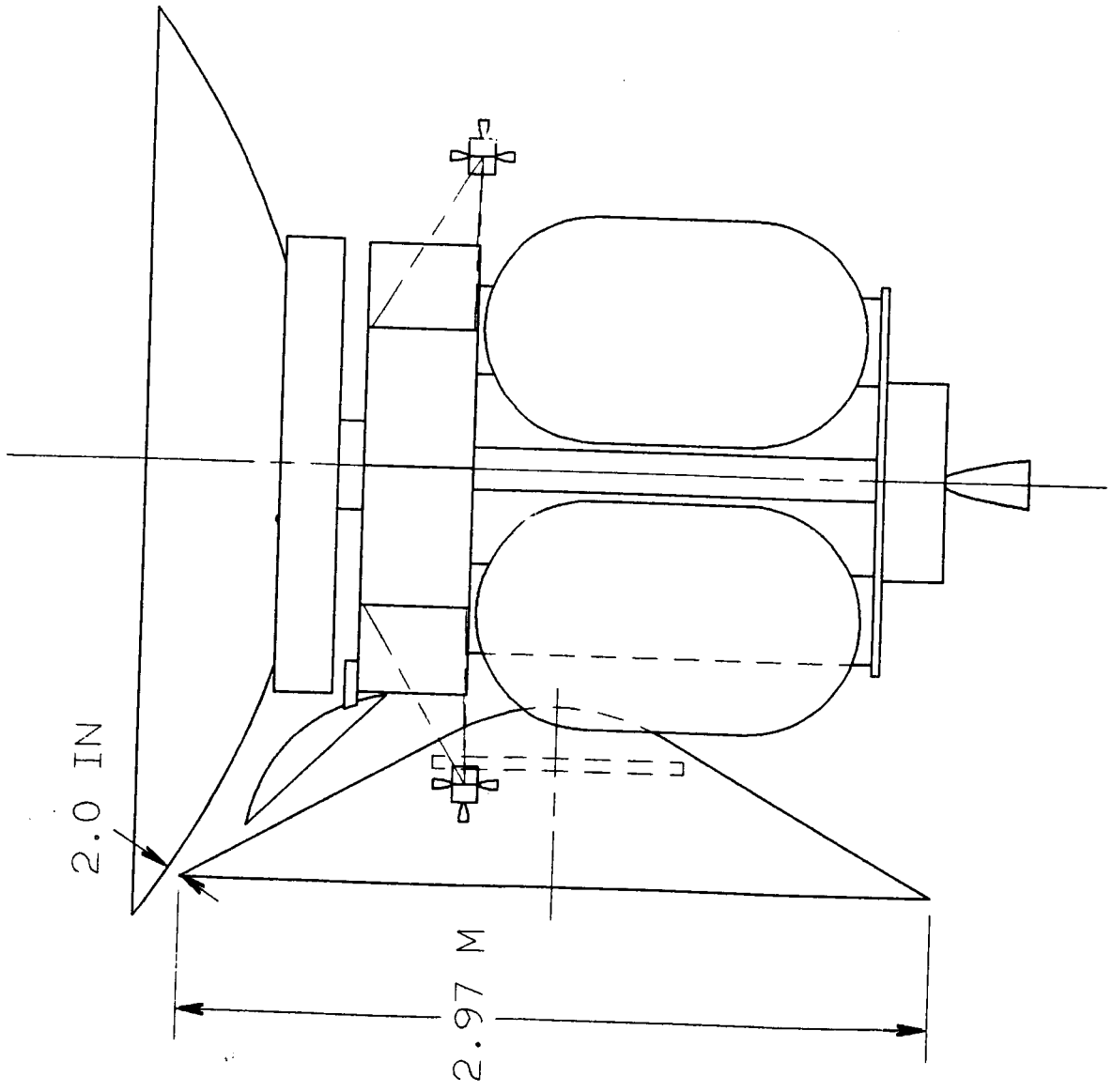

5.3 Receiver

The mission analysis in section 2.4 shows two ways that the receiver design is a determining factor in the performance of the system. The receiver design sets both the requirement for Eb/N_0 (energy to noise level ratio) as well as the tolerable level of doppler rate. These requirements limit the time that at a given rate can be supported.

The key driver in the receiver design is the requirement for two data rates: one at 100 bps and the other at 10 Kbps. Both data rates must be received with an error rate better than one in a thousand. In addition, the receiver must detect when the transition between the two data rates occurs. The purpose of the higher rate is to allow for an imaging device which requires a data rate of at least 2 kbps and preferably 10 Kbps. The preliminary strategy is to initiate the imaging at an altitude of 10 km with the Probe clock triggering the switch to the higher data rate. As a point of reference, the Galileo Probe has a simplification of only one data rate of 128 bps and a complication of a lower C/N_0 (carrier to noise ratio) at acquisition.

Modulation Formats

The first step in the receiver design is to determine the means of transmitting digital data from the Probe to the receiver. Given that there are no bandwidth constraints, three modulation formats are applicable: (1) non-coherent frequency shift keying (NC FSK), (2) non-coherent differentially encoded phase shift keying (NC DPSK) and (3) coherent binary phase shift keying (BPSK). NC FSK provides the least complex receiver structure while BPSK is the most complex. If the Eb/N_0 requirements for the different modulation formats were identical, then NC FSK would be the obvious choice for implementation; however, Table 5.3-1 demonstrates that this is not the case.

Table 5.3-1 shows the theoretical (implementation losses are not included) Eb/N_0 required to achieve a bit error rate of 10^{-3}. Requirements are listed for both uncoded data and rate 1/2, constraint length 7, convolutionally encoded data. Constraints on the receiver's output data rate preclude the use of soft decision information (see section 4.6). The requirements for the convolutionally encoded data assume that the error rate on the Carrier to Earth link is not significant. Note that while elimination of coding would seem to reduce receiver complexity, this is not really the case. Removal of the convolutional code would require the inclusion of Manchester encoding to ensure enough bit transitions for proper signal synchronization.

For coded data, BPSK clearly provides the best performance while NC FSK is the worst performer. The issue is whether the reduced complexity of NC FSK offsets the 5.2 dB penalty in the Eb/N_0 requirement. This higher Eb/N_0 requirment lowers the time that can be supported at a given data rate (section 2.4); however, if both NC FSK and BPSK provide sufficient time, then NC FSK is the proper choice. To quantitatively evaluate the differences in receiver complexity, specific receiver designs must be examined. NC DPSK was not included in this study because it was marginally less complex than BPSK.

Receiver Design Tradeoff - BPSK

The simple NC FSK mechanization comes at a cost of higher required Eb/No to achieve a given bit error rate. BPSK requires significantly less link power at some increased complexity. In BPSK, the transmitter modulates the carrier with a signal which generates one of two phases. Typically, the two phases are 0 and 180 degrees; or equivalently, the modulating signal is plus or minus 1. To distinguish between the two transmitted phases, the receiver must generate a coherent phase reference. This process is known as carrier recovery and is typically accomplished with a phase-locked-loop (PLL). The PLL accounts for the additional complexity of the BPSK receiver.

Since coherent BPSK is used on the Galileo Probe, one conceptual approach for Titan Probe is to modify the Galileo receiver. Galileo uses a microprocessor based digital receiver designed to support a single data rate of 128 bps. There are two ways the Galileo design can be modified to accomodate higher rates: (1) replace the existing components with faster equivalents and/or (2) use the Galileo receiver concept, but map as many software functions as possible into dedicated hardware (to aleviate microprocessor loading). The fastest spacequalified microprocessor (3 MHz clock) applied to the Galileo design supports a data rate of only 660 bps. Mapping software functions into dedicated hardware yields a maximum supportable data rate of only 1300 bps. The Galileo design, therefore, can not be modified to meet the 10 kbps requirement. Though excellent for the low rate Galileo application, the all digital receiver is too computationally intensive in its implementation of carrier recovery and symbol synchronization loops.

The alternative BPSK receiver with analog carrier recovery and symbol synchronization loops (Figure 5.3-4) handles a data rate of 10 kbps without difficulty. The feedback loop at the front end recovers the phase of the carrier and demodulates the incoming BPSK signal. The acquisition logic and lock detector estimates carrier frequency to recover the phase of the carrier. The acquisition logic sweeps the center frequency of the voltage-controlled oscillator (VCO) until the lock detector indicates that the loop is in lock. Once the carrier frequency has been located, the data are demodulated. The output of the low pass filter (LPF) is the plus or minus one signal which, integrated over a bit time, estimates whether a "1" or a "0" has been received. As mentioned previously, the data rate decision and symbol synchronization functions are common to both the BPSK and NC FSK receivers.

The doppler performance of the BPSK receiver depends on the ability of the carrier recovery loop to track the phase and frequency variation of the carrier. Conceptually, the recovery loop is a feedback loop which reacts to the phase of the input signal. Hence, the loop must be at least second order to track the doppler variation. A third order loop (as chosen for Galileo) provides improved tracking ability. The degree to which the loop can track the frequency variation is dependent upon the functional form of the doppler variation.

Figure 5.3-5 shows a doppler rate profile for a typical mission. With an exponential approximation, the doppler limitations of the carrier recovery loop can be determined both by simulation and analysis. The performance limits depend on the order and bandwidth of the loop. For the second order loop, a loop bandwidth of 20 Hz satisfies the constraints on phase degradation, mean

time to cycle slip, and loop sweep rate. Simulations show that the second order loop can track doppler rates up to 2 Hz/s with a bandwidth of 20 Hz.

Simulations also show that the third order loop can track doppler rates up to 110 Hz/s with a loop bandwidth of only 5 Hz. This is well above any mission requirements. In fact, the third order loop can probably be designed with a larger loop bandwidth, allowing even higher doppler rates to be tracked. The difficulty with using a third order loop is that under certain conditions, the loop can become unstable. Consequently, the time to design a third order loop is significantly longer than for a second order loop.

The ability to take radio science measurements is also dependent on the order of the carrier recovery loop. With a second order loop, an estimate of the carrier frequency is available. A third order loop provides estimates of both carrier frequency and frequency rate. In any case, D/A converters are required to digitize the measurements.

Tradeoff Summary

Table 5.3-2 summarizes the investigation of NC FSK and BPSK receivers. Recalling from the mission analysis of section 2.4 that a doppler rate limit of 8 Hz/s is not a severe constraint, we conclude the additional hardware required by a four filter receiver is not justified. Likewise, the second order recovery loop provides adequate doppler rate protection for the BPSK receiver. The additional design time required for the third order loop is not warranted.

The tradeoff between NC FSK and BPSK is power efficiency versus implementation complexity. Section 2.4 shows that NC FSK supports inadequate time at the high data rate. Another consideration is the fact that BPSK provides radio science measurements while NC FSK does not. The choice for a baseline design is BPSK with a 2nd order carrier recovery loop.

Data Rate Detection

Although the baseline design has been chosen, there are still two more receiver issues which must be pinned down: (1) data rate change detection and (2) radio science frequency estimation. The change in data rate must be detected so that the symbol synchronization loop can be properly adjusted. There are two ways this can be done. The first technique simply uses a clock onboard the carrier to indicate the switch from the low data rate to the high data rate. Given that the carrier and probe clocks are synchronized just before separation, it is possible to compute the uncertainty of timing the transition to the high data rate. Assuming a 20 day coast period and clock stabilities on the order of 20 parts per million, the timing uncertainty is approximately 69 seconds.

Hypothesis testing yields a higher degree of accuracy. The output of the LPF in the BPSK receiver (see Figure 5.3-4) is the sum of the data signal plus noise. The objective is to distinguish the high rate from the low rate. After integrating the signal plus noise over a certain period of time if the output of the integrator exceeds a threshold, then the low rate is present; otherwise, the high rate is present (Figure 5.3-5).

To understand how this works, recall that the high data rate is an integral multiple of the low data rate. Hence, an integer number of "fast" bits occupy the same time period as one "slow" bit (See Figure 5.3-7). Let T be the time for one slow bit. Assume there is a 50 percent bit transition probability. If the high data rate is present, then integrating the signal over T will yield zero. However, if the low rate is present, integrating the signal over T will yield a non-zero value (see Figure 5.3-8). Returning to Figure 5.3-6, if no noise is present, then integrating over T will indicate which data rate is present.

The addition of noise does not really complicate the problem. Instead of being zero or non-zero, the output of the integrator is a gaussian process with zero mean, (Figure 5.3-9). If the low rate is present, there is some probability that the output of the integrator exceeds the threshold. Thus, if the low rate is present, then the output of the integrator will be a non-zero mean gaussian process. If the high rate is present, then the gaussian process will be zero mean.

Based on noise statistics, the performance of the hypothesis test gives a 0.005 second mean time to correctly detect the high data rate. The mean time to incorrectly decide high when the low rate is present is 10^{15} hours. The mean time to incorrectly decide low when the high rate is present is also 10^{15} hours. Thus, hypothesis testing provides an extremely quick and accurate estimate of the data transition time.

Since using an onboard clock to predict the time of rate transition is much less complex than hypothesis testing, it was chosen as the baseline. Should more accuracy be required, the use of hypothesis testing is a viable alternative.

Frequency Estimation

The output of the VCO in the 2nd order PLL is a noisy estimate of the carrier frequency. By periodically sampling this output and then smoothing it, a more accurate estimate of the carrier frequency is obtained. This is exactly the technique that was used on Galileo to obtain radio science measurements. Although Galileo used a third order loop, the parameter which sets the performance of the estimator is proportional to it. Galileo used a loop bandwidth of 8 Hz. This yielded a frequency estimation accuracy of 0.25 Hz, assuming the doppler rate is not significant over the integration time of 2/3 second. To accomodate the doppler rate, the baseline BPSK receiver requires a loop bandwidth of 20 Hz. Hence, we would expect a frequency estimation accuracy of about 0.40 Hz and a corresponding wind measurement accuracy of 0.29 m/s at initial descent and 0.71 m/s at impact (Table 5.5-3). The actual performance should be better since the C/No for Titan is higher than for Galileo.

Coding Scheme	NC FSK	NC DPSK	BPSK
Without coding	10.9 dB	7.9 dB	6.8 dB
With rate 1/2, constraint length 7 convolutional code - hard decisions	10.0 dB	7.0 dB	4.8 dB

Table 5.3-1: Theoretical E_b/N_0 Requirements

	NC FSK	NC FSK 4 Filter	BPSK 2nd Order PLL	BPSK 3rd Order PLL
E_b/N_0 Required With Coding	10 dB	10 dB	4.8 dB	4.8 dB
Doppler Considerations	Doppler Variation $\leq$5 kHz (occurs at ~9 Hz/s)	$\leq$80 kHz	$\leq$2.0 Hz/s	$\leq$110 Hz/s
Radio Science Estimates Available	---	---	f	f, $\dot{f}$

Table 5.3-2: Receiver Comparison

TABLE 5.3-3 WIND VELOCITY MEASUREMENT ACCURACY

- CAN MEASURE DOPPLER TO 0.4 Hz
- DIRECTLY LINKED TO RANGE RATE MEASUREMENT OF 0.052 M/S
- THIS CORRESPONDS TO A WIND VELOCITY INCREMENT PARALLEL TO PLANET'S SURFACE OF
  - AT BEGINNING OF DESCENT, .29 M/S
  - AT SURFACE, .71 M/S

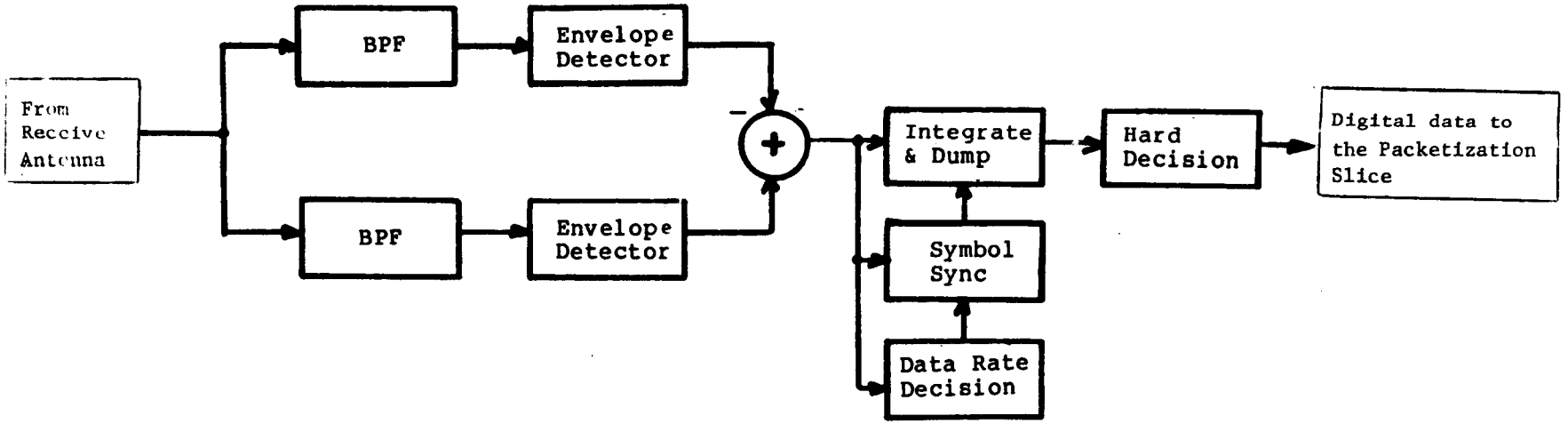

Figure 5.3-1: NC FSK Receiver Functional Diagram

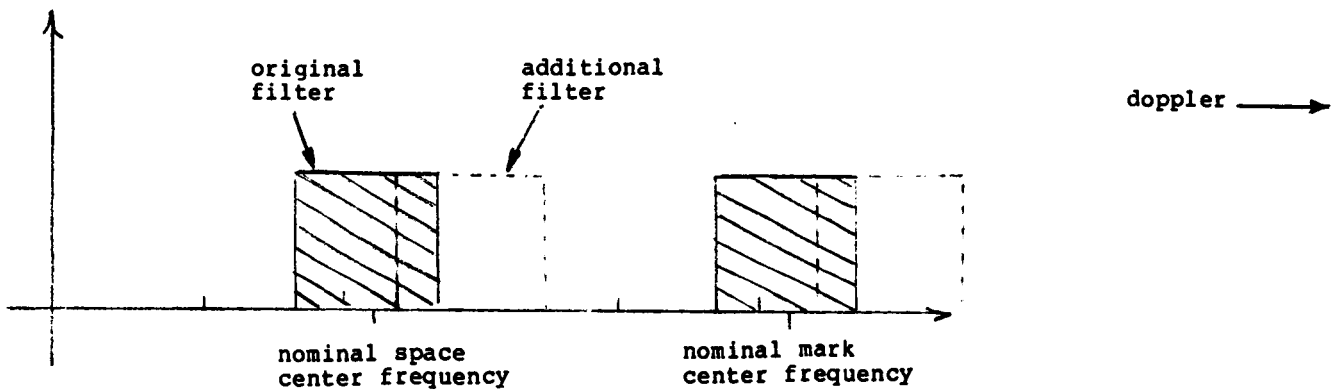

Figure: 5.3-2 Additional Filters Can Accommodate Carrier Frequency Doppler Shift

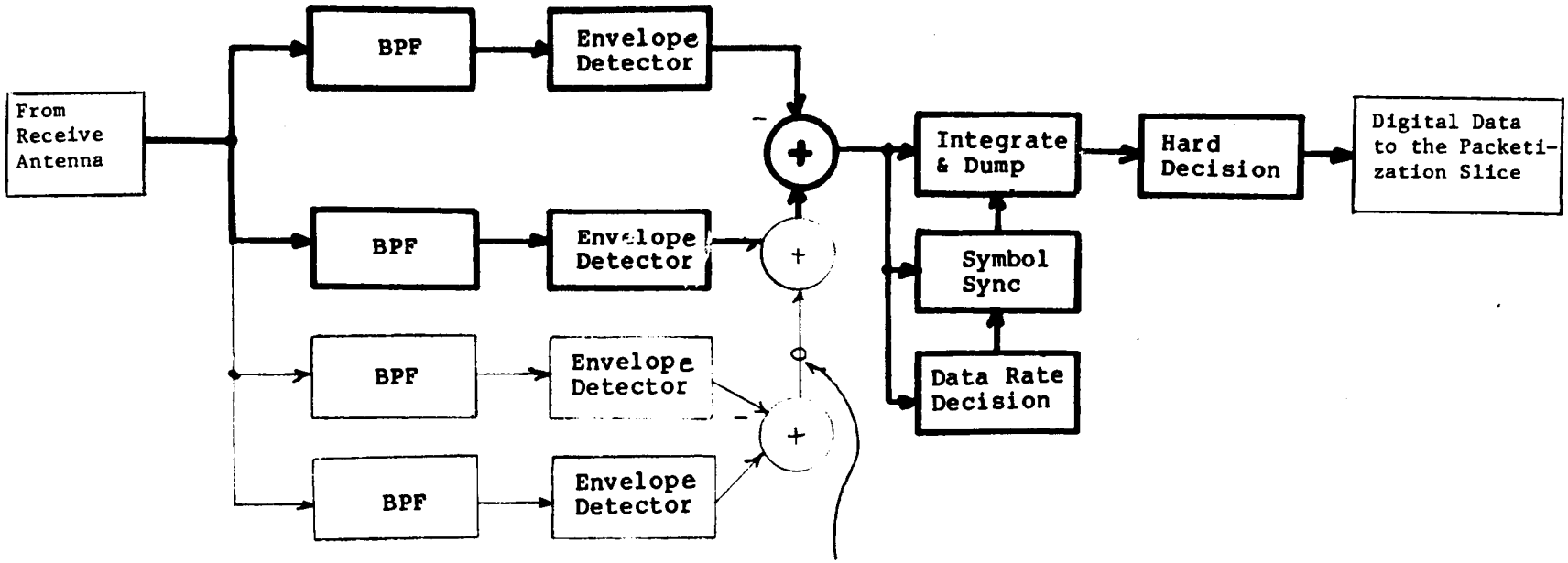

Closed by Stored Command After a Given Time

Figure 5.3-3: Modified NC FSK Receiver

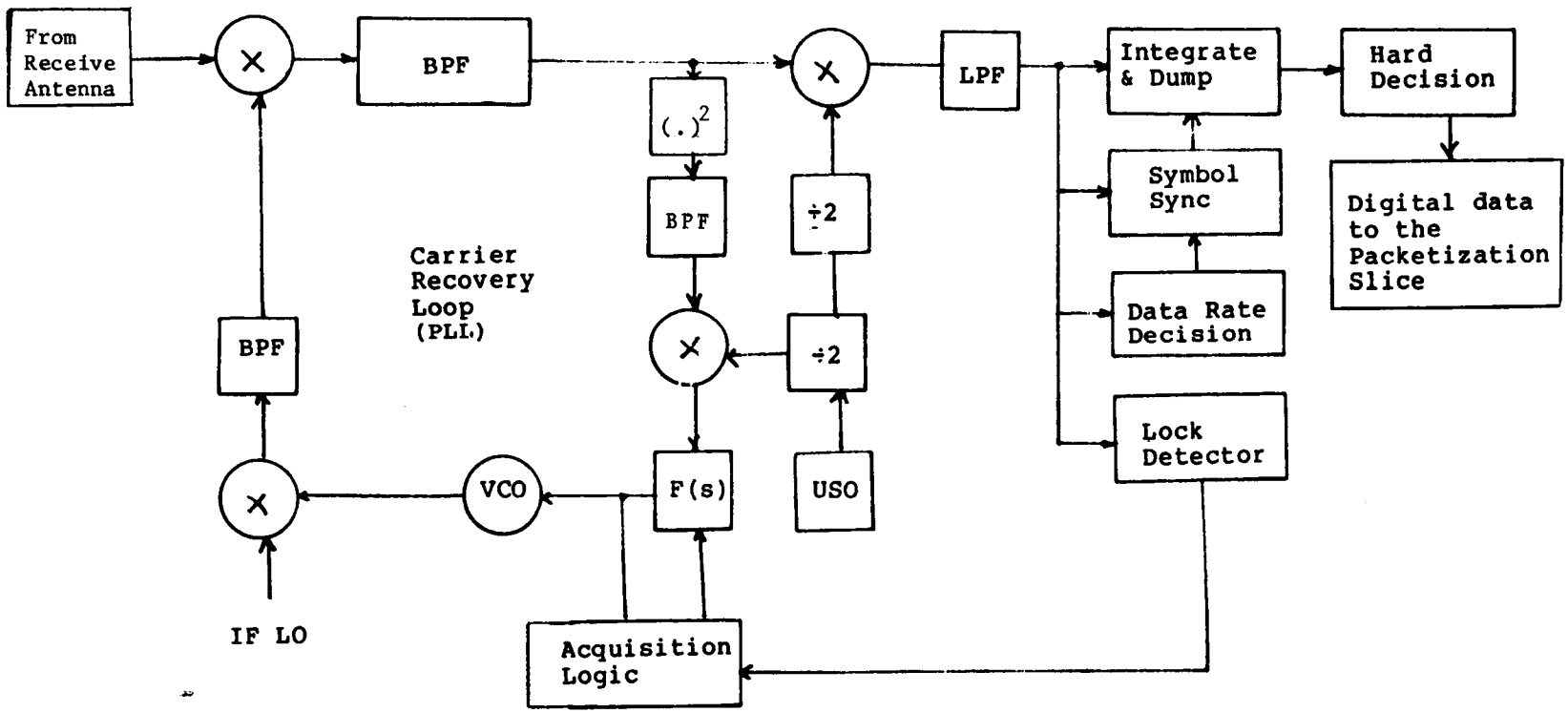

Figure 5.3-4: BPSK Receiver Functional Diagram

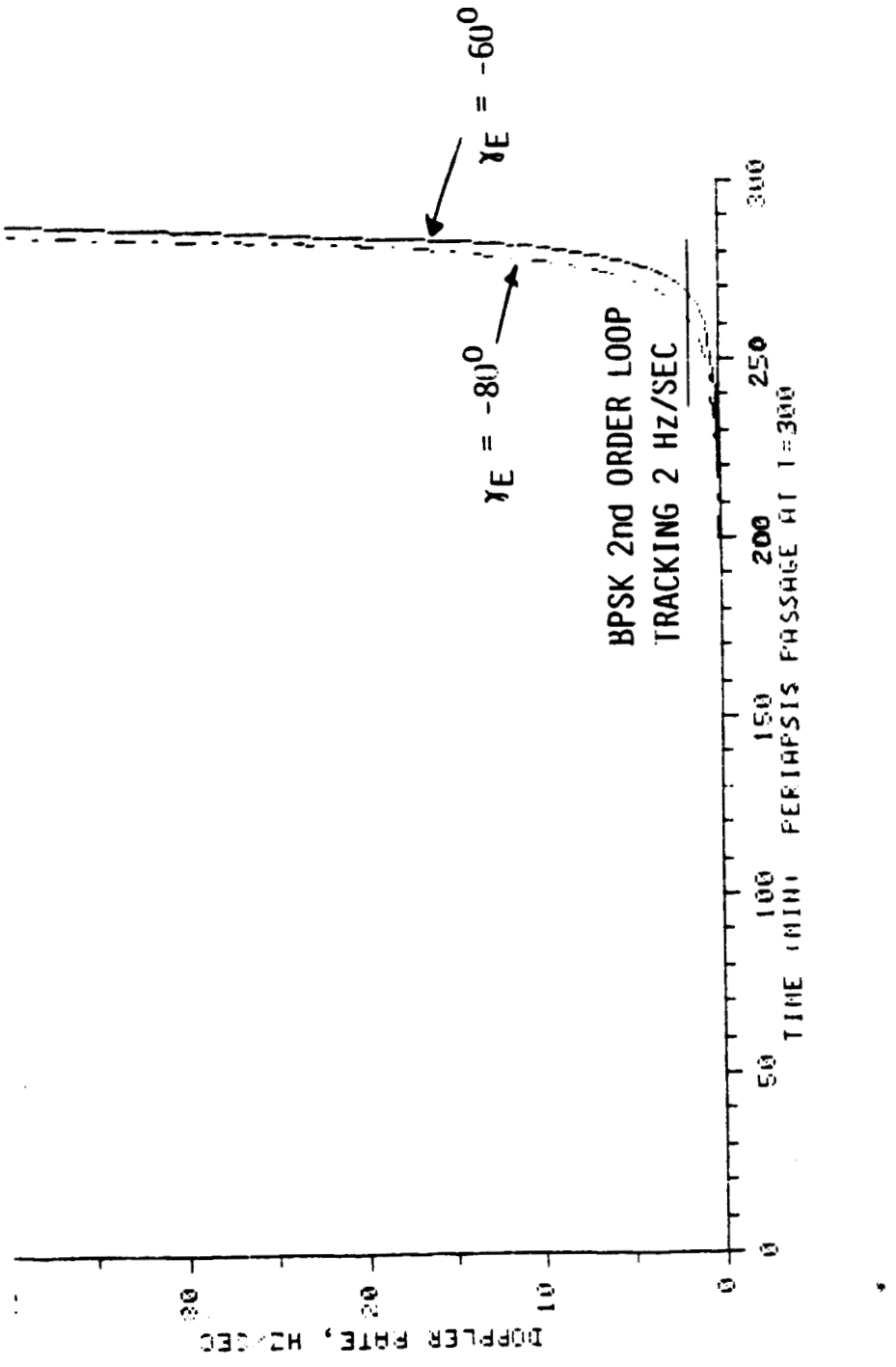

Figure 5.3-5: Typical Doppler Profiles

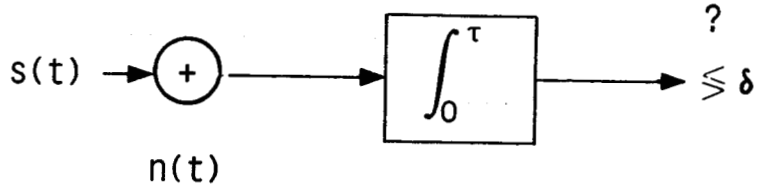

H_0: s(t) is low rate

H_1: s(t) is high rate

Choose H_0 if integrator output exceeds δ; otherwise choose H_1

Figure 5.3-6: Hypothesis Test for Data Rate Change

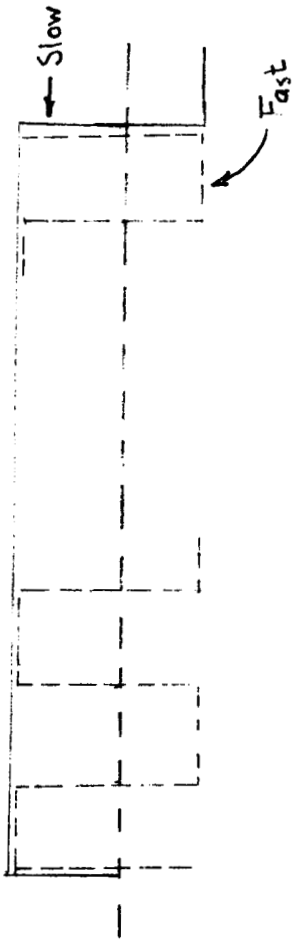

Figure 5.3-7: Relationship Between Slow and Fast Bits

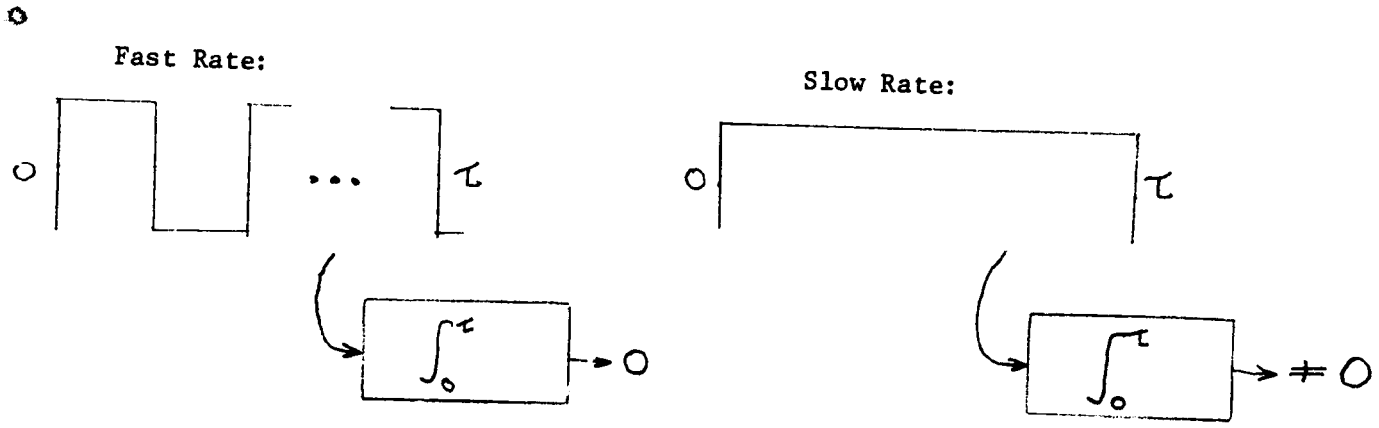

Figure 5.3-8: Integrating Over a Slow Bit Time for Slow and Fast Rates

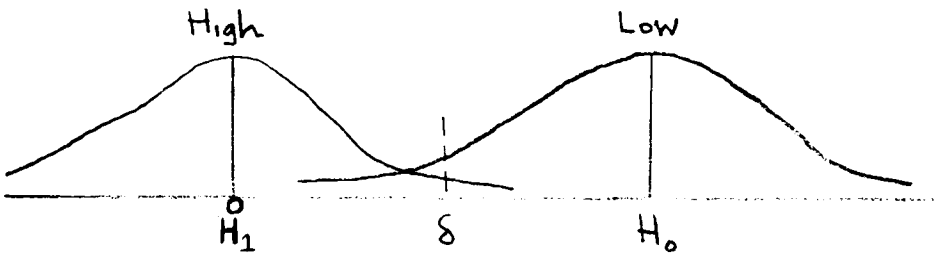

Figure 5.3-9: Distributions when Noise is Added

6. CONCLUSIONS

This study has demonstrated that some new design concepts can enable a Titan Probe to meet new science objectives while maintaining acceptable risk and cost.

Table 6-1 summarizes the results of the major tradeoffs of this study. The preceding sections have addressed each of these in detail and defined a baseline selection.

The baseline mission and probe design demonstrates that haze layer sampling can be accomplished together with an adequate descent time for atmospheric sampling and a high data rate for surface imaging. However, the atmospheric wind uncertainty compromises the data link. If wind bounds can be established the analysis in section 2.4 should be repeated. Fortunately, the automated computer simulations will facilitate this analysis during a future study.

The fixed decelerator configuration with attachment to the Carrier through the probe nose offers the lowest cost and risk design while still providing adequate drag to facilitate high altitude measurements. Integrating a beryllium heat sink decelerator nose with the descent module eliminates any nose separation risk. Differential drag enables low risk aft separation of the skirt. The only complication inherent to the baseline design is the need to deploy instrument sensors. As instruments become better defined, further study can define the deployment mechanisms.

Though somewhat more complicated than an FSK receiver, a BPSK receiver is required to support high rate data transmission. A 2nd order loop receiver provides adequate tracking considering that antenna geometry constrains the mission timing away from periods of peak doppler. Antenna sizing depends on wind model and Carrier pointing capability and is an appropriate subject for further study refinement.

The selected redundancy implementation has no single point failures but does require redundant and asynchronous instrument data interfaces. After instruments are somewhat better defined, further study can compare the impact of this approach on instrument complexity as compared with other approaches which maintain a single interface with each instrument and use internal spacecraft switching to handle redundancy.

6.1 Technology Readiness

Part of this Titan Probe study has been to define any needed technology breakthrough so that appropriate enabling research can be undertaken before program start in the 1988 time frame. Although a number of further studies have been described throughout this report (summarized in table 6.1-1), the study has identified no need for enabling technology before hardware go-ahead.

There are some desirable early activities to be accomplished before the development decision. These activities include verification of entry stability based on 6 DOF simulations, consideration of less costly heat sink designs than beryllium, definition of detailed instrument integration and sensor deployment concepts, and refinement of the relay link analysis and design based on a more detailed wind model including uncertainties. More detailed decelerator design definition and analysis may show advantages of a ribbed or semi monocoque design over the baseline honeycomb construction. A coupon test or tests would validate candidate heatshield materials.

Finally, the new separation technique of splitting the decelerator and allowing differential drag to pull the skirt aft of the descent module nose would benefit from a flight demonstration similar to the PAET demonstration of parachute extraction. It is suggested that such a demonstration be based on an Earth re-entry vehicle and balloon/rocket mechanization simulating the desired properties and staging sequence.

TABLE 6.-1 STUDY CONCLUSIONS

MISSION:	• ENTRY PATH ANGLE -80^{O}
	• CARRIER PERIAPSIS ALTITUDE 1000 KM
	• CARRIER PHASING 40 MIN
	• STAGING TWO SECTION DECELERATOR WITH FORWARD DESCENT MODULE EXTRACTION, SINGLE DESCENT PARACHUTE
	• SURFACE SURVIVAL POSSIBLE BUT NOT LIKELY
CONFIGURATION:	• 2.97 M DIAMETER FIXED DECELERATOR
	• 1M DIAMETER SINGLE SHELF DESCENT MODULE
	• PROBE/CARRIER SEPARATION BY THREE SPRINGS
	• DECELERATOR NOSE RETAINED WITH DESCENT MODULE
COMMUNICATIONS:	• MODULATION BPSK, CONVOLUTIONAL ENCODING
	• PROBE ANTENNA 0.384 DIAMETER
	• RECEIVE ANTENNA 0.75M DIAMETER, POINTED
REDUNDANCY:	• FULLY REDUNDANT DESIGN
	• 3 $LiSO_2$ BATTERY MODULES, 2 REQUIRED
	• ASYNCHRONOUS INSTRUMENT DATA SAMPLING
	• CRITICAL COMMAND PROTECTION
SCIENCE:	• GC DEPLOYMENT ALTITUDE 196 KM
	• IMAGING ALTITUDE (10,000 bps)~10 KM TO SURFACE

TABLE 6.1-1

TECHNOLOGY READINESS

- BASELINE CONFIGURATION IS WITHIN CURRENT STATE OF THE ART. REQUIRING NO TECHNOLOGY DEVELOPMENT
- RECOMMENDED FURTHER STUDY
  - 6DOF DEMONSTRATION OF ENTRY STABILITY
  - MORE DETAILED MISSION OPTIMIZATION FOR BEST ESTIMATE WIND MODEL
  - CONCEPT AND PERFORMANCE ESTIMATE OF RECEIVE ANTENNA POINTING MECHANIZATION
  - ACCOMMODATION OF REVISED SCIENCE PAYLOAD INCLUDING SENSOR DEPLOYMENT
  - VERIFICATION OF ASYNCHRONOUS REDUNDANT INSTRUMENT DATA INTERFACE
  - COST TRADE-OFF OF CANDIDATE HEAT SINK MATERIALS FOR NOSE
  - DEFINE SPIN RATE CONTROL CAPABILITY
  - OPTIMIZE DECELERATOR MASS
  - VERIFY HEATSHIELD PERFORMANCE WITH COUPON TEST
- RE-ENTRY PROBE WOULD VALIDATE DECELERATOR/STAGING DESIGN

APPENDIX A - Symbols and Abbreviations

A/D	Analog to Digital
A-hr	Ampere hour
ASI	Atmospheric Structure Instrument
BIU	Bus Interface Unit
bps	bit per second
BPSK	Binary Phase Shift Keying
BTU	British Thermal Unit
C	Celsius
CCSDS	Consultative Committee on Space Data Systems
CDP	Command and Data Processor
CDS	Command and Data Subsystem
cg	center of gravity
CM	Centimeter
C/N_o	Carrier-to-Noise ratio
dB	Decibel
DC	Direct Current
deg/hr	degree per hour
DOF	Degree of Freedom
DPSK	Differentially Encoded Phase Shift Keying
E-20	Entry minus 20 minutes
E_b/N_o	Energy-to-Noise Level ratio
ESM	Elastomeric material
EXC	Exciter
FIFO	First in First Out
FSK	Frequency Shift Keying
ft	feet
g	gram, force of gravity at Earth sea-level
GC	Gas Chromatograph
HS-376	Hughes Spacecraft Model 376
Hz	Hertz
HYB	hybrid
IPIU	Instrument Power Interface Unit
K	Kelvin
kg	kilogram
kHz	kiloHertz
km	kilometer
kbps	kilobits per second
Li SO_2	Lithium Suphur Dioxide
LPF	Low Pass Filter
JPL	Jet Propulsion Laboratory
m	meter
MHz	MegaHertz
mm	millimeter
N_2	Diatomic Nitrogen
NC	non-coherent
Nep	Nephelometer
NFR	Net Flux Radiometer
Nms	Newton meter second
NMS	Neutral Mass Spectrometer
Ns	Newton second
PAET	Planetary Atmospheric Entry Test

PCU	Pyro Control Unit
PLL	Phase Locked Loop
PPIU	Probe Power Interface Unit
PSF	pound per square foot
RF	Radio Frequency
RHU	Radioisotope Heater Unit
rpm	revolutions per minute
RSS	Root Sum Square
RTG	Radioisotope Thermal Generator
RTV	Room Temperature Vulcanizing
SPIU	Subsystem Power Interface Unit
VCO	Voltage-controlled oscillator
VOIR	Venus Orbiting Imaging Radar
V_∞	Approach Velocity
W	Watt

REFERENCES

Conrath, 85 - Conrath, B.J., Titan atmosphere model presented at the Cassini Science Working Group meeting of March 20-22, 1985.

Flasar, 81 - Flasar, M., Nature, 292, 693, 1981.

Hughes, 82 - Hughes Aircraft Company, Saturn/Titan Probe Final Report, Contract NAS 2-10841, June 1982

Hunten, 82 - Hunten, D.M., "A Review of Titan," 1982.

Lindal, 83 - Lindal et al, "The Atmosphere of Titan: An Analysis of the Voyager 1 Radio Occultation Measurements," Icarus, 53, 348-363 (1983).

Lunine, 83 - Lunine, J.I., Stevenson, D.J., and Yung, Y.L., "Ethane Ocean on Titan," Science 222, 1229 (1983).

Swenson, 84 - Swenson, B.L., et al, "A New System concept for a Titan Atmospheric Probe," AIAA paper 84-0456, January 1984.

Tiwari, 81 - Tiwari, S.N., Chow, H., Moss, J.N., "Analysis of Aerothermodynamic Environment of a Titan Aerocapture Vehicle," AIAA paper 81-1128, June 1981.

1. Report No.	2. Government Accession No.	3. Recipient's Catalog No.
NASA CR-177394		

4. Title and Subtitle	5. Report Date
STUDY OF NEW SYSTEMS CONCEPTS FOR A TITAN ATMOSPHERIC PROBE. Final Technical Report.	April 1986
	6. Performing Organization Code
7. Author(s) Doug Bernard, Todd Citron, Robert Drean, Scott Lewis, Martin Lo, John McCarthy, Robert Soderblom, Dave Steffy, Tina Vargas, Marty Wolff	8. Performing Organization Report No.
	10. Work Unit No.
9. Performing Organization Name and Address Hughes Aircraft Company Space and Communications Group P.O. Box 92919 Airport Station Los Angeles, CA 90009	11. Contract or Grant No. NAS2-12049
	13. Type of Report and Period Covered Contractor Report
12. Sponsoring Agency Name and Address National Aeronautics and Space Administration Washington, DC 20546	14. Sponsoring Agency Code 186-30-21

15. Supplementary Notes

Point of Contact: Contract Monitor, Byron L. Swenson, Ames Research Center, Moffet Field, CA 94035 (415) 694-5705

16. Abstract

The second Mariner Mk II mission scheduled for launch in the mid 1990's offers an opportunity for in-situ sampling of Saturn's mysterious moon, Titan. Though not bounded by existing hardware, this conceptual study assumes only readily available and low risk hardware projected for the late 1980's time frame. This study reflects the latest thoughts of planetary scientists in investigation goals: the desire to sample the organic haze layer which surrounds Titan at high altitude, up to 200 km above the surface; a 2 to 4 hour descent time, for adequate gas sampling; and the ability to image the surface before impact. The baseline Probe configuration consists of two major parts, the central probe element, a descent module, attaches directly to the nose of the Probe which is a solid beryllium decelerator. The 1 meter diameter descent module compartment houses the instruments and support subsystems. The fixed (no deployment) outer decelerator skirt provides the necessary low entry ballistic coefficient (high drag area). The Probe attaches to the Carrier at three points through the beryllium nose. A simple three spring simultaneous spin/eject mechanism, BPSK receiver, and 0.75m dia antenna comprise the hardware retained on the Mariner Mk II Carrier.

The report describes the mission analysis performed to determine compliance with the high altitude sampling and descent time requirements and the selection of Probe/Carrier relay geometry to enable high rate surface imaging. Comparison of staging concepts indicates aft skirt separation by differential drag is the most cost effective approach with minimal risk. Entry thermodynamics analysis determines decelerator materials and thickness. Aerodynamic stability constrains the shape. The most significant advancement from previous probe technology is the Command/data subsystem designed for the much higher data rate and increased emphasis on redundancy. The study conclusions include design solutions to all the major science objectives without requiring significant technology advancement.

17. Key Words (Suggested by Author(s))	18. Distribution Statement
Titan Probe, gas sampling, communications relay, beryllium decelerator, surface imaging.	Unclassified - Unlimited Subject Category 88

19. Security Classif. (of this report)	20. Security Classif. (of this page)	21. No. of Pages	22. Price*
Unclassified	Unclassified	192	

*For sale by the National Technical Information Service, Springfield, Virginia 22161